Studies on Bio-inspired N, O-donor Ligands-Based Cu(II) Complexes in Photocatalysis

Ph.D. Thesis

By

RISHI RANJAN

DEPARTMENT OF CHEMISTRY

INDIAN INSTITUTE OF TECHNOLOGY INDORE

DECEMBER 2022

Studies on Bio-inspired N, O-donor Ligands-Based Cu(II) Complexes in Photocatalysis

A THESIS

Submitted in partial fulfillment of the requirements for the award of the degree of

DOCTOR OF PHILOSOPHY

by

RISHI RANJAN

DEPARTMENT OF CHEMISTRY

INDIAN INSTITUTE OF TECHNOLOGY INDORE

DECEMBER 2022

INDIAN INSTITUTE OF TECHNOLOGY INDORE

I hereby certify that the work which is being presented in the thesis entitled "**Studies on Bio-inspired N, O-donor Ligands-Based Cu(II) Complexes in Photocatalysis"** in the partial fulfillment of the requirements for the award of the degree of **DOCTOR OF PHILOSOPHY** and submitted in the **Department of Chemistry, Indian Institute of Technology Indore**, is an authentic record of my own work carried out during the time period from **September 2017** to **November 2022** under the supervision of **Dr. Suman Mukhopadhyay**, Professor, Department of Chemistry, Indian Institute of Technology Indore.

The matter presented in this thesis has not been submitted by me for the award of any other degree of this or any other institute.

06/12/2022
Signature of the student with date
(RISHI RANJAN)

This is to certify that the above statement made by the candidate is correct to the best of my knowledge.

06/12/2022
Signature of Thesis Supervisor with date
(Prof. Suman Mukhopadhyay)

Mr. Rishi Ranjan has successfully given his Ph.D. Oral Examination held on April 21st 2023

21/04/2023
Signature of Thesis Supervisor with date
(Prof. Suman Mukhopadhyay)

ACKNOWLEDGEMENTS

It is my great pleasure to express my deep sense of gratitude to my PhD thesis supervisor, Prof. Dr. Suman Mukhopadhyay for his constant guidance, encouragement and help throughout the whole course of the thesis work. I am greatly indebted to him for his support, motivation and guidance. His vision and dedication in developing the thesis injected a remarkable impact on my academic career. His assurance and encouragement during the hard times when research plans did not work are gratefully acknowledged. I am thankful to my PSPC committee members, Dr. Amrendra K. Singh and Dr. Hem Chandra Jha for their valuable suggestions and guidance. I wish to express my gratitude to Prof. Suhas S. Joshi, Director, IIT Indore for his continuous support in every aspect. I would like to thank University Grant Comission and SIC, IIT Indore for providing financial support and instrumentation facility, respectively. I am also thankful to SERB for International travel grant (ITS/2022/001983) for providing financial support to attend the conference in RUDN University Moscow, Russian federation. I am thankful also to Dr. Rakesh Ganguly, Dr. Pabitra Baran Chatterjee, Dr. Preeti S. Bhobe, Dr. Komal M. Vyas, Dr. Sivranjana R. Vennapusa and Mr. Probal Nag, for their active support in various research projects. I would also like to thank all the faculty members of Department of Chemistry, IIT Indore for their guidance and help during the course of the thesis work. I personally extend my heartiest gratitude to Dr. Poulami mandal, Dr. Bidyut Kumar Kundu, Dr. Novina Malviya, Dr. Rinky Singh and Dr. Chanchal Sonkar for their constant guidance, help and support at all the ups and downs in those initial days of the PhD programme. I convey my deep thanks to my dear group members, Ms. Pragti, Ms. Reena, Mr. Argha Chakraborty, Mr. Sayantan Sarkar, Ms. Ritika, Mr. Amardeep, Ms. Srijita Pal, Mr. Ritik and Dr. Shilpi Misra for their selfless co- operation and help to make my work successful. I would also like to thank Mr. Kinny Pandey, Dr. Ravinder Kumar, Mr. Ghanshyam Bhavsar, Mr. Manish Kushwaha, Mr. Rameshwar Dohare, Mr. Nitin, Ms. Mitali Dave, Mr. Ranjeet Raghuvanshi and Ms. Vinita Kothari for their technical support without which it would not be possible to continue my work. I would also like to thank Mr. Rajesh Kumar, Mr. Lala Ram Ahirwar, Dr. Ripan Ranjan Biswas, Mr. Satish Bisen, Mr. Divyanshu Jain, Mr. Nipul G. Shihora Powar and other library staffs for their constant support, whenever required. I would like to thank all my co-

researchers at IIT Indore. I would like to acknowledge all the technical and non-technical staffs of IIT Indore for their assistance and service. It has been a wonderful experience to work with many friends during my Ph.D. who really helped me in many aspects. I would like to record my thanks to Dr. Rohit G. Jhadhav, Dr. Soumitra Guin, Dr. Soumya Kanti De, Dr. Sayan Maity, Dr. Debashis Majee, Dr. Shyama Charam Mandal, Dr. Akhil S. Nair, Ms. Manju, Dr. Faizal Khan, Mr. Indresh Singh Yadav, Mr. Tapas Ghosh, Mr. K. Sarathkumar, Mr. Vinod Sahu, Mr. Avijit Maity, Mr. Debanjan Bagchi, Mr. Devraj Singh, Mr. Sourav Bhowmik, Mr. Vikash Sahu and many more in my friend circle.

Most importantly, I thank my beloved parents (Mr. Arun Kumar and Mrs. Sharda Devi) for their wise counsel and sympathetic ear. They are always there for me. I don't have enough word to describe all the sacrifices they continue to make to see me through this milestone. Without your constant support and unconditional love, it would not have been possible. I want to say thanks to my family members Mr. Divyesh Ranjan, Mr. Bibesh Ranjan, Mrs. Archana Anjali, Mrs. Kavita Kumari, and Mrs. Shakshi Suman.

There are many more who have directly or indirectly contributed in making this journey successful. I wish I could thank them all but time and space compel me to stop here!!!

RISHI RANJAN

IIT INDORE

Dedicated to My Beloved Family

ABSTRACT

1. Introduction

Ligands are ions or molecules that formally donate at least one electron pair to the metal center [1]. The interaction(s) between the metal and donor system can be significantly influenced by both the electronic as well as steric properties of the ligand [2]. It follows that the design and synthesis of new ligands have significantly enriched the field of organometallic and transition-metal coordination chemistry. The diversities in structures and reactivity of the ligands have led to the synthesis of an extensive range of transition metal coordination and organometallic complexes. The synthesized compounds can show enormous potential to get utilized in pharmaceuticals (drug development), material industries (polymers), and biomedical applications (Figure 1) [3-6]. In addition, these transition metal complexes can also play significant roles in catalysis (organic transformation), sensing, and different biological processes and can act as metalloenzyme mimics.

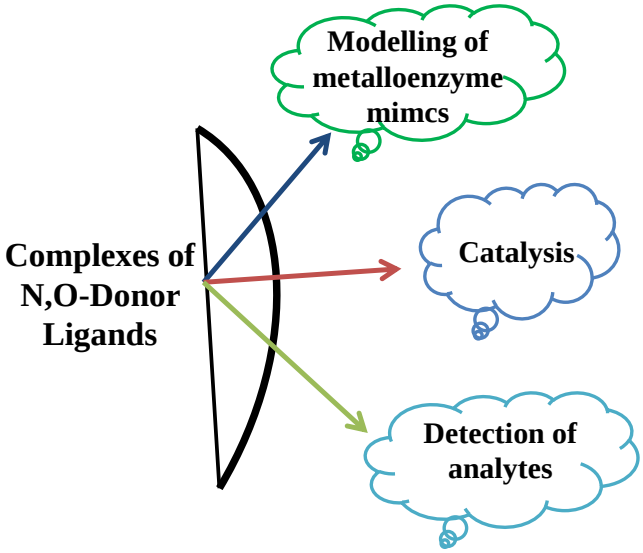

Figure 1. Various applications of 'N, O-donor' ligands and their complexes.

Numerous types of ligands can be developed by varying the combinations of aza (N), oxa (O), sulfa (s) and phospha (P) ligating atoms. To accommodate the specific metal ions, the ligands can be fabricated by the modulating the features such as nature of the donor atoms, donor arrays, ligand conjugation, donor sets, ligand substitution, number and sizes of the chelate rings, ligand flexibility and nature of the ligand backbone, *etc* [7]. Among various donor sets, ligands having 'N', 'O' donor atoms are found to be very effective in complexation due to smaller size of the donor atoms, ability to form neutral and anionic ligands, easily

available lone pair(s) for chelation and ability to form metal complexes with moderate stability [2]. These features make N, O-donor ligands as excellent contenders for the critical applications in many areas, including bioinorganic and medicinal chemistry, homogeneous catalysis, and environmental chemistry [1, 8]. With the broad aim of development of improved N, O-donor ligands (*ca*. Mannich base and Schiff base) and tune their property through introduction of flexibility in the backbone and varying the number of donor sites, a number of ligands and metal complexes have been designed and synthesized and the complexes have been explored for various applications in different facets of usability with a specific focus of bio-inspired catalytic reactions [9, 10].

2. Objectives

The primary objectives which have been set for this thesis are the following:

- To develop target-specific metalloenzyme mimics by employing N, O-donor ligands around copper center. Following enzyme mimics are mostly explored in this thesis.

Galactose oxidase mimicking activity: Galactose oxidase induces homogeneous organic transformation of primary alcohols to corresponding aldehydes. Developing galactose oxidase mimicking center can provide new oxidative catalyst for improved oxidation transformation in a less demanding reaction conditions.

Laccase mimicking activity: Laccase is an enzyme which catalyzes the depolymerization of lignin into monomers through one electron oxidation. Laccase mimicking complex can provide new ways to overcome the crises of renewable source of energy.

- To explore the sensing of analytes (nitro-aromatics) by photo-luminescence spectroscopy: Sensing and quantification of analytes have profound importance in terms of environmental and biological chemistry. Easy detection of molecules can be helpful to arrest environmental pollution as well as disease progression in biological systems.

- To explore the efficacy of developed catalysts towards the photocatalytic organic synthesis: the extensive use of galactose oxidase mimicked compound as homogeneous catalysts towards the C-N coupling reactions has been explored to overcome the chemical waste.

• To explore the efficacy of developed catalysts in homogeneous and heterogeneous conditions: comparative study of a compound as homogeneous and heterogeneous catalysts has been explored for better oxidative catalytic performance.

• To investigate the possible mechanistic pathway(s) to determine the mode of action of synthesized compounds.

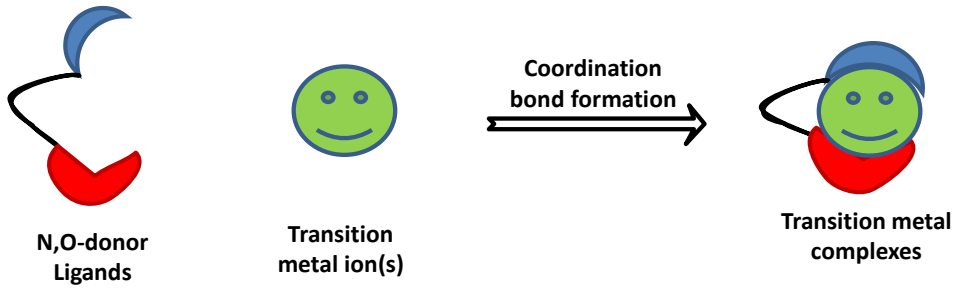

Figure 2. General representation of the synthesis of coordination complexes.

3. Summary of research work

The contents of each chapter included in the thesis are discussed briefly as follows:

3.1. Chapter 1: General Introduction and Background

A brief overview of the basic concepts and recent scientific developments towards the generation of N, O-donor based ligands and derived complexes (*ca*. Mannich base or Schiff base transition metal complexes) and their potential applications in various biological, chemical and material fields have been presented. A summary of the research work reported in this thesis and the relevance in the prospects of recent developments have been also included in this chapter.

3.2. Chapter 2: Mono- and hexa-nuclear copper complexes of mannich base ligand: Synthesis, ligand transformation study, X-ray crystal structure, enzymatic catalysis and nitro aromatic sensing applications

Over the years, researchers have been developed various coordination complexes based on flexible Mannich base ligands because of their significant electronic and conformational diversity which is driven by the various group(s) attached to the backbone of the ligand. Therefore, to understand the potential effect of this ligand towards enzymatic reactions as well as nitro-aromatics detection activity, this chapter has been divided into two parts as described below:

3.2.1. Chapter 2A: Synthesis of mono-nuclear Cu(II) complexes by N,O-donor ligand transformation and their catalytic role in visible-light-driven alcohol oxidation

In this part, galactose oxidase (GOase) which is the metalloenzyme of copper with monomeric sites of co-ordination, has been taken into account. This work summarizes the results of the structural, spectral and catalytic properties of new mononuclear copper (II) complexes [$CuHL_a^1$] (**1**), and [$CuHL_b^1$] (**2**) which are derived from the internal transformation of the ligand from H_2L^1 **[H_2L^1** = 2,4-dichloro-6-{[(2'-dimethylaminoethyl)methylamino]methyl}phenol], which can mimic the functionalities of the metalloenzyme GOase under visible light irradiation. The GOase catalytic results were explored by GC-MS and analyzed by HPLC at room temperature. It has been found that the amount of conversion of benzyl alcohol to benzaldehyde is significant in presence of 2,2,6,6-Tetramethyl-1-piperidinyloxy (TEMPO). The generation of reactive intermediates during organic transformation of ligand and GOase catalysis was investigated by ESI-MS. Furthermore, it has been found that H_2O_2 is the byproduct for the GOase catalysis, thus, confirming the generation of reactive oxygen species during the catalytic procedure. A plausible mechanistic pathway for photocatalytic oxidation reaction has been explored through ESI-MS, cyclic voltammetry, UV-Vis and computational study. Notably, complex **1** has shown superior catalytic activity in comparison to complex **2**.

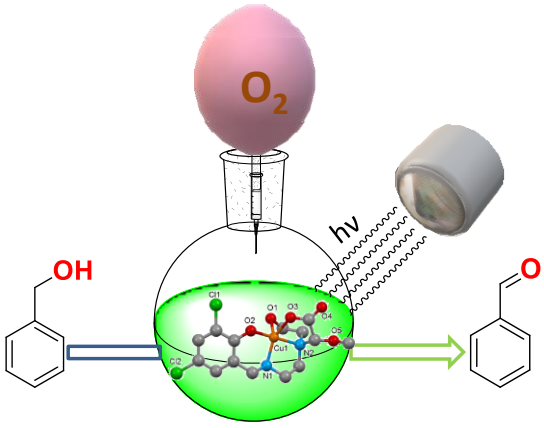

Figure 3. *Photocatalytic oxidation of benzyl alcohol in to benzaldehyde.*

3.2.2. Chapter 2B: Picric acid detection by a hexanuclear Cu(II) complex synthesized through N,O-donor ligand transformation

Chapter 2B is about the synthesis, characterization and sensing ability of one hexanuclear Cu(II) complex $[Cu(HL_c^1)]_6$ (**3**). The complex **3** also derived from the transformed ligand of H_2L^1 to $H_3L_c^1$ [$\mathbf{H_3L_c^1}$ = 1-(3,5-dichloro-2-hydroxybenzyl)-3-(2-hydroxyethyl) imidazolidine-2-carboxylic acid] and the probable pathway of organic transformation has been explored through the ESI-MS. Furthermore, the practical applicability of the synthesized complex was investigated as a fluorescence sensor for the sensitive detection of picric acid.

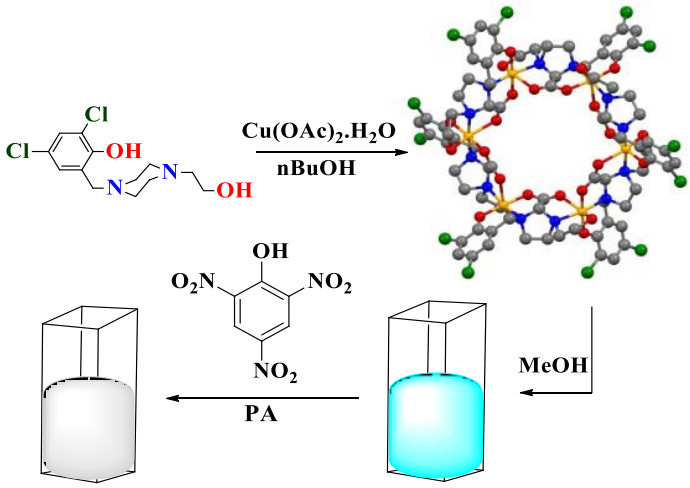

Figure 4. *Schematic diagram of synthesis and application of hexanuclear complex.*

3.3. Chapter 3: Binuclear Cu(II) complex as an efficient Photocatalyst for Benzyl alcohol oxidation and in-situ N-alkylation of aromatic amines

The chapter 3 is about the synthesis and photo-catalytic ability of two binuclear Cu(II) Mannich base complexes $[Cu(HL^1)(OAc)]_2$ **(4)** and $[Cu(HL^2)(NO_3)]_2$ **(5)** [$\mathbf{H_2L^2}$ =2,4-dibromo-6-((4-(2-hydroxyethyl) piperazin-1-yl)methyl)phenol]. The extensive use of galactose oxidase mimicked compound as homogeneous catalysts towards the C-N coupling reactions were carried out at room temperature in the presence of visible light. The catalytic results were explored by GC-MS and analyzed by HPLC. The plausible mechanistic pathway for catalytic reactions has been explored through ESI-MS spectrometric, UV-Vis spectroscopic and computational study. Notably, complex **4** has shown superior catalytic activity in comparison to complex **5** towards both of the reactions.

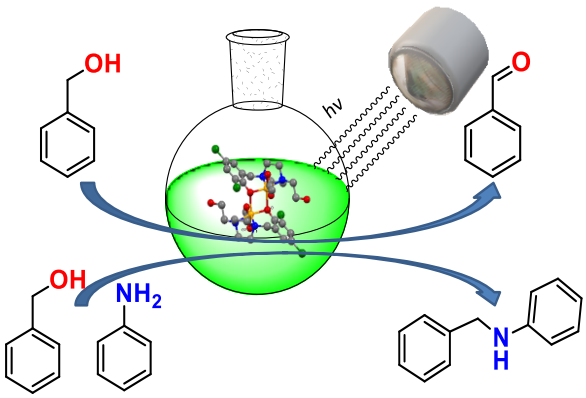

Figure 5. *Schematic diagram of photocatalytic oxidation and C-N coupling reactions.*

3.4. Chapter 4: Employing Cu(II) complexes of N,O-donor ligand for the catalysis of visible light driven cleavage of lignin C-C bonds

In this chapter, we discussed about the synthesis, characterization and photocatalytic application of two new binuclear Cu(II) Schiff base complexes $[Cu(L^3)Cl]_2$ **(6)** and $[Cu(L^3)(N_3)]_2$ **(7)** [$\mathbf{HL^3}$ = 2-[((3-(dimethylamino)-2,2-dimethylpropyl)imino)(phenyl) methyl]phenol]. Under visible light irradiation, the synthesized complexes are able to cleave the C-C bonds of 2-phenoxy-1-phenylethanone, as well as authentic lignin in the presence of H_2O as a solvent as suggested by HPLC data. A plausible mechanistic pathway for the degradation reaction has been explored through ESI-MS spectrometry, NMR spectroscopy, UV-Vis and computational study. Complex **6** has shown superior catalytic activity in comparison to complex **7**.

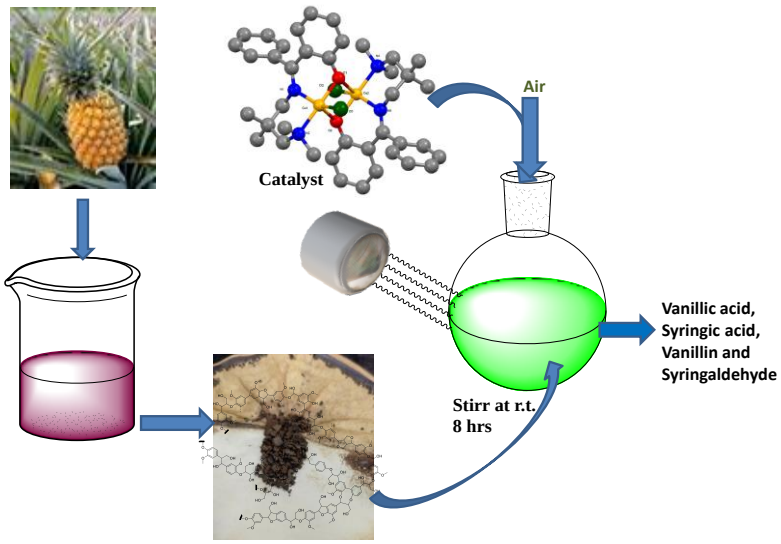

Figure 6. *Schematic diagram of extraction and photocatalytic degradation of the lignin.*

3.5. Chapter 5: Zeolite encapsulated host-guest Cu(II) Schiff base complexes: superior activity towards degradation of lignin C=C bonds

Being inspired by the results of the previous chapter, this chapter is particularly focused on the enhancement of the photo catalytic efficiency *via* fine tuning of the N,O-based ligand systems. Thus, two crystalline copper Schiff base complexes of general formula $[CuL^3(OAc)]_2$ **(8)** and $[Cu(HL^4)(OAc)]_2$ **(9)** $[H_2L^4$ = 2-(((2-(methylamino)ethyl)imino) (phenyl)methyl)phenol] were prepared and characterized. The guest, metal complexes were entrapped in the supercages of NaY zeolite (host) in the solvent phase through two stage process (i) ion exchange of the selected transition metal (Cu(II)-ion) in the porous structure and (ii) encapsulation of Schiff-base ligands (**HL^3**/ **HL^4**) in Cu(II) exchanged zeolite. Herein, this study reveals the advantage of heterogeneous catalytic method for the stability of metal complexes into the supercages of zeolite-Y and the photocatalytic degradation of lignin in presence of TBHP at mild reaction conditions. The catalytic activities of the zeolite entrapped Cu(II) complexes were tested for comparison with their homogeneous analogous. The heterogeneous catalysts can be re-used after recovering from several cycles without much decay in the activity.

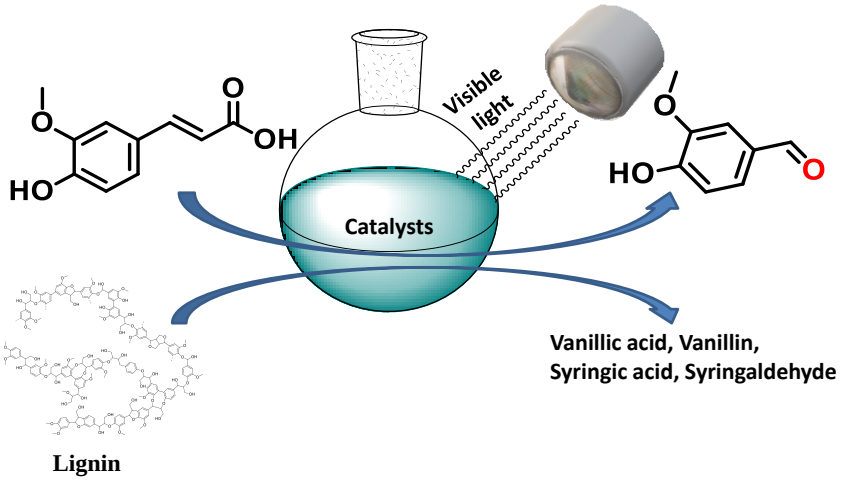

Figure 7. *Schematic diagram of photocatalytic degradation reactions by homo- and heterogeneous catalysts.*

3.6. Chapter 6: General conclusions and future scope

This chapter summarizes the salient features of the work and its future prospects.

4. References

[1] Cotton, F.A., Wilkinson, G., Murillo, C.A., Bochmann, M., Grimes, R., Advanced inorganic chemistry, Wiley New York, 1988

[2] Milstein, D., Ligand Design in Metal Chemistry: Reactivity and Catalysis, John Wiley & Sons, 2016

[3] Haas, K.L., Franz, K.J. (2009), Application of Metal Coordination Chemistry To Explore and Manipulate Cell Biology, Chemical Reviews, 109, 4921-4960. (DOI: 10.1021/cr900134a)

[4] Hoof, S., Limberg, C. (2019), The Behavior of Trispyrazolylborato-Metal(II)-Flavonolate Complexes as Functional Models for Bacterial Quercetinase-Assessment of the Metal Impact, Inorg. Chem., 58, 12843-12853. (DOI: 10.1021/acs.inorgchem. 9b01795)

[5] Rebilly, J. N., Colasson, B., Bistri, O., Over, D., Reinaud, O. (2015), Biomimetic cavity-based metal complexes, Chem. Soc. Rev., 44, 467. (DOI: 10.1039/c4cs00211c)

[6] Willms, H., Frank, W., Ganter, C. (2009), Coordination Chemistry and Catalytic Application of Bidentate Phosphaferrocene-Pyrazole and -Imidazole Based P,N-Ligands, Organometallics, 28, 3049-3058. (DOI: 10.1021/om8012025)

[7] Yang, L., Zhang, D., Yan, H., Dong, Y., Zhou, Z., Wang, S. (2019), Flexible-Ligand-Based Self-adaptive Metal−Organic Material for Supramolecular Selective Recognition of Similar Natural Molecules, Inorg. Chem., 58, 4067-4070. (DOI: 10.1021/acs. inorgchem.9b00148)

[8] Ayipo, Y. O., Osunniran, W. A., Babamale, H. F., Ayinde, M. O., Mordi, M. N. (2022), Metalloenzyme mimicry and modulation strategies to conquer antimicrobial resistance: Metal-ligand coordination perspectives, Coordination Chemistry Reviews, 453, 214317. (DOI: 10.1016/j.ccr.2021.214317)

[9] Robin, A.Y., Fromm, K.M. (2006), Coordination polymer networks with O- and N-donors: What they are, why and how they are made, Coordination Chemistry Reviews, 250, 2127-2157. (DOI: 10.1016/j.ccr.2006.02.013)

[10] Gogoi, G., Nath, J. K., Hoque, N., Biswas, S., Gour, N. K., Kalita, D. J., Bora, S. R., Bania, K. K., (2022), Single and multiple site Cu(II) catalysts for benzyl alcohol and catechol oxidation reactions, Applied Catalysis A: General, 644, 118816.(DOI: 10.1016/j.apcata.2022.118816)

LIST OF PUBLICATIONS

[1]. Ranjan, R., Kundu, B. K., Reena, Ganguly, R., and Mukhopadhyay, S. (2022), Synthesis of Cu(II) complexes by N,O-donor ligand transformation and their catalytic role in visible-light-driven alcohol oxidation. Appl. Organomet. Chem., 36(1), e6450.(DOI: 10.1002/aoc.6450)

[2]. Ranjan, R., Reena, Chakraborty, A., Ganguly, R. and Mukhopadhyay, S. Synthesis of fluorescent hexa-nuclear Cu(II) complex by N,O-donor ligand transformation for picric acid detection. (Manuscript under preparation)

[3]. Ranjan, R., Reena, Chakraborty, A., Ganguly, R. and Mukhopadhyay, S. (2022) A binuclear Cu(II) complex as an efficient photocatalyst for N-alkylation of aromatic amines. Dalton trans. 51(35), 13288-13300.(DOI: 10.1039/ D2DT01771G)

[4]. Ranjan, R., Chakraborty, A., Ganguly, R. and Mukhopadhyay, S. Employing Cu(II) complexes of N,O-donor ligand for catalysis in visible light driven cleavage of lignin C-C bonds. Molecular Catalysis, 537, 112947.(D.O.I. 10.1016/j.mcat.2023.112947)

[5]. Ranjan, R., Sarkar, S., Ganguly, R. and Mukhopadhyay, S. Zeolite encapsulated host-guest Cu(II) Schiff base complexes: superior activity towards degradation of lignin C=C bonds (Manuscript under preparation)

[6]. Kundu, B. K., Ranjan, R., Mukherjee, A., Mobin, S. M. and Mukhopadhyay, S. (2019), Mannich base Cu(II) complexes as biomimetic oxidative catalyst. J. Inorg. Biochem. 195, 164.(DOI: 10.1016/j.jiorgbio .2019.03.023)

[7]. Malviya, N., Ranjan, R., Sonkar, C., Mobin, S. M. and Mukhopadhyay, S. (2019), Self-healable Lanthanoid-based metallogels: Dye removal and crystallization in the confind in the gel state. ACS Appl. Nano Mater., 2, 8005. (DOI: 10.1021/acsanm.9b02064)

[8]. Chhabra, V., Kundu, B. K., Ranjan, R., Pragti, Mobin, S. M., and Mukhopadhyay, S. (2020), Coligand driven efficiency of catecholase activity and proteins binding study of redox active copper complexes. Inorganica Chimica Acta., 502, 119389. (DOI: 10.1021/acsanm.9b02064)

[9]. Sonkar, C., Malviya, N., **Ranjan**, **R.,** Mukherjee, A., Mobin, S. M. and Mukhopadhyay, S. (2020), Mechanistic insight for targeting biomolecules by Ruthenium (II) NSAID complexes. ACS Applied Bio Materials., 3(7), 4600. (DOI:10.1021/acsabm.0c00501)

[10]. Sarkar, S., Chakraborty, A., **Ranjan**, **R.,** Nag, P., Vennapusa, S. and Mukhopadhyay, S. (2022) A bifunctional imidazolium-functionalized ionic porous organic polymer in water remediation. Materials Chemistry Frontiers, 6, 3070-3083. (DOI: 10.1039/D2QM00636G)

[11]. Chakraborty, A., Sarkar, S., Nag, P., **Ranjan**, **R.,** Vennapusa, S., and Mukhopadhyay, S., (2023), Exploring Multifunctional Applications of a Luminescent Covalent Triazine Polymer in Acid Vapour Sensing, CO_2 Capture, Dye Removal, and Turn-off Fluorescence Sensing of Dichromate Ions. Materials Chemistry Frontiers. (DOI: 10.1039/D2QM01329K)

[12]. Patel, B. **Ranjan**, **R.,** Chauhan, N. R., Mukhopadhyay, S., Roychoudhury A., and Vyas, K. M. (2023), N-coordinated Ru(II) Catalyzed Solvent Free N-alkylation of Primary Amines with Alcohols through Borrowing Hydrogen Strategy. New J. Chem.,(DOI: 10.1039/D3NJ00210A)

(*N. B. Publications 6-12 are not included in the thesis work*)

LIST OF CONFERENCES

1. In-house chemistry symposium CHEM 2019 (Organized by department of Chemistry, IIT Indore) on 28th Feb, 2019.(Poster Presented)

2. International conference on “Emerging Trends in Chemistry” (Organized by IIT Indore) on 12th- 15th July, 2019.(Poster Presented)

3. In-house chemistry symposium CHEM 2020 (Organized by department of Chemistry, IIT Indore) on 12th Feb, 2020.

4. Attended the ‘ACS Fall 2020 Virtual meeting and Exposition’ (Organized by American Chemical Society) on 17th-20th Aug, 2020.

5. In-house chemistry symposium CHEM 2022 (Organized by department of Chemistry, IIT Indore) on 11th March, 2022.

6. 29th CRSI national symposium and CRSI-ACS symposium series in chemistry (CRSI-NSC-29) (Organized by IISER, Mohali, with the celebration of CRSI India and ACS) on 7th-9th July, 2022. (Poster Presented)

7. The Sixth International Scientific Conference “Advances in Synthesis and Complexing” (Organized by Peoples’ Friendship University of Russia, Moscow) on 26th – 30th Sept, 2022. (Poster Presented)

Table of Contents

List of Nomenclature

A	Alpha
B	Beta
Γ	Gama
T	Fluorescence Lifetime
Å	Angstrom
X	Chi
Λ	Wavelength
μ	Micro
Π	Pi
Nm	Nanometer
Ns	Nanosecond
mM	Milli Molar
μM	Micro Molar
Ksv	Stern Volmer Quenching Constant
ε	Molar Extinction coefficient
Cm	Centimeter
°	Degree
K	Kelvin
mL	Milliliter
μL	Microliter
a. u.	Arbitrary Unit
Λ_{ex}	Excitation Wavelength
λ_{em}	Emission Wavelength
pH	The negative logarithm of hydronium-ion concentration
H	Eta (Efficiency)
K_a	Binding Constant

List of Acronyms

CCDC	Cambridge Crystallographic Data Centre
$CDCl_3$	Chloroform - *d*
DCM	Dichloromethane
DFT	Density Functional Theory
DMF	Dimethylformamide
DMSO-d_6	Dimethyl sulfoxide – d_6
ESI-MS	Electron Spin Ionization Mass Spectroscopy
FE-SEM	Field-emission Scanning Electron Microscope
GOF	Goodness of Factor
HOMO	Highest Occupied Molecular Orbital
IR	Infrared
LUMO	Lowest Unoccupied Molecular Orbital
MeOH	Methanol
NMR	Nuclear Magnetic Resonance
PA	Picric Acid
PXRD	Powder X-ray diffraction
SCXRD	Single Crystal X-Ray Diffraction
TOF	Turn Over Frequency
TON	Turn Over Number
UV	Ultra Violet
XPS	X-ray photoelectron spectroscopy

List of Figures

Chapter 1

Chapter 2

Chapter 2A

Chapter 2B

Chapter 3

Chapter 4

Chapter 5

List of Schemes

Chapter 3

Chapter 4

Chapter 5

List of Tables

Chapter 5

Chapter 6

Chapter 1

General introduction and background

Chapter 1

General introduction and background

1.1 Introduction

Each layer of discovery and creation arises from initial ideas and investigation, making science a pyramidal effort. Chemistry, primarily an experimental science, relies heavily on available observations and findings. Apart from the database available through scientific research, scientists have found a lot of motivations from nature by understanding how the biological and chemical process occurs spontaneously, even with an energy-demanding scenario. The chemistry of metal ions, particularly in biological systems, gets strongly dictated by coordination chemistry, a subdivision of inorganic chemistry. It primarily deals with the synthesis, structure, and reactivity of coordination complexes which generally get formed by the attachment of one or more ligands surrounding a central metal atom or ion by covalent coordinate bonds. Ligands have different numbers of atoms to coordinate with the central metal atom to satisfy the coordination sphere, known as the donor sites of the ligand. Depending on the number of donor sites, the ligand shows variable denticity. The properties of the coordination complexes depend upon the engaged and available sites for attachment of the incoming ligands [1, 2]. This phenomenon helped nature to design many enzymes/ bio-active molecules for specific targeted activities. From this clue, in the past few decades, researchers have developed various complexes based on metal-ligand interaction, which mimic the activities of enzymes [3, 4]. It is now well known that for better catalytic activity, metal-based catalysts must have a vacant site(s) to interact with the incoming substrate(s). Therefore, designing and synthesis of appropriate metal complexes remain at the heart of biomimetic metalloenzyme chemistry. Throughout this process, it has been evident that ligands have the potential to shape the future metal-based biomimetic chemistry and their applications [5]. Among numerous classes and sub-classes of ligands, it has been observed that N, O-donor ligands play a vital role in forming stable and active coordination compounds [6, 7]. Transition metal complexes made by Mannich bases and Schiff bases ligands have been extensively explored due to their capability to stabilize metal ions with their attractive physical and

chemical properties for extensive range of applications in various research zones. Most of the cases this kind of ligands provide a N, O- donor system which can play a dynamic role to make the metaloenzymes mimic model [8, 9]. This type of complexes act as a homogeneous catalyst and comes with some serious disadvantages like reusability and separation of such complexes from reaction medium are often very laborious, whereas easy to separate from the reaction mixture and reusability of heterogeneous system encourage scientists to move towards them, which may lucractive on the homogeneous N, O- donor ligand based complexes. Therefore, the utilization of such ligand-based metal complexes in homogeneous and heterogeneous conditions has been extensively studied and explored. As the solid support for these metal complexes, the importance of zeolites has been widely established, [10-13] and widespread use of such heterogeneous systems with transition-metal coordination and organometallic complexes is reported [14, 15]. Notably, the separation techniques for zeolite encapsulated transition metal complexes are relatively easy, [16] can accommodate metal ions in various oxidation states, and most importantly, they are found to be environmentally benign systems for various organic transformations [17, 18]. It’s challenging to cover the whole discussion about the Mannich base and Schiff base metal complexes in a single chapter that grasps wide and differentiated subjects, containing immense territories of coordination chemistry and different parts of bioinorganic, chemical, and material science. Therefore, this chapter is limited to a brief discussion on N, O-donor based flexible Mannich base, and Schiff base ligands, their complexes, and their interaction with zeolite to form a host-guest heterogeneous system and their general applications in the field of enzyme and heterogeneous catalysis.

1.2 N, O-donor ligands

N, O-donor ligands broadly can be classified into two major categories: (a) Mannich base, (b) Schiff base ligands. The brief introduction about these ligand systems are given below:

1.2.1 Mannich base ligand. It's a type of aminomethylated product that's made by combining a primary or secondary amine with a nonenolizable aldehyde, phenol, or an enolizable ketone [19]. In 1912 Carl Mannich discovered the mechanism of this synthesis, the name of this reaction was honored to him for that discovery (scheme 1.1) [20, 21].

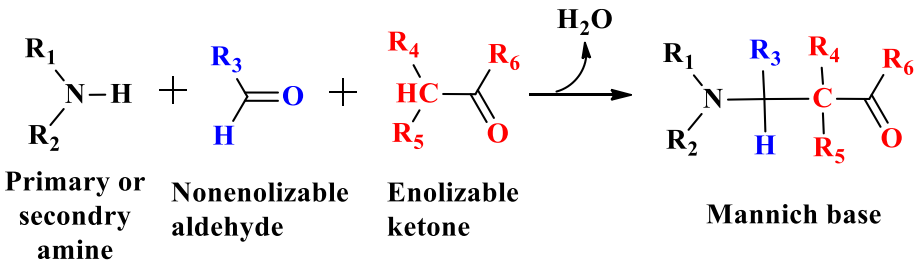

Scheme 1.1. *Synthesis of Mannich base ligands.*

The Mannich reaction has been utilized to make alkylamines, peptides, nucleotides, alkaloids, agrochemicals, antibiotics, crosslinking polymers, pharmaceutical drugs, α, β-unsaturated ketones and cleaning applications (soap and detergents), among other biologically significant molecules (scheme 1.2) [22].

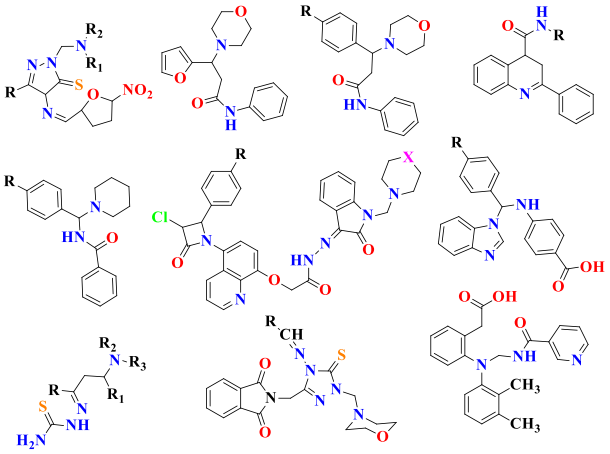

Scheme 1.2. *Some example of Mannich base ligands (R stands for alkyl or aryl groups).*

1.2.2 Schiff base ligand. Hugo Schiff, in 1864 discovered an azomethine (>C=N-) functional group containing compounds known as Schiff bases (scheme 1.3) [23, 24]. The azomethine groups have lone pairs of electrons which can donate to the metal ions for binding during complexation. The Schiff base shows some special character *viz* synthetic flexibility, sensitivity, and selectivity towards the central metal ion attributable to their structural resemblances with natural biological molecules, which makes them an important class of ligands [25].

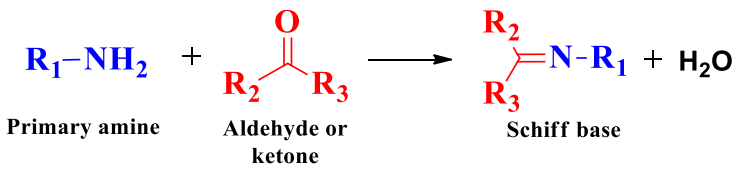

Scheme 1.3. *Typical synthesis of Schiff bases.*

Important features of Schiff bases. (a) By coordinating through the azomethine (>C=N-) group along with one or more than one donor atoms, it can behave as poly-dentate chelating ligands or macrocycles. (b) As a lone pair of electrons is available in the sp^2 hybridized orbital of the N-atom, the azomethine group has a lot of biological and chemical relevance [26]. (c) It can govern the formations of transition metal complexes through various types of interactions and a wide range of beneficial catalytic reactions by balancing the oxidation state of the central metal atom [27]. Examples of few Schiff base compounds are shown in scheme 1.4.

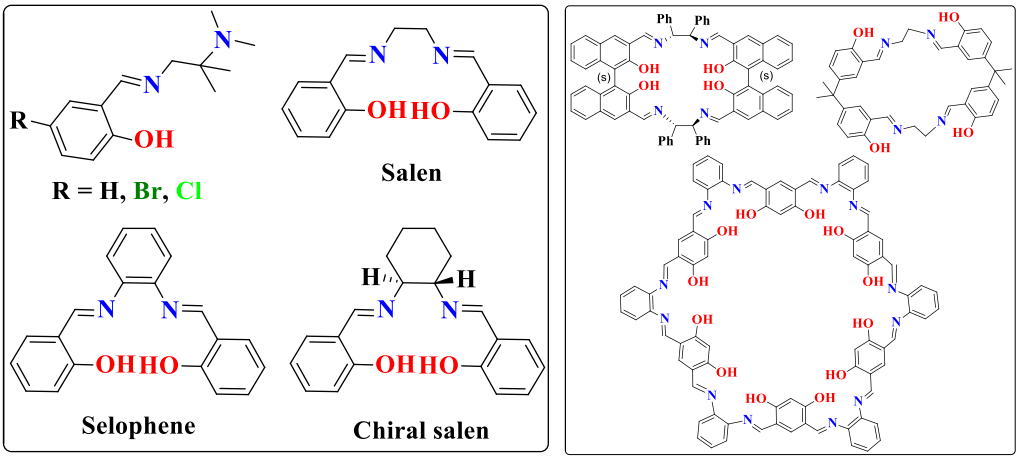

Scheme 1.4. *Some example of achiral, chiral and macrocyclic Schiff bases.*

The flexibility of the ligand is one of the important factors in tuning various architectures of the metal-ligand framework. The ligand flexibility is mainly defined on the basis of phenomena described below-

- Flexibility in denticity – Some ligand system possess different types of denticity depending upon the external factor *i.e.*, pH, solvent effect, temperature etc.
- Flexibility in charge – Depending on the external effects mentioned above, a few ligands can acquire different charges on them and this

adaptable phenomenon enables the entire moiety to diversely coordinate with charged metal ions.

- Flexibility in geometry – The preferable geometry of the ligand can change the coordination behaviour, gaining flexibility towards different kinds of structures.

In this regards piperazine derived ligand got an attention in recent scenario (figure 1.1) [28]. The conformation of the piperazine ring plays a crucial role in determining the structure of the metal complexes [29]. According to previous report, the size of the metal ion and the presence of certain co-ligands have an impact on the conformation adopted by the piperazine ring [30-32].

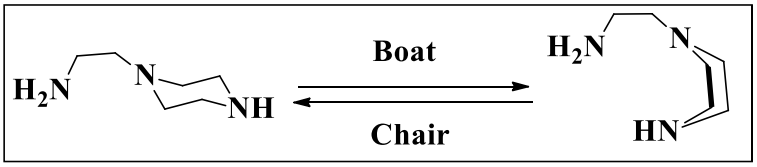

Figure 1. 1. *Chair-boat conformations of amino ethyl piperazine moiety.*

1.3 Synthesis of transition metal complexes by N, O-donor ligands

Because of the diversity of the complex produced, the reaction of N, O-donor ligands with transition metal salts remains an interesting topic over the years. The synthetic procedures of the corresponding metal complexes by using N, O-donor ligands are described below in brief.

1.3.1 Formation of Mannich base complexes

The Mannich reaction is an immensely advantageous synthetic transformation due to the formation of both 'C-C' and 'C-N' bonds during this aminomethylation technique, as shown in the accompanying scheme 1.5 [33].

Herein, an examples of phenol based Mannich base complex of mixed metal Ln(III) and Co(II) shows catalytic oxidase activity [34]. Furthermore, Cu(II) Mannich base complexes can also show oxidase activity (scheme 1.6) [35-37].

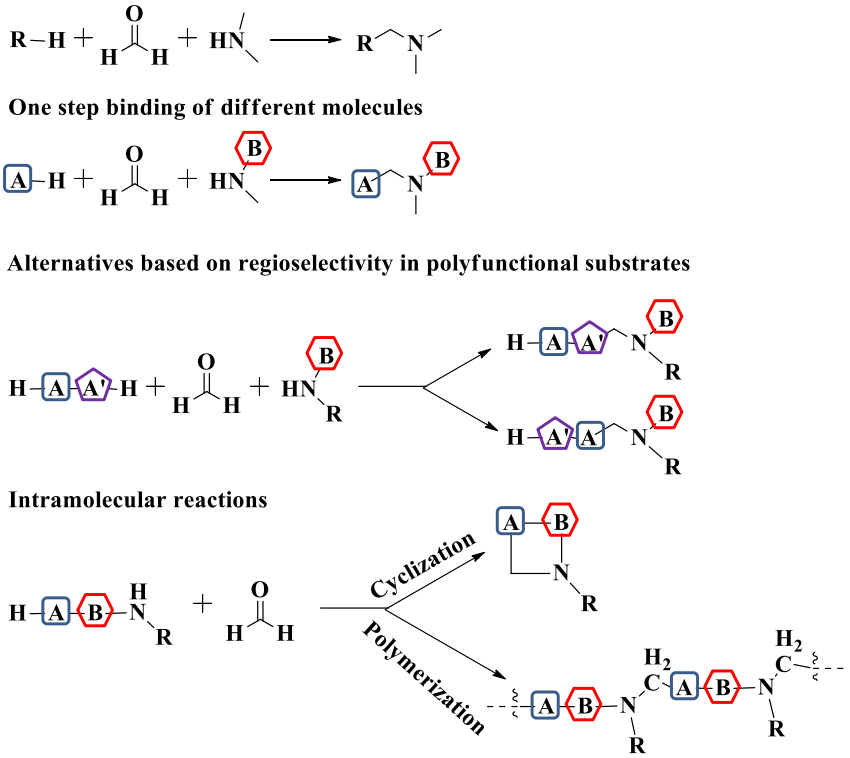

Scheme 1.5. *General scheme for the preparation of denticity variated Mannich bases*

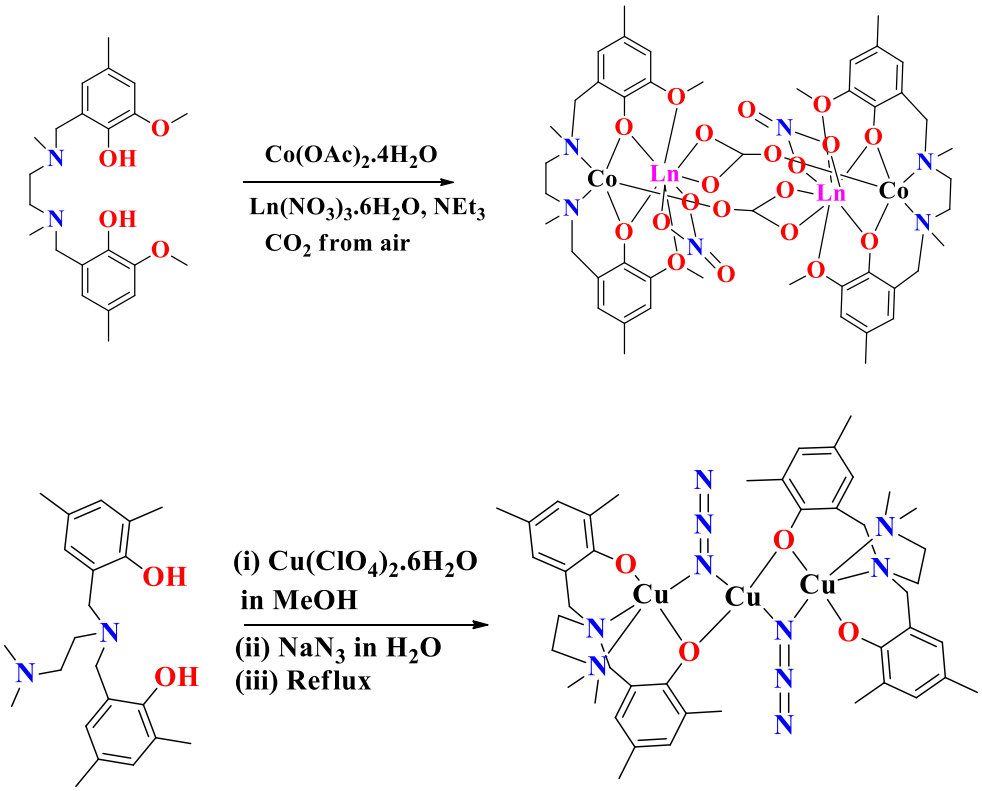

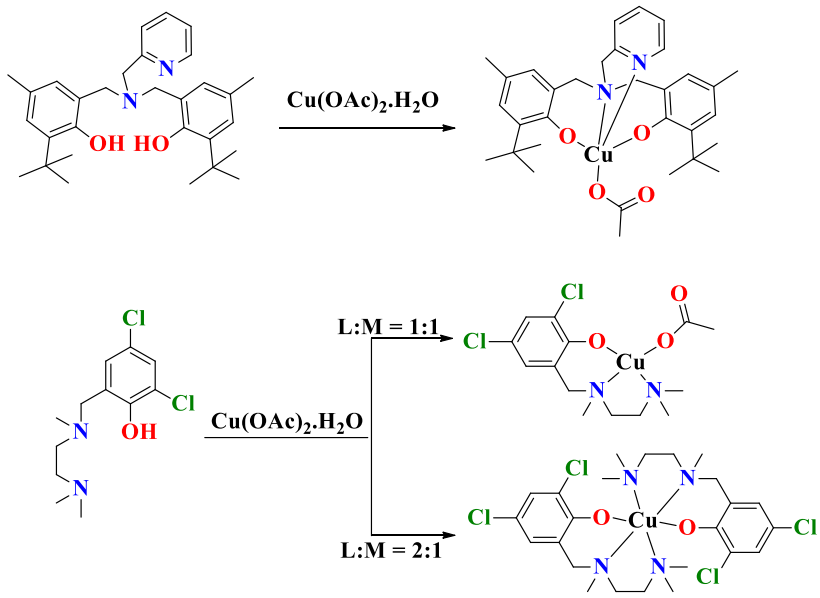

Scheme 1.6. *Synthetic route of some catalytically active Mannich base complexes.*

Therefore, Mannich base ligand has been elected for a part of this thesis due to its great impact in mimicking the meteloenzymes to explore the field of catalysis.

1.3.2 Formation of Schiff base complexes

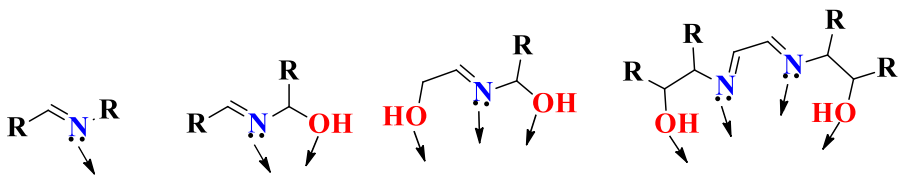

Scheme 1.7. *Denticity variated Schiff base ligands.*

According to the number of donor sites, Schiff base ligands are categorized as uni- or multi-dentate. When ligand is coordinate with central metal ion through two or more donor sites, complex is formed as a closed ring. This type of bonding is termed as “Chelate”. Morgan and Drew were the first to use the term "Chelate" to describe a type of chelation in 1920 [24]. Schiff base ligands contains hetero atoms primarily as a donor sites *viz* N, O, and sometimes S, but they shows the mixed donor capabilities as per the scheme 1.7 [38].

The basic nature of the Schiff base ligands assumes a crucial role in the development and stabilization of the transition metal complexes [39]. The different electronic properties of the N and O donor atoms of Schiff bases are ideal for the making of stable complexes. Generally, oxygen act as a hard donor

and prefer hard metal ions for binding which have higher oxidation states, whereas nitrogen act as a borderline donor, it can bind with those metal ions which have lower oxidation states [40]. In this regard, P.G. Cozzi presented five unique synthetic methods for the synthesis of Schiff base metal complexes, as shown in scheme 1.8 [27].

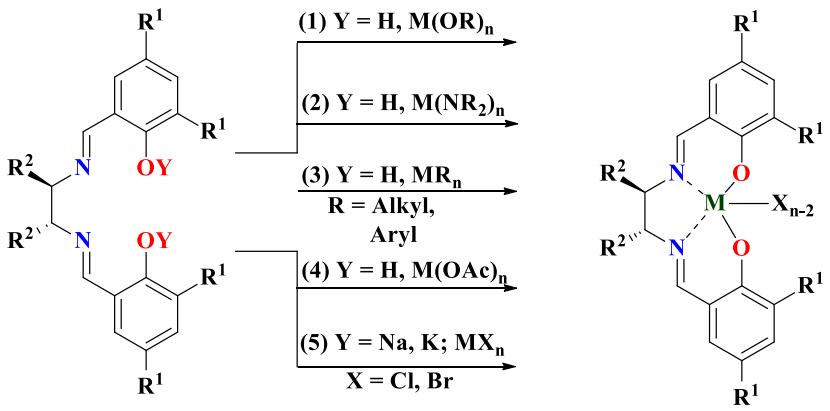

Scheme 1.8. *Synthetic routes of metal Schiff base complexes.*

In the next sections, five different routes of synthesis of Schiff base transition metal complexes are discussed:

• The synthetic ***Route 1*** involves the usage of metal alkoxides [M(OR)n]. Early transition metal alkoxides (M = Ti, Zr) are commercially available and easy to handle, however other alkoxide derivatives, particularly moisture sensitive lanthanide derivatives, are challenging to employ.

• Metal amides [$M(NMe_2)_4$] (M = Ti, Zr) are also utilised as precursors in the synthesis of Schiff base metal complexes of early transition metals, as shown in ***Route 2***. The reaction is initiated by the production of volatile $NHMe_2$ from the acidic phenolic proton of the Schiff bases.

• One of the primary routes for the synthesis of Schiff base metal complexes is ***Route 3***, which explains the clean and effective technique of employing metal alkyl complexes as precursors. Commercially accessible metal alkyls from the main group of metals ($AlMe_3$, $GaMe_3$, $InMe_3$) can be employed in the manufacture of Schiff base complexes via a direct exchange reaction.

• Many Schiff base metal complexes can be synthesized by treating the Schiff base with the corresponding metal acetate, usually by heating the Schiff base in the presence of the metal salt under reflux conditions, as shown in ***Route 4***. The

corresponding acetate [$M(OAc)_2$] (M = Ni, Cu, Co) is used to make copper, cobalt, and nickel Schiff bases.

• ***Route 5*** represents the making of salen type metal complexes, which is a two-step reaction involving deprotonation of Schiff bases followed by reactivity with metal halides.

1.4 Applications of N, O-donor ligands based complexes

N, O-donor ligands' versatility, as well as their potential biological, analytical, and industrial uses, make them promising candidates for further research. Transition metal complexes also have a wide range of applications in technology, industry, and medicine. This thesis focuses on a few specific topics within the broad areas of relevant applications for N, O-donor ligands and their complexes. Those domains, as well as some related applications, are categorized in the flow chart (figure 1.2), which is followed by a detail description.

Properties of transition metal complexes synthesized by N, O-donor based ligands and their applications		
Biological	**Chemical**	**Material**
➢ Enzyme Catalysis • Galactose oxidase activity • Laccase activity	➢ Coupling reaction • C-N coupling ➢ Degradation reaction • Polymer degradation	➢ Gas adsorption ➢ Solar cell application ➢ Organic transformation reaction

1.4.1 Biological applications

The interest in Mannich base and Schiff base complexes has developed as bioinorganic chemistry has advanced, owing to their diverse interactions with other molecules. Despite the fact that the transition metal Mannich base and Schiff base complexes have been associated to a diverse area of biological significances, only a few topics pertinent to the thesis study have been covered.

1.4.1.1 Enzymatic catalysis

It is about the interaction of enzyme with substrate molecules to form an enzyme–products complex, which leads to the synthesis of the products [41, 42]. In 1890, Emil Fischer proposed a mechanism to describe the interaction between substrate molecules and the active sites of an enzyme [43]. The active site of the enzyme considered to a fixed geometry (the lock), which matched the structure of a certain substrate (the key) followed by the release of product from the active site which is no longer fits into it (figure 1.2).

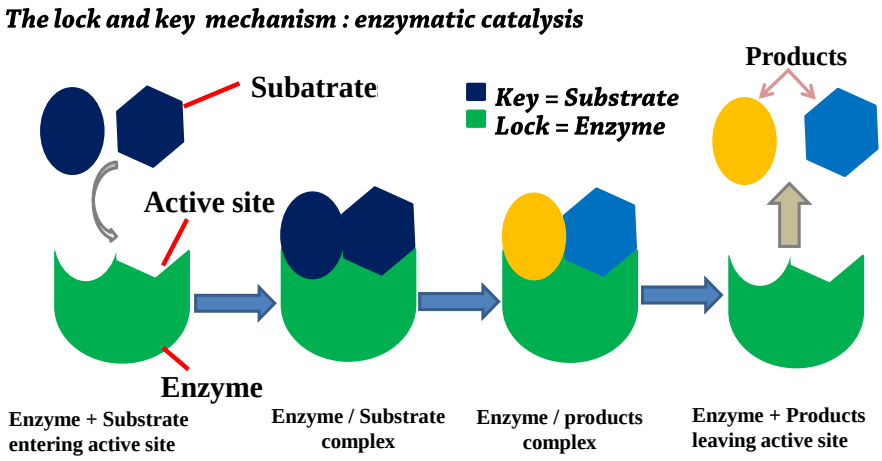

Figure 1.2. *General representation of the product formation during enzymatic catalysis.*

One of the primary purposes of the synthesis of transition metal complexes with biological relevance is to synthesize compounds with significant catalytic activity, which work analogous to the function of natural enzymes. Ideally an enzyme mimic should have a similar coordination environment to the main metalloenzyme, and it should be able to follow the native enzymes' mechanistic pathways. Although there are plenty of the metalloenzymes are identified and to be explored, but this thesis is mainly focused on two enzymes *viz* galactose oxidase (GOase), and laccase.

1.4.1.1.1 Galactose oxidase

Many metalloenzymes are found in nature and are used to catalyze the controlled and selective oxidation of organic molecules. Galactose oxidase (GOase) is one of the most important enzymes among them. GOase is a fungal metalloenzyme-

based radical copper oxidase that catalyzes the conversion of primary alcohols to aldehydes and the reduction of O_2 to H_2O_2 or H_2O.[44, 45]

$$R^{\prime}CH_2OH + O_2 \xrightarrow[\text{Enzyme}]{\text{GOase}} R^{\prime}CHO + H_2O_2$$

The wide-ranging trait of substrate allows the enzyme to metabolize an extensive range of alcohols (ca. benzyl alcohol) in the environment to selectively produce biologically important products.

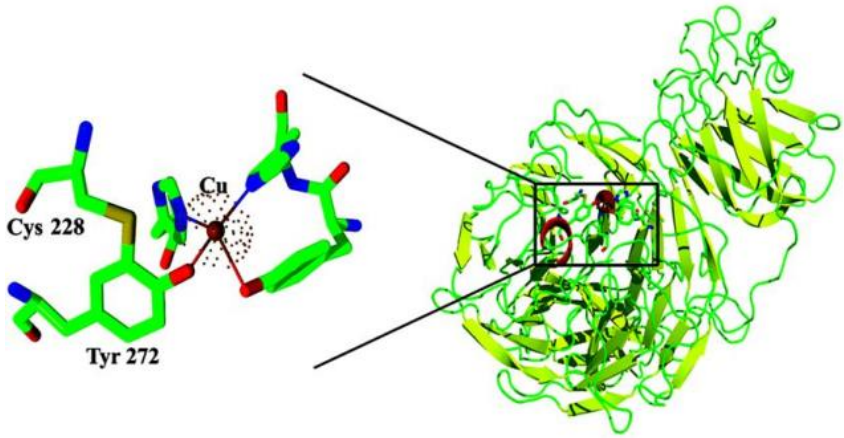

Figure 1.3. *Active sites of the mononuclear copper(II) centre of GOase (PDB ID: 1GOG)[46].*

The GOase's catalytic process has drawn scientist's attention to its unusual structural sites, which have been determined by the spectroscopic and crystallographic methods (figure 1.3). GOase contains a novel protein free radical in its active form that coordinates to a Cu(II) metal centre forming a radical-copper complex whose special reactivity serves for rapidly expanding field of free radical enzymology as metalloradical catalysis [46, 47].

A tyrosyl side chain of GOase stabilizes the free radical, which is covalently linked by cross linking to a cysteinyl residue to form a tyrosinecysteine dimer in the protein. This radical formation equilibrium follows a mechanism *viz* ping-pong turnover reaction (scheme 1.9) [48].

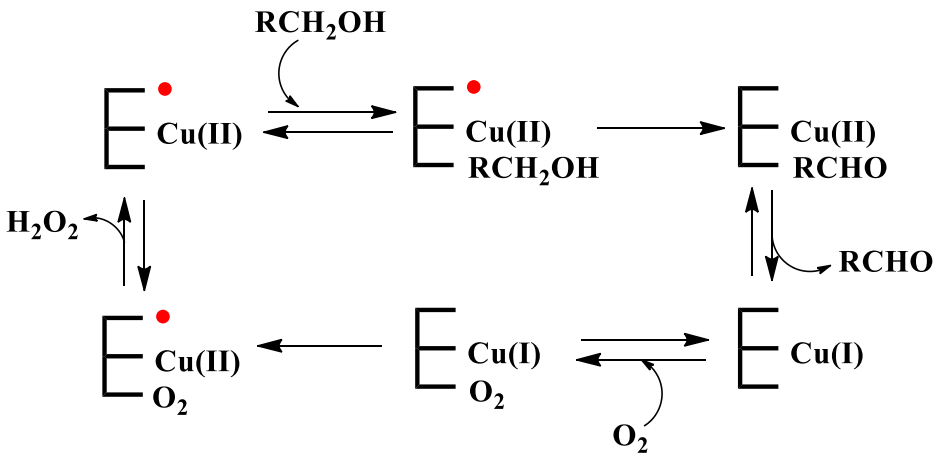

Scheme 1.9. *Representation of ping-pong turn over mechanism.[48]*

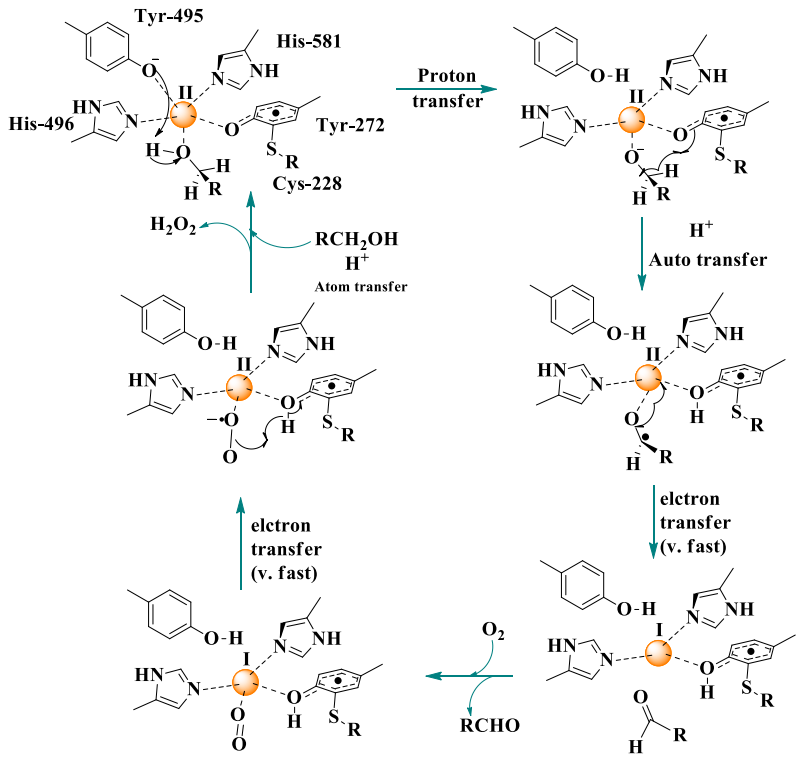

Scheme 1.10. *A postulated mechanism for galactose oxidase [48].*

Scheme 1.10 represents a mechanistic pathway of GOase catalysis [48]. Some Cu(II) complexes have already been prepared to mimic the GOase activity using phenolic oxygen atom as donor center [49]. Furthermore, it has been assumed that tyrosine (Tyr495), which is coordinated axially plays a crucial role in controlling the redox potential of Cu-centre and act as a base for abstracting a proton from the alcoholic substrate, thus enhancing the electron donating ability of the substrate [50].

The galactose oxidase mimicking field is largely unexplored till now. There are very few reports available till now in which the copper complexes shows the activity like galactose oxidase. Alex John *et al*. [36], Chandan Mukherjee *et al*. [51], and Bidyut Kumar Kundu, *et al*. [37], reported some mononuclear and Striegler *et al*. [53], and Alamsetti *et al*. [54] reported some binuclear copper complexes with the galactose oxidase like activities (figure 1.4). Numerous primary alcohols have been used as substrate to check this enzymatic activity. However, all of them reported the catalytic activities in traditional method of heating condition. However, the visible light driven GOase activity as alternative environmentally friendly procedure is not explored very much and required to be developed. Hence, this thesis presents the visible light driven GOase mimicking activity of some mono- and bi-nuclear Mannich base copper complexes.

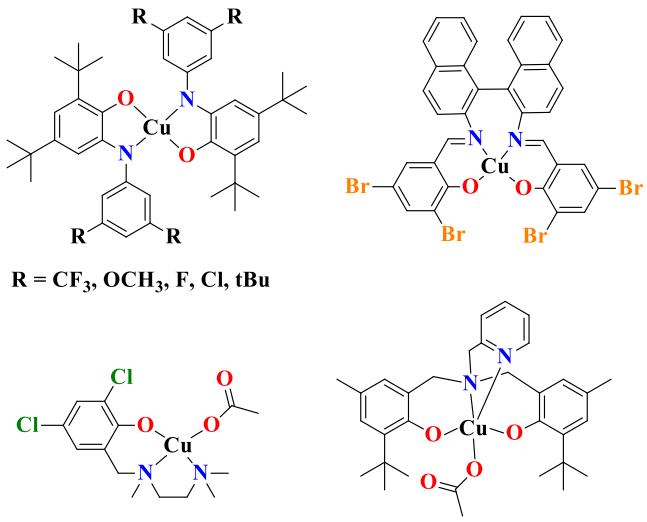

Figure 1.4. *Galactose oxidase mimicking complexes [36, 37, 51].*

1.4.1.1.2 Laccase

Laccase is multi-copper oxidase enzyme which contains type I, type II and type III Cu(II) system in its active site. In 2003, Enguita *et al.* elaborated the crystal structure of laccase enzyme (figure 1.5) [55].

In general, laccase starts reaction by reducing oxygen molecule into H_2O by the tri-copper center composed by type II and III copper followed by the electron abstraction from substrate through the type I copper center (scheme 1.11) [56]. In some cases due to complex structure of the enzyme the substrate can't directly approach, and for this mediator can bind with the enzyme and facilitates the oxidation reactions (figure 1.6) [57].

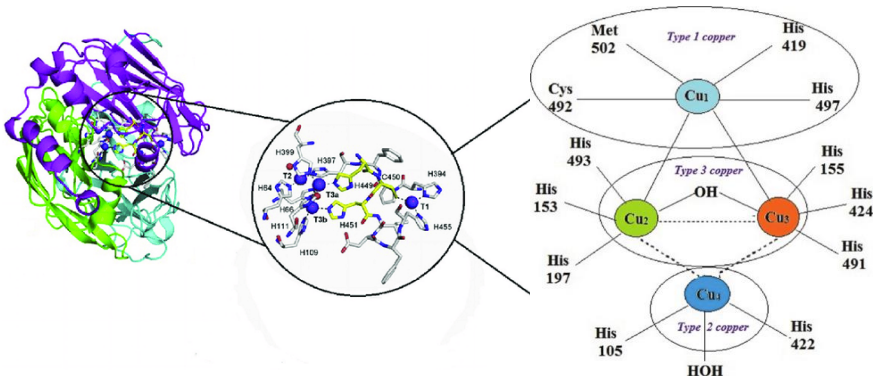

Figure 1.5. *Active sites of laccase enzyme [55].*

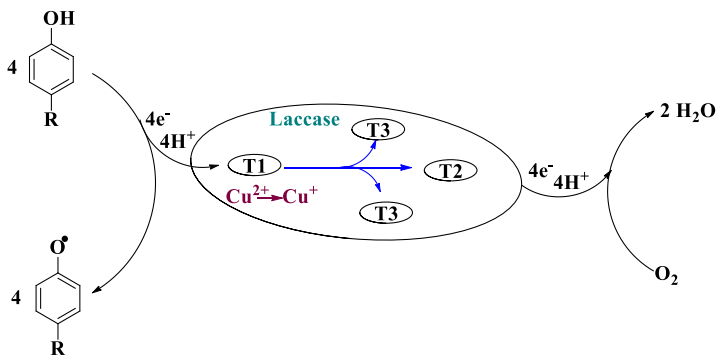

Scheme 1.11. *Mechanistic pathways of laccase enzyme*

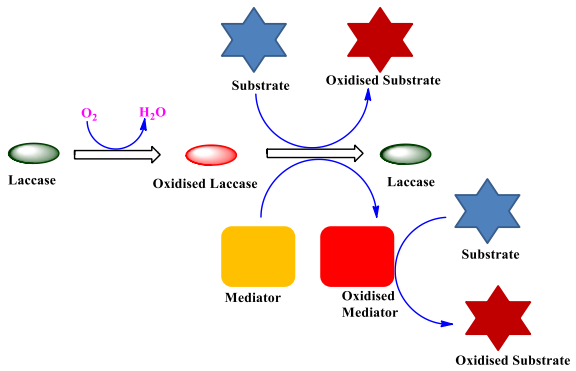

Figure 1.6. *General representation of the product formation during catalysis by Laccase enzyme.*

Laccases are found in the plants, bacteria and fungi. Laccase enzymes catalyze some polymerization, de-polymerization, oxidation and reduction reactions. The ligninification process in higher plants includes the cross-linking of phenolic precursors by laccases and is one of the polymerization reaction, which helps in growth of the plants (scheme 1.12) [58, 59]. Laccases found in fungus like Pleurotus ostreatus, used to degrade complex natural polymers, such as lignin or humic acids (figure 1.7) [60].

There are very few reports available till now in which the multicopper complexes shows the activity like laccase. C. M. Edmund *et al*. [61], and Zhen Yu *et al*. [62] reported some multi- copper complexes with the laccase like activities (figure 1.8).

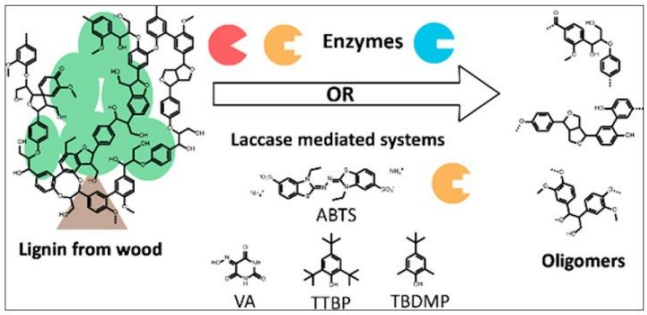

Figure 1.7. *Laccase mimicking complexes [61, 62].*

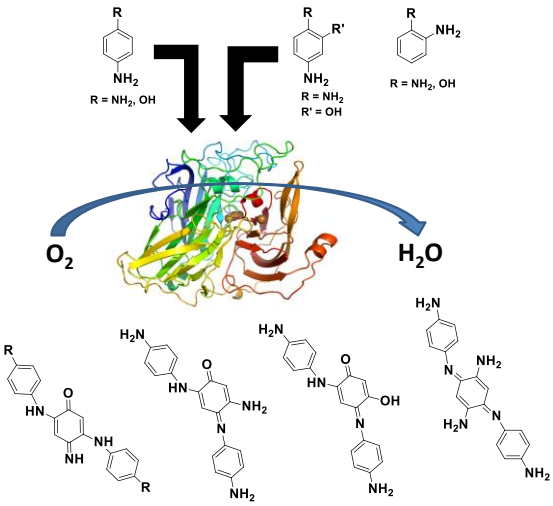

Scheme 1.12. *Laccase catalyzed coupling reactions.*

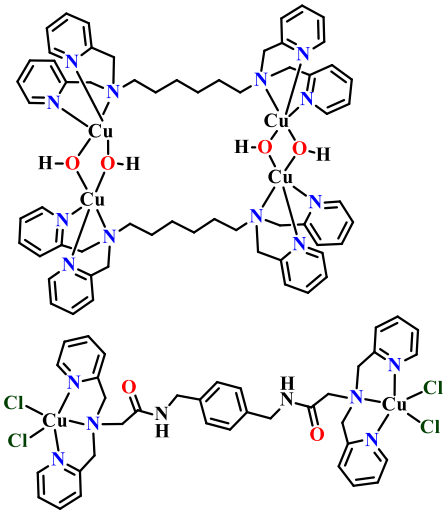

Figure 1.8. *Depolymerization of lignin by laccase mediated system [63].*

Because of its wide range of substrates and numerous functions, laccase has recently been a research hotspot. The laccase-catalyzed reaction only produced water as reduction product, making it an environmental friendly process.

1.4.2 Chemical applications

Transition metal complexes composed by N, O-donor ligand systems have shown catalytic properties towards various chemical reactions.

1.4.2.1 Coupling Reactions

In the coupling reaction, two chemical species joins together to form a new chemical species. There are two types of coupling reactions are known, homo-coupling and hetero-coupling (cross coupling) reactions (figure 1.9). The coupling reactions generally take place in the presence of metal as catalyst.

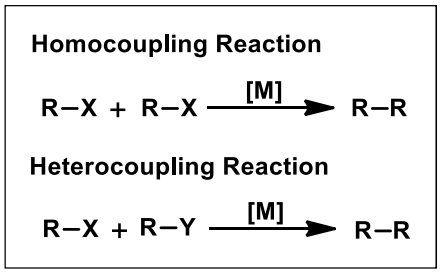

Figure 1.9. *General representation of homo- and hetero-coupling reaction.*

Charles Adolphe Wurtz in 1855 reported the first sodium catalyzed homo-coupling reaction. Transition metal complexes can catalyze various types of homo- and hetero-coupling reactions using various strategies. This thesis mainly focuses on C-N coupling by borrowing hydrogen strategy. Borrowing hydrogen reaction is an atom economy reaction, which gets completed in three steps (scheme 1.13). In the first step of this reaction, dehydrogenation takes place in the presence of metal catalyst, after that the dehydrogenated product gets coupled with second substrate and forms unsaturated compound which further gets reduced in last step by metal hydrides generated during the dehydrogenation step [64].

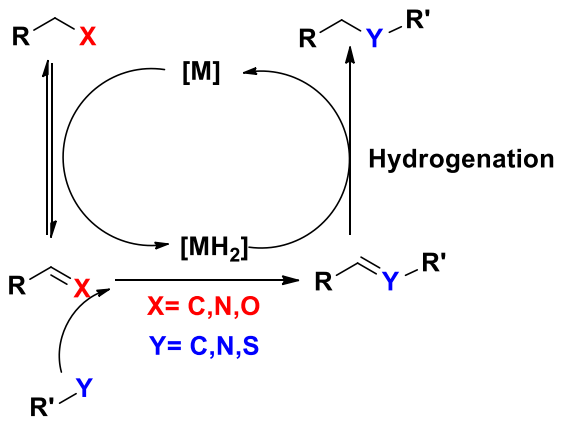

Scheme 1.13. *Basic Scheme of the BH Methodology.*

In 1981, Grigg *et al.* first reported the formation of N-alkylated amine upon reaction of amine with primary alcohols using rhodium, iridium and ruthenium complexes as catalysts through borrowing hydrogen strategy [65]. After that, in last few decades researchers introduced Cu, Os, Pd, Co, Mn and Ni complexes [66-71]. Among these metals copper is relatively cheaper and abundant in earth.

1.4.2.2 Degradation Reaction

In this reaction, large molecule breaks into two or more smaller molecules. In this thesis degradation of has been explored.

1.4.2.2.1 Polymer Degradation (Depolymerization)

Mainly three types of polymers are available in our environment (1) natural (2) semi-synthetic and (3) synthetic polymers. Among these, natural polymers are reach source of energies and fuels. Cellulose, proteins, wool, silk, hemicellulose, DNA, silk and lignin are the natural polymers, and out of these lignin is a polymer of phenolic precursors [72]. In lignin p-coumaryl alcohol, coniferyl alcohol, and sinapyl alcohol are linked by various C-C, C=C, and C-O bonds via β-1, β-O-4, 4-O-5, β-β, 5-5′, α-1 and other linkages [73]. It can act as a reach source of the valuable chemicals and fuels which might be isolated by the degradation of lignin through the cleavage of C-C, C=C or C-O bonds (figure 1.10) [74]. Lignin's are found in the cell walls of the hard wood and soft wood.

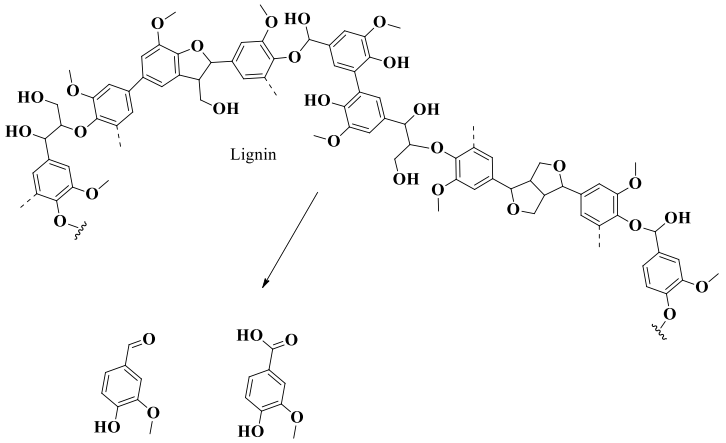

Figure 1.10. *General representation of depolymerization of lignin.*

As a result of the exhaustion of fossil fuels as a source of energy, fuels and chemicals, it is reasonable to anticipate that in the near future, a greater proportion of energy and chemicals will be produced from renewable resources, such as biomass. To achieve this goal we need to develope technologies for depolymerization of the lignin. In this regards, researchers have developed some methods like pyrolysis, [75-78] acid or alkali hydrolysis, [79-81] reduction [82-85] and oxidation [86-89]. Among these, oxidative cleavage has attractive advantages on chemical point of view. The lignin contains high percentage of C-C bonds this can be cleave by oxidation, that is why the oxidative depolymerization of the lignin is grown up in last few years. In last decade researchers have reported certain systems which can catalyze the oxidative lignin degradation reactions. Toste's and Hanson's group reported vanadium-based catalysts [90-92], Bozell and co-workers reported Co-Schiff base catalysts for the oxidative cleavage of C-O and C-C bonds of the lignin models to the corresponding benzoquinones [93]. Later on, Corma and co-workers introduced copper with vanadium catalyst for the oxidative cleavage of lignin [94]. After that, some heterogeneous systems also reported such as, Pd/CeO_2, Co_3O_4, [95, 96] Mn−Co(mixed oxide) [97], and Co-ZIF-9 [98]. Recent reports showed that the copper-based catalytic systems, such as $Cu(OAc)_2$/1,10-phenanthroline/ methanol [99], CuCl/TEMPO/2,6-lutidine/toluene [100], $CuBr_2$/N-methyl TBD/ DMSO [101], $Cu(OAc)_2/BF_3{\cdot}OEt_2$/methanol [102], $CuCl_2$/N-iodosuccinimide/ DMSO [103], etc., are efficient as catalysts to depolymerizes the lignin. However, in all these cases they have used the toxic solvents, high temperatures and pressure to depolymerizes the authentic lignins. However, in this thesis photocatalytic oxidative degradation of lignin model compounds as well as

authentic lignins degradation by cleavage of C-C and C=C bonds have been reported by photocatalytic route.

1.4.3 Applications in material science

Schiff base transition metal complexes exhibited a variety of materialistic properties, including gas absorption, organic transformation reaction, oxidation catalysis, photo-physical properties and so on. These properties are found to be particularly beneficial for a variety of industrial uses [104].

Why is heterogenization of transition metal complexes so important for oxidation catalysis?

The homogeneous nature of Schiff base metal complexes restricted them a certain limit, although these are possess various oxidation state and exhibits good catalytic activity for various types of reactions. However there are certain disadvantages like they fail in terms of reusability after some reactions, have a lower thermal stability, and their separation from reaction mixture is a challenging task for the researchers.

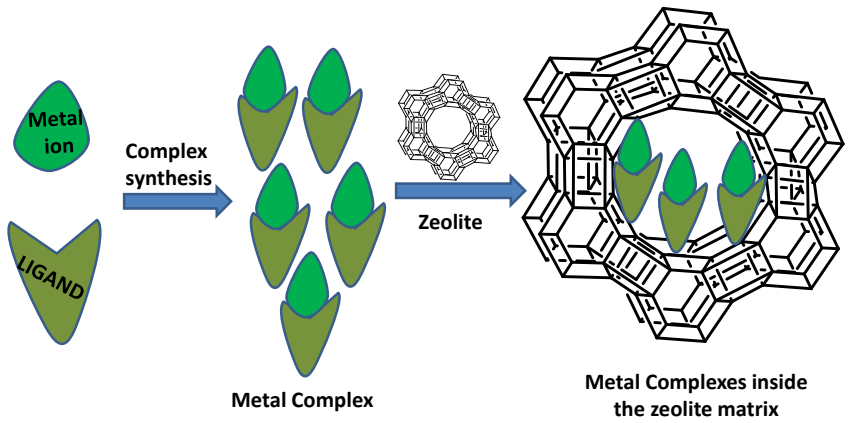

Scheme 1.14. *Illustration of zeolite encapsulated host-guest complex formation.*

Therefore, lots of attention has been given to develop catalysts, which are long lasting and easily recoverable with 100% efficiency. In these conditions, the heterogeneous material, which are synthesized by loading/encapsulation of the metal complexes on the various supports, provides an alternative routes for achieving some of these objectives, like reducing the waste, increasing efficiency, reusability and selectivity towards important catalytic process (scheme 1.14) [105].

1.4.3.1 Importance of zeolite encapsulated complexes in catalysis

Special Notes on Zeolite!

About Zeolite

Zeolites are 3D crystalline aluminosilicates of natural or synthetic origin with highly ordered structures, which consists SiO_4^{4-} or Al_4^{5-} tetrahedral. In the centre of the tetrahedra are atoms with relatively low electronegativities (Si^{IV}, Al^{III}, P^{V}, Zn^{II}, etc.) and in the corners are oxygen anions (O^{2-}). These combinations can be depicted as $[SiO_4]$, $[AlO_4]$, $[PO_4]$, *etc.* and are commonly designate as TO_4 unit where T stands for any tetrahedral species. The tetrahedra in zeolite materials are somewhat rigid. In general, the O-T-O angle is close to the "ideal" value of 109°28′ for a geometrically perfect tetrahedron and deviations of more than a few degrees are not frequent.

Structural Features

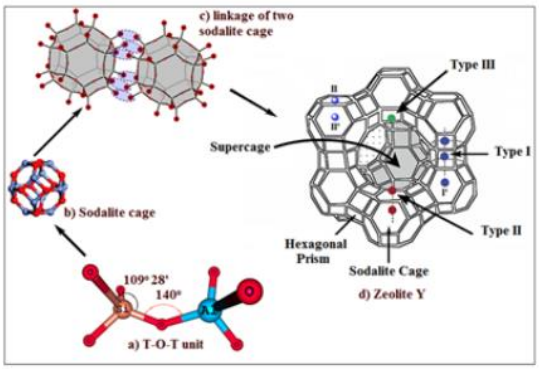

a) T-O-T unit b) sodalite cage c) linkage between two sodalite cages d) structure of zeolite-Y showing the cation sites (I, II, III, I′, II′).

The encapsulation of homogeneous catalysts in the voids of the zeolite is a reliable approach for heterogenizing it. Encapsulating transition metals and organometallic complexes within the pores of the microspores zeolite has drawn attention in last decade, because, it offers a simple method of coupling the reactivity of the metal complexes with the stereochemistry and stoutness of the host zeolite [106, 107]. The magnetic, electronic and redox behaviours of the loaded complexes are altered due to steric constrain of the wall of the zeolite matrix. Increments of chemical properties were observed in comparison of homogeneous counterparts. The heterogeneous compounds provide a straightforward extraction procedure for reusability, making them significant for commercial usage. Encapsulation based catalyst development has advanced quickly in recent years due to their applications in wide range of organic transformation. Nowadays, researchers use these hybrid materials to mimic the biosystems in addition to their use in catalytic reactions. Encapsulated metal complexes which can mimic the metalloenzyme, are termed as zeozymes [108, 109]. Figure 1.11 illustrates a zeozyme like activity.

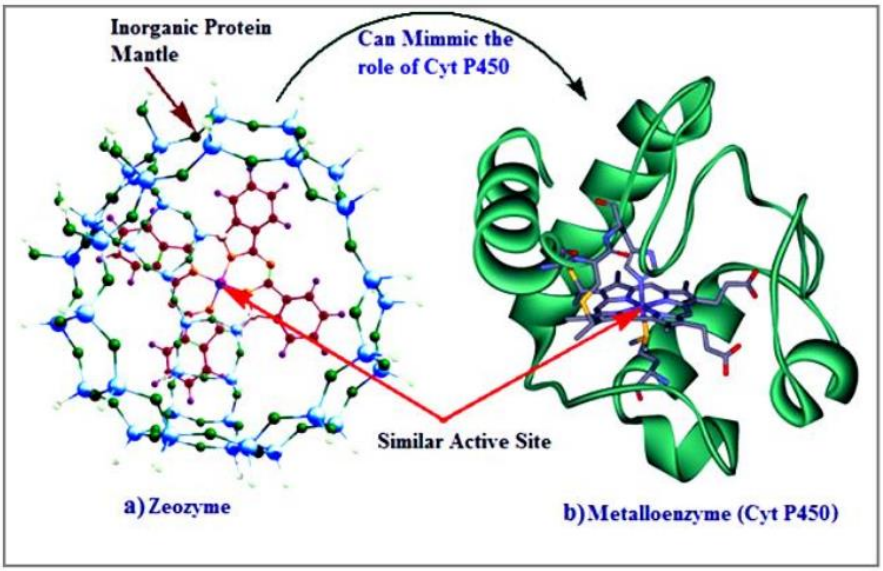

Figure 1.11. *a) Metal phthalocyanine complex inside zeolite-Y (Zeozyme) b) Cytochrome P450 enzymes.*

To develop new catalytic systems in the present scenario of host-guest transition metal complexes, researchers are focused on the following aspects:

- Physiochemical and spectroscopic characterization of hybrid materials
- Catalytic application of encapsulated transition metal complexes
- Calculations based on density functional theory of zeolite supported complexes
- Biologically active molecule heterogenization to mimic the biosystems

1.4.3.1.1 Applications of zeolite encapsulated complexes

Zeolite encapsulated metal complexes have found extensive application as metalloenzyme mimic and as catalyst for a variety of organic reactions. Recently, they have also been utilized as molecular sensors and switches (figure 1.12) [110]. In addition, several recent studies have focused on the use of complexes encapsulated in zeolite-Y as zeozymes and some significant catalytic reactions that these hybrid complexes have mediated [111-113]. By adopting the notion of catalyst encapsulated in zeolite mediated organic reaction, this thesis is mainly focused on the application of Cu(II) Schiff base complexes in the field of oxidative photocatalysts for the degradation of the biopolymer into the valuable chemicals [114]. The central atom of the catalyst has been selected to be copper since it has strong redox properties that can increases the reaction rate of the catalytic reaction [115].

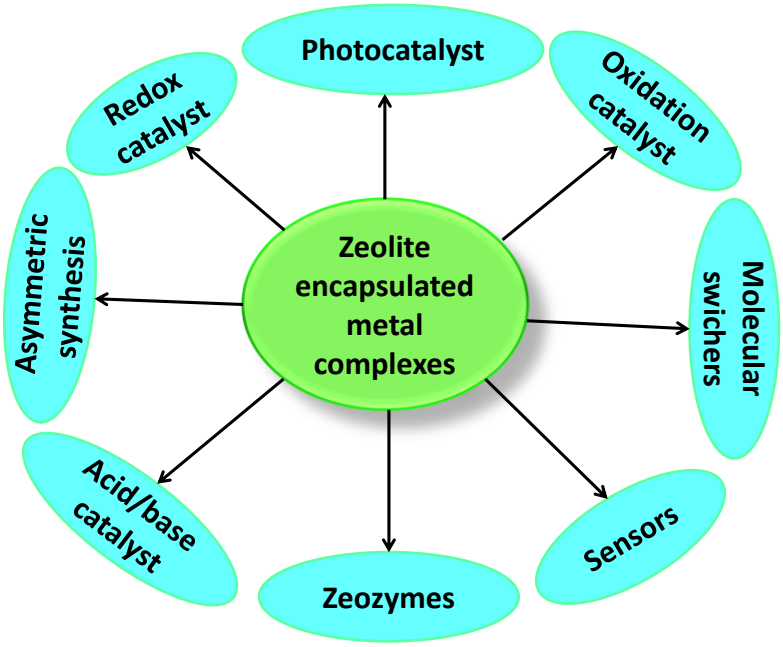

Figure 1.12. *Various application of zeolite encapsulated complexes.*

1.4.3.1.1 Zeolite encapsulated complexes as oxidation catalyst

Based on their chemical, structural and redox behavior, Bania *et.al* and Meier *et.al* are being used as base catalyst, acid catalyst and electro- or photo-catalyst [116, 117]. Since it would be impossible to explain all of the catalytic applications for such zeolite encapsulated metal complexes, the discussion in this thesis has been limited to photocatalytic oxidation processes. In recent time, complexes encapsulated in zeolite have been found to be catalytically active towards the oxidative degradation reactions [118]. According to reports, the encapsulated complexes also exhibit high yield, selectivity along with the reusability for several times [119].

1.5 Purpose and span of present investigation

The purpose of present work to explore the structure-activity relationship between various N, O- donor based ligands and their Cu(II) complexes to compare their biological, chemical as well as materialistic properties with the reported analogues.

In this regard the following Mannich base and Schiff base ligands were selected in this study.

a) 2,4-dichloro-6-((4-(2-hydroxyethyl)piperazin-1-yl)methyl)phenol (**H_2L^1**)
b) 2,4-dibromo-6-((4-(2-hydroxyethyl)piperazin-1-yl)methyl)phenol (**H_2L^2**)

c) 2-(((3-(dimethylamino)-2,2-dimethylpropyl)imino)(phenyl)methyl)phenol (**HL^3**)

d) 2-(((2-(methylamino)ethyl)imino)(phenyl)methyl)phenol (**HL^4**)

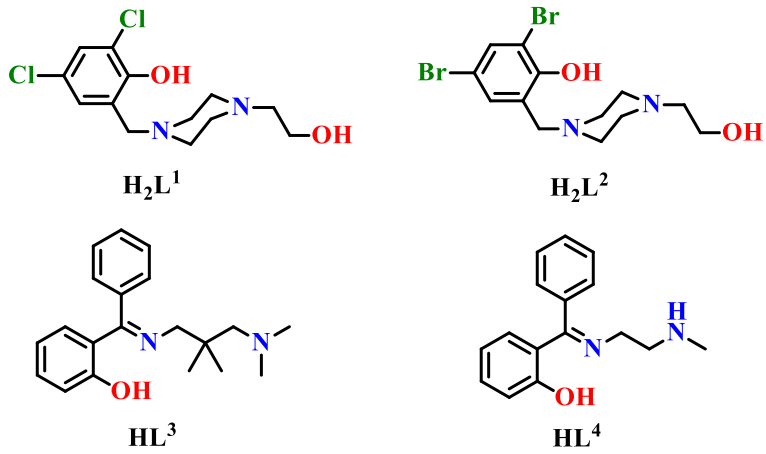

Figure 1.13. *Structure of Ligands.*

Using these ligands total **eleven** metal complexes of Cu^{2+} metal ion have been synthesized and characterized thoroughly using several analytical techniques along with single crystal XRD. All the complexes up to this have been studied in a broad application zone, as described in this chapter.

Hence, the chapter wise distribution of ligands and complexes are summarized below:

Chapter	Ligand(s)	Complex(s)
Chapter 2A	**HL^1**	[CuHL$^{1'}$] **(1)**, [CuHL$^{1''}$] **(2)**
Chapter 2B	**HL^1**	[CuHL$^{1'''}$]$_6$ **(3)**
Chapter 3	**HL^1 and HL^2**	[Cu(HL^1)(OAc)]$_2$ **(4)**, [Cu(HL^2)(NO$_3$)]$_2$ **(5)**
Chapter 4	**HL^3**	[Cu(L^3)Cl]$_2$ **(6)**, [Cu(L^3)(N$_3$)]$_2$**(7)**
Chapter 5	**HL^3 and H$_2$L^4**	[CuL^3(OAc)]$_2$ **(8),** [Cu(HL^4)(OAc)]$_2$ **(9),** [CuL^3(OAc)@Y] **(10),** [Cu(HL^4)(OAc)@Y] **(11)**

1.6 References

[1] Elsevier, C.J., Reedijk, J., Walton, P.H., Ward, M.D. (2003), Ligand design in coordination chemistry: approaches to new catalysts, new materials, and a more sustainable environment, Dalton Transactions, 1869-1880.(DOI: 10.1039 /B303975G)

[2] Peris, E., Crabtree, R.H. (2018), Key factors in pincer ligand design, Chemical Society Reviews**,** 47, 1959-1968.(DOI: 10.1039/C7CS00693D)

[3] Riccardi, L., Genna, V., De Vivo, M. (2018), Metal–ligand interactions in drug design, Nature Reviews Chemistry**,** 2, 100-112.(DOI: 10.1038/s41570-018-0018-6)

[4] Amgoune, A., Bourissou, D. (2011), σ-Acceptor, Z-type ligands for transition metals, Chemical Communications**,** 47, 859-871.(DOI: 10.1039/C0CC04109B)

[5] Levason, W., Monzittu, F.M., Reid, G. (2019), Coordination chemistry and applications of medium/high oxidation state metal and non-metal fluoride and oxide-fluoride complexes with neutral donor ligands, Coordination Chemistry Reviews, 391, 90-130.(DOI: 10.1016/j.ccr.2019.04.005)

[6] Argent, S.P., Adams, H., Riis-Johannessen, T., Jeffery, J.C., Harding, L.P., Mamula, O., Ward, M.D. (2006), Coordination Chemistry of Tetradentate NDonor Ligands Containing Two Pyrazolyl-Pyridine Units Separated by a 1,8-Naphthyl Spacer: Dodecanuclear and Tetranuclear Coordination Cages and Cyclic Helicates, Inorganic Chemistry, 45, 3905-3919.(DOI: 10.1021/ic060157d)

[7] Karia, P.S., Vekariya, P.A., Patidar, A.P., Patel, M.N. (2015), Copper(II) Complexes with N,O-Donor Ligands and Ofloxacin Drug as Antibacterial, DNA Interacting, Cytotoxic and SOD Mimic Agent, Indian journal of microbiology, 55, 302-312.(DOI: 10.1007/s12088-015-0525-9)

[8] Kaim, W. and Schwederski, B. (2010) Non-innocent ligands in bioinorganic chemistry, Coord. Chem. Rev., 254, 1580–1588.(DOI:10.1016/j.ccr.2010.01.009)

[9] Fedushkin, I. L., Maslova, O. V., Morozov, A. G., Dechert, S., Demeshko, S. and Meyer, F. (2012), Genuine Redox Isomerism in a Rare-Earth-Metal complex, Angew. Chem., Int. Ed., 2012, 51, 10584–10587.(DOI: 10.1002/anie.201204452)

[10] Yilmaz, B., Müller, U. (2009), Catalytic Applications of Zeolites in Chemical Industry, Topics in Catalysis, 52, 888-895.(DOI: 10.1007/s11244-009-9226-0)

[11] Liang, J., Liang, Z., Zou, R., Zhao, Y. (2017), Heterogeneous Catalysis in Zeolites, Mesoporous Silica, and Metal–Organic Frameworks, Advanced Materials, 29, 1701139.(DOI: 10.1002/adma.201701139)

[12] Li, Y., Li, L., Yu, J. (2017), Applications of Zeolites in Sustainable Chemistry, Chem, 3, 928-949.(DOI: 10.1016/j.chempr.2017.10.009)

[13] Naber, J.E., de Jong, K.P., Stork, W.H.J., Kuipers, H.P.C.E., Post, M.F.M. (1994), Industrial applications of zeolite catalysis, in: J. Weitkamp, H.G. Karge, H. Pfeifer, W. Hölderich (Eds.) Studies in Surface Science and Catalysis, Elsevier, 84, 2197-2219.(DOI: 10.1016/S0167-2991(08)63783-0)

[14] Choplin, A. (1994), Surface organometallic chemistry on zeolites: A tool for modifying the sorption properties of zeolites, Journal of Molecular Catalysis, 86, 501-512.(DOI: 10.1016/0304-5102(93)E0214-2)

[15] Corma, A., Iglesias, M., Del Pino, C., Sanchez, F. (1991), New rhodium complexes anchored on modified USY zeolites. A remarkable effect of the support on the enantioselectivity of catalytic hydrogenation of prochiral alkenes, Journal of the Chemical Society, Chemical Communications, 1253-1255.(DOI: 10.1039/C39910001253)

[16] Ramanjaneya Reddy, G., Balasubramanian, S., Chennakesavulu, K. (2014), Zeolite encapsulated Ni(ii) and Cu(ii) complexes with tetradentate N2O2 Schiff base ligand: catalytic activity towards oxidation of benzhydrol and degradation of rhodamine-B, Journal of Materials Chemistry A, 2, 15598-15610.(DOI: 10.1039/C4TA01869A)

[17] Kumar, B.S., Dhakshinamoorthy, A., Pitchumani, K. (2014), K10 montmorillonite clays as environmentally benign catalysts for organic reactions, Catalysis Science & Technology, 4, 2378-2396.(DOI: 10.1039/C4CY00112E)

[18] John, J.M. (2003), Zeolite encapsulated complexes of Fe, Co, Ni, Cu, and Pd: synthesis, characterization, and catalysis.

[19] Al-Nuzal, S.M.D., Al-Azzawi, H.M.A.K., Al-Mosawy, Z.M.J. (2013), Synthesis of multidentate ligands with amido or amino donor groups for the preparation of rhenium and technetium radiopharmaceuticals, Journal of radioanalytical and nuclear chemistry, 295, 1599-1604.(DOI: 10.1007/s10967-012-2356-z)

[20] Thompson, B.B. (1968), The mannich reaction. Mechanistic and technological considerations, Journal of Pharmaceutical Sciences, 57, 715-733.(DOI: 10.1002/jps.2600570501)

[21] Shi, Y., Wang, Q., Gao, S. (2018), Recent advances in the intramolecular Mannich reaction in natural products total synthesis, Organic Chemistry Frontiers, 5, 1049-1066.(DOI: 10.1039/C7QO01079F)

[22] Bala, S., Sharma, N., Kajal, A., Kamboj, S., Saini, V. (2014), Mannich Bases: An Important Pharmacophore in Present Scenario, International Journal of Medicinal Chemistry, 2014, 15.(DOI: 10.1155/2014/191072)

[23] Yousif, E., Majeed, A., Al-Sammarrae, K., Salih, N., Salimon, J., Abdullah, B. (2017), Metal complexes of Schiff base: Preparation, characterization and antibacterial activity, Arabian Journal of Chemistry, 10, S1639-S1644.(DOI: 10.1016/j.arabjc.2013.06.006)

[24] Abu-Dief, A.M., Mohamed, I.M.A. (2015), A review on versatile applications of transition metal complexes incorporating Schiff bases, BeniSuef University Journal of Basic and Applied Sciences, 4, 119-133.(DOI:10.1016/j.bjbas.2015.05.004)

[25] Al Zoubi, W., Al-Hamdani, A.A.S., Ahmed, S.D., Ko, Y.G. (2018), A new azo-Schiff base: Synthesis, characterization, biological activity and theoretical studies of its complexes, Applied Organometallic Chemistry, 32, 3895.(DOI: 10.1002/aoc.3895)

[26] da Silva, C.M., da Silva, D.L., Modolo, L.V., Alves, R.B., de Resende, M.A., Martins, C.V.B., de Fátima, Â. (2011), Schiff bases: A short review of their antimicrobial activities, Journal of Advanced Research, 2, 1-8.(DOI:10.1016/j.jare.2010.05.004)

[27] Cozzi, P.G. (2004), Metal–Salen Schiff base complexes in catalysis: practical aspects, Chemical Society Reviews, 33, 410-421.(DOI: 10.1039/ B307853C)

[28] Keypour, H.,Rezaeivala, M.,Valencia, L.,Pérez-Lourido, P.,Khavasi, H. R. (2009), Synthesis and characterization of some new Co(II) and Cd(II) macroacyclic Schiff-base complexes containing piperazine moiety, Polyhedron, 28, 3755-3758.(DOI: 10.1016/j.poly.2009.08.021)

[29] Costişor, O.,Pantenburg, I.,Tudose, R.,Meyer, G. (2004), New Copper(II) and Cobalt(II) Complexes with the N,N′-Bis(antipyryl-4-methyl)-piperazine

(BAMP) Ligand: $Co_2(BAMP)Cl_4$ and $[Cu(BAMP)(H_2O)](ClO_4)_2$, Zeitschrift für anorganische und allgemeine Chemie, 630, 1645-1649.(DOI: 10.1002/ zaac.200400239)

[30] Kubono, K.,Hirayama, N.,Kokusen, H.,Yokoi, K. (2003), Crystal Structure of {1,4-Bis[1-(3,5-dichlorophenolato-2-ylmethyl)-ylpropylamino- κ^2N,O]piperazine κ^2N,N'}cobalt(II), Analytical Sciences, 19, 645-646.(DOI:10.2116/analsci. 19.645)

[31] Paital, A. R., Mandal, D., Huang, X., Li, J., Aromi, G., Ray, D. (2009), Structure and dimensionality of coordination complexes correlated to piperazine conformation: from discrete $[Cu^{II}_2]$ and $[Cu^{II}_2]_n$ complexes to a [τ]1,3-N -bridged $[Cu^{II}_2]_n$ chain, Dalton Transactions, 1352-1362. (DOI: 10.1039/B814681K)

[32] Cretu, C., Tudose, R., Cseh, L.,Linert, W.,Halevas, E.,Hatzidimitriou, A.,Costisor, O.,Salifoglou, A. (2015), Schiff base coordination flexibility toward binary cobalt and ternary zinc complex assemblies. The case of the hexadentate ligand N,N′-bis[(2 hydroxybenzilideneamino)-propyl]-piperazine, Polyhedron, 85, 48-59.(DOI: 10.1016/j.poly.2014.08.035)

[33] Noble, A., Anderson, J.C. (2013), Nitro-Mannich Reaction, Chemical Reviews, 113, 2887-2939.(DOI: 10.1021/cr300272t)

[34] Das, A., Goswami, S., Sen, R. and Ghosh, A. (2019), Inclusion of Ln(III) in the Complexes of Co(II) with a Mannich Base Ligand: Development of Atmospheric CO_2 Fixation and Enhancement of Catalytic Oxidase Activities, Inorg. Chem. 58, 5787−5798.(DOI: 10.1021/acs.inorgchem.9b00121)

[35] Das, A., Bhattacharya, K., Das, L. K. and Ghosh, A. (2018) Mixed azido/phenoxido bridged trinuclear Cu(II) complexes of Mannich bases: Synthesis, structures, magnetic properties and catalytic oxidase activities, Dalton Trans., 47, 9385-9399.(DOI: 10.1039/C8DT01400K)

[36] John, A., Mobin, S. M., Gosh, P., (2008) Structural and functional mimic of galactose oxidase by a copper complex of a sterically demanding [N2O2] ligand, Dalton Trans., 2815-2824.(DOI: 10.1039/b801496e)

[37] Kundu, B. K., Ranjan, R., Mukherjee, A., Mobin, S. M., Mukhopadhyay, S., (2019) Mannich base Cu(II) complexes as biomimetic oxidative catalyst, J. Inorg. Biochem., 195, 164-173. (DOI: 10.1016/j.jinorgbio.2019.03.023)

[38] Badwaik, V.B., Deshmukh, R.D., Aswar, A.S. (2009), Transition metal complexes of a Schiff base: synthesis, characterization, and antibacterial studies, Journal of Coordination Chemistry, 62, 2037-2047. (DOI: 10.1080/00958970 902741244)

[39] Zoubi, W.A. (2013), Biological Activities of Schiff Bases and Their Complexes: A Review of Recent Works, International Journal of Organic Chemistry, 03, 73.(DOI: 10.4236/ijoc.2013.33A008)

[40] Sen, P., Yildiz, S.Z., Atmaca, G.Y., Erdoğmuş, A. (2018), Synthesis, photophysics, and photochemistry of peripherally Schiff base-zinc complex substituted zinc phthalocyanine, Journal of Coordination Chemistry, 71, 1258-1267.(DOI: 10.1080/00958972.2018.1455094)

[41] Robinson, P.K. (2015), Enzymes: principles and biotechnological applications, Essays in biochemistry, 59, 1-41.(DOI: 10.1042/bse0590001)

[42] Pattammattel, A., Deshapriya, I.K., Chowdhury, R., Kumar, C.V. (2013), Metal-Enzyme Frameworks: Role of Metal Ions in Promoting Enzyme SelfAssembly on α-Zirconium(IV) Phosphate Nanoplates, Langmuir, 29, 2971-2981.(DOI: 10.1021/la304979s)

[43] Koshland Jr, D.E. (1995), The Key–Lock Theory and the Induced Fit Theory, Angewandte Chemie International Edition in English, 33, 2375-2378.(DOI: 10.1002/anie.199423751)

[44] Arends, I.W.C.E., Gamez, P., Sheldon, R.A. (2006), Green oxidation of alcohols using biomimetic Cu complexes and Cu enzymes as catalysts, in: R. van Eldik, J. Reedijk (Eds.) Advances in Inorganic Chemistry, Academic Press, 58, 235-279.(DOI: 10.1016/S0898-8838(05)58006-1)

[45] Vaidyanathan, M., Palaniandavar, M. (2000), Models for the active site in galactose oxidase: Structure, spectra and redox of copper(II) complexes of certain phenolate ligands, Journal of Chemical Sciences, 112, 223-238.(DOI: 10.1007/BF02706175)

[46] Sun, L., Petrounia, I.P., Yagasaki, M., Bandara, G., Arnold, F.H. (2001), Expression and stabilization of galactose oxidase in Escherichia coli by directed evolution, Protein Engineering, Design and Selection, 14, 699-704.(DOI: 10.1093/protein/14.9.699)

[47] Abad, J.M., Gass, M., Bleloch, A., Schiffrin, D.J. (2009), Direct Electron Transfer to a Metalloenzyme Redox Center Coordinated to a MonolayerProtected Cluster, Journal of the American Chemical Society, 131, 10229-10236.(DOI: 10.1021/ja9026693)

[48] Blaza, J.N., Bridges, H.R., Aragão, D., Dunn, E.A., Heikal, A., Cook, G.M., Nakatani, Y., Hirst, J. (2017), The mechanism of catalysis by type-II NADH: quinone oxidoreductases, Scientific Reports, 7, 40165.(DOI: 10.1038/srep40165)

[49] Himo, F., Eriksson, L.A., Maseras, F., Siegbahn, P.E.M. (2000), Catalytic Mechanism of Galactose Oxidase: A Theoretical Study, Journal of the American Chemical Society, 122, 8031-8036.(DOI: 10.1021/ja994527r)

[50] Reynolds, M.P., Baron, A.J., Wilmot, C.M., Vinecombe, E., Stevens, C., Phillips, S.E.V., Knowles, P.F., McPherson, M.J. (1997), Structure and mechanism of galactose oxidase: catalytic role of tyrosine 495, JBIC Journal of Biological Inorganic Chemistry, 2, 327-335.(DOI: 10.1007/s007750050139)

[51] Ryland, B.L., McCann, S.D., Brunold, T.C., Stahl, S.S. (2014), Mechanism of alcohol oxidation mediated by copper(II) and nitroxyl radicals, Journal of the American Chemical Society, 136, 12166-12173.(DOI: 10.1021/ja5070137)

[52] Mukherjee, C., Pieper, U., Bothe, E., Bachler, V., Bill, E., Weyhermu¨ller, T. and Chaudhuri, P. (2008), Ligand-Derived Oxidase Activity. Catalytic Aerial Oxidation of Alcohols (Including Methanol) by Cu(II)-Diradical Complexes, Inorg. Chem, 47, 8943-8956.(DOI: 10.1021/ic8009767)

[53] Striegler, S., Dunaway, N.A., Gichinga, M.G., Barnett, J.D., Nelson, A.-G.D. (2010), Evaluating Binuclear Copper(II) Complexes for Glycoside Hydrolysis, Inorganic Chemistry, 49, 2639-2648.(DOI: 10.1021/ic9014064)

[54] Alamsetti, S.K., Mannam, S., Mutupandi, P., Sekar, G. (2009), Galactose Oxidase Model: Biomimetic Enantiomer-Differentiating Oxidation of Alcohols

by a Chiral Copper Complex, Chemistry – A European Journal, 15, 1086-1090.(DOI: 10.1002/chem.200802064)

[55] Claus, H. (2004) Laccase: structure, reactions, distributin, Micron, 35, 93-96.(DOI: 10.1016/j.micron.2003.10.029)

[56] prajapati, H. (2018), Laccase- A Wonder Molecule : A Review of its Properties and Applications, Int. J. Pure App. Biosci. 6, 766-773.(DOI: 10.18782/2320-7052.6233)

[57] D'Acunzo, F., Galli, C., Masci, B. (2002), Oxidation of phenols by laccase and laccase mediator systems, Eur. J. Biochem., 269, 5330–5335.(DOI: 10.1046/ j.14321033.2002.03256.x.)

[58] Kramer, K. J., Kanost, M. R., Hopkins, T. L., Zhu, Yu C., Xu, R., Kerwin, J. L., Turecek, F. (2001), Oxidative conjugation of catechols with proteins in insect skeletal systems, Tetrahedron 57, 385–392.(DOI: 10.1016/S0040-4020(00) 00949-2)

[59] Sousa, A. C., Piedade, M. F. M. M., Martins, L. O., Robalo, M. P. (2016), Eco-friendly synthesis of indo dyes mediated by a bacterial laccase, Green Chemistry, 18, 6063-6070.(DOI: 10.1039/C6GC02050J)

[60] Claus, H., Filip, Z. (1998), Degradation and Transformation of Aquatic Humic Substances by Laccase-producing Fungi Cladosporium cladosporioides and Polyporus versicolor, Acta Hydrochim. Hydrobiol., 26, 180–185.(DOI: 10.1002/(SICI)1521-401X(199805))

[61] Edmund, C. M., Tse, D. S., Danielle, L. G., Thomas, B. R., and Andrew, A. G., (2014), Multicopper Models for the Laccase Active Site: Effect of Nuclearity on Electrocatalytic Oxygen Reduction, Inorg. Chem., 53, 8505−8516.(DOI: 10.1021/ic501080c)

[62] Yu, Z., Thompson, Z., Behnke, S. L., Fenk, K. D., Huang, D., Shafaat, H. S., and Cowan, J. A. (2020), Metalloglycosidase Mimics: Oxidative Cleavage of Saccharides Promoted by Multinuclear Copper Complexes under Physiological Conditions, Inorg. Chem., 59, 11218−11222.(DOI: 10.1021/acs.inorgchem .0c01193)

[63] Longe, L. F., Couvreur, J., Grandchamp, M. L., Garnier, G., Allais, F., Saito, K., (2018), Importance of Mediators for Lignin Degradation by Fungal Laccase, ACS Sustainable Chem. Eng., 6, 10097−10107. (DOI: 10.1021/ acssuschemeng. 8b01426)

[64] Corma, A., Navas, J., Sabater, M. J. (2018), Advances in One-Pot Synthesis through Borrowing Hydrogen Catalysis, Chem. Rev., 118, 1410-1459. (DOI: 10.1021/acs.chemrev. 7b00340)

[65] Grigg, R., Mitchel, T. R. B., Sutthivaiyakit, S., Tongpenyai, N. (1981), Transition metal-catalysed N-alkylation of amines by alcohols, J. Chem.Soc., Chem. Commun., 611-612.(DOI: 10.1039/C39810000611)

[66] Li, F., Shan, H., Kang, Q., Chen, L. (2011), Regioselective N-alkylation of 2 aminobenzothiazoles with benzylic alcohols, Chem. Comm., 47, 5058-5060.(DOI: 10.1039/C1CC10604J)

[67] Bertoli, M., Choualeb, A., Lough, A. J., Moore, B., Spasyuk, D., Gusev, D. G. (2011), Osmium and Ruthenium Catalysts for Dehydrogenation of Alcohols, Organometallics, 30, 3479-3482.(DOI: 10.1021/om200437n)

[68] Tuan Thanh, D., Ramalingam, B., Shan, S. P., Seayad, A. M. (2013), An Efficient Palladium-Catalyzed N-Alkylation of Amines Using Primary and Secondary Alcohols, ACS Catal., 3, 2536-2540.(DOI: 10.1021/cs400799n)

[69] Roesler, S., Ertl, M., Irrgang, T., Kempe, R. (2015) Cobalt-Catalyzed Alkylation of Aromatic Amines by Alcohols, Angew. Chem. Int. Ed., 54, 15046-15050.(DOI:10.1002/anie. 201507955)

[70] Elangovan, S., Neumann, J., Sortais, J.-B., Junge, K., Darcel, C., Beller, M. (2016), Efficient and selective *N*-alkylation of amines with alcohols catalysed by manganese pincer complexes, Nat. Commun., 7, 12641. (DOI: 10.1038/ ncomms12641)

[71] Vellakkaran, M., Singh, K. and Banerjee, D. (2017), An Efficient and Selective Nickel-Catalyzed Direct N-Alkylation of Anilines with Alcohols, ACS Catal., 7, 8152-8158.(DOI: 10.1021/acscatal.7b02817)

[72] Zhang, C., Wang, F. (2020), Catalytic Lignin Depolymerization to Aromatic Chemicals, Acc. Chem. Res., 53, 470−484.(DOI: 10.1021/acs.accounts.9b00573)

[73] Xu, C., Arancon, R. A. D., Labidi, J., Luque, F. (2014), Lignin depolymerisation strategies: towards valuable chemicals and fuels, Chem. Soc. Rev., 43, 7485–7500.(DOI: 10.1039/ C4CS00235K)

[74] Zakzeski, J., Bruijninicx, P. C. A., Jongerius, A. L., Weckhuysen, B. M. (2010), The Catalytic Valorization of Lignin for the Production of Renewable Chemicals, Chem. Rev., 110, 3552–3599.(DOI: 10.1021/cr900354u)

[75] Yang, H., Yan, R., Chen, H., Zheng, C., Lee, D. H., Liang, D. T. (2006), In-Depth Investigation of Biomass Pyrolysis Based on Three Major Components: Hemicellulose, Cellulose and Lignin, Energy Fuels, 20, 388–393.(DOI: 10.1021/ef0580117)

[76] Yang, H., Yan, R., Chen, H., Zheng, C. (2007), Characteristics of hemicellulose, cellulose and lignin pyrolysis, Fuel, 86, 1781–1788.(DOI: 10.1016/j.fuel.2006.12.013)

[77] Patwardhan, P. R., Brown, R. C., Shanks, B. H. (2011), Understanding the Fast Pyrolysis of Lignin, ChemSusChem, 4, 1629–1636.(DOI: 10.1002/cssc.201100133)

[78] Wang, S., Ru, B., Lin, H., Sun, W., Luo, Z. (2015), Pyrolysis behaviors of four lignin polymers isolated from the same pine wood, Bioresour. Technol., 182, 120–127.(DOI: 10.1016/j.biortech.2015.01.127)

[79] Deuss, P. J., Scott, M., Tran, F., Westwood, N. J., Vries, J. G. de, Barta, K. (2015), Aromatic Monomers by in Situ Conversion of Reactive Intermediates in the Acid-Catalyzed Depolymerization of Lignin, J. Am. Chem. Soc., 137, 7456–7467.(DOI: 10.1021/jacs.5b03693)

[80] Li, B., filpponen, I., Argyropoulous, D. S. (2010), Acidolysis of Wood in Ionic Liquids, Ind. Eng. Chem.Res., 49, 3126–3136.(DOI: 10.1021/ie1000983)

[81] Dabral, S., Engel, J., Mottweiler, J., Spoehrle, S. S. M., Lahive, W. C., Bolm, C. (2018), Mechanistic studies of base-catalysed lignin depolymerisation in dimethyl carbonate, Green Chem., 20, 170–182.(DOI: 10.1039/C7GC03110F)

[82] Song, Qi, Wang, F., Cai, J., Wang, Y., Zhang, J., Yu, W., Xu, J. (2013), Lignindepolymerization (LDP) in alcohol over nickel-based catalysts*via* a

fragmentation–hydrogenolysis process, Energy Environ. Sci., 6, 994–1007.(DOI: 10.1039/C2EE23741E)

[83] Laskar, D. D., Tucker, M. P., Chen, X., Helms, G. L., Yang, B. (2014), Noble-metal catalyzed hydrodeoxygenation of biomass-derived lignin to aromatic hydrocarbons, Green Chem., 16, 897–910.(DOI: 10.1039/C3GC42041H)

[84] Huang, Y., Duan, Y., Qiu, S., Wang, M., Ju, C., Cao, H., Fang, Y., Tan, T. (2018), Lignin-first biorefinery: a reusable catalyst for lignin depolymerization and application of lignin oil to jet fuel aromatics and polyurethane feedstock, Sustainable Energy Fuels, 2, 637–647.(DOI: 10.1039/C7SE00535K)

[85] Shu, R., Xu, Y., Ma, L., Zhang, Qi, Wang, C., Chen, Y. (2018), Controllable production of guaiacols and phenols from lignin depolymerization using Pd/C catalyst cooperated with metal chloride, Chem. Eng. J., 338, 457–464.(DOI: 10.1016/j.cej.2018.01.002)

[86] Rahimi, A., Azarpira, A., Kim, H., Stahi, S. S. (2013), Chemoselective Metal-Free Aerobic Alcohol Oxidation in Lignin, J. Am. Chem. Soc., 135, 6415–6418.(DOI: 10.1021/ja401793n)

[87] Rahimi, A., Ulbrich, A., Coon, J. J., Stahi, S. S. (2014), Formic-acid-induced depolymerization of oxidized lignin to aromatics, Nature, 515, 249–252.(DOI:10.1038/ nature13867)

[88] Lancefield, C. S., Ojo, O. S., Tran, F., Westwood, N. J. (2015), Isolation of Functionalized Phenolic Monomers through Selective Oxidation and C-O Bond Cleavage of the β-O-4 Linkages in Lignin, Angew. Chem., Int. Ed., 54, 258–262.(DOI: 10.1002/anie.201409408)

[89] Zhang, C., Li, H., Lu, J., Zhang, X., MacArthur, K. E., Heggen, M., Wang, F. (2017), Promoting Lignin Depolymerization and Restraining the Condensation via an Oxidation−Hydrogenation Strategy, ACS Catal., 7, 3419–3429.(DOI: 10.1021/acscatal.7b00148)

[90] Sedai, B., Diaz-Urrutia, C., Baker, R. T., Wu, R., Silks, L. A. Pete, Hanson, S. K. (2011), Comparison of Copper and Vanadium Homogeneous Catalysts for Aerobic Oxidation of Lignin Models, ACS Catal., 1, 794−804.(DOI: 10.1021/ cs200149v)

[91] Hanson, S. K., Wu, R., Silks, L. A. Pete, (2012), C-C or C-O Bond Cleavage in a Phenolic Lignin Model Compound: Selectivity Depends on Vanadium Catalyst, Angew. Chem., Int. Ed., 51, 3410−3413.(DOI: 10.1002/anie. 201107020)

[92] Baburam, S., Christian, D.-U., Tom, B. R., Ruilian, W., Silks, L. A. Pete, Hanson, S. K. (2013), Aerobic Oxidation of β-1 Lignin Model Compounds with Copper and Oxovanadium Catalysts, ACS Catal., 3, 3111−3112.(DOI: 10.1021/cs400636k)

[93] Biannic, B., Bozel, J. J. (2013), Efficient Cobalt-Catalyzed Oxidative Conversion of Lignin Models to Benzoquinones, Org. Lett., 15, 2730−2733. (DOI: 10.1021/ol401065r)

[94] Mottweiler, J., Puche, M., Rauber, C., Concepcion, P., Corma, A., Bolm, C. (2015), Copper- and Vanadium-Catalyzed Oxidative Cleavage of Lignin using Dioxygen, ChemSusChem, 8, 2106−2113.(DOI: 10.1002/cssc.201500131)

[95] Mate, V. R., Shirai, M., Rode, C. V. (2013), Heterogeneous Co_3O_4 catalyst for selective oxidation of aqueous veratryl alcohol using molecular oxygen, Catal. Commun., 33, 66−69.(DOI: 10.1016/j.catcom.2012.12.015)

[96] Mate, V. R., Jha, A., Joshi, U. D., Patil, K. R., Shirai, M., Rode, C. V. (2014), Effect of preparation parameters on characterization and activity of Co_3O_4 catalyst in liquid phase oxidation of lignin model substrates, Appl. Catal., A, 487, 130−138.(DOI:10.1016/j.apcata. 2014.08.023)

[97] Jha, A., Patil, K. R., Rode, C. V. (2013), Mixed Co-Mn Oxide-Catalysed Selective Aerobic Oxidation of Vanillyl Alcohol to Vanillin in Base-Free Conditions, ChemPlusChem, 78, 1384−1392.(DOI: 10.1002/cplu.201300247)

[98] Zakzeski, J., Debczak, A., Bruijnincx, Pieter C. A., Weckhuysen, Bert M. (2011), Catalytic oxidation of aromatic oxygenates by the heterogeneous catalyst Co-ZIF-9,Appl. Catal., A, 394 (1−2), 79−85.(DOI: 10.1016/j.apcata.2010.12.026)

[99] Wang, M., Lu, J., Zhang, X., Li, L., Li, H., Luo, N., Wang, F. (2016), Two-Step, Catalytic C-C Bond Oxidative Cleavage Process Converts Lignin Models and Extracts to Aromatic Acids, ACS Catal., 6, 6086–6090.(DOI: 10.1021/ acscatal.6b02049)

[100] Hanson, S. K., Baker, R. T. (2015), Knocking on Wood: Base Metal Complexes as Catalysts for Selective Oxidation of Lignin Models and Extracts, Acc. Chem. Res., 48, 2037–2048.(DOI: 10.1021/acs.accounts.5b00104)

[101] Kim, Si A., Kim, S. E., Kim, Yu K., Jang, H.-Y. (2020), Copper-Catalyzed Oxidative Cleavage of the C-C Bonds of β-Alkoxy Alcohols and β-1 Compounds, ACS Omega, 5, 31684–31691.(DOI: 10.1021/acsomega.0c04162)

[102] Wang, M., Li, L. H., Lu, J. M., Li, H. J., Zhang, X. C., Liu, H. F., Luo, N. C., Wang, F. (2017), Acid promoted C-C bond oxidative cleavage of β-O-4 and β-1 lignin models to esters over a copper catalyst, Green Chem., 19, 702–706.(DOI: 10.1039/C6GC02970A)

[103] Liu, M., Zhang, Z., Yan, J., Liu, S., Liu, H., Liu, Z., Wang, W., He, Z., Han, B. (2020), Aerobic Oxidative Cleavage and Esterification of C(OH)-C Bonds, Chem, 6, 3288–3296.(DOI: 10.1016/j.chempr.2020.09.006)

[104] Al Zoubi, W., Ko, Y.G. (2017), Schiff base complexes and their versatile applications as catalysts in oxidation of organic compounds: part I, Applied Organometallic Chemistry, 31, 3574.(DOI: 10.1002/aoc.3574)

[105] Çapan, A., Uruş, S., Sönmez, M. (2018), Ru(III), Cr(III), Fe(III) complexes of Schiff base ligands bearing phenoxy Groups: Application as catalysts in the synthesis of vitamin K3, Journal of Saudi Chemical Society, 22, 757-766.(DOI: 10.1016/j.jscs.2017.12.007)

[106] De Vos, D.E., Thibault-Starzyk, F., Knops-Gerrits, P.P., Parton, R.F., Jacobs, P.A. (1994), A critical overview of the catalytic potential of zeolite supported metal complexes, Macromolecular Symposia, 80, 157-184.(DOI:10.1002/masy. 19940800112)

[107] Bania, K.K., Deka, R.C. (2013), Zeolite-Y Encapsulated Metal Picolinato Complexes as Catalyst for Oxidation of Phenol with Hydrogen Peroxide, The Journal of Physical Chemistry C, 117, 11663-11678.(DOI: 10. 1021/jp402439x)

[108] Bedioui, F. (1995), Zeolite-encapsulated and clay-intercalated metal porphyrin, phthalocyanine and Schiff-base complexes as models for

biomimetic oxidation catalysts: an overview, Coordination Chemistry Reviews, 144, 39-68.(DOI: 10.1016/0010-8545(94)08000-H)

[109] Maurya, M.R., Kumar, M., Titinchi, S.J., Abbo, H.S., Chand, S. (2003), Oxovanadium (IV) Schiff base complexes encapsulated in zeolite-Y as catalysts for the liquid-phase hydroxylation of phenol, Catalysis Letters, 86, 97-105.(DOI: 10.1023/A:102261931)

[110] Zhou, X.-F. (2014), Application of zeolite-encapsulated Cu(II) [H_4] salen derived from [H_2]salen in oxidative delignification of pulp, RSC Advances, 4, 28029-28035.(DOI: 10.1039/C4RA04175E)

[111] Bennur, T.H., Srinivas, D., Ratnasamy, P. (2001), EPR spectroscopy of copper and manganese complexes encapsulated in zeolites, Microporous and Mesoporous Materials, 48, 111-118.(DOI: 10.1016/S1387-1811(01)00345-6)

[112] Kundu, B. K.,Das, M., Ganguly, R., Bhobe, P. A., Mukhopadhyay, S. (2020), Role of zeolite encapsulated Cu(II) complexes in electron transfer as well as peroxy radical intermediates formation during oxidation of thioanisole, Journal of Catalysis, 389, 305-316.(DOI: 10.1016/j.jcat.2020.06.005)

[113] Kundu, B. K., Chhabra, V., Malviya, N., Ganguly, R., Mishra, G. S., Mukhopadhyay, S. (2018), Zeolite encapsulated host-guest Cu(II) Schiff base complexes: Superior activity towards oxidation reactions over homogenous catalytic systems, Microporous and Mesoporous Materials 271, 100-117.(DOI: 10.1016/j.micromeso.2018.05.046)

[114] Tuck, C. O., Perez, E., Horvath, I. T., Sheldon, R. A., Poliakoff, M. (2012), Valorization of Biomass: Deriving More Value from Waste, Science, 337, 695-699.(DOI:10.1126/science. 1218930)

[115] Rayati, S., Khodaei, E., Jafarian, M. (2017), Catalytic activity and electrochemical properties of Cu(II)-Schiff base complex encapsulated in the nanocavities of zeolite-Y for oxidation of olefins and sulfides, Journal of Coordination Chemistry, 70, 2736-2750.(DOI: 10.1080/00958972.2017.1369052)

[116] Bania, K. K., Bharali, D., Viswanathan, B., Deka, R.C. (2012), Enhanced Catalytic Activity of Zeolite Encapsulated Fe(III)-Schiff-Base Complexes for

Oxidative Coupling of 2-Napthol, Inorganic Chemistry, 51, 1657-1674.(DOI: 10.1021/ic201959g)

[117] Meier, B., Werner, T., Klimant, I., Wolfbeis, O.S. (1995), Novel oxygen sensor material based on a ruthenium bipyridyl complex encapsulated in zeolite Y: dramatic differences in the efficiency of luminescence quenching by oxygen on going from surface-adsorbed to zeolite-encapsulated fluorophores, Sensors and Actuators B: Chemical, 29, 240-245.(DOI:10.1016/ 0925-4005(95)01689-9)

[118] Li, S., Liu, M., Liu, Q., Pan, F., Zhang, Li, Ma, K. (2022), Zeolite encapsulated Cu(II)-salen complexes for the catalytic degradation of dyes in a neutral condition, Colloids and Surfaces, A: Physicochemical and Engineering Aspects, 648, 129153.(DOI:10.1016/j.colsurfa. 2022.129153)

[119] Anpo, M., Zhang, S. G., Mishima, H., Matsuoka, M., Yamashita, H. (1997), Design of photocatalysts encapsulated within the zeolite framework and cavities for the decomposition of NO into N_2 and O_2 at normal temperature, Catalysis Today, 39, 159-168. (DOI: 10.1016/S0920-5861(97)00097-7)

Chapter 2

Mono- and hexa-nuclear copper complexes of Mannich base ligand: Synthesis, ligand transformation study, X-ray crystal structure, enzymatic catalysis and nitro aromatic sensing applications.

Chapter 2

Mono- and hexa-nuclear copper complexes of Mannich base ligand: Synthesis, ligand transformation study, X-ray crystal structure, enzymatic catalysis and nitro aromatic sensing applications.

N, O-donor based Mannich ligand, H_2L^1 [2,4-dichloro-6-((4-(2 hydroxyethyl)piperazin-1-yl)methyl)phenol] promoted synthesis of two new mononuclear Cu(II) complexes (1-2) and one new hexanuclear Cu(II) complex has been achieved (3) through ligand transformation. The metalloenzyme mimicking properties of complexes (1, 2) and nitroaromatic sensing interactions of complex (3) have been explored. Structural features and different applications of these newly synthesized metal complexes are discussed in two parts.

2A- Synthesis of mono-nuclear Cu(II) complexes by N,O-donor ligand transformation and their catalytic role in visible-light-driven alcohol oxidation.

And

2B- Picric acid detection by a hexanuclear Cu(II) complex synthesized through N,O-donor ligand transformation.

Chapter 2A

Synthesis of mono-nuclear Cu(II) complexes by N,O-donor ligand transformation and their catalytic role in visible-light-driven alcohol oxidation

2A.1 Introduction

The conformation of ligands can bring about interesting aspects in the structure of transition metal complexes and associated properties. A flexible ring or open structure as a ligand with one or more than one donor center can induce structural preferences in the formation of metal complexes in various ways [1-6]. It has been also noticed that in a sterically demanding situation or for the sake of less strainer chelating environment certain ligands can decyclize or ring-opening of the ligands can happen [7-15]. In point of view of the catalytic properties, in-built flexibility of the associated ligands in terms of denticity, ability to engage in different non-covalent interactions with substrate and providing an efficient and robust platform remain very crucial as per earlier reports [16-21]. Among various catalytic activities aerobic oxidation of primary alcohol is an important sub-class of catalytic reaction in terms of biological as well as industrial viewpoint [22, 23]. In biological systems, oxidation of alcohols gets catalyzed by various enzymes like alcohol dehydrogenase or galactose oxidase. While alcohol dehydrogenase contains zinc ion; galactose oxidase is a mononuclear type II copper fungal metalloenzyme. In the active center of galactose oxidase copper(II) ion is surrounded by two nitrogen atoms of histidine (His496 and His581) and two oxygen atoms of tyrosine (Tyr272 and Tyr495) along with a labile water molecule (pH 7) to form a distorted square pyramidal geometry. Sometimes at lower pH(~3.5), acetate group replaces the water [24]. These natural enzymes provide us clues for how to go forward for greener catalytic systems based on bio-inspired perception. It is also evident from the fact that a N/O donor system for copper ions can provide an ideal environment to shuttle between Cu(II) and Cu(I) state to act as an oxidation catalyst.

In an effort to develop flexible ligands [6, 25, 26] and oxidation catalysts, [26-30] hereby a new ligand *viz.* 2,4-dichloro-6-((4-(2-hydroxyethyl)piperazin-1-yl)methyl)phenol [$\mathbf{H_2L^1}$] has been designed to investigate its ability to form copper(II) complexes. The idea was to provide an N_2O_2 environment surrounding the copper center like the active center of galactose oxidase and an alcoholic arm has been purposefully inducted to investigate the fate of it while copper(II) complex of the $\mathbf{H_2L^1}$ assists as a catalyst in alcohol oxidation reactions.

Alcohol oxidation by the copper catalyst is a well-known process and extensively studied as reported in the literature [31-39]. However, it is noteworthy to mention that though photocatalytic systems as a part of green synthetic processes have emerged as a research hotspot in current sustainable research scenario, there are very limited examples of photocatalytic oxidation of alcohol oxidation are reported so far [40-46].

In this chapter, synthesis and characterization oftwo mono-nuclear copper complexes derived from ligand $\mathbf{H_2L^1}$ have been reported. Upon reaction with copper(II) acetate in methanol an unprecedented piperizinyl ring cleavage has been observed with further organic transformation to yield [$Cu(HL_a^1)$] **1** [$\mathbf{H_3L_a^1}$ = 2-((2-((3,5-dichloro-2 hydroxybenzyl)amino)ethyl)(2-hydroxyethyl)amino)-2-methoxyacetic acid] [Scheme 2A.2]. A similar result is also obtained when the reaction was carried out in ethanol medium and a corresponding copper complex [$Cu(HL_b^1)$] **2** [$\mathbf{H_3L_b^1}$ = 2-((2-((3,5-dichloro-2-hydroxybenzyl)amino) ethyl)(2-hydroxyethyl)amino)-2-ethoxyacetic acid] is obtained. The probable mechanistic pathway of organic transformation and photocatalytic activity of both the complexes towards alcohol oxidation reaction in presence of aerial oxygen is explored herewith.

2A.2 Experimental

2A.2.1 Materials and methods

All the chemical reagents required were purchased from Sigma and used without further purification. Infrared spectra (4000 to 500 cm^{-1}) were recorded with a BRUKER TENSOR 27 instrument in KBr pellets. NMR spectra were recorded on an AVANCE III 400 Ascend Bruker BioSpin machine at ambient temperature.

Mass spectrometric analyses were done on Bruker- Daltonics, microTOF-Q II mass spectrometer and elemental analyses were carried out with a ThermoFlash 2000 elemental analyzer. Spectrophotometric measurements were performed on a Perkin Elmer UV-Vis-NIR spectrophotometer (Model: Lambda 1050) and a Fluoromax-4p spectrofluorometer from Horiba JobinYvon (Model: FM-100) (for emission) using a quartz cuvette with a path length of 2 cm. HPLC analysis was done through a Dionex HPLC-Ultimate 3000 (High-Performance Liquid Chromatography) pump, which was used to analyze products onto a Dionex Acclaim ® 120 C18 column. GC-MS analysis was performed using GC-Hewlett Packard 6890 equipped with HP-5 column. All voltammetric experiments were performed using a CHI 104 electrochemical workstation (CH Instruments Model CHI62OD series). Potentials were referenced vs the Ag/AgCl electrode and ferrocene was added as an internal standard. The Gaussian 09 D.01 package has been used for the computational study [47]. The Pople diffuse basis set 6-31G(d,p) has been considered for non-metals (C, H, O, and N), whereas the effective core potential (ECP) LANL2DZ has been considered for the Cu atom [48-50]. All the calculations are performed using Becke's three-parameter hybrid exchange functional and Lee–Yang–Parr's correlation functional (B3LYP) [51-53].

2A.2.2 X-ray crystallography

Single crystal X-ray structural studies of 1 and 2 were performed on a CCD Agilent Technologies (Oxford Diffraction) SUPER NOVA diffractometer. Data for all the complexes were collected at 150(2) K using graphite-monochromoated MoKα radiation ($\lambda\alpha$ = 0.71073 Å). The strategy for the data collection was evaluated by using the CrysAlisPro CCD software. The data were collected by the standard 'phi-omega scan techniques and were scaled and reduced using CrysAlisPro RED software. The structures were solved by direct methods using SHELXS-97 and refined by full-matrix least-squares with SHELXL-97, refining on F^2 [54]. The positions of all the atoms were obtained by direct methods. All non-hydrogen atoms were refined anisotropically. The remaining hydrogen atoms were placed in geometrically constrained positions and refined with isotropic temperature factors, generally 1.2 U_{eq} of their parent atoms. The crystal and refinement data are summarized in Table 2A.1.

Table 2A. 1. *Crystallographic data and structure refinement parameters for* ***1****, and* ***2****.*

Complex	**1**	**2**
Empirical Formula	$C_{14}H_{18}Cl_2CuN_2O_5$	$C_{17}H_{26}Cl_2CuN_2O_6$
Formula weight	428.74	488.84
Crystal system	Triclinic	Monoclinic
Space group	P -1	P 1 21/c 1
a (Å)	10.2953(5)	13.9091(15)
b (Å)	12.1715(5)	11.8179(11)
c (Å)	15.3072(7)	12.9126(15)
α (°)	70.350(3)	90
β (°)	70.494(3)	92.753(4)
γ (°)	78.232(3)	90
V ($Å^3$)	1693.65(14)	2120.1(4)
λ (Å)	0.71073	0.71073
ρcalcd (mgm^{-3})	1.681	1.532
Z	4	4
T (K)	103(2)	100(2)
μ (mm-1)	1.632	1.317
F(0 0 0)	876	1012
Crystal size (mm^3)	0.040 × 0.100 × 0.140	0.200 × 0.240 × 0.320
θ ranges (°)	1.48 - 31.15	2.34 - 25.70
h/k/l	-14,14/-17,17/-22,22	-16,16/-14,14/-15,15
Reflections Collected	49244	34221
Independent Reflections	10878	4038
T_{max} and T_{min}	0.9380 and 0.8040	0.7790 and 0.6780
Data/restraints/paRameters	10878 / 0 / 447	4038 / 0 / 259
GOF	0.856	1.052
Final R indices [I > 2σ(I)]	R1 = 0.0542, wR2 = 0.1372	R1 = 0.0518, wR2 = 0.1024
R indices (all data)	R1 = 0.0904, wR2 = 0.1675	R1 = 0.0884, wR2 = 0.1181
Largest peak and hole(e Å-3)	0.617 and -0.895	0.714 and -0.550

2A.2.3 Synthesis of 2,4-dichloro-6-((4-(2-hydroxyethyl) piperazin-1-yl) methyl)phenol (H_2L^1)

1.63 g (10 mmol) of 2,4-di-chlorophenol was added to a 30 mL ethanolic solution of 1-(2-hydroxyethyl) piperazine (1.25 g, 10 mmol) and formaldehyde (0.44 g, 14.8 mmol). The solution was refluxed overnight under nitrogen atmosphere and then cooled to room temperature. After that the solution was removed under reduced pressure, hydrobromic acid (1.82 mL, 16.1 mmol, 48% solution) was added and the liquid solution began to gel which was washed with n-hexane to remove the impurity. The white solid obtained was dissolved in water (50 mL), neutralized with NaOH (checked by litmus paper) followed by the extraction with CH_2Cl_2/diethyl ether (3 × 50 mL). The combined organic layers were dried over anhydrous Na_2SO_4 and the solvent was removed in vacuo to give a light orange oil (2.11 g, 7.6 mmol, yield 73%). ^{1}H NMR (400.13 MHz, 298K, $CDCl_3$): δ 7.18 (1H, s, ArH), 6.81 (1H, s, ArH), 5.23 (1H, s, ArOH), 3.63 (2H, s, -NCH_2Ar), 3.57 (2H, t, -CH_2OH), 2.57 (8H, s, -piperazine ring), 2.52 (2H, t, -NCH_2), ppm; ^{13}C NMR (100.61 MHz, 298 K, $CDCl_3$): δ 152.5 (C of ArOH), 128.8 (CH of Ar), 126.8 (CH of Ar), 123.6 (C of $ArCH_2$), 123.1 (C of ArCl), 121.4 (C of ArCl), 60.7 (C of –NCH_2), 59.2 (C of –CH_2OH) , 57.7 (CH_2 of –NCH_2Ar), 52.5 (CH_2 of –piperazine ring), 52.2 (CH_2 of –piperazine ring) ppm (figure 2A.1). Anal. Calcd (%) for $C_{13}H_{18}Cl_2N_2O_2$: C, 51.16; H, 5.94; N, 9.18. Found (%): C, 51.64; H, 6.12; N, 9.43. FTIR (in KBr υ in cm^{-1}): 3500–3100 {υO-H, (s)}; 3000–2820 {υC-H, (m)}; 1120–1010 {υC-N,C-O (m)}; 900-850 { υC-Cl, (s)}. ESI-MS in HPLC MeOH (m/z): 303.3 (100%) (in negative mode) (figure 2A.2).

2A.2.4 Synthesis of complex [Cu(HL_a^1)] (1)

A 10 mL methanolic solution of $Cu(OAc)_2.H_2O$ (0.1 g; 0.5 mmol) was added dropwise to a 10 mL methanolic solution of H_2L^1 (0.15 g; 0.5 mmol) and triethylamine (70 μL; 0.5 mmol). Then the mixture was stirred at room temp for 4 hrs. The resulting green solution was concentrated up to 5-6 mL by evaporating the solvents in vacuo. The concentrated mixture was filtered and then left for slow evaporation in the air. Finally, after three or four days, dark green square-shaped defractable crystals were obtained from the reaction mixture. Crystals were collected by filtration and washed with diethyl ether. ESI-MS $[C_{14}H_{18}Cl_2CuN_2O_5 + Na]^+$ 452.3 (figure 2A.3). Anal. Calcd (%) for $C_{14}H_{18}Cl_2CuN_2O_5$: C, 39.22; H, 4.23; N, 6.53. Found (%): C, 39.56; H, 4.26; N,

6.41; FTIR (in KBr υ in cm^{-1}): 3600–3100 {υN-H,O-H (s); 3000–2800 {υC-H, (m)}; 1120–1010 {υC-N,C-O (s)}; 920-850 { υC-Cl, (s)}. Yield 75%

2A.2.5 Synthesis of complex $[Cu(HL_b^1)]\cdot C_2H_5OH$ (2)

This compound was obtained following the same procedure as above by using ethanol instead of methanol. The concentrated solution was filtered and kept in a test tube for slow evaporation of ethanol. After three days green square-shaped crystals are obtained which were further washed with diethyl ether to obtain a pure compound. ESI-MS $[C_{17}H_{26}Cl_2CuN_2O_6 + Na - EtOH]^+$ 465.9 (figure 2A.3). Anal. Calcd (%) for $C_{17}H_{26}Cl_2CuN_2O_6$: C, 41.77; H, 5.36; N, 5.73. Found (%): C, 41.85; H, 5.46; N, 5.79; FTIR (KBr υ in cm^{-1}): 3600–3100 {υN-H,O-H (s); 3000–2800 {υC-H, (m)}; 1110–1000 {υC-N,C-O (m)}; 900-860 { υC-Cl, (s)}. Yield 72%

2A.2.6 Selective primary alcohols by Cu^{2+} complexes oxidation of

All the photocatalytic reactions were performed in a 50 mL two-necked borosil round bottom flask at ambient temperature. In a typical sealed reaction system, copper complex (1 mol%, 0.0096 mmol) and TEMPO (3 mol%, 0.0288 mmol) were added to the two necked round bottom flask with a magnetic stirrer under O_2 (balloon pressure), and it was followed by addition of the relevant substrate (0.96 mmol) and 1 mL of DCM. Two 6 watts LED bulbs which are provided on two sides of the reactor, act as the source of the visible light (λ 400-800 nm). After the reaction, 20 μL of the reaction mixture was taken out and filtered through the Whatman filter paper and diluted by acetonitrile and injected into the HPLC equipped with VWD detector (Agilent Technologies, GC7890A) for analysis. The results were analyzed by HPLC analysis at the wavelength maximum of 254 nm and 280 nm, respectively. A HP-5 5% phenyl methyl siloxane column (30 m × 0.32 mm × 0.5 μm) was used. The chemical structures of the products were confirmed by comparison with standard chemicals and GC-MS (Agilent Technologies, GC6890N, MS 5973). The conversion for the substrate was described as the ratio of the moles of the reactant consumed in the reaction to the initial moles of the reactant. The selectivity was defined as the ratio of the moles of the product to that of the reactant consumed in the reaction.

2A.2.7 Detection of hydrogen peroxide in the catalytic reactions

Modification of the iodometric method is employed to detect H_2O_2 quantitatively during the catalytic reaction. Reaction mixtures were prepared as in the kinetic experiments. After 1 h of reaction, an equal volume of water was added to extract the formed quinone using dichloromethane. The aqueous layer was acidified with H_2SO_4 to pH ~2 to stop further oxidation, and 1 mL of a 10% solution of KI and three drops of a 3% solution of ammonium molybdate were added. In the presence of hydrogen peroxide I^- is oxidized to I_2, $H_2O_2 + 2I^- + 2H^+ \rightarrow 2H_2O + I_2$, and with an excess of iodide ions, the tri-iodide ion is formed according to the reaction $I_2(aq) + I^- \rightarrow I_3^-$. The reaction rate is slow but increases with increasing concentrations of acid, and the addition of an ammonium molybdate solution condenses the reaction almost immediately. The formation of I_3^- could be monitored by UV-vis spectroscopy due to the development of the characteristic I_3^- band (λ = 353 nm, ε = 26 000 M^{-1} cm^{-1}).

2A.3 Results and discussion

2A.3.1 Synthesis and characterization

The reaction of 2,4-di-chlorophenol, 1-(2-hydroxyethyl) piperazine and formaldehyde in a 1:1:1.5 molar ratio in ethanol lead to the formation of mannich base (**H_2L^1**) (scheme 2A.1.a). Upon reaction of (**H_2L^1**) with $Cu(OAc)_2.H_2O$ in methanol/ethanol, green colored solution was obtained. Slow evaporation of the concentrated solution leads to the green square-shaped crystals of $[Cu(HL_a^1)]$ **(1)** and $[Cu(HL_b^1)]\cdot C_2H_5OH$ **(2),** respectively (scheme 2A.1.b).

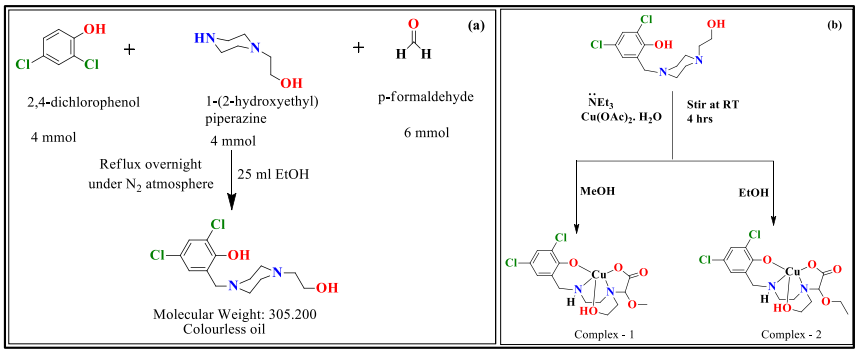

Scheme 2A.1. Synthesis of (a) Ligand and (b) Complexes **1** and **2**.

Ligand **(H_2L^1)** has been characterized by ^1H and ^{13}C NMR and ESI-MS spectroscopy. The ligand has shown all the characteristic peaks in ^1H NMR and ^{13}C NMR (figure 2A.1).

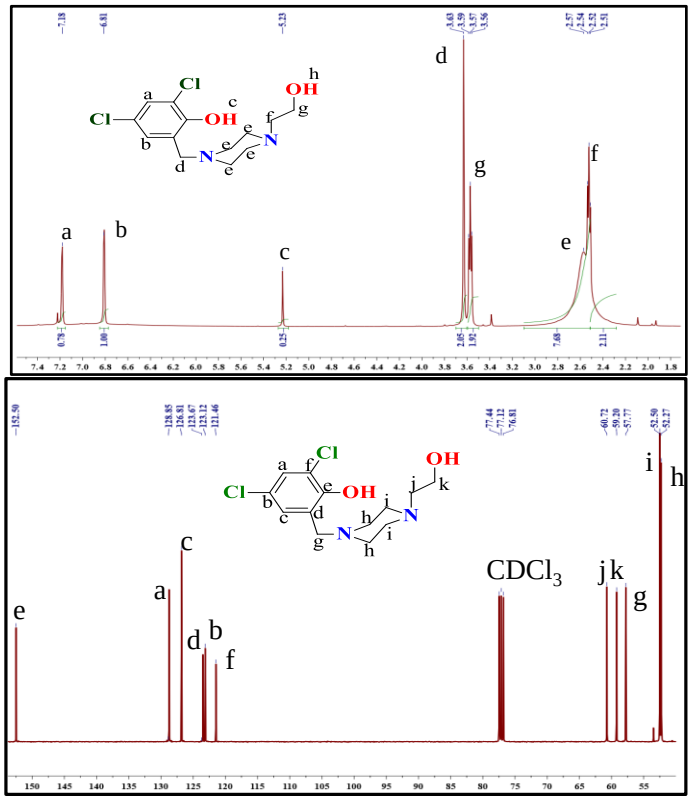

***Figure 2A. 1**. ^1H and ^{13}C NMR of H_2L^1.*

The molecular ion peak of the ligand H_2L^1 was observed at 303.3 $[M–H]^+$ in the negative mode in ESI-MS spectrum (Figure 2A.2). All the complexes have been characterized by ESI-MS spectroscopy, elemental analysis and singly crystal X-ray crystallography. IR spectra of complexes **1** and **2** have shown metal carboxylate starching bands around 1421 and 1627 cm^{-1} due to the symmetric and asymmetric stretching.

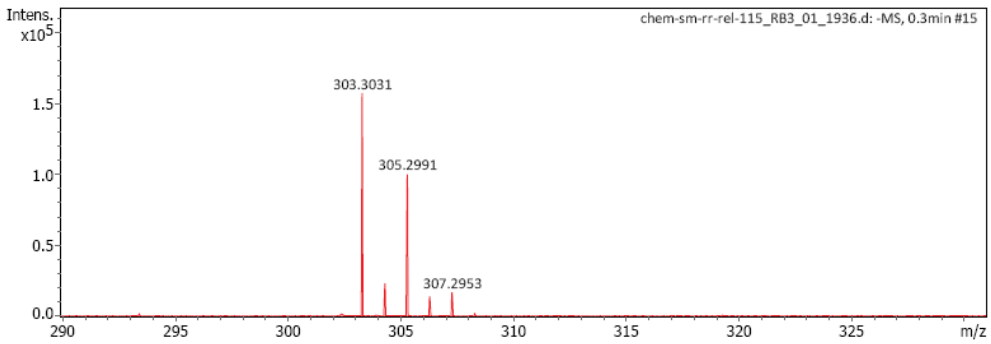

***Figure 2A. 2**. ESI- MS spectrum of H_2L^1.*

Furthermore the broad stretching band for –N-H around 3450 cm^{-1} masks the alcoholic stretching band which is visible around 2985 cm^{-1} in the original ligand. The ESI-Mass spectra of compound **1** and **2** show the molecular ion peak at 452.3 $[M + Na]^+$ and 465.9 $[M + Na – EtOH]^+$, respectively (figure 2A.3).

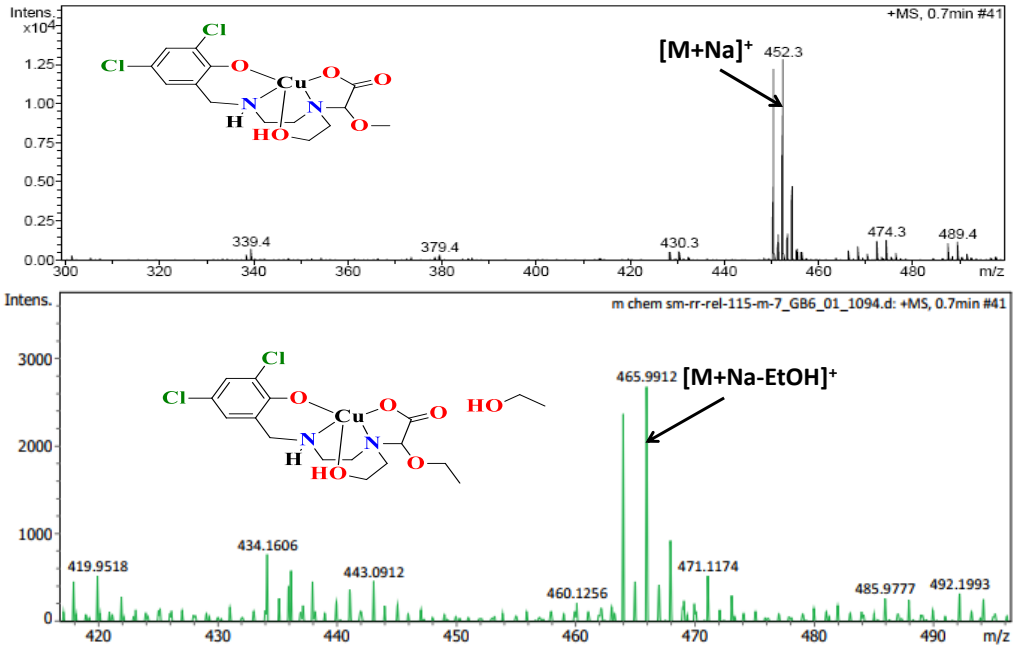

***Figure 2A. 3**. ESI- MS spectrum of **1** and **2**. (top to bottom)*

2A.3.2 Investigation on the mechanistic pathway of ligand transformation

The ligand upon treatment with copper acetate in methanolic/ethanolic solution undergoes an unprecedented transformation with oxidation of piperazine ring. To get a better idea about how the ligand transformation is taking place in presence of copper acetate, the reaction has been monitored through ESI-MS spectrometry in 30 mins of intervals. Literature reveals that piperazine ring tends to get oxidized to lactam in various oxidative conditions in the presence and absence of metal catalysts [55-57]. It is assumed herein that the copper complex gets oxidized to mono keto form as depicted in scheme 2A.2 structure A. The keto form tautomerizes into enol and forms an intermediate B (scheme 2A.2), identified by ESI-MS with simulated pattern peaks with as $[M + H^+]$ ion at 881.0. In the presence of aerial oxygen the enol gets oxidized, and subsequent nucleophilic attack by methanol and dissociation of the dimeric species generates the α-methoxy product (scheme 2A.2, structure C) which is alsoidentified in ESI-MS with the signature fragmented peak at 530.8 (figure 2A.4) [58]. Further hydrolysis of the amide bond leads to the ring cleavage and generates the obtained complexes **1** and **2,** respectively [59].

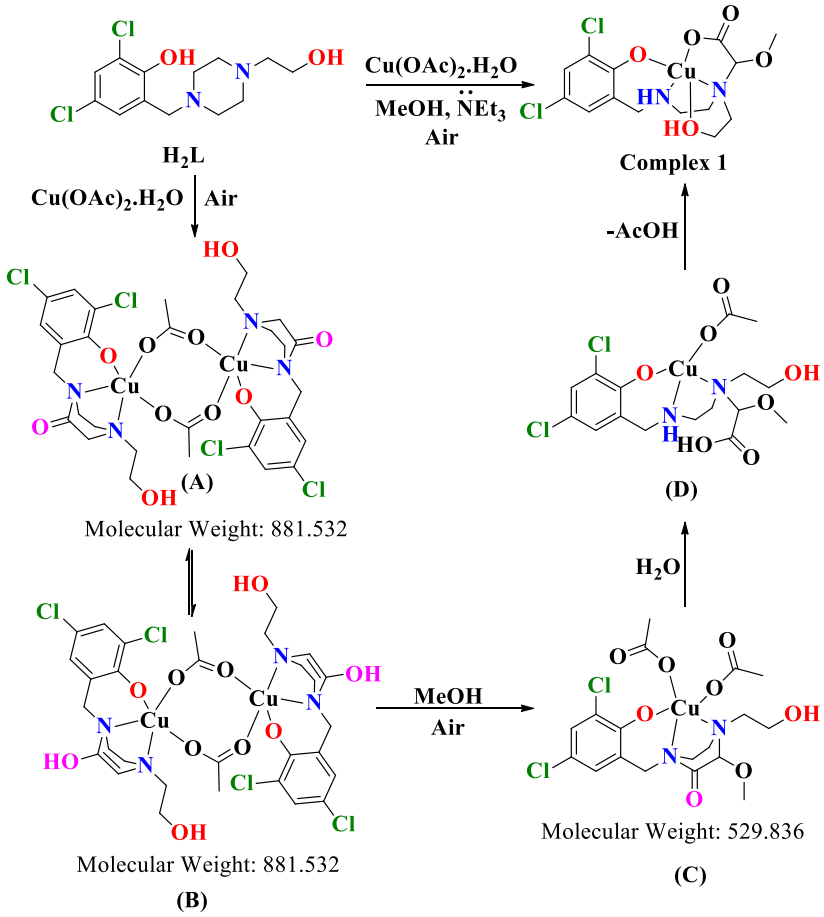

Scheme 2A.2. *Mechanistic pathway for the formation of complex-**1**.*

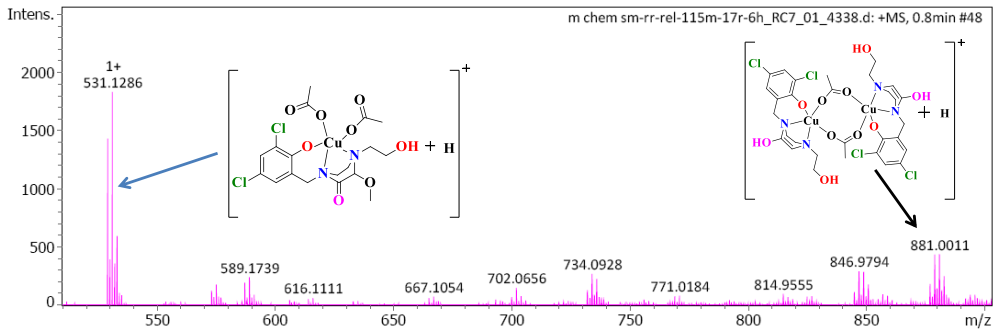

Figure 2A.4*. ESI-MS spectrum in MeOH for complex-**1** reaction intermediates*

2A.3.3 Structural description of the complexes (1) and (2)

These two structures are monomeric in nature and with the distorted square pyramidal environment surrounding the copper ions. The ligands are acting in a pentadentate fashion with two N and three O atoms (figure 2A.5) acting as donor sites.

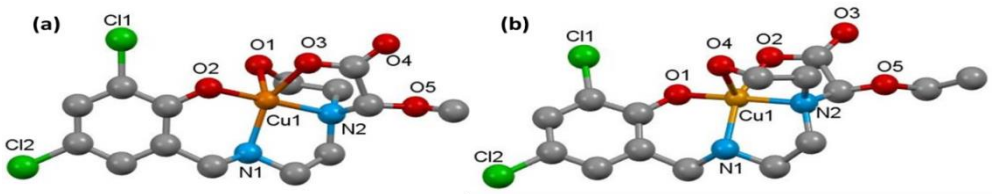

Figure 2A. 5**. The solid-state crystal structure for (a) complex **1** (b) complex **2.

The calculated **τ** values for compound **1** are 0.20 and 0.21 for two crystallographically independent centers. In complex **2** the **τ** value is 0.22. In both the complexes the value of **τ** is near more towards zero suggesting the square pyramidal geometry around the Cu center [60].

Table 2A. 2**. Selected bond lengths (Å) and bond angles (°) for **1** and **2.

Complex-1		**Complex-2**	
Cu1-O2	1.906(2)	Cu1-O1	1.908(3)
Cu1-O3	1.985(2)	Cu1-O2	1.973(3)
Cu1-N1	2.003(3)	Cu1-N1	2.001(4)
Cu1-N2	2.051(3)	Cu1-N2	2.044(3)
Cu1-O1	2.208(2)	Cu1-O4	2.286(3)
C12-O4	1.234(4)	C10-O3	1.229(5)
C13-O5	1.397(4)	C11-O5	1.396(5)
O2-Cu1-O3	94.13(10)	O1-Cu1-O2	94.40(12)
O2-Cu1-N1	95.55(11)	O1-Cu1-N1	96.66(14)
O3-Cu1-N2	83.20(10)	O2-Cu1-N2	82.93(13)
O2-Cu1-O1	101.96(10)	O1-Cu1-O4	104.60(12)
O3-Cu1-O1	93.00(10)	O2-Cu1-O4	96.53(12)
N1-Cu1-O1	113.01(10)	N1-Cu1-O4	97.96(14)
N2-Cu1-O1	81.89(10)	N2-Cu1-O4	80.94(13)
N1-Cu1-N2	85.05(11)	N1-Cu1-N2	84.32(14)
O2-Cu1-N2	175.46(10)	O1-Cu1-N2	174.13(14)
O3-Cu1-N1	149.54(10)	O2-Cu1-N1	158.91(15)

The average coordination bond angle around the Cu center of square pyramidal geometry is around 80° to 113° whereas the largest bond angle was observed for O(2)-Cu(1)- N(2) (~175°) (Table 2A.2).

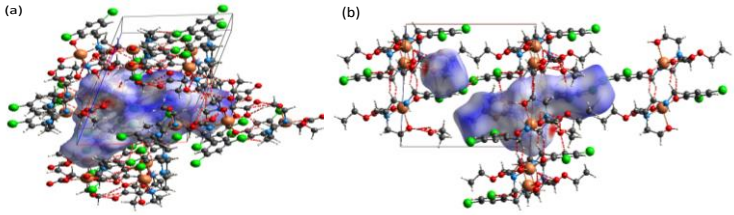

***Figure 2A. 6**. The Hirshfeld surface for (a) complex **1**, and (b) complex **2**.*

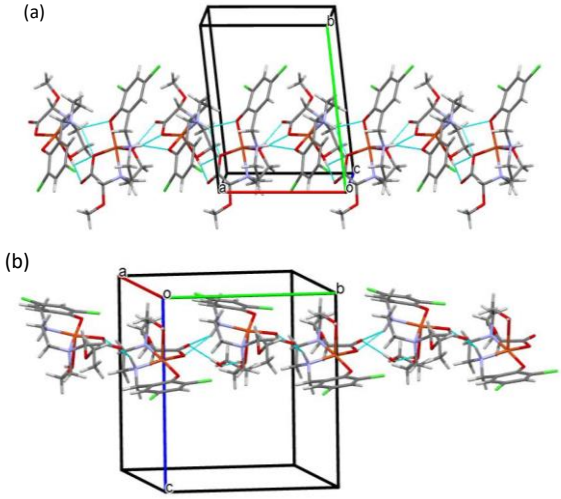

***Figure 2A. 7**. 1D polymeric extension through intermolecular H-bonding for (a) complexes **1**, and (b) complex **2**.*

The hydrogen bond interactions and close contacts in the crystal structure were visualized by carrying out the Hirshfeld surface analysis [61]. The hydrogen bond interactions were envisaged through dark red spots obtained as a result of hydrogen bond acceptors of types N-H···O, C-H···O and O-H···O (figure 2A.6(a)), red dotted lines show the H-bond) on the Hirshfeld surface of **1**. Intra- as well as inter-molecular hydrogen bonds, are exhibited by the molecule. O1-H1O···O9 and O7-H2O···O4 form strong intermolecular hydrogen bonds while N1-H1N···O6, N1-H1N···O8, N3-H2N···O2, N3-H2N···O3 and O1-H1O···O8 also forms rather strong intermolecular hydrogen bonds resulting in Type 3 1D infinite chain along *a*-axis (figure 2A.7 (a)). In complex **2**, N1-H1···O2, N1-H1···O3, O6-H6···O3 and O4-H4O···O6 form Type 3 infinite 1D chain through hydrogen bonds along *b*-axis (figure 2A.6(b) and 2A.7(b)). The details of hydrogen bonds are given in Tables 2A.3 and 2A.4.

Table 2A.3. *Hydrogen Bonds (Angstrom, Deg), for complex **1**.*

Donor--- H....Acceptor	D – H (Å)	H...A (Å)	D...A (Å)	D - H...A (°)	Symmetry Code
N1 --H1N ..O6	0.93	2.39	3.143	138	-1+x,y,z
N1 --H1N ..O8	0.93	2.17	2.956	143	-1+x,y,z
O1 --H1O ..O8	0.83	2.54	3.094	125	-1+x,y,z
O1 --H1O ..O9	0.83	1.83	2.660	175	-1+x,y,z
N3 --H2N ..O2	0.89	2.51	3.142	129	x,y,z
N3 --H2N ..O3	0.89	2.12	2.944	154	x,y,z
O7 --H2O ..O4	0.66	1.98	2.635	174	x,y,z
C4 --H4B ..O8	0.99	2.51	3.208	127	-1+x,y,z
C14 --H14A ..O4	0.98	2.46	3.062	119	Intra
C15 --H15B ..Cl1	0.99	2.73	3.491	134	x,y,z
C17 --H17A ..O1	0.99	2.58	3.242	125	1-x,-y,1-z
C28 --H28C ..O9	0.98	2.49	3.071	117	Intra

Table 2A.4. Hydrogen Bonds (Angstrom, Deg), for complex **2**.

Donor--- H....Acceptor	D – H (Å)	H...A (Å)	D...A (Å)	D- H...A (°)	Symmetry Code
N1--H1..O2	1.00	2.26	3.153	148	2-x,1/2+y,3/2-z
N1--H1..O3	1.00	2.50	3.351	143	2-x,1/2+y,3/2-z
O4--H4O..O6	0.91	1.72	2.609	165	1+x,1/2-y,1/2+z
O6--H6 ..O3	0.84	1.86	2.698	179	1-x,-y,1-z
C7 --H7B..O2	0.99	2.44	3.269	142	2-x,-y,1-z
C8 --H8B..O4	0.99	2.58	3.517	159	2-x,1/2+y,3/2-z
C13--H13A..O2	0.99	2.59	3.574(4)	174	2-x,1/2+y,3/2-z
C14--H14A..O3	0.99	2.57	3.122(7)	115	Intra

2A.3.4. Electronic spectra

Complex **1** and **2** have shown d-d absorption at 670 nm as a broad peak as expected for Cu(II) complexes with square pyramidal geometry (figure 2A.8) [62]. The other bands appeared as shoulders below 350 nm due to ligand internal transitions.

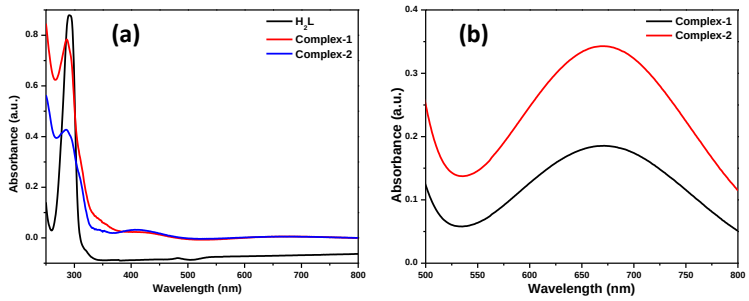

Figure 2A.8. *UV-Vis spectra in dichloromethane for (a) Ligand and Complexes, and (b) complex **1** and **2**.*

2A.3.5. Electrochemistry

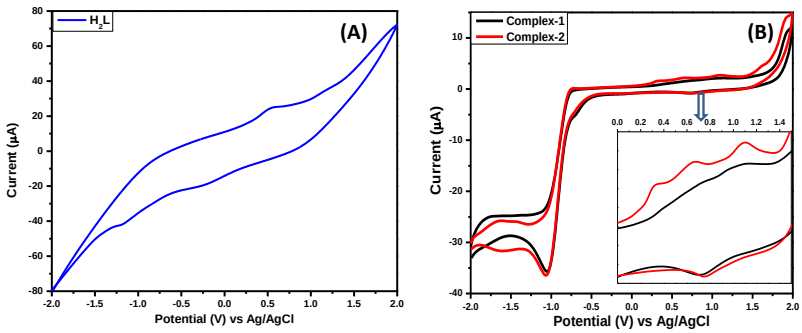

Figure 2A.9. *Cyclic voltammograms of (1.0 × 10^{-4} M) solution of (a) Ligand, **H_2L^1** and (b) complexes in CH_2Cl_2 containing 0.1 M Bu_4NPF_6 as the supporting electrolyte. The data were recorded at a scan speed of 100 mV s^{-1} at 25 °C.*

Upon oxidation of the ligand, an anodic peak at Epa = +0.55 V was observed, showing the oxidation of the phenol [63]. whereas in case of complexes shows an anodic peak around Ep_a = +1.10 V along with cathodic peaks around Ep_c = +0.739 V, revealing a quasi-reversible behavior of the complex due to the oxidation of phenolate ion to phenoxyl moiety (figure 2A.9) [24]. An irreversible cathodic peak is observed in the negative potential for both of the complexes at Epa = - 1.06 V and Epa = -1.05 respectively, which indicates the reduction of Cu (II) to Cu(I) [64].

2A.3.6. Oxidation of benzyl alcohols

Both the complexes have been tested for their abilities to catalyze the oxidation of alcohols under irradiation of visible light. Oxidation of alcohol to aldehyde and carboxylic acid is a very important reaction in organic as well as biochemistry. On the other hand photocatalysis emerged as an important tool to carry out such reaction in a more environmentally friendly condition without the application of external heat. To verify the ability of the synthesized copper complexes to catalyze the oxidation reaction of alcohols; we have tested our compounds for their activities upon irradiation with visible light (LED bulb). Both compounds have shown promising results in the oxidation reaction.

Table 2A.5. *Photocatalytic Oxidation of Benzyl Alcohol by Complex-**1**/Solvent*[a]

Entry No	Solvent	Time [h]	Conversion [%]	Selectivity [%]	Yield [%]	TON
1	DCM	3	96	99	95	95
2[b]	DCM	3	76	99	75	75
3[c]	DCM	3	96	99	98	98
4[d]	DCM	3	39	86	34	34
5	ACN	3	92	93	86	86
6	Acetone	3	92	90	83	83
7	DMF	3	90	90	81	81
8	Toluene	3	96	86	83	83
9	DMSO	3	82	80	66	66
10[e]	DCM	3	00	00	00	00

[a]*General reaction conditions: benzyl alcohol (1 mmol, 108 mg), catalyst **1** (1 mol%, 4.3 mg), TEMPO (3 mol%, 4.6 mg), solution volume (1 mL), O_2 atmosphere (balloon pressure), light intensity (12 Watt LED bulb, 400−800 nm wavelength range), room temperature (~25 °C), Stir.*[b]*light intensity (9 Watt LED bulb).*[c]*light intensity (15 Watt LED bulb).*[d]*without TEMPO.* [e]*without irradiation of light.*

To optimize the reaction conditions first benzyl alcohol has been taken as the substrate and the oxidation reaction has been tested in different solvents for

better reactivity as per Table 2A.5. The reaction was carried out under visible light (irradiated by 12 watts of the LED bulb) for 3 h at room temperature in presence of TEMPO and oxygen atmosphere. Complex **1** in dichloromethane (DCM) afforded 96% conversion of benzyl alcohol with a selectivity of 99% for benzaldehyde, (entry 1) which is the best with respect to the other solvents. The reactions are monitored through HPLC (figure 2A.10). When dichloromethane was replaced by other solvents such as acetonitrile, acetone, or N, N-dimethylformamide it afforded more than 90% conversion of benzyl alcohol with a selectivity of 90% for benzaldehyde, respectively (entries 5, 6 and 7). Toluene afforded 96% conversion of benzyl alcohol but the selectivity is less, 86% towards the benzaldehyde (entry 8). When we used dimethyl sulfoxide instead, then the conversion of benzyl alcohol goes down to 82% with a selectivity of 80% for benzaldehyde (entry 9). In the absence of light irradiation, no conversion of benzyl alcohol was observed. The photocatalytic oxidation reaction was also not observed in the absence of Cu complex. In absence of TEMPO the yield remains low (entry 4). Upon irradiation with high-energy visible light (15 watts), the percentage yield remains almost the same as with 12-watt energy (entry 3).

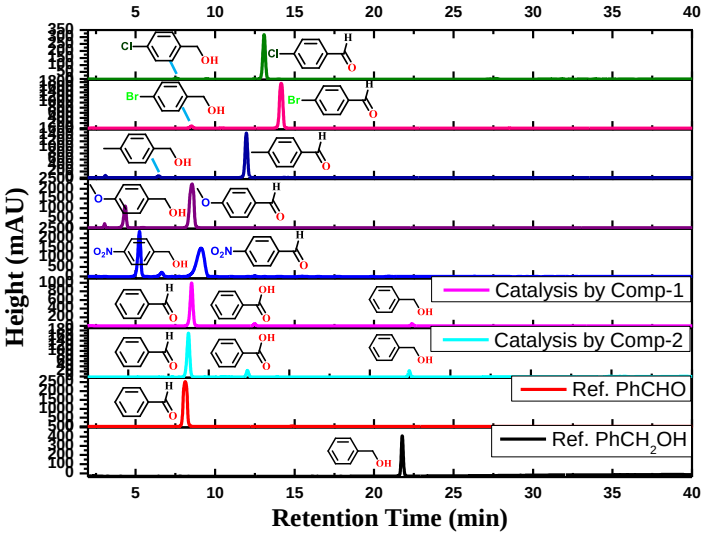

Figure 2A.10. *HPLC interpretation of some oxidation reactions after catalysis ('Ref.' signifies the standard sample).*

The scope of this photocatalytic oxidation of benzyl alcohol was further extended to a variety of substituted benzyl alcohols with catalysts **1** and **2** by using dichloromethane as the solvent for the study of substitution effects (Table 2A.6).

Table 2A.6. *Percentage conversion of substituted benzyl alcohol by homogeneous catalysts* ***1*** *and* ***2****.*

Entry	Substrates	Conversion [%]		Product	Selectivity [%]	
		1	2		1	2
1	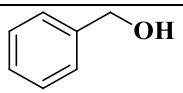	96	92	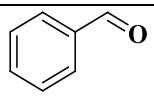	99	90
2	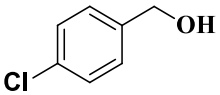	99	94	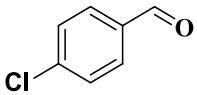	99	95
3	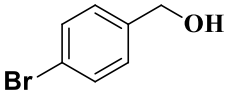	96	93	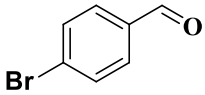	99	99
4	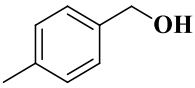	96	91	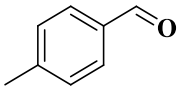	98	98
5	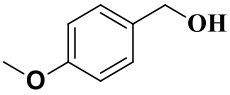	77	70	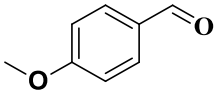	99	99
6	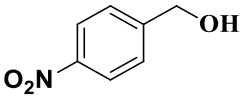	64	53	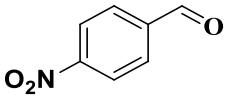	94	98

General reaction conditions: benzyl alcohol (1 mmol), catalyst ***1*** *or* ***2*** *(1 mol%), TEMPO (3 mol%), DCM (1 mL),* O_2 *atmosphere,12 Watt LEDs bulb, stir for 3h.*

The result of these photocatalytic reactions follows a regular trend according to the electronic properties of the other substituent which is attached to the phenyl ring. The conversion of a primary alcohol to aldehyde decreases with decreasing electron density at the aromatic ring. In the presence of a strong electron-withdrawing group such as nitro-, it results in lower conversion with respect to the presence of other electron-donating groups such as chloro-, bromo-, methyl- or methoxy- groups. These trends are followed in the presence of both photocatalysts **1** and **2**. 4-chloro-substituted benzyl alcohol has shown a better conversion rate with respect to 4-bromo, 4-methyl, 4-methoxy, or 4-nitro substituted benzyl alcohol as well as benzyl alcohol. In presence of photocatalyst **1**, 4-chlorobenzyl alcohol affords 99% conversion whereas 4-bromo, 4-methyl, 4-methoxy, and 4-nitro benzyl alcohol affords 96%, 96%, 77%, and 64% conversion of benzyl alcohol, respectively. Whereas in presence of photocatalyst

2, 4-chloro, 4-bromo, 4-methyl, 4-methoxy, and 4-nitro benzyl alcohol affords 94%, 93%, 91%, 70%, and 53% conversion of benzyl alcohol, respectively. In all photocatalytic reactions, the selectivity towards the formation of benzaldehyde remains higher than 95%. However, it is interesting to note that the selectivity towards the formation of a carboxylic acid obtained by over-oxidation of aldehyde remains limited to 5% in each case.

2A.3.7. Change in electronic spectra during photocatalysis

Benzyl alcohol has been taken as a substrate for alcohol oxidation, with a λ_{max} (wavelength maxima) of 256 nm ($\pi \rightarrow \pi^*$ transition) [24]. In CH_2Cl_2 solution, the catalytic mixture was subjected to perform UV–Vis analysis after 0.5 h of interval. At beginning of the catalytic reaction, the absorbance around 400 nm ($\pi \rightarrow \pi^*$ transition) due to the oxidized phenoxyl radical get sharply increased.

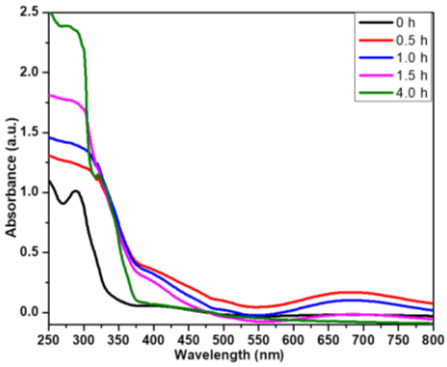

Figure 2A.11. *UV-Vis spectra of the catalytic mixture at 25°C.*

After half an hour of reaction, the absorbance around 400 nm starts to decrease with increasing time duration. At the end of the reaction, absorbance goes down to the initial position, indicating the end of the reaction (figure 2A.11). Absorbance at 290 nm increases with increasing the duration of catalysis which is assigned to the formation of benzaldehyde as an oxidized product.

In the presence of benzyl alcohol, the dichloromethane (DCM) solution of complexes **1** and **2** showed a weak anodic peak at E_{pa} = +0.744 and +0.726 V, respectively. A subtle cathodic peak at E_{pc} = +0.736 and +0.715 V was also observed due to phenoxyl to phenolate reduction, revealing the reversible behavior of the phenoxyl radical (figure 2A.12). However, the large deviation of i_{pa}/i_{pc} ratio from 1 indicates lesser reversibility of the system which might be due to the involvement of the generated phenoxyl radical in alcohol oxidation. This

result also indicates that the phenoxide ligand of the complex gets easily oxidized into phenoxyl radical in the presence of benzyl alcohol [64].

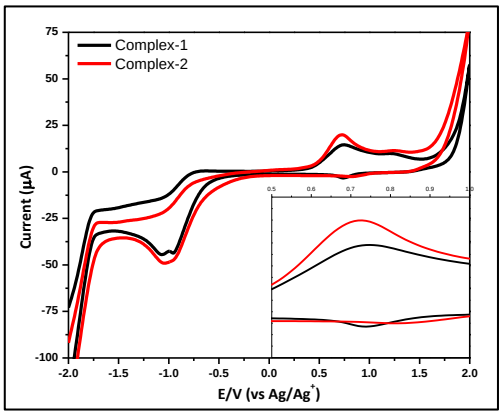

Figure 2A.12. *Cyclic voltammograms of (1.0 × 10^{-4} M) solutions of the complex with adding 50 µL of Benzyl alcohol in CH_2Cl_2 containing 0.1 M Bu_4NPF_6 as the supporting electrolyte. The data were recorded at a scan speed of 100 mV s^{-1} at 25 °C.*

2A.3.8 Mechanism for photocatalytic oxidation

The proposed simplified mechanism based on UV-Vis, CV, and ESI-MS data for benzyl alcohol oxidation is depicted in scheme 2A.3. Benzyl alcohol binds to complex A through an unshared pair of electrons of hydroxyl oxygen at the beginning of the reaction, forming B. TEMPO is converted into TEMPOH by abstract hydrogen from benzyl alcohol forms intermediate C. According to UV-Vis and CV results in the presence of visible light phenoxide ions get oxide to phenoxyl radical by donating a single electron to Cu(II) which is reduced to Cu(I) species D, which gives the desired product benzaldehyde, and E. ESI-MS spectrometry of the reaction mixture reveals a molecular ion peak at 347.32 and 536.84 indicating formation of intermediate B and C (figure 2A.13). TEMPO is regenerated from TEMPOH which leads to the formation of Cu(II) complex (A) by the oxidation of Cu(I) species in the presence of molecular oxygen under visible light irradiation.

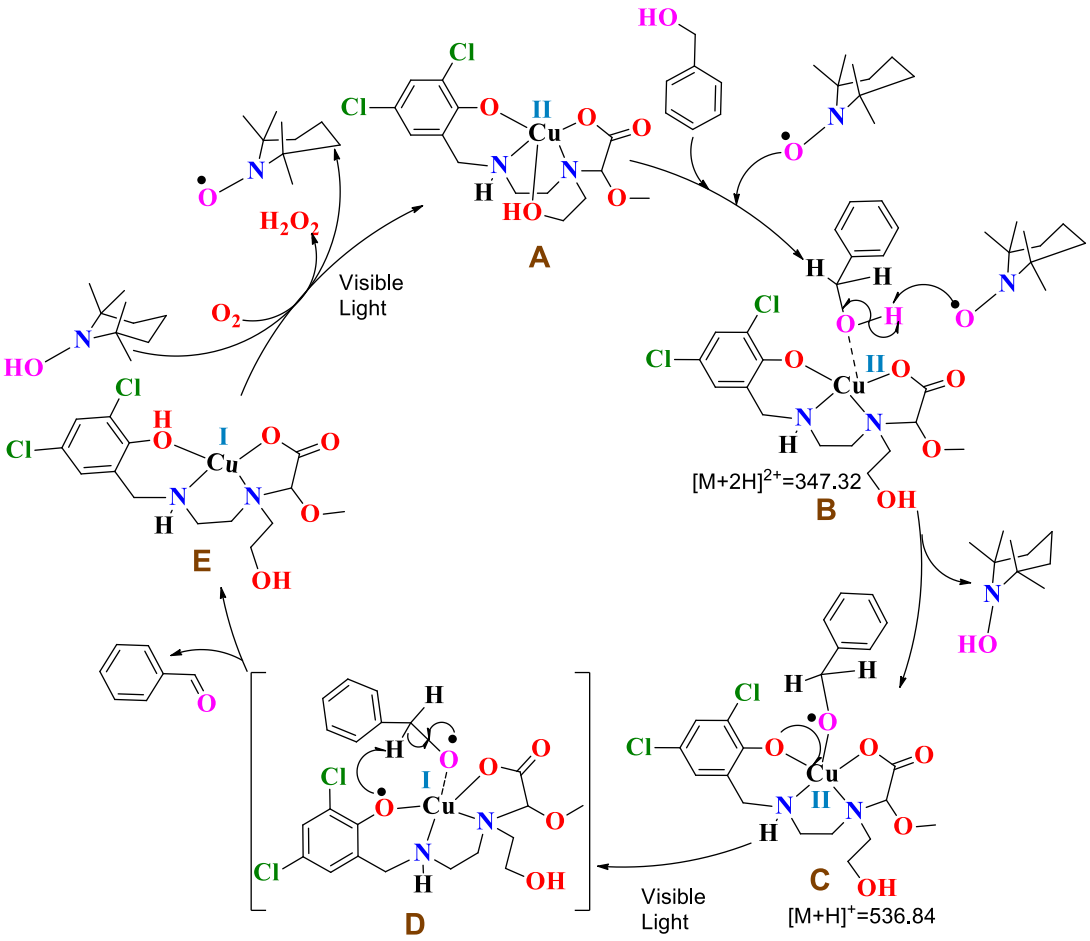

Scheme 2A.3. *Proposed mechanism for the photocatalytic oxidation of benzyl alcohol by complex* ***1****.*

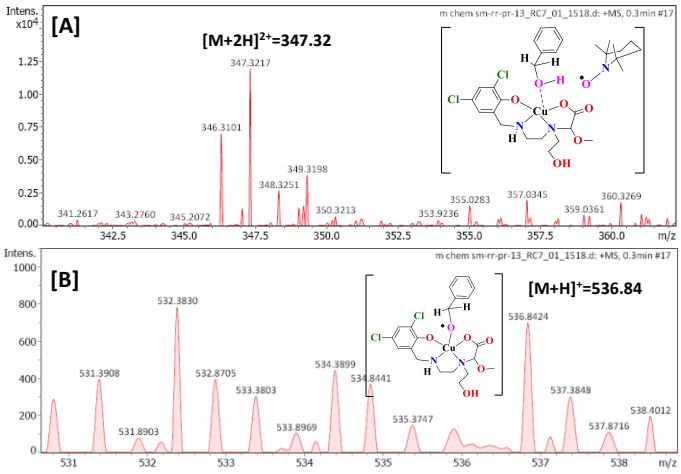

Figure 2A.13. *ESI-MS Spectrum in MeOH for complex* ***1*** *photocatalytic reaction intermediate.*

Furthermore, DFT calculations were employed to confirm and further elucidate the proposed photocatalytic oxidation mechanism (scheme 2A.3). Complex '**A**' is

the active catalyst, in which copper is present in (II) oxidation state. According to the reaction free energy profile diagram (scheme 2A.4), the free energy of (B + TEMPO) is less than the free energy of (cat A + BnOH + TEMPO), so this step is favorable. Whereas, in the second step of the mechanism 42.7 kcal/mol energy is required, this may be provided by visible light irradiation. The energy of intermediate 'C' is higher than the energy of (E + BnO) similarly in the next step the free energy of (A + TEMPO + H_2O_2) is much lower than the energy of (E + TEMPOH + O_2), therefore we can expect these steps are energetically favorable. At last, the intermediate E can be converted easily to active catalyst A for the restart of the next cycle.

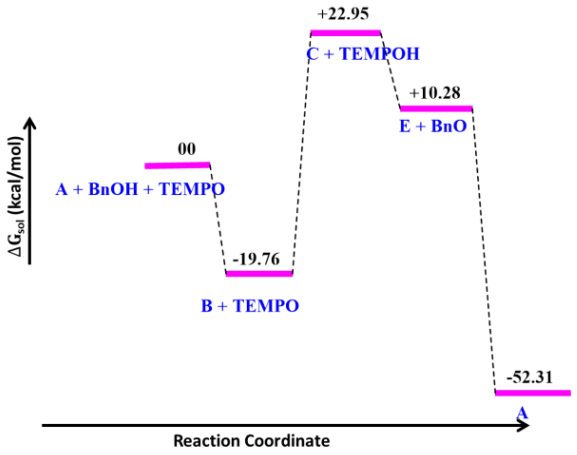

Scheme 2A.4. *Reaction-free energy profile diagram of proposed mechanism for the photocatalytic oxidation of benzyl alcohol by complex* ***1****.*

2A.3.9. Detection of hydrogen peroxide during catalysis

According to the iodometric reaction: $H_2O_2 + 2I^- + 2H^+ \rightarrow 2H_2O + I_2$ (aq.), then I^- ions may further be oxidized into I_2 in the presence of H_2O_2. An excess of iodide ions reacts with molecular iodine to produce a highly stable tri-iodide ion (I_3^-) by following a reaction: I_2(aq.) + $I^- \rightarrow I_3^-$. The rate of reaction is slow but increases with increasing concentrations of acid. However, the reaction can immediately cease with the addition of an ammonium molybdate solution. Shnyrev and co-workers have shown the characteristic bands of I_3^- are appears at 286 and 350 nm (figure 2A.14) [65]. Therefore the predominant band at 286 nm might be due to the combination of I_3^- and benzaldehyde. Hence, all the above experiments hereby support the radical mechanism pathways for catalysis [25].

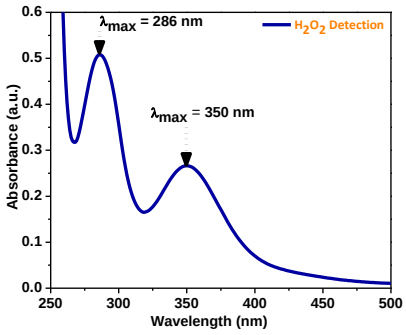

Figure 2A.14. *Detection of hydrogen peroxide in the catalytic reaction: formation of H_2O_2 (λ_{max}=350 nm) as well as PhCHO (λ_{max}=286 nm) during catalysis.*

2A.3.10. Recyclability and reusability of catalysts

Photocatalyst **1** and **2** has been tested for recyclability and reusability with benzyl alcohol as the substrate. The catalyst can be recovered almost quantitatively from DCM by filtration, washed with ether and dried in a vacuum and the molecular structure of the catalyst remain almost intact as can be seen from the PXRD pattern from before and after the reaction (figure 2A.15).

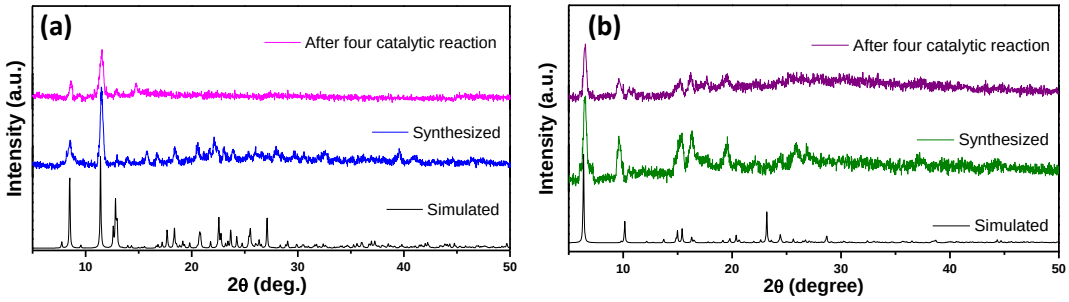

Figure 2A.15. *Powder X-ray diffraction patterns for (a) photocatalyst **1** and (b) photocatalyst **2** before and after four catalytic cycles.*

The recovered catalyst can be utilized for four cycles without much decrement of its activity (figure 2A.16) or significant change in PXRD, IR, and LCMS pattern (figure 2A.17 and 2A.18).

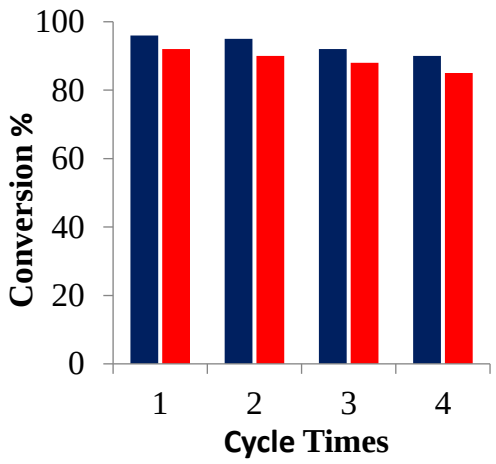

Figure 2A.16. *Recyclability of the photocatalyst* ***1*** *and* ***2****. The blue and red bar indicates the conversion of benzyl alcohol into benzaldehyde in the presence of catalysts* ***1*** *&* ***2*** *at 3 h for a separate run, respectively.*

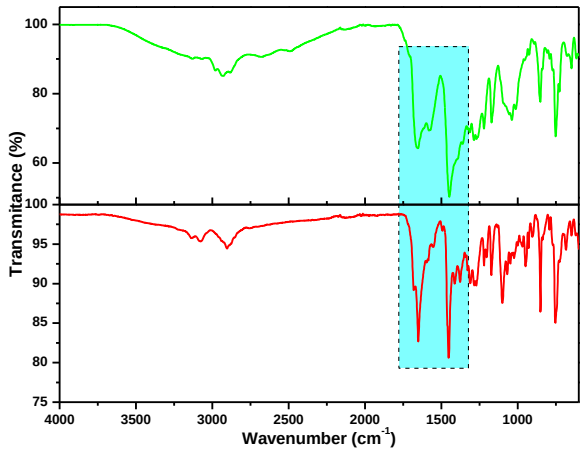

Figure 2A.17. *FTIR stretching frequencies of complex* ***1****, (a) before and (b) after the catalytic reaction.*

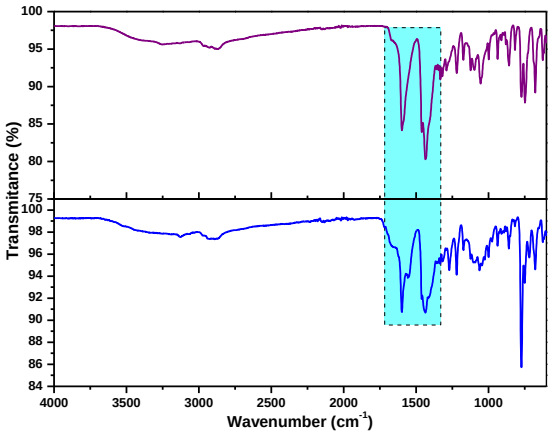

Figure 2A.18. *FTIR stretching frequencies of complex* ***2****, (a) before and (b) after the catalytic reaction.*

2A.4. Conclusions

An unprecedented piperazine ring cleavage leads to the formation of two mononuclear copper complexes **1** and **2** with square-pyramidal geometry**.** The ESI-MS spectrometric analysis indicates that the organic transformation occurs via oxidation of the piperazine ring and subsequent nucleophilic substitution reaction in α-amino ketone carbon by alcohol which propagates further through hydrolysis of amide bond resulting in piperazine ring cleavage.

Both complexes have shown their ability to act as efficient photo-catalyst to oxidize primary alcohol into the corresponding aldehyde at ambient temperature and in presence of aerial oxygen and TEMPO in an environmentally friendly manner. Photocatalyst **1** selectively produces only aldehyde with a conversion of 96% whereas photocatalyst **2** afforded up to 92% conversion in 3 h. The synthesized catalysts survived many cycles of reuse without significant loss of catalytic activity. A plausible mechanistic pathway for alcohol oxidation has been explored through ESI-MS spectrometry, cyclic voltammetry, UV-vis and computational study. TEMPO abstracted a hydrogen radical from benzyl alcohol after binding with Cu(II) center generated a benzyloxy radical. Aftrethat, in the presence of visible light phenoxide ion reduced the Cu(II) into Cu(I) by donating an electron. The phenoxyl radical abstract a hydrogrn radical from benzylic carbon, leads to the formation of product benzaldehyde. Aftreward, molecular oxygen converts the TEMPOH into TEMPO and generates active catalyst.

2A.5 Declaration:

This chapter is adapted from Appl. Organomet.Chem., 2022, 36, e6450. (DOI: 10.1002/aoc.6450)

2A.6 References

[1] Spiridonova, Y. S., Nikolaeva, Y. A., Balueva, A. S., Musina, E. I., Litvinov, I. A., Strelnik, I. D., Khrizanforova, V. V., Budnikova, Y. G. and Karasik, A. A., (2020), Ferrostatin-1 alleviates lipopolysaccharide-induced acute lung injury via inhibiting ferroptosis, Molecules, 25, 10–13.(doi:10.1186/s11658-020-00205-0)

[2] Tay, D. W. P., Nobbs, J. D., Romain, C., White, A. J. P., Aitipamula, S., Van Meurs, M. and Britovsek, G. J. P. (2020), gem-Dialkyl Effect in Diphosphine

Ligands: Synthesis, Coordination Behavior, and Application in Pd-Catalyzed Hydroformylation, ACS Catal., 10, 663–671.(DOI:10.1021/acscatal. 9b03007)

[3] Tanase, T., Urabe, M., Mori, N., Hatada, S., Noda, S.,Takenaka, H., Nakamae, K. and Nakajima, T. (2019), N-Acyclic carbene complexes supported by meso-$Ph_2PCH_2P(Ph)CH_2P(Ph)CH_2PPh_2$ (meso-dpmppm) as an asymmetric pincer ligand, J. Organomet. Chem., 879, 47–59.(DOI: 10.1016/j.jorganchem. 2018. 10.005)

[4] Kennedy, A. R., Klett, J., McGrath, G., Mulvey, R. E., Robertson, G. M., Robertson, S. D. and O'Hara, C. T. (2014), Synthesis of an alkylmagnesium amide and interception of a ring-opened isomer of the important utility amide 2,2, 6,6-tetramethylpiperidide (TMP) *Inorganica Chim. Acta*, 411, 1–4. (DOI: 10.1016/j.ica.2013.11.015)

[5] Franz, J. A., O'Hagan, M., Ho, M. H., Liu, T., Helm, M. L., Lense, S., Dubois, D. L., Shaw, W. J., Appel, A. M., Raugei, S. and Bullock, R. M. (2013), Conformational Dynamics and Proton Relay Positioning in Nickel Catalysts for Hydrogen Production and Oxidation, Organometallics, 32, 7034–7042.(DOI:10.1021/om400695w)

[6] Mukhopadhyay, S., Mandal, D., Ghosh, D., Goldberg, I. and Chaudhury, M. (2003), Equilibrium Studies in Solution Involving Nickel(II) Complexes of Flexidentate Schiff Base Ligands: Isolation and Structural Characterization of the Planar Red and Octahedral Green Species Involved in the Equilibrium, Inorg. Chem., 42, 8439–8445. (DOI: 10.1021/ic0346174)

[7] Bilyj,J. K., Silajew, N. V., Hanson, G. R., Harmer, J. R. and Bernhardt, P. V. (2019), Trivalent copper stabilized by acetylacetone dithiocarbazate Schiff base ligands: structural, spectroscopic and electrochemical properties *Dalt. Trans.*, *48*, 15501–15514.(DOI: 10.1039/c9dt02071c)

[8] Al-Jibori, S. A., Ali, S. H., Al-Janabi, A. S., Wagner, C. and Hogarth, G. (2019), Phosphine-promoted ring-opening of benzisothiazolinate ligands at a nickel(II) centre: a convenient synthesis of Ni(II)-thiolate complexes Dalt. Trans., 48, 5520–5522.(DOI: 10.1039/c9dt00953a)

[9] Liu, M. J., Yuan, J., Tao, J., Zhang, Y. Q., Liu, C. M. and Kou, H. Z. (2018), Rhodamine Salicylaldehyde Hydrazone Dy(III) Complexes: Fluorescence and

Magnetism, Inorg. Chem., 57, 4061–4069.(DOI: 10.1021/acs.inorgchem. 8b00219)

[10] Paul, G. C., Banerjee, S. and Mukherjee, C. (2017), Dioxygen Reactivity of an Iron Complex of 2-Aminophenol-Appended Ligand: Crystallographic Evidence of the Aromatic Ring Cleavage Product of the 2-Aminophenol Unit, Inorg. Chem., 56, 729–736.(DOI:10.1021/acs.inorgchem.6b01474)

[11] Das, U. K., Daifuku, S. L., Gorelsky, S. I., Korobkov, I., Neidig, M. L., Le Roy, J. J., Murugesu, M. Baker, R. T. (2016), Mononuclear, Dinuclear, and Trinuclear Iron Complexes Featuring a New Monoanionic SNS Thiolate Ligand, Inorg. Chem., 55, 987–997.(DOI: 10.1021/acs.inorgchem.5b02833)

[12] Cheaib, K., Herrero, C., Guillot, R., Banse, F., Mahy, J. P. and Avenier, F. (2017), Imidazolidine Ring Cleavage upon Complexation with First-Row Transition Metals Eur. J. Inorg. Chem., 2017, 3884–3891.(DOI: 10.1021/acs. inorgchem.5b02833)

[13] Roy, S., Banerjee, A., Lima, S., Horn, A., Sampaio, R. M. S. N., Ribeiro, N., Correia, I., Avecilla, F., Carvalho, M. F. N. N., Kuznetsov, M. L., Pessoa, J. C., Kaminsky, W. and Dinda, R. (2020), Unusual chemistry of Cu(II) salan complexes: synthesis, characterization and superoxide dismutase activity, New J. Chem., 44, 11457–11470.(DOI: 10.1039/d0nj01892a)

[14] Danopoulos,A. A., Massard, A., Frison, G. and Braunstein, P. (2018), Iron and Cobalt Metallotropism in Remote-Substituted NHC Ligands: Metalation to Abnormal NHC Complexes or NHC Ring Opening, Angew. Chemie - Int. Ed., 57, 14550–14554.(DOI:10.1002/anie.201808008)

[15] Wenz, J., Rettenmeier, C. A., Wadepohl, H. and Gade, L. H. (2016), Catalytic C-F bond activation of geminal difluorocyclopropanes by nickel(I) complexes via a radical mechanism, Chem. Commun., 52, 202–205. (DOI: 10.1039/C5CC08950F)

[16] Hao, Y., Tian, T., Kang, Y., Chang, T., Fu, X., Zhu, Z., Meng, X., Panchal, B. and Qin, S. (2020), Potassium iodide and bis(pyridylcarbamate) electrostatic synergy in the fixation reaction of CO2 and epoxides, New J. Chem., 44, 15811–15815.(DOI: 10.1039/d0nj02597f)

[17] Huang, M., Paretsky, J. and Schomaker, J. M. (2020),Rigidifying Ag(I) Complexes for Selective Nitrene Transfer, Chemcatchem., 12, 3076-3081.(DOI: 10.1002/cctc.202000336)

[18] Salzmann, K., Segarra. C. and Albrecht, M. (2020), Donor-Flexible Bis(pyridylidene amide) Ligands for Highly Efficient Ruthenium-Catalyzed Olefin Oxidation, Angew. Chem. Int. Ed., 59, 8932-8936. (DOI: 10.1002/anie.202002014)

[19] Storey, C. M., Kalpokas, A., Gyton, M. R., Krämer, T. and Chaplin, A. B. (2020), A shape changing tandem Rh(CNC) catalyst: preparation of bicyclo[4.2.0]octa-1,5,7-trienes from terminal aryl alkynes, Chem. Sci., 11, 2051–2057. (DOI: 10.1039/c9sc06153c)

[20] Falconer, R. L., Nichol, G. S., Cowley, M. J. (2019), Flexible Coordination of N,P-Donor Ligands in Aluminum Dimethyl and Dihydride Complexes, Inorg. Chem., 58, 11439–11448.(DOI: 10.1021/acs.inorgchem. 9b01061)

[21] Peng, Q., Wang, Z., Zarić, S. D., Brothers, E. N., Hall, M. B. (2018), Unrav eling the Role of a Flexible Tetradentate Ligand in the Aerobic Oxidative Carbon-Carbon Bond Formation with Palladium Complexes: A Computational Mechanistic Study, J. Am. Chem. Soc., 140, 3929–3939. (DOI: 10.1021/jacs. 7b11701)

[22] Ju,S., Yusuf, M., Jang, S., Kang, H., Kim, S. and Park, K. H. (2019), Simple Transformation of Hierarchical Hollow Structures by Reduction of Metal-Organic Frameworks and Their Catalytic Activity in the Oxidation of Benzyl Alcohol, Chem. - A Eur. J., 25, 7852–7859.(DOI: 10.1002/chem. 201900231)

[23] Paul, A., Martins, L. M. D. R. S., Karmakar, A., Kuznetsov, M. L., Da Silva, M. F. C. G., Pombeiro, A. J. L. (2020), Zn(II)-to-Cu(II) transmetalation in an amide functionalized complex and catalytic applications in styrene oxidation and nitroaldol coupling, Molecules, 25, 2644. (DOI: 10.3390/ molecules25112644)

[24] Kundu, B. K., Ranjan, R., Mukherjee, A., Mobin, S. M., Mukhopadhyay, S., (2019), Mannich base Cu(II) complexes as biomimetic oxidative catalyst, J. Inorg. Biochem., 195, 164–173.(DOI: 10.1016/j.jinorgbio.2019.03.023)

[25] Das, M., Nasani, R., Saha, M., Mobin, S. M., Mukhopadhyay, S. (2015), Ni (II) complexes with a flexible piperazinyl moiety: studies on DNA and protein binding and catecholase like properties, Dalt. Trans., 44, 2299–2310.(DOI: 10.1039/C4DT02675F)

[26] Das, M., Kundu, B.K., Tiwari, R., Mandal, P., Nayak, D., Ganguly, R. and Mukhopadhyay, S. (2018), Investigation on chemical protease, nuclease and catecholase activity of two copper complexes with flexidentate Schiff base ligands, Inorganica Chim. Acta, 469, 111–122.(DOI: 10.1016/j.ica. 2017.09.013)

[27] Kundu, B. K., Das, M., Ganguly, R., Bhobe, P. A. and Mukhopadhyay, S. (2020), Role of zeolite encapsulated Cu(II) complexes in electron transfer as well as peroxy radical intermediates formation during oxidation of thioanisole J. Catal. 389, 305-316.(DOI: 10.1016/j.jcat.2020.06.005)

[28] Chhabra,V., Kundu, B. K., Ranjan, R., Pragti, Mobin, S. M., and Mukhopadhyay, S. (2020), Coligand driven efficiency of catecholase activity and proteins binding study of redox active copper complexes, Inorganica Chim. Acta, 502, 119389.(DOI: 10.1016/j.ica.2019.119389)

[29] Malviya,N., Sonkar, C., Kundu, B. K., Mukhopadhyay, S. (2018), Disco -tic Organic Gelators in Ion Sensing, Metallogel Formation, and Bioinspired Catalysis Langmuir, 34, 11575–11585.(DOI: 10.1021/acs.langmuir.8b02352)

[30] Kundu, B. K., Chhabra, V., Malviya, N., Ganguly, R., Mishra, G. S. and Mukhopadhyay, S. (2018), Zeolite encapsulated host-guest Cu(II) Schiff base complexes: Superior activity towards oxidation reactions over homogenous catalytic systems, Microporous Mesoporous Mater. 271, 100-117.(DOI: 10.1016/ j.micromeso.2018.05.046)

[31] Ma, R., Xiao, Z., Zhong, W., Lu, C., Shen, Z., Zhao, D., Liu, X. (2021), The superiority of cuprous chloride to iodide in the selective aerobic oxidation of benzylic alcohols at ambient temperature, Appl. Organomet. Chem., 35, e6245. (DOI: 10.1002/aoc.6245)

[32] Senthilkumar, S., Zhong, W., Natrajan, M., Lu, C., Xu, B.and Liu, X. (2021), A green approach for aerobic oxidation of benzylic alcohols catalysed by CuI-Y zeolite/TEMPO in ethanol without additional additives, New J. Chem., 45, 705-713.(DOI: 10.1039/d0nj03776a)

[33] Yang, Y., Zhong, W., Ma, R., Lu, C., Shen, Z., Liu, X., Zhang, S., Wang, H. (2021), Engineering the surface of cuprous oxide via surface coordination for efficient catalysis on aerobic oxidation of benzylic alcohols under ambient conditions, Appl. Surf. Sci., 543, 148840.(DOI: 10.1016/j.apsusc.2020.148840)

[34] Sutradhar, M., Alegria, E. C. B. A., Barman, T. R., Guedes da Silva, M. F. C., Liu, C. M. and Pombeiro, A. J. L. (2020), Supramolecular photothermal nanomedicine mediated distant tumor inhibition via PD-1 and TIM-3 Blockage, Front. Chem., 8, 1–10.(DOI: 10.3389/fchem.2020.00001)

[35] Xu, B., Senthilkumar, S., Zhong, W., Shen, Z., Lu, C. and Liu, X. (2020), Magnetic core-shell Fe_3O_4@Cu_2O and Fe_3O_4@Cu_2O-Cu materials as catalysts for aerobic oxidation of benzylic alcohols assisted by TEMPO and N-methylimidazole, RSC Adv., 10, 26142–26150.(DOI: 10.1039/d0ra04064a)

[36] Lai, Y. L., Wang, X. Z., Dai, R. R., Huang, Y. L., Zhou, X. C., Zhou, X. P. and Li, D. **(**2020), Self-assembly of mixed-valence and heterometallic metallocycles: Efficient catalysts for the oxidation of alcohols to aldehydes in ambient air, Dalt. Trans., 49, 7304–7308.(DOI: 10.1039/d0dt01340d)

[37] Liu, Z., Shen,Z., Zhang, N., Zhong, W., Liu, X. (2018), Aerobic Oxidation of Alcohols Catalysed by Cu(I)/NMI/TEMPO System and Its Mechanistic Insights, Catal. Lett., 148, 2709.(DOI: 10.1007/s10562-018-2485-2)

[38] Zhang, Z., Zhong, W., Wei, Z., Liu Z. and Liu, X. (2017), Roles of phenol groups and auxiliary ligand of copper(II) complexes with tetradentate ligands in the aerobic oxidation of benzyl alcohol, Dalt. Trans., 46, 8286-8297.(DOI: 10.1039/C7DT01716B)

[39] Nasani, R., Saha, M., Mobin, S. M., Martins, L. M. D. R. S., Pombeiro, A. J. L., Kirillov A. M. and Mukhopadhyay, S. (2014), Copper–organic frameworks assembled from in situ generated 5-(4-pyridyl)tetrazole building blocks: synthesis, structural features, topological analysis and catalytic oxidation of alcohols. Dalt. Trans., 43, 9944–9954.(DOI: 10.1039/c4dt00531g)

[40] Dong, Y., Su, Y., Hu, Y., Li, H. and Xie, W. (2020), Ag2S-CdS p-n Nanojunction-Enhanced Photocatalytic Oxidation of Alcohols to Aldehydes. Small., 2001529.(DOI: 10.1002/small.202001529)

[41] Shi, Z., Qu, X., Dai, J., Zou, H., Zhang, Z., Wang, R., Qiu, S. (2021), Photoactive amphiphilic nanoreactor: A chloroplast-like catalyst for natural oxidation of alcohols, Chem. Eng., 408, 127243. (DOI: 10.1016/j.cej.2020. 127243)

[42] Zhu, X., Liu, C., Liu, Y. , Yang, H.,Fu, H. (2020), A sodium trifluoromethanesulfinate-mediated photocatalytic strategy for aerobic oxidation of alcohols, Chem. Commun., 56, 12443–12446.(DOI: 10.1039/D0CC05799A)

[43] Sun, D., Li, P., Wang, X., Wang, Y., Wang, J., Wang, Y., Lu, Y. , Duan, L. , Sarina, S., Zhu, H. , Liu, J. (2020), Heterogeneous photocatalytic anaerobic oxidation of alcohols to ketones by Pt-mediated hole oxidation, Chem. Commun., 56, 11847–11850.(DOI: 10.1039/D0CC03325A)

[44] Luo, S., Zeng, Z., Zeng, G., Liu, Z., Xiao, R., Chen, M., Tang, L., Tang, W., Lai, C., Cheng, M., Shao, B., Liang, Q., Wang, H., Jiang, D. (2019), Metal Organic Frameworks as Robust Host of Palladium Nanoparticles in Heterogeneous Catalysis: Synthesis, Application, and Prospect, ACS Appl. Mater. Interfaces., 11, 32579–32598.(DOI: 10.1021/acsami.9b11990)

[45] Meng, C., Yang, K., Fu, X.,Yuan, R. (2015), Photocatalytic Oxidation of Benzyl Alcohol by Homogeneous $CuCl_2$/Solvent: A Model System to Explore the Role of Molecular Oxygen, ACS Catal., 5, 3760–3766.(DOI:10.1021/ acscatal. 5b00644)

[46] Zhou, J., Huang-Fu, X., Huang, Y. Y., Cao, C. N., Han, J., Zhao, X. L., Chen, X. D. (2020), Metal–Organic Framework Based on Heptanuclear Cu–O Clusters and Its Application as a Recyclable Photocatalyst for Stepwise Selective Catalysis, Inorg. Chem., 59, 254-263.(DOI: 10.1021/acs. inorgchem.9b02084)

[47] Frisch, M. J. et al., Gaussian Revision D.01, Gaussian, Inc., Wallingford CT, 2013.

[48] Frisch, M. J., Trucks, G. W., Schlegel, H. B., Scuseria, G. E., Robb, M. A., Cheeseman, J. R., Scalmani, G., Barone, V., Mennucci, B., Petersson, G. A., et al. Gaussian 09, revision A.02; Gaussian, Inc.: Wallingford, CT, 2009.

[49] Lee, C., Yang, W., Parr, R. G. (1988), Development of the Colle-Salvetti correlation-energy formula into a functional of the electron density, Phys. Rev. B: Condens. Mater. Phys. 37, 785-789.(DOI: 10.1103/PhysRevB. 37.785)

[50] Becke, A. D. (1993), A new mixing of Hartree-Fock and local-density-functional theories, J. Chem. Phys. 98, 1372−1377.(DOI: 10.1063/1.464304)

[51] Becke, A. D. (1988), Density-functional exchange-energy approximation with correct asymptotic behavior, Phys. Rev. A, 38, 3098–3100.(DOI: 10.1103/PhysRevA.38.3098)

[52] Becke, A. D. (1993), Density-functional thermochemistry. III. The role of exact exchange, J. Chem. Phys., 98, 5648–5652.(DOI: 10.1063/1.464913)

[53] Becke, A. D. (1997), Density-functional thermochemistry. V. Systematic optimization of exchange-correlation functionals, J. Chem. Phys., 107, 8554–8560.(DOI: 10.1063/1.475007)

[54] Sheldrick, G. (2008), A short history of SHELX, Acta Crystallographica Section A, 64, 112-122.(DOI: 10.1107/S0108767307043930)

[55] khusnutdinova, J. R., Ben-David, Y. and Milstein, D. (2014), Oxidant-Free Conversion of Cyclic Amines to Lactams and H2 Using Water As the Oxygen Atom Source, J. Am. Chem. Soc., 136, 2998–3001.(DOI: 10.1021/ja500026m)

[56] Griffiths, R. J., Burely, G. A. and Talbot, Eric P. A. (2017), Transition-Metal-Free Amine Oxidation: A Chemoselective Strategy for the Late-Stage Formation of Lactams, Org. Lett., 19, 870–873.(DOI: 10.1021/acs. orglett.7b00021)

[57] Moehrle, H. and Azodi, K. (2006), Piperazines as model substrates for oxidations, Pharmazie, 61, 815–822. (https://pubmed.ncbi.nlm.nih.gov/ 17069419)

[58] Christina Chai, L. L., Elix, John A. and Huleatt, Paul B. (2005),The synthetic versatility of alkoxycarbonyl- and hydroxymethyl-piperazine-2,5-diones, Tetrahedron, 61, 8722–8739.(DOI: 10.1016/j.tet.2005.06.084)

[59] Ahmed Farghaly and Salwa A.Elgebaly, (2006), PCT Int. Appl. 13th July, 2006073923.

[60] Crans, D. C., Tarlton, M. L. and McLauchlan, C. C. (2014), Trigonal Bipyramidal or Sqare pyramidal Coordination Geometry? Investigation the Most potent Geometry for Vanadium Phosphatase Inhibitors, Eur. J. Inorg. Chem., 2014(27), 4450-4468.(DOI: 10.1002/ejic.201402306)

[61] Spackman, M. A. and Jayatilaka, D. (2009), Hirshfeld surface analysis, CrystEngComm, 11, 19–32.(DOI: 10.1039/B818330A)

[62] Roy, S., Sarma, M. J., Kashyap, B. and Phukan, P. (2016),A quick Chan-Lam C-N and C-S cross coupling at room temperature in the presence of square pyramidal [Cu(DMAP)4I]I as a catalyst, Chem. Commun., 52, 1170–1173.(DOI: 10.1039/C5CC04619J)

[63] Dutta, S., Biswas, S., Maji, R. C. and Saha, R. (2018), Environmentally Sustainable Fabrication of Cu1.94S-rGO Composite for Dual Environmental Application: Visible-Light-Active Photocatalyst and Room-Temperature Phenol Sensor, ACS Sustainable Chem. Eng. 6, 835–845.(DOI: 10.1021/ acssuschemeng.7b03186)

[64] Sénèque, O., Campion, M., Douziech, B., Giorgi, M., Mest, Y. L. and Reinaud, O. (2003), Supramolecular control of an organic radical coupled to a metal ion embedded at the entrance of a hydrophobic cavity, Dalton Trans., 22, 4216– 4218.(DOI: 10.1039/B308255E)

[65] Kireev, S. V. and Shnyrev, S. L. (2015), Study of molecular iodine, iodate ions, iodide ions, and triiodide ions solutions absorption in the UV and visible light spectral bands, Laser Phys. 25, 075602.(DOI: 10.1088/1054-660X/25/7/075602)

Chapter 2B

Picric acid detection by a hexanuclear Cu(II) complex synthesized through N,O-donor ligand transformation.

Chapter 2B

Picric acid detection by a hexanuclear Cu(II) complex synthesized through N,O-donor ligand transformation

2B.1 Introduction

The employment of multidentated ligand system can make it possible to synthesize a wide range of metal complexes with various structures. Among various chelateing ligands, piperazine ring can show intersesting coordination properties by adopting either chair or boat confirmation and acting as mono- or bi-dentate mode cosidering the reaction conditions and the nature of metal ion involved [1, 2]. Sometimes, it can act as a bridging ligand as well [3]. The piperazine ring with aromatic and/or aliphatic arm can also act as a chelating and/or as bridging ligand [2]. The hydroxyl-group containing ligands with other donor sites like nitrogen are used to synthesize complexes with structural diversity [4-7]. Coordination chemists frequently employ the self-assembly synthetic strategy using transition metal cations and multidentate ligands because this approach produces an extensive range of fascinating structures with multiple metal centers. Researchers are more interested in these complexes because of their high nuclearity and the interaction that can occur between the metal cations [8-10].

On the other hand the development of explosive materials was started with invention of gunpowder and dynamite. These are extensively used in mining, military exercises, civil construction, rocket propellant, etc. Due to terror attacks, such explosives have become a threat to human civilization. The common chemical components of frequently used explosives are nitro-aromatics, such as 2,4,6-trinitrotoluene (TNT), 2,4-dinitrophenol (2,4-DNP) and 2,4,6-trinitrophenol/picric acid (TNP/PA). Furthermore nowadays, picric acid is being used in industries like pharmaceuticals, the production of rocket fuels, dye and leather industries, chemical laboratories, etc [11, 12]. It has an extremely high solubility in water and contaminates the groundwater easily upon exposure affecting human and animal health. PA causes diseases such as nausea, anemia, asphyxiation, vomiting, sycosis, damaged liver malfunction, skin/eye itching, and

chronic diseases such as cyanosis and cancer [13-16]. In groundwater, up to 0.001 mg L^{-1} of picric acid is the acceptable tolerance level [17]. From the environmental safety and security screening point of view, there is a need to develop an efficient methodology to detect the trace amount of PA.

Various researchers have developed various instrumental techniques to detect nitroaromatic compounds (NACs) so far [18-20]. Due to its high sensitivity, quick response time, low cost, mobility and simple sample preparation, the fluorescence-based technique has emerged as a potential tool to detect the NACs [21-24]. Numerous fluorescence sensors, including small molecules [25-28], MOFs [29-31], polymers [32-34], gels [35, 36], and discrete macro cycles /cages [37, 38], etc., have been reported in the literature in this regard. The N, O-donor ligand systems can also play an important role to generate luminescent metal complexes [39, 40]. Though the number of luminescent Cu(II) complexes are comparatively less in literature, few reports are available and it has been found that in all these cases at least one of the donor atom is attached with the aromatic systems [41-44].

This chapter presents one hexanuclear copper complex made out of ligand $\mathbf{H_2L^1}$ where the phenolic arm is purposefully incorporated in the ligand system. Upon reaction with copper(II) acetate in n-butanol an unprecedented piperazinyl ring cleavage and rearrangement into a five-membered ring has been observed with further organic transformation to yield $[Cu(HL_c^1)]_6$ **3** [$\mathbf{H_3L_c^1}$ = 1-(3,5-dichloro-2-hydroxybenzyl)-3-(2-hydroxyethyl)imidazolidine-2-carboxylic acid] [scheme 2B. 2]. Compound **3** has been found to be fluorescent in nature and the sensing ability of the complex towards the nitroaromatics is explored herewith.

2B.2 Experimental

2B.2.1 Materials and methods

All the chemical reagents are purchased from sigma and used without further purification. The specifications of all the instruments used for analytical purposes were the same as described in section 2A.2.1 of the previous chapter 2A. The ligand $\mathbf{H_2L^1}$ synthesis is also described in section 2A.2.3 of the previous chapter 2A.

2B.2.2 X-ray crystallography

Table 2B. 1. *Crystallographic data and structure refinement parameters for* ***3****.*

Complex	3
Empirical Formula	$C_{78}H_{84}Cl_{12}Cu_6N_{12}O_{24}$
Formula weight	2380.27 g/mol
Crystal system	trigonal
Space group	R-3 (No. 148)
a (Å)	25.0144(18)
b (Å)	25.0144(18)
c (Å)	17.2665(10)
α (°)	90
β (°)	90
γ (°)	120
V ($Å^3$)	9356.5(17)
λ (Å)	0.71073
ρcalcd (g cm^{-3})	1.267
Z	3
T (K)	100
μ (mm^{-1})	1.320
F(0 0 0)	3618
Crystal size (mm^3)	0.04 × 0.12 × 0.18
θ ranges (°)	2.2 to 26.4
h/k/l	-31,27/-29,29/-18,21
Reflections collected	4253
Independent reflections	233
Tmax and Tmin	0.949 and 0.827
R indices (all data)	R1 = 0.1038, wR2 = 0.3433
Largest peak and hole (e $Å^{-3}$)	-0.60 and 1.64

Single crystal X-ray structural studies of **3** were performed following a similar protocol as mentioned in section 2A.2.2 of previous chapter 2A. The crystal refinement data are summarized in Table 2B.1

2B.2.3 Synthesis of the complex $[Cu(HL_c^1)]_6$ (3)

A butanolic 8 mL solution of $Cu(OAc)_2.H_2O$ (0.07 g; 0.35 mmol) was added drop-wise into an 8 mL butanolic solution of $\mathbf{H_2L^1}$ (0.106 g; 0.35 mmol) and triethylamine (50 μL; 0.35 mmol). The resulting green solution was stirred for 4 hrs at room temperature. After that, the volume of the reaction mixture was reduced to 6 mL by evaporating in vacuo. It was then left for slow evaporation after filtration. Finally, after two weeks, dark green square-shaped crystals were obtained. Crystals were collected by separation followed by washing with diethyl ether. Anal. Calcd (%) for $C_{78}H_{84}Cl_{12}Cu_6N_{12}O_{24}$: C, 39.36; H, 3.56; N, 7.06. Found (%): C, 39.34; H, 3.58; N, 7.05; FTIR (υ in cm^{-1}): 3310–3165 {υN-H,O-H (s); 2980–2810 {υC-H, (m)}; 1600-1528 {υC=C and υC=O (s)}; 1470-1360 {υC=O (s)} 1340–990 {υC-N, C-O (s)}; 780-670 { υC-Cl, (d)} (figure 2B.1). Yield 75%

2B.2.4 Preparation of solutions for photophysical studies

To record UV-Vis spectra, 1.0 mM solution (working solution) was prepared by dissolving 0.002 mmol of complex **3** (4.76 mg) in 2 mL of MeOH. 20 μL of the working solution was diluted up to 2 mL by the solvent to get 10 μM solution and UV-Vis spectra of the resultant solution were recorded.

A similar procedure was followed for the preparation of the solution of nitro aromatics according to the experimental requirement. Furthermore, the concentration of complex sometimes selectively has chosen according to the experimental requirement during PL spectroscopy.

2B.2.5 Fluorescence titrations

20 μL of stock solution (as prepared above) of complex **3** was taken in a cuvette followed by the addition of 2.98 mL of solvent to obtain a 10 μM resultant solution. Nitro aromatic solution (5 mM) of 2.0-20 μL was then mixed with each 10 μM complex solution. Reasonable spectral change in the fluorimeter was recorded for every single experiment within a short time window (<1 min). It shows that quenching in fluorescence intensity proportionally with the increase of nitro aromatic concentration at room temperature.

2B.2.6 Limit of detection for picric acid

To calculate the LOD value, Eqn. (i) given as per the following is used [45].

Detection limit (DL) = 3.3σ/ k …… (i)

Where σ is the standard deviation (S_d) of complex **3**, and k denoted the slope, obtained from the plot of PL intensity changes versus the concentration of picric acid. The fluorescence intensity of the solution of **3** was recorded several times to calculate the standerd deviation.

2B.3 Results and discussion

2B.3.1 Synthesis and Characterization

Upon reaction of (**H_2L^1**) with $Cu(OAc)_2.H_2O$ in n-butanol a green-colored solution was obtained which upon further concentration furnished green square-shaped crystals of $[Cu(HL_c^1)]_6$ **(3)** (scheme 2B.1.).

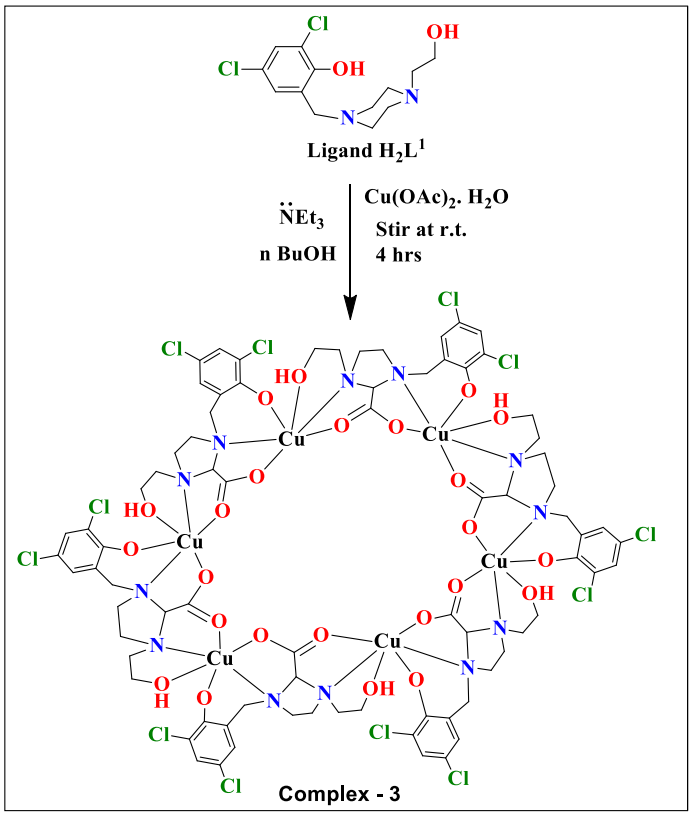

Scheme 2B.1. *Synthesis of Complexes **3**.*

Complex **3** has been characterized by singly crystal X-ray crystallography and elemental analysis. The bands appeared in the region of 1530-1610 cm^{-1} and 1370-1450 cm^{-1} in the FTIR spectra of the complex suggest the presence of

antisymmetric and symmetric vibrations of the bridging carboxylate group of the ligand (figure 2B.1).

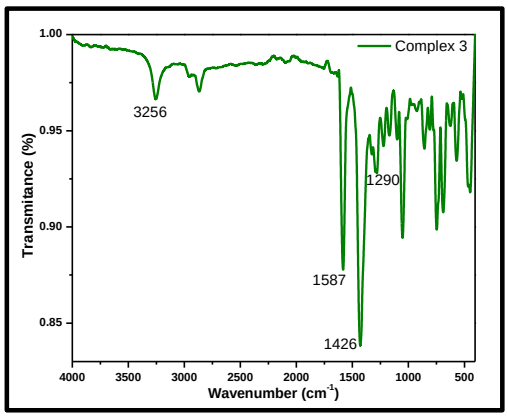

Figure 2B.1. *FTIR spectrum of* ***3****.*

2B.3.2 Investigation on the mechanistic pathway of ligand transformation

The synthesis reaction was monitored through ESI-MS spectrometry in thirty mins of the interval, to get a better understanding about the ligand transformation in the presence of copper acetate (figure 2B.2).

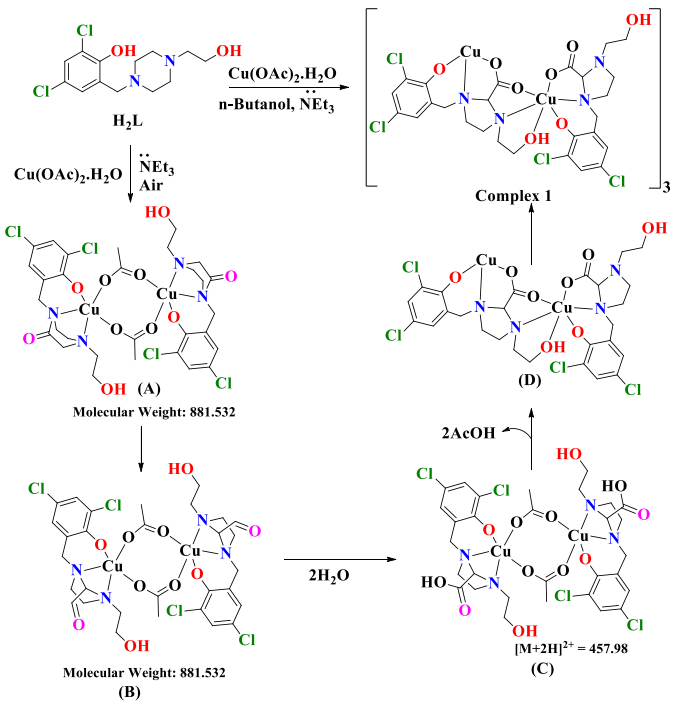

Scheme 2B.2. *Mechanistic pathway for the formation of complex-3.*

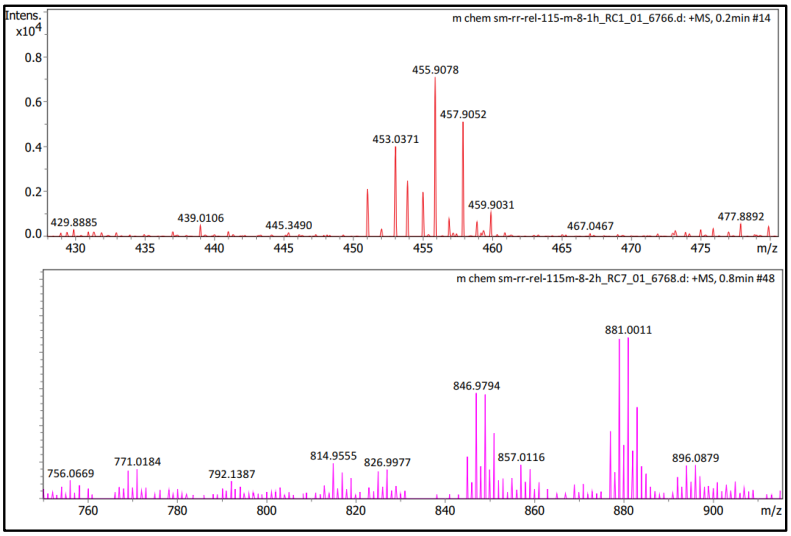

***Figure 2B.2**. ESI-MS spectrum in MeOH for complex-**3** reaction intermediates*

Some intermediate fragments have been identified and given in scheme 2B.2. However, it is very difficult to propose the complete mechanism from this data and further detailed investigation is required for that.

2B.3.3 Structural description of the complex (3)

With the help of single-crystal X-ray crystallographic techniques, the solid-state structure of the complex has been confirmed. The ball and stick structural presentation of the crystal is shown in figure 2B.3 and refinement parameters are described in Table 2B.1 and the selected bond angles and distances are described in Table 2B.2. Complex **3** crystallizes in trigonal space group R-3.

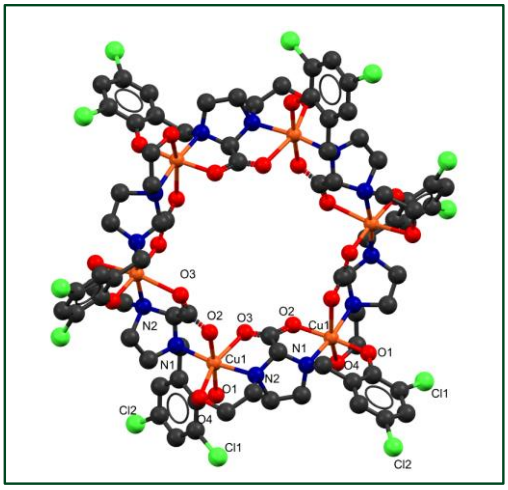

***Figure 2B.3.** The solid state crystal structure of complex **3**, hydrogen atoms are omitted for clarity*

The crystallographic data revealed that six Cu^{2+} ions are present in the macrocyclic compound. The deprotonated ligand (HL_c^1) links between two Cu(II) centers through the carboxylate and imidazolidine bridge. The two nitrogen atoms of the imidazolidine ring are coordinated with two different Cu(II) ions. The ligand bridges between two Cu(II) ions by two different oxygen atoms of the carboxylate group.

. The transformed deprotonated ligand coordinates hexadentately, and forms four chelate rings (one six-membered and three five-membered). All the Cu(II) ions in this complex are shows the distorted octahedral geometry around it and formed a cavity. The diameter of the cavity is 8.299 Å (figure 2B.4A).

Table 2B. 2. *Selected bond lengths (Å) and bond angles (°) for* ***3****.*

Complex	**3**
Cu(1)-O(1)	1.890(11)
Cu(1)-N(1)	2.019(7)
Cu(1)-N(2)	2.092(7)
Cu(1)-O(2)	1.917(10)
Cu(1)-O(3)	2.289(8)
Cu(1)-O(4)	2.421(14)
O(1)-Cu(1)-O(2)	174.8(4)
O(1)-Cu(1)-N(1)	94.8(4)
O(2)-Cu(1)-N(1)	84.6(3)
O(1)-Cu(1)-N(2)	89.4(4)
O(2)-Cu(1)-N(2)	91.8(4)
O(4)-Cu(1)-N(2)	81.1(6)
O(1)-Cu(1)-O(3)	96.2(4)
N(1)-Cu(1)-N(2)	171.6(4)
O(4)-Cu(1)-N(1)	104.2(6)
O(1)-Cu(1)-O(4)	109.6(8)
O(2)-Cu(1)-O(3)	89.0(4)
O(1)-Cu(1)-O(4)	65.7(8)
O(3)-Cu(1)-N(1)	94.5(3)
O(3)-Cu(1)-N(2)	77.8(3)
O(3)-Cu(1)-O(4)	146.3(7)

The cooperative hydrogen bonding interactions of the ligand is pivotal for the formation of self-assemble extended structure of the macrocycles. In this structure, macrocycles are stacked in alternating a-b-c fashion. They form 24

hydrogen bonds per macrocycle (four per ligand) with its six neighboring units within the structure (figure 2B.4).

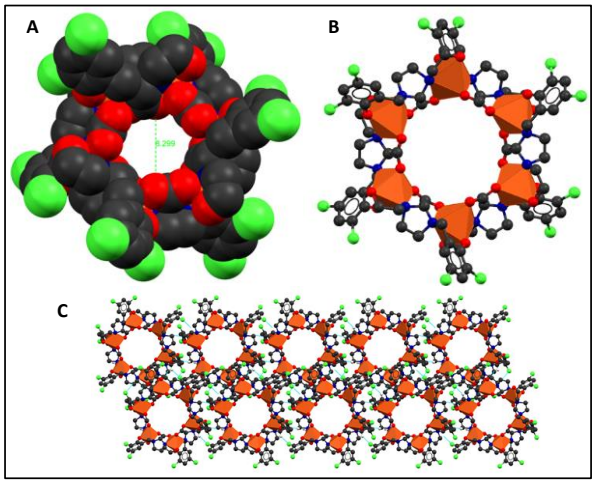

Figure 2B.4. *Top view of (A) space-filling model, (B) polyhedral model and (C) 2D- packing structure.*

The powder X-ray diffraction (PXRD) pattern of complex **3** is similar to the simulated pattern of the crystallographic data, which confirms the bulk synthesis of the complex **3** (figure 2B.5).

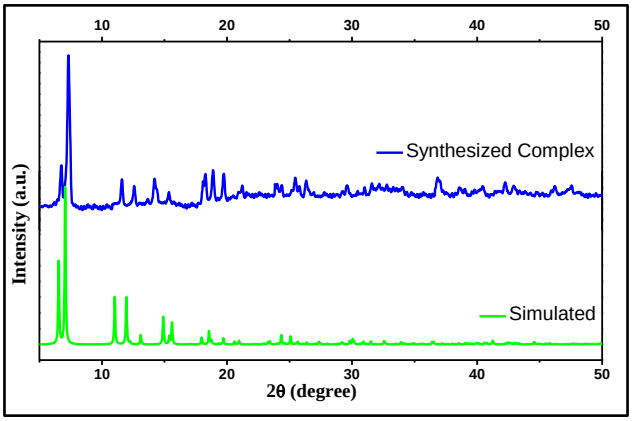

Figure 2B.5. *Powder X-ray diffraction pattern for complex **3**.*

2B.3.4. Electronic spectra

A broad band at 640 nm corresponds to the d-d absorption, indicates the octahedral geometry of the complex **3** (figure 2B.6) [46]. Internal transitions of the ligand are responsible for the shoulders at 395 and 285 nm.

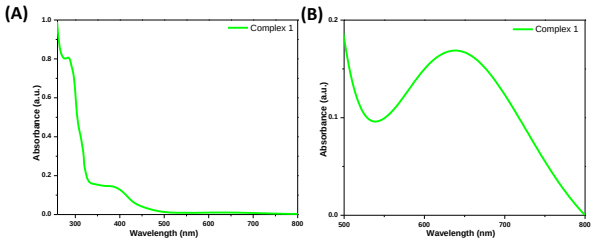

***Figure 2B.6**. UV-Vis spectra in MeOH of Complexes **3**.*

2B.3.5. Photophysical studies

The solvatochromic properties of complex **3** with known common solvents have been tested at room temperature. In MeOH, complex **3** shows luminescent properties. The fluorescence spectrum of complex **3** in methanol exhibits strong transitions at 400 and 425 nm with a shoulder peak at 448 nm (figure 2B.7A).

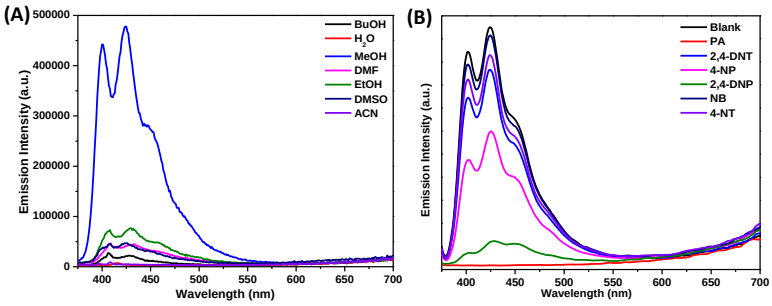

***Figure 2B.7.** Fluorescence spectra of complex **3** (10 μM) (A) in the presence of different solvent (B) in the presence of (0.1 mM) nitroaromatics in H_2O solvent.*

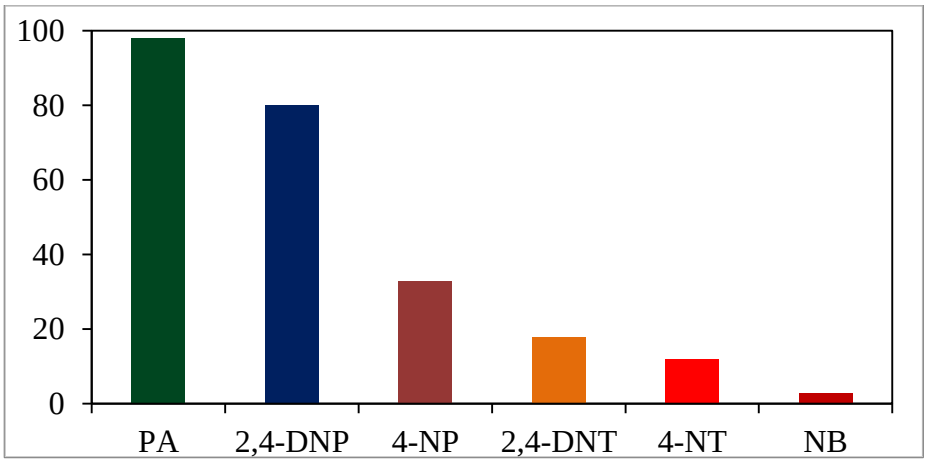

***Figure 2B.8.** The luminescence quenching efficiencies of **3** in the presence of other analytes.*

PA, 4-nitrotoluene (4-NT), 2,4-dinitrophenol (2,4-DNP), 2,4-dinitrotoluene (2,4-DNT), 4-nitrophenol (4-NP), nitrobenzene (NB) were selected to explore the sensing ability of complex **3**. First, the fluorescence emission of the complex **3** was measured in the MeOH with the addition of other analytes to better grasp the capability of the complex to detect the nitroaromatics. Upon the addition of ten equivalents of PA, the fluorescence intensity of **3** was quenched ~97% (figure 2B.7B). In the following order, PA > 2,4-DNP > 4-NP > 2,4-DNT > 4-NT > NB, the other analytes are found to have much lower quenching efficiency than the PA (figure 2B.8). The fluorescence intensity of the methanolic solution of **3** is got interestingly affected in different ways by different aromatic compounds depending on the electronic factor.

When analytes such as 2,4-DNT, NB and 4-NT were added, the fluorescence intensity of solution of **3** remains almost unchanged, but there was a notable quenching of fluorescence intensity was observed upon the addition of nitrophenols. Among nitrophenols, the PA shows drastic quenching efficiency than others.

2B.3.6. Calculation of quenching efficiency and detection limit

To measure the luminescence quenching efficiency of **3**, a series of emission spectra are recorded with the increasing concentration of PA (figure 2B.9a). The Stern-Volmer (S-V) equation ($K_{sv}[Q] + 1 = I_0/I$) was used to calculate the quenching efficiency. Where K_{sv} is the quenching constant (M^{-1}), Q is the quencher concentration, I_0 and I are the fluorescence intensity in the absence and presence of the quencher respectively [16, 47].

K_{sv} for PA is calculated from the linear fitting of the plot is 9.8×10^4 M^{-1}, which illustrates the high quenching capability of **3** towards the PA (figure 2B.9). To examine the sensitivity of **3**, the fluorescence quenching experiment was carried out at a low concentration of PA.

Table 2B. 3 *Comparison of the detection of PA by luminescent* $[Cu(HL_c^1)]_6$ ***(3)*** *with the other reported data*

S. No.	material	K_{sv} (M^{-1})	detection limit	reference
1	Zn-TDPAT MOF	NA	4×10^{-4} M	48
2	Cd-NDC MOF	3.5×10^{4}	NA	49
3	Zr-MOF	5.8×10^{4}	NA	50
4	$[Cd(NDC)(H_2O)]_n$	2.385×10^{4}	4×10^{-6} M	51
5	$\{[Cd_4(L)_2(L_2)_3(H_2O)_2].8DMF.8H_2O\}_n$	3.84×10^{4}	8.6×10^{-6} M	52
6	$Zn_2L_2(NO_3)_4$ and $Ag_2L_2(BF_4)_2$	1.52×10^{3} and 1.01×10^{3}	6.38×10^{-4} M and 6.72×10^{-4} M	37
7	Cu(II)-MOF	1.3×10^{5}	2.7×10^{-6} M	53
8	Cu(II)-(HBU-166) MOF	7.3×10^{4}	3.19×10^{-3} M	54
9	$[Cu(Biphen)(Meim)(H_2O)]$	3.49×10^{4}	14×10^{-6} M	44
10	$[Cu(HL_c^1)]_6$	9.8×10^{4}	3×10^{-6} M	This work

The standard formula (3S/k) was used for the calculation of the detection limit (LOD) value. Where S is the standard deviation obtained by the fluorescence intensity of the **3** and k (slope) is derived from the fluorescence intensity versus concentration of PA [55]. The calculated LOD value for the detection of PA by complex **3** is found to be 3.02 μM indicating the high selectivity and sensitivity. The standard deviation for complex **3** is 4%.

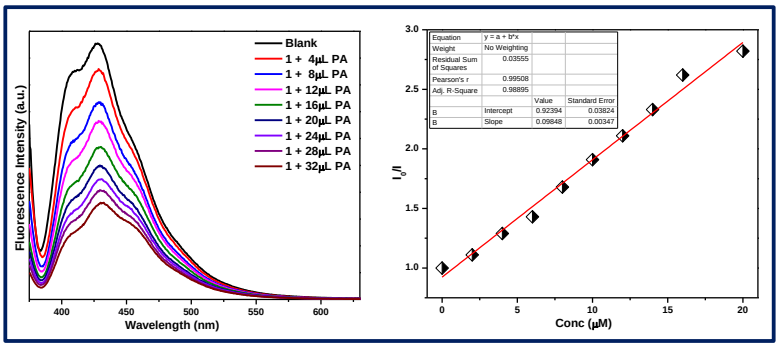

Figure 2B.9. *Fluorescence titration of* ***3*** *(10 μM) with PA (0.1 mM) and linear fitting for calculation of quenching constant.*

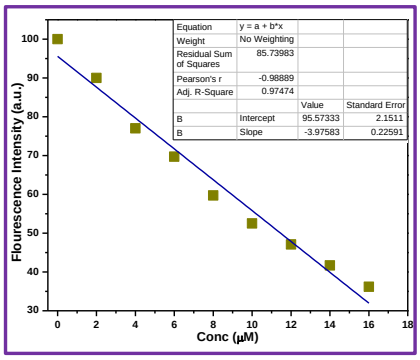

Figure 2B.10. *Relation of fluorescence intensity against PA added into the solution of* ***3*** *and their linear fit curve for the estimation of LOD.*

2B.4. Conclusions

An unprecedented organic transformation of the ligand system leads to the formation of one hexanuclear copper complex **3**. The synthesized complex **3** was characterized by single crystal X-ray crystallography, powder X-ray diffraction and FTIR techniques. The methanolic solution of complex **3** is fluorescent in nature which selectively detects the picric acid among the various nitro-aromatics. It shows ~97% quenching in fluorescence with quenching constant of 9.8×10^4 M^{-1}. The detection limit towards picric acid is 3.02 μM, which shows better turn-off fluorescence quenching than some earlier report.

2B.5. References

[1] Das, M., Nasani, R., Saha, M., Mobin, S. M., Mukhopadhyay, S. (2015), Nickel (II) complexes with a flexible piperazinyl moiety: studies on DNA and protein binding and catecholase like properties, Dalton Trans., 44, 2299-2310. (DOI: 10.1039/C4DT02675F)

[2] Das, M., Mandal, P., Malviya, N., Choudhuri, I., Charmier, M. A. J., Morgado, S., Mukhopadhyay, S. (2016), Copper complexes with a flexible piperazinyl arm: nuclearity driven catecholase activity and interactions with biomolecules, J. Coord. Chem., 69, 3619-3637.(DOI: 10.1080/00958972.2016.1236193)

[3] Cooper, T., Novak, A., Humphreys, L. D., Walker, M. D., Woodward, S. (2006), User-Friendly Methylation of Aryl and Vinyl Halides and Pseudohalides

with DABAL-Me_3, Adv. Synth. Catal., 348, 686-690.(DOI: 10.1002/adsc.20050 5405)

[4] Dutta, N., Haldar, S., Majumder, A., Vijaykumar, G., Carrella, L., Bera, M. (2020), Synthesis, structure and properties of a novel self-assembled tetranuclear copper (II) complex derived from carboxylate-based multidentate ligand, Inorg. Chem. Commun., 121, 108208. (DOI: 10.1016/j.inoche.2020.108208)

[5] Gungor, E., Kara, H. (2015), A new tetranuclear distorted open-cubane copper (II) Schiff base complex: Structural, spectral and magnetic characterizations, J. Struct. Chem., 56, 1646-1652.(DOI: 10.1134/ S002247 6615080296)

[6] Shit, S., Nandy, M., Rosair, G., El Fallah, M. S., Ribas, J., Garribba, E., Mitra, S. (2013), A hexanuclear copper (II) Schiff base complex incorporating rare “bicapped cubane” core: Structural aspects, magnetic properties and EPR study, Polyhedron, 52, 963-969.(DOI: 10.1016/j.poly.2012.07.016)

[7] Sari, M., Atakol, O., Svoboda, I., Fuess, H. (2006), Di-μ-acetato-bis [μ-2-hydroxy-N, N′-bis (2-oxidobenzyl) propane-1, 3-diamine] bis (N, N′-dimethylformamide) trinickel (II) N, N′-dimethylformamide disolvate, Acta Crystallogr. E., 62, m563-m565. (DOI: 10.1107/S1600536806005976)

[8] Haldar, S., Dutta, N., Vijaykumar, G., Das, A., Carrella, L., Oliver, A., Bera, M. (2019), Synthesis, structure and properties of new heterometallic octanuclear $Li_2Na_2Cu_4$ and decanuclear Li_2Zn_8 complexes. Polyhedron, 172, 58-66.(DOI: 10.1016/j.poly.2019.03.013)

[9] Bonanno, N. M., Lough, A. J., Lemaire, M. T. (2018), Polynuclear Cu_4L_4 copper (II) aminyl radical coordination complexes, Inorg. Chem., 57, 4837-4840.(DOI: 10.1021/acs.inorgchem.8b00785)

[10] Yang, X. Y., Li, Y., Pullarkat, S. A. (2014), A one-pot diastereoselective self assembly of C-stereogenic copper (I) diphosphine clusters. Inorg. Chem., 53, 10232-10239.(DOI: 10.1021/ic501233w)

[11] Muthurajan, H., Sivabalan, R., Talawar, M. B., Asthana, S. N. (2004), Computer simulation for prediction of performance and thermodynamic

parameters of high energy materials, J. Hazar. Mater., 112, 17-33.(DOI: 10.1016/j.jhazmat.2004.04.012)

[12] Beyer, C., Böhme, U., Pietzsch, C., Roewer, G. (2002), Preparation, characterization and properties of dipolar 1, 2-N, N-dimethylaminomethyl ferrocenylsilanes, J. Organomet. Chem., 654, 187-201.(DOI: 10.1016/S0022-328X(02)01427-4)

[13] Maiti, K., Mahapatra, A.K., Gangopadhyay, A., Maji, R., Mondal, S., Ali, S.S., Das, S., Sarkar, R., Datta, P., Mandal, D. (2017), Simple bisthiocarbonohydrazone as a sensitive, selective, colorimetric, and ratiometric fluorescent chemosensor for picric acids. ACS Omega, 2, 1583-1593.(DOI: 10.1021/acsomega.6b00288)

[14] Huynh, T.P., Wojnarowicz, A., Kelm, A., Woznicki, P., Borowicz, P., Majka, A., D'Souza, F. and Kutner, W. (2016), Chemosensor for selective determination of 2, 4, 6-trinitrophenol using a custom designed imprinted polymer recognition unit cross-linked to a fluorophore transducer, Acs Sensors, 1, 636-639.(DOI: 10.1021/acssensors.6b00055)

[15] Shanmugaraju, S., Mukherjee, P. S. (2015), π-Electron rich small molecule sensors for the recognition of nitroaromatics. Chem. Commun., 51, 16014-16032.(DOI: 10.1039/ C5CC07513K)

[16] Kundu, B. K., Mobin, S. M., Mukhopadhyay, S. (2019), Mechanistic and thermodynamic aspects of a pyrene-based fluorescent probe to detect picric acid, New J. Chem., 43, 11483-11492.(DOI: 10.1039/C9NJ02342A)

[17] Senapati, S., Nanda, K. K. (2018), MgO nanocubes as self-calibrating optical probes for efficient ratiometric detection of picric acid in the solid state, ACS Sustain. Chem. Eng., 6, 13719-13729.(DOI: 10.1021/ acssuschemeng. 8b01330)

[18] Luggar, R. D., Farquharson, M. J., Horrocks, J. A., Lacey, R. J. (1998), Multivariate analysis of statistically poor EDXRD spectra for the detection of concealed explosives, X-Ray Spectrom., 27, 87-94.(DOI: 10.1002/(SICI)1097-4539(199803/04)27)

[19] Moore, D. S. (2004), Instrumentation for trace detection of high explosives, Rev. Sci. Instrum., 75, 2499-2512.(DOI: 10.1063/1.1771493)

[20] Håkansson, K., Coorey, R. V., Zubarev, R. A., Talrose, V. L., Håkansson, P. (2000), Low-mass ions observed in plasma desorption mass spectrometry of high explosives, J. Mass Spectrom., 35, 337-346.(DOI: 10.1002/(SICI)1096-9888(200003)35)

[21] Guan, W., Zhou, W., Lu, J., Lu, C. (2015), Luminescent films for chemo- and biosensing, Chem. Soc. Rev., 44, 6981-7009.(DOI: 10.1039/C5CS00246J)

[22] Bradberry, S. J., Savyasachi, A. J., Martinez-Calvo, M., Gunnlaugsson, T. (2014). Development of responsive visibly and NIR luminescent and supramolecular coordination self-assemblies using lanthanide ion directed synthesis, Coord. Chem. Rev., 273, 226-241.(DOI: 10.1016/j.ccr.2014.03.023)

[23] Nolan, E. M., Lippard, S. J. (2008), Tools and tactics for the optical detection of mercuric ion, Chem. Rev., 108, 3443-3480.(DOI: 10.1021/ cr068000q)

[24] Bell, T. W., Hext, N. M. (2004), Supramolecular optical chemosensors for organic analytes, Chem. Soc. Rev., 33, 589-598.(DOI: 10.1039/B207182G)

[25] Chowdhury, A., Mukherjee, P. S. (2015), Electron-rich triphenylamine-based sensors for picric acid detection, J. Org. Chem., 80(8), 4064-4075.(DOI: 10.1021/acs.joc.5b00348)

[26] Shanmugaraju, S., Jadhav, H., Patil, Y. P., Mukherjee, P. S. (2012), Self-assembly of an Octanuclear platinum (II) tetragonal prism from a new PtII4 organometallic star-shaped acceptor and its Nitroaromatic sensing study, Inorg. Chem., 51(24), 13072-13074.(DOI: 10.1021/ic301716y)

[27] Vajpayee, V., Kim, H., Mishra, A., Mukherjee, P. S., Stang, P. J., Lee, M. H., Kim, H. K., Chi, K.W., (2011), Self-assembled molecular squares containing metal-based donor: synthesis and application in the sensing of nitro-aromatics, Dalton Trans., 40, 3112-3115.(DOI: 10.1039/C0DT01481H)

[28] Roy, B., Bar, A. K., Gole, B., Mukherjee, P. S. (2013), Fluorescent tris-imidazolium sensors for picric acid explosive, J. Org. Chem., 78, 1306-1310.(DOI: 10.1021/jo302585a)

[29] Gole, B., Bar, A. K., Mukherjee, P. S. (2014), Modification of extended open frameworks with fluorescent tags for sensing explosives: competition between size selectivity and electron deficiency, Chem. Eur. J., 20, 2276-2291.(DOI: 10.1002/chem.201302455)

[30] Gole, B., Bar, A. K., Mukherjee, P. S. (2011), Fluorescent metal–organic framework for selective sensing of nitroaromatic explosives, Chem. Commun., 47, 12137-12139.(DOI: 10.1039/C1CC15594F)

[31] Xu, H., Liu, F., Cui, Y., Chen, B., Qian, G. (2011), A luminescent nanoscale metal–organic framework for sensing of nitroaromatic explosives, Chem. Commun., 47, 3153-3155.(DOI: 10.1039/C0CC05166G)

[32] Nie, H., Zhao, Y., Zhang, M., Ma, Y., Baumgarten, M., Müllen, K. (2011), Detection of TNT explosives with a new fluorescent conjugated polycarbazole polymer, Chem. Commun., 47, 1234-1236.(DOI: 10.1039/C0CC03659E)

[33] He, G., Peng, H., Liu, T., Yang, M., Zhang, Y., Fang, Y. (2009), A novel picric acid film sensor via combination of the surface enrichment effect of chitosan films and the aggregation-induced emission effect of siloles, J. Mater. Chem., 19, 7347-7353.(DOI: 10.1039/B906946A)

[34] Thomas, S. W., Joly, G. D., Swager, T. M. (2007), Chemical sensors based on amplifying fluorescent conjugated polymers, Chem. Rev., 107, 1339-1386.(DOI: 10.1021/cr0501339)

[35] Dey, N., Samanta, S. K., Bhattacharya, S. (2013), Selective and efficient detection of nitro-aromatic explosives in multiple media including water, micelles, organogel, and solid support, ACS Appl. Mater. Interfaces, 5, 8394-8400.(DOI: 10.1021/am401608q)

[36] Bhalla, V., Gupta, A., Kumar, M., Rao, D. S., Prasad, S. K. (2013), Self-assembled pentacenequinone derivative for trace detection of picric acid, ACS Appl. Mater. Interfaces, 5, 672-679.(DOI: 10.1021/am302132h)

[37] Guzmán-Percástegui, E., Vonlanthen, M., Quiroz-García, B., Flores-Alamo, M., Rivera, E., Castillo, I. (2015), Supramolecular fluorescence enhancement via coordination-driven self-assembly in bis-picolylcalixarene blue-emitting $M_2L_2X_n$ macrocycles, Dalton Trans., 44, 15966-15975.(DOI: 10.1039/C5DT02058A)

[38] Acharyya, K., Mukherjee, P. S. (2014), A fluorescent organic cage for picric acid detection, Chem. Commun., 50, 15788-15791.(DOI: 10.1039/C4CC06 225F)

[39] Azhdari Tehrani, A., Esrafili, L., Abedi, S., Morsali, A., Carlucci, L., Proserpio, D.M., Wang, J., Junk, P.C., Liu, T., (2017), Urea metal–organic frameworks for nitro-substituted compounds sensing, Inorg. Chem., 56, 1446-1454.(DOI: 0.1021/acs.inorgchem.6b02518)

[40] Li, A. L., Qu, Y. H., Fu, L., Han, C., Cui, G. H. (2020), Multidimensional luminescent cobalt (ii)-coordination polymers as sensors with extremely high sensitivity and selectivity for detection of acetylacetone, benzaldehyde and $Cr_2O_7^{2-}$, CrystEngComm, 22, 2656-2666.(DOI: 10.1039/D0CE00077A)

[41] Pearce, B. H., Ogutu, H. F., Luckay, R. C. (2017), Synthesis of Pyrazole-Based Pyridine Ligands and Their Use as Extractants for Nickel (II) and Copper (II): Crystal Structure of a Copper (II)–Ligand Complex, Eur. J. Inorg. Chem., 2017, 1189-1201.(DOI: 10.1002/ejic.201601410)

[42] Devi, L. R., Raza, M. K., Musib, D., Ramu, V., Devi, J., Roy, M. (2020), Nucleus targeting anthraquinone-based copper (II) complexes as the potent PDT agents: Synthesis, photo-physical and theoretical evaluation, Inorganica Chim. Acta, 500, 119208.(DOI: 10.1016/j.ica.2019.119208)

[43] Wang, Z., Chen, B., Rogach, A. L. (2017), Synthesis, optical properties and applications of light-emitting copper nanoclusters, Nanoscale Horizons, 2, 135-146.(DOI: 10.1039/C7NH00013H)

[44] Tella, A. C., Olayemi, V. T., Adekola, F. A., Oladipo, A. C., Adimula, V. O., Ogar, J. O., Mokaya, R. (2021), Synthesis, characterization and density functional theory of copper (II) complex and cobalt (II) coordination polymer for detection of nitroaromatic explosives, Inorganica Chim. Acta, 515, 120048. (DOI: 10.1016/j.ica.2020.120048)

[45] Malviya, N., Das, M., Mandal, P., Mukhopadhyay, S. (2017), A smart organic gel template as metal cation and inorganic anion sensor, Soft Matter, 13, 6243-6249.(DOI: 10.1039/C7SM01199G)

[46] Nandy, M., Shit, S., Garribba, E., Gomez-Garcia, C. J., Mitra, S. (2015), Double azido/cyanato bridged copper (II) dimers incorporating tridentate nitrogen donors Schiff base: Structure, EPR and magnetic studies, Polyhedron, 102, 137-146.(DOI: 10.1016/j.poly.2015.07.034)

[47] Srivastava, S., Gupta, B. K., Gupta, R. (2017), Lanthanide-based coordination polymers for the size-selective detection of nitroaromatics, Crys. Growth Des., 17, 3907-3916.(DOI: 10.1021/acs.cgd.7b00536)

[48] Ma, D., Li, B., Zhou, X., Zhou, Q., Liu, K., Zeng, G., Li, G., Shi, Z. Feng, S., (2013), A dual functional MOF as a luminescent sensor for quantitatively detecting the concentration of nitrobenzene and temperature, Chem. Commun., 49, 8964-8966.(DOI: 10.1039/C3CC44546A)

[49] Nagarkar, S. S., Joarder, B., Chaudhari, A. K., Mukherjee, S., Ghosh, S. K. (2013), Highly selective detection of nitro explosives by a luminescent metal–organic framework, Angew. Chem., 125, 2953-2957.(DOI: 10.1002/ange. 201208885)

[50] Nagarkar, S. S., Desai, A. V., Samanta, P., Ghosh, S. K. (2015), Aqueous phase selective detection of 2, 4, 6-trinitrophenol using a fluorescent metal–organic framework with a pendant recognition site, Dalton Trans., 44, 15175-15180.(DOI: 10.1039/C5DT00397K)

[51] Ghosh, P., Saha, S. K., Roychowdhury, A., Banerjee, P. (2015), Recognition of an explosive and mutagenic water pollutant, 2, 4, 6-trinitrophenol, by cost-effective luminescent MOFs, Eur. J. Inorg. Chem., 2015, 2851-2857.(DOI: 10.1002/ejic.201500233)

[52] Pal, T. K., Chatterjee, N., Bharadwaj, P. K. (2016), Linker-induced structural diversity and photophysical property of MOFs for selective and sensitive detection of nitroaromatics, Inorg. Chem., 55, 1741-1747.(DOI: 10.1021/acs.inorgchem.5b02645)

[53] Zhuang, X., Zhang, N., Zhang, X., Wang, Y., Zhao, L., Yang, Q. (2020), A stable Cu-MOF as a dual function sensor with high selectivity and sensitivity detection of picric acid and CrO_4^{2-}in aqueous solution, Microchem. J., 153, 104498.(DOI: 10.1016/j.microc. 2019.104498)

[54] Xin, X., Ai, J., Li, F., Zhao, J., Zhang, L. (2020), An imidazole functionalized copper (II)-organic framework for highly selective sensing of picric acid and metal ions in water, Appl. Organomet. Chem., 34(9), e5803. (DOI: 10.1002/aoc.5803)

[55] Malviya, N., Sonkar, C., Kundu, B. K., Mukhopadhyay, S. (2018), Discotic organic gelators in ion sensing, metallogel formation, and bioinspired catalysis, Langmuir, 34, 11575-11585.(DOI: 10.1021/acs.langmuir.8b02352)

Chapter 3

Binuclear Cu(II) complexes as the efficient Photocatalyst for Benzyl alcohol oxidation and in-situ N-alkylation of aromatic amines

Chapter 3

Binuclear Cu(II) complexes as the efficient Photocatalyst for Benzyl alcohol oxidation and in-situ N-alkylation of aromatic amines

3.1 Introduction

N-alkylamines have found wide applications in pharmaceuticals, biologically active compounds, agrochemicals, and as a potential ligand for catalysis [1-4]. Traditionally, N-alkylated aliphatic or aromatic amines are obtained by C-N bond coupling reactions [5]. Alkylation of amines with an alkyl halide or reductive amination of carbonyl compounds in presence of amines with suitable reducing agents is also employed to obtain N-alkylated amines [6-9]. However, these reactions are stoichiometric in nature with drawbacks like the generation of a large amount of waste and side products and the toxicity of the reactants. Transition metal-based catalytic methods like hydroamination and hydroaminomethylation reactions are other important methodologies adopted for such synthesis. Hydrogen auto-transfer or borrowing hydrogen reaction is an atom-efficient and greener approach for the synthesis of N-alkylated amines by using alcohols as an inexpensive and green alkylating reagent in presence of different transition metal ions [10]. Direct N-alkylation of amines with primary alcohols through hydrogen auto-transfer reaction has been explored with rhodium [11-13], iridium [14-17], ruthenium [18-21], osmium [22] metal-containing catalysts. Due to the ecological and economic benefits, it is desirable to use cheap metal-based catalysts in organic synthesis. In this regard, manganese [23-24], iron [25-28], cobalt [29-31], nickel [32-35], and earth-abundant copper [36, 37] based catalysts are also reported for such reactions. This methodology is treated as an environmentally friendly process as the water gets generated as the only by-product. However, in all cases, high temperature is a pre-requirement for effective conversion.

Interestingly despite considerable advancement in this field of formation of N-alkyl amine, no visible light-mediated photo-catalysis for such a reaction is reported. Herein, the synthesis and characterization of two dimeric copper complexes which can effectively catalyze the formation of N-alkyl amine from

aromatic amines and benzyl alcohol when activated with visible light without the application of any heat energy from an external source in presence of TEMPO is reported and discussed.

As per the literature report oxidation of alcohols is an important step to initiate the borrowing hydrogen reactions. Among the various catalytic activities, aerobic oxidation of primary alcohol is an important sub-class of catalytic reaction in terms of an industrial as well as a biological viewpoint [38]. In biological systems, the oxidation of alcohols gets catalyzed by various enzymes like galactose oxidase or alcohol dehydrogenase. Zn(II) and Cu(II) ions are present in alcohol dehydrogenase and galactose oxidase enzymes respectively, facilitates the catalytic reactions. Two histidine nitrogen atoms (His496 and His581), two tyrosine oxygen atoms (Tyr272 and Tyr495), and a labile water molecule (pH 7) surround the copper(II) ion in the active center of galactose oxidase to form a distorted square pyramidal geometry. At lower pH (~3.5), acetate group sometimes replaces the water [39]. These natural enzymes provides idea how to develop a greener catalytic systems based on bio-inspired perception. It is also evident from the fact that a N/O donor environment for copper ion can provide an ideal environment to shuttle between Cu(II) and Cu(I) state to act as an oxidation catalyst.

3.2 Experimental section

3.2.1 Materials and methods

All the chemical reagents required were purchased from Sigma and used without further purification. The specifications of all the instruments used for analysis purposes were the same as described in section 2A.2.1 of the previous chapter 2A. The synthesis of ligands $\mathbf{H_2L^1}$ is described in section 2A.2.3 of the previous chapter 2A.

3.2.2 X-ray crystallography

Single crystal X-ray structural studies of **4** and **5** were performed following a similar protocol as mentioned in section 2A.2.2 of previous chapter 2A. The crystal and refinement data are summarized in Table 3.1

Table 3. 1. *Crystallographic data and structure refinement parameters for* ***4****, and* ***5****.*

Complex	**4**	**5**
Empirical Formula	$C_{15}H_{20}Cl_2CuN_2O_4$	$C_{13}H_{17}Br_2CuN_3O_5$
Formula weight	426.77 g/mol	518.66 g/mol
Crystal system	Monoclinic	Monoclinic
Space group	P 1 21/n 1	P 1 21/n 1
a (Å)	10.4399(4)	8.1936(19)
b (Å)	14.9215(5)	11.490(2)
c (Å)	11.5303(5)	17.350(3)
α (°)	90	90
β (°)	102.329(13)	96.244(8)
γ (°)	90	90
V ($Å^3$)	1754.75(12)	1623.7(6)
λ (Å)	0.71073	0.71073
ρ_{calcd} (g cm^{-3})	1.615	2.122
Z	2	2
T (K)	148(2)	273(2)
μ (mm^{-1})	1.571	6.297
F(0 0 0)	876	1020
Crystal size (mm^3)	0.04 × 0.06 × 0.10	0.10 × 0.12 × 0.18
θ ranges (°)	2.27 to 28.30	2.95 to 29.65
h/k/l	-13,13/-19,19/-15,15	-11,11/-15,15/-24,24
Reflections collected	35789	28374
Independent reflections	4353	4571
T_{max} and T_{min}	0.9400 and 0.8590	0.5720 and 0.3970
Data/restraints/parameters	4353 / 0 / 219	4571 / 1 / 220
Goodness-of-fit	1.065	1.045
Final R indices [I > 2σ(I)]	R1 = 0.0428, wR2 = 0.0828	R1 = 0.0297, wR2 = 0.0714
R indices (all data)	R1 = 0.0888, wR2 = 0.1059	R1 = 0.0374, wR2 = 0.0757
Largest peak and hole (e $Å^{-3}$)	0.560 and -0.512	0.880 and -0.874

3.2.3 Synthesis of 2,4-dibromo-6-((4-(2-hydroxyethyl) piperazin-1-yl)methyl) phenol (H_2L^2)

The ligand $\mathbf{H_2L^2}$ was synthesized by following the same procedure as the synthesis of $\mathbf{H_2L^1}$, by using 2,4-di-bromophenol instead of 2,4-dichlorophenol, which is described in section 2.2.3 of the previous chapter 2. The ligand $\mathbf{H_2L^2}$ was furnished as orange semiliquid with a 72% of yield. ^{1}H NMR (400.13 MHz, 298K, $CDCl_3$): δ 7.18 (1H, s, ArH), 6.81 (1H, s, ArH), 5.23 (1H, s, ArOH), 3.63 (2H, s, $-NCH_2Ar$), 3.57 (2H, t, $-CH_2OH$), 2.57 (8H, s, -piperazine ring), 2.52 (2H, t, $-NCH_2$), ppm; ^{13}C NMR (100.61 MHz, 298 K, $CDCl_3$): δ 152.5 (C of ArOH), 128.8 (CH of Ar), 126.8 (CH of Ar), 123.6 (C of $ArCH_2$), 123.1 (C of ArBr), 121.4 (C of ArBr), 60.7 (C of $–NCH_2$), 59.2 (C of $–CH_2OH$) , 57.7 (CH_2 of $–NCH_2Ar$), 52.5 (CH_2 of –piperazine ring), 52.2 (CH_2 of –piperazine ring) ppm

(figure 3.1). Anal. Calcd (%) for $C_{13}H_{18}Br_2N_2O_2$: C, 39.62; H, 4.60; N, 7.11. Found (%): C, 39.64; H, 4.63; N, 7.10. FTIR (in KBr υ in cm^{-1}): 3500–3100 {υO-H, (s)}; 3000–2820 {υC-H, (m)}; 1120–1010 {υC-N,C-O (m)}; 900-850 { υC-Cl, (s)}. ESI-MS in HPLC MeOH (m/z): $[M + H]^+$ 394.99 (100%) (figure 3.2).

3.2.4 Synthesis of $[Cu(HL^1)(OAc)]_2$ (4)

A solution of $\mathbf{H_2L^1}$ (0.152 g; 0.5 mmol), triethylamine (70 μL; 0.5 mmol) and $Cu(OAc)_2.H_2O$ (0.1 g; 0.5 mmol) in dichloromethane (20 mL) was stirred at room temperature for 4 hrs; the resulting green solution was concentrated up to 4-5 mL by evaporating the solvents in vacuum (scheme 1). The concentrated mixture was filtered and layered with acetonitrile (3 mL) and then left for slow diffusion. Finally, after three days, dark green square-shaped crystals suitable for diffraction were obtained from the reaction mixture. Crystals were collected by filtration and washed with diethyl ether. Anal. Calcd (%) for $C_{30}H_{40}Cl_4Cu_2N_4O_8$: C, 42.11; H, 4.72; N, 6.56. Found (%): C, 42.37; H, 4.73; N, 6.60; FTIR (in KBr υ in cm−1): 3670–3050 {υN-H,O-H (s); 3000–2810 {υC-H, (m)}; 1735-1500 {υC=O (m)}; 1150–990 {υC-N,C-O (s)}; 835-750 { υC-Cl, (s)} (figure 3.3). ESI-MS $[C_{30}H_{40}Cl_4Cu_2N_4O_8]$ (m/z) calculated – 852.05 (m); obtained – 438.20 $[M + Na + H]^{2+}$ (figure 3.4).Yield 78%

3.2.5 Synthesis of $[Cu(HL^2)(NO_3)]_2$ (5)

8 mL of methanolic solution of Cu(NO3)2.3H2O (0.12 g, 0.5 mmol) was added dropwise to a 10 mL solution of $\mathbf{H_2L^2}$ (0.197 g, 0.5 mmol) and triethylamine (70 μL; 0.5 mmol) and the resultant mixture was stirred at room temp for 3 hr and then the solution was concentrated by evaporating the solvent up to 4 mL. The concentrated reaction mixture was left for slow evaporation after filtration with filter paper. After 2-3 days, bluish-green square-shaped crystals were obtained from the reaction mixture which is suitable for diffraction. Anal. Calcd. (%): $C_{26}H_{34}Br_4Cu_2N_6O_{10}$; C, 30.11; H, 3.30; N, 8.10. Found (%): C, 30.16; H, 3.34; N, 8.08. Selected IR in KBr (ν/cm^{-1}): 1588 (–C=N), 1450 ($NO3^-$) (figure 3.3). $[C_{26}H_{34}Br_4Cu_2N_6O_{10}]$ (m/z) calculated – 1037.29 (M); obtained – 1056.742 $(M+H_2O+H)^+$ (figure 3.4). Yield: 80%

3.2.6 Selective oxidation and hydrogen auto-transfer reaction of 1° alcohols by Cu(II) complexes

All the photocatalytic activities of complexes **4** and **5** were also studied following a similar procedure as described in section 2A.2.6 of previous chapter 2A.

3.2.7 Detection of hydrogen peroxide in the catalytic reactions

Modification of the iodometric method as described in section 2A.2.7 of chapter 2A, is employed to detect H_2O_2 during the catalytic reaction.

3.3 Results and discussion

3.3.1 Syntheses of the ligands and complexes

The ligands $\mathbf{H_2L^1}$ and $\mathbf{H_2L^2}$ are obtained by simple mannich reaction using previously reported methodology describe in an earlier chapter with sufficient purity and yield. $\mathbf{H_2L^2}$ is synthesized according to scheme 3.1.

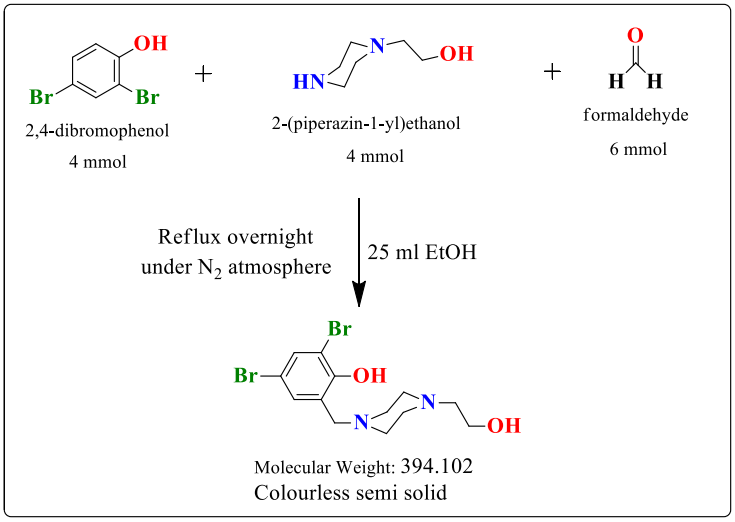

Scheme 3.1. *Synthesis of ligand H_2L^2.*

Ligand **(H_2L^2)** has been characterized by ^{1}H and ^{13}C NMR and ESI-MS spectroscopy. The ligand has shown all the characteristic peaks in ^{1}H NMR and ^{13}C NMR (figure 3.1). The molecular peak was observed at 394.995 $[M+ H]^+$ in the ESI-MS spectrum (figure 3.2).

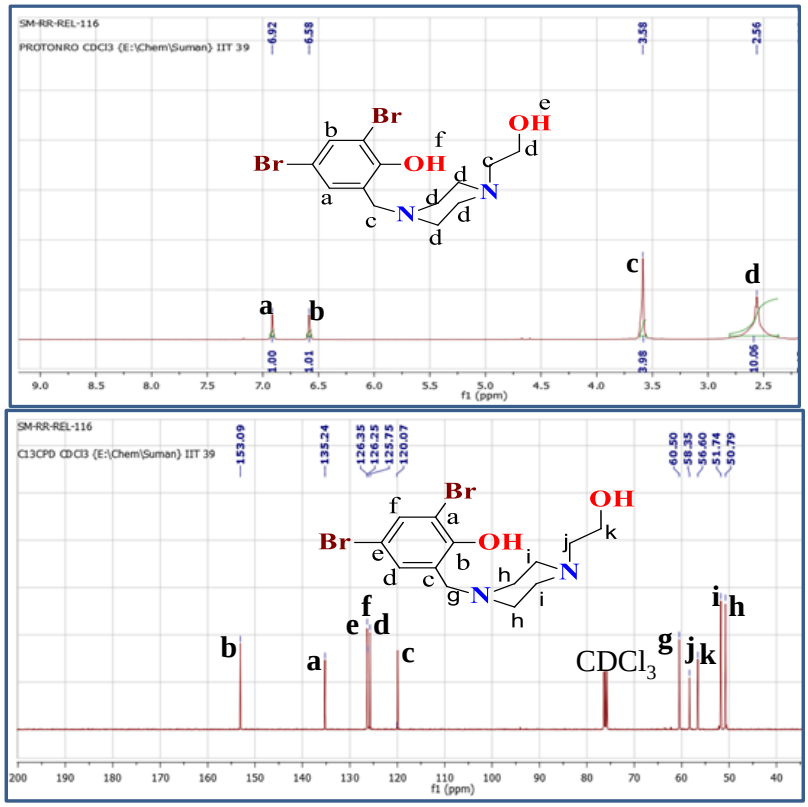

Figure 3.1. *^{1}H and ^{13}C NMR of* $\boldsymbol{H_2L^2}$.

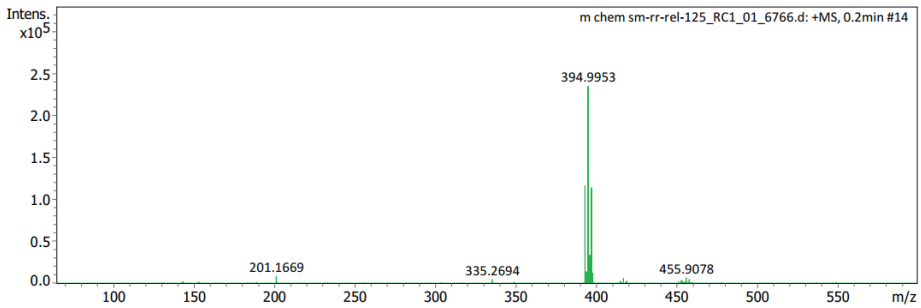

Figure 3.2. *ESI- MS spectrum of* $\boldsymbol{H_2L^2}$.

Ligand $\mathbf{H_2L^1}$ was used without further purification in the synthesis of bi-nuclear copper(II) complex **4**. Complex **4** is synthesized according to scheme 3.2.

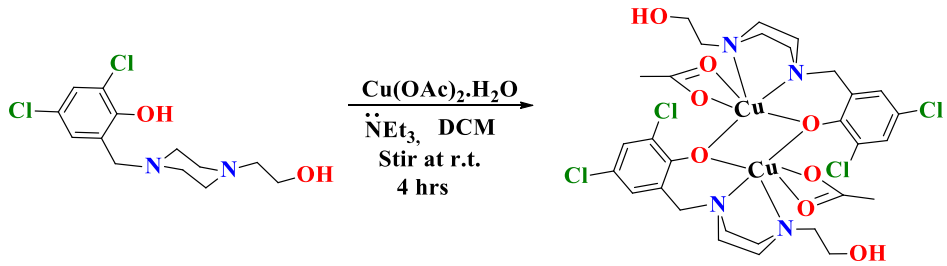

Scheme 3.2. *Formation of binuclear metal complex* ***4***.

We have tried many times for the synthesis of binuclear Cu(II) complex with acetate co-ligand system by using ligand **H_2L^2** and **$Cu(OAc)_2.H_2O$**, but we are unsuccess to synthesized. After that, we got a diffractable green square-shaped single crystal of binuclear Cu(II) complex **$[Cu(HL^2)(NO_3)]_2$ (5)** by reacting ligand **H_2L^2** and **$Cu(NO_3)_2.3H_2O$** salt in methanol (scheme 3.3). Afterward, we have also try to synthesize the binuclear Cu(II) complex by using **$Cu(NO_3)_2.3H_2O$** with **H_2L^1**, but we again unsuccess to find any single crystal.

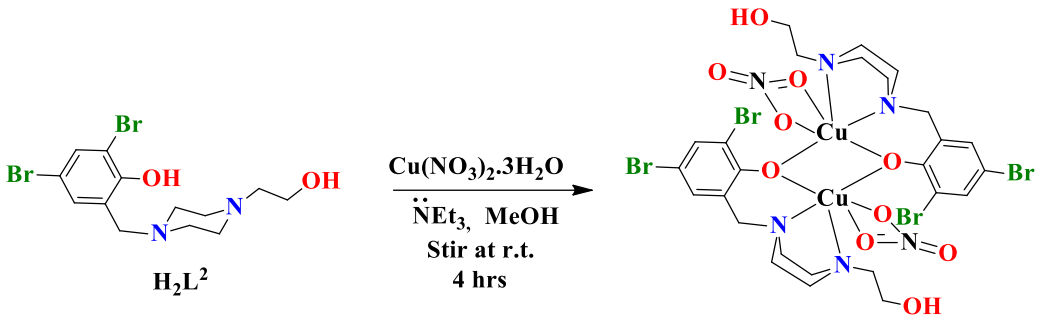

Scheme 3.3. *Formation of binuclear metal complex **5**.*

Both complexes have been characterized by ESI-MS spectroscopy, elemental analysis, and singly crystal X- ray crystallography. IR spectra of complex **4** have shown metal carboxylate starching bands around 1421 and 1627 cm^{-1} due to the symmetric and asymmetric stretching. Whereas, in the case of complex **5,** the band appears around 1400-1480 indicating the presence of nitrate ion (figure 3.3).

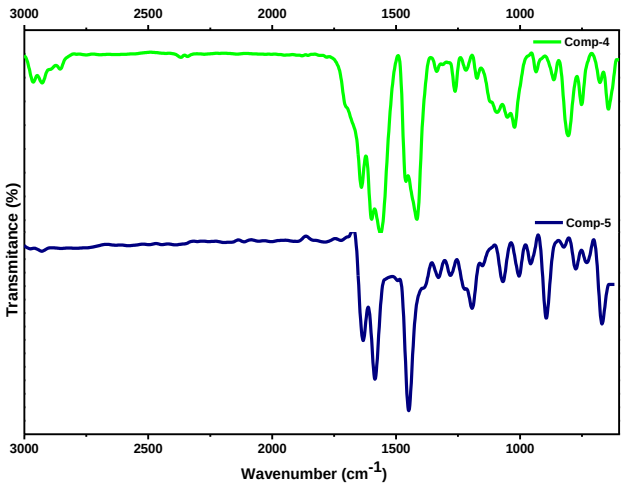

Figure 3.3*. FTIR spectrum of **4** and **5**. (top to bottom)*

The ESI-Mass spectra of compound **4** and **5** show the molecular ion peak at 438.20 $[M + Na + H]^{2+}$ and 1056.742 $[M + H_2O + H]^+$, respectively (figure 3.4).

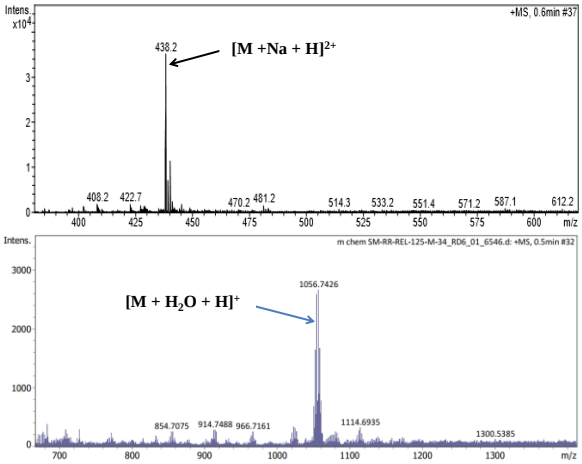

***Figure 3.4**. ESI- MS spectrum of **4** and **5**. (top to bottom)*

The electronic spectra of ligands $\mathbf{H_2L^1}$ and $\mathbf{H_2L^2}$ and complexes **4** and **5** (figure 3.5) have been studied in the solution state using CH_3OH as solvent. The solutions of ligands and complexes in methanol exhibit absorption in 270-690 nm ranges [$\mathbf{H_2L^1}$ and $\mathbf{H_2L^2}$: 290 nm; **4**: 287, 424, 660 nm; **5**: 291, 433, 660 nm]. The transition around 600-700 nm corresponds to a d-d transition of copper (II) moiety and band around 420 nm for intramolecular LMCT transition [26]. In the case of complexes **4** and **5**, d-d transitions are observed at about 660 nm which indicates hexacoordinated structures around the central atom [27, 28].

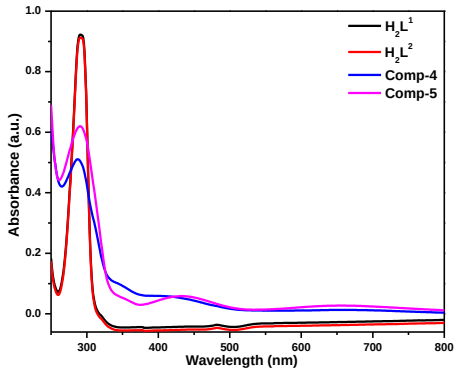

***Figure 3. 5.** UV-Vis Spectra of ligands $\mathbf{H_2L^1}$, $\mathbf{H_2L^2}$, complex-**4** and complex-**5**.*

3.3.2. Electrochemistry

Upon oxidation of the ligand, an anodic peak at Epa = +0.55 V was observed, showing the oxidation of the phenol [40]. Whereas, the case of complexes shows anodic peaks around Ep_a = +1.10 V along with cathodic peaks around Ep_c = +0.739 V, revealing a quasi-reversible behavior of the complex due to the oxidation of phenolate ion to phenoxyl moiety (figure 3.6). Irreversible cathodic

peak is observed in the negative potential for both of the complexes at Epa = -1.06 V and Epa = -1.05 respectively, which indicates the reduction of Cu (II) to Cu(I) [41].

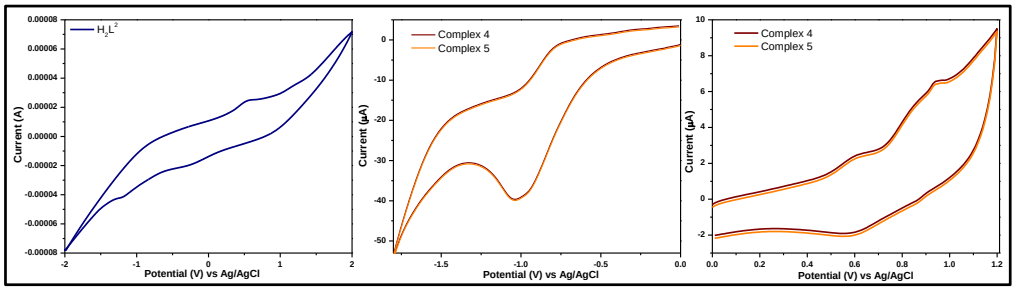

Figure 3.6. *Cyclic voltammograms of (1.0 × 10^{-4} M) solution of (a) Ligand,* ***H_2L^2*** *and (b) complexes* ***4*** *and* ***5*** *in CH_2Cl_2 containing 0.1 M Bu_4NPF_6 as the supporting electrolyte. The data were recorded at a scan speed of 100 mV s^{-1} at 25 °C.*

3.3.3. Crystal structure of complex 4 and 5

Table 3. 2. *Selected bond lengths (Å) and bond angles (°) for* ***4****, and* ***5***

Complex	**4**	**5**
Cu(1)-O(1)	1.943(2)	1.944(2)
Cu(1)-N(1)	2.020(3)	2.019(2)
Cu(1)-N(2)	2.066(3)	2.028(2)
Cu(1)-O(2)	1.947(2)	.....
Cu(1)-O(3)	2.719	2.023(2)
Cu(1)-O(4)	.....	2.564
O(1)-Cu(1)-O(2)	91.90(10)	.....
O(1)-Cu(1)-N(1)	92.52(10)	93.29(8)
O(2)-Cu(1)-N(1)	164.74(10)	.....
O(1)-Cu(1)-N(2)	165.28(10)	167.06(8)
O(2)-Cu(1)-N(2)	100.06(11)	.....
N(1)-Cu(1)-N(2)	73.76(11)	74.15(9)
O(1)-Cu(1)-O(1)	84.96(9)	83.18(7)
O(2)-Cu(1)-O(1)	92.86(9)	.....
N(1)-Cu(1)-O(1)	102.07(9)	97.70(7)
N(2)-Cu(1)-O(1)	102.81(9)	101.29(8)
O(1)-Cu(1)-O(3)	.....	92. 95(8)
N(1)-Cu(1)-O(3)	.....	160.83(8)
O(3)-Cu(1)-N(2)	.....	98.04(8)
O(3)-Cu(1)-O(1)	.....	101.03(7)

The crystal structure of these two binuclear complexes shows the Cu (II) center having distorted octahedral geometry. In both complexes, the major coordination

bond lengths between Cu atom and N/O-donor centers are within the range of 1.943(2) to 2.386(2) Å (Table 3.2), which matches perfectly with the earlier report [42.] However, few exceptions are found in the form of Cu(1)-O(3) in complex **4** and Cu(1)-O(4) in complex **5**, which are mainly caused by Jahn-Teller distortion as mentioned in the previous report [43-45].

Complexes **4** and **5** are crystalized in the space group *P 1 21/n 1*. The central metal atom is coordinated to the tridentate Mannich base ligands **HL**^{1} and **HL**^{2} in which the phenoxide oxygen act as a bridging between two metal center and two oxygen of acetate and nitrate group is also bound with the metal atom in the complex **4** and **5** respectively (figure 3.7). In the complex **4**, N, N, O donor sites of Schiff base **HL**^{1} and one O donor site of acetate group are on the equatorial face of distorted octahedral geometry while O donor site from phenoxide group of other Schiff base **HL**^{1} ligand and one O donor site of acetate group are on the axial position of distorted octahedral geometry. The piperazinyl ring takes the boat confirmation.

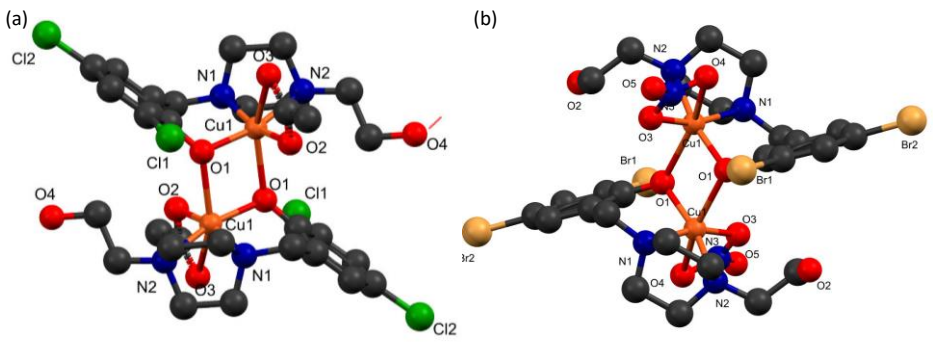

Figure 3.7**. The solid-state crystal structure for (a) complex **4** (b) complex **5

3.3.4. Photocatalytic oxidation of benzyl alcohols

Initially, we started to investigate the photocatalytic oxidation of benzyl alcohol by homogeneous binuclear Cu^{2+} complex **4** in different solvents as shown in Table 3.3. Under visible light irradiation (by 12 watts of the LEDs), the reaction mixture in the presence of air was stirred for 3 h at room temperature, and the catalyst in dichloromethane (DCM) brings out 97% conversion of benzyl alcohol with a selectivity of 98% in favor of benzaldehyde, (entries 1). Furthermore, changing the solvent from DCM to polar solvents like DMF or DMSO resulted in 90 and 92% conversion, respectively with high selectivity (> 95%) (entries 6 and 7).

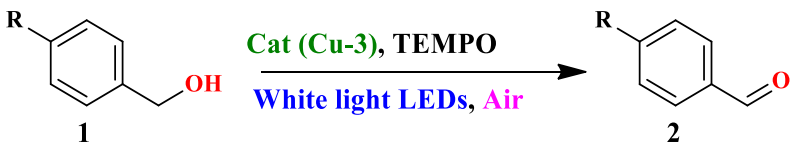

Table 3.3. *Photocatalytic Oxidation of Benzyl Alcohol by complex-4/Solvent*[a]

Entry No	Solvent	Time [h]	Conversion [%]	Selectivity [%]	Yield [%]	TON
1	DCM	3	97	98	95	190
2[b]	DCM	3	95	98	93	186
3[c]	DCM	3	94	97	91	182
4[d]	DCM	3	97	98	95	190
5[e]	DCM	3	74	96	71	142
6	DMF	3	90	96	87	174
7	DMSO	3	92	95	86	172
8	ACN	3	90	88	79	158
9	Toluene	3	95	88	83	166
10	Acetone	3	87	90	78	156

[a]*General reaction conditions: benzyl alcohol (1 mmol), complex-**4** (0.5 mol%), TEMPO (2 mol%), solution volume (1 mL), light intensity (12 Watt LED bulb, 400−800 nm wavelength range), room temperature (~25 °C), Stir.* [b]*Complex-**5**.* [c]*light intensity (9 Watt LED bulb).* [d]*light intensity (15 Watt LED bulb).* [e]*without TEMPO.*

When acetonitrile or toluene was used in place of DCM, we observed more than 90% conversion of benzyl alcohol but the selectivity is less (88%) towards the benzaldehyde (entries 8 and 9). Furthermore when acetone was used then the conversion of benzyl alcohol goes down to 87% with a selectivity of 90% (entry 10). The complex **5** afforded 95% conversion with 98% of selectivity (entry 2). In the absence of light irradiation or TEMPO, no conversion of benzyl alcohol was observed. Similarly, the photocatalytic oxidation reaction was also not observed in the absence of the Cu complex. Upon irradiation with low-intensity visible light (9 Watt), a decrease in yields of benzaldehyde was observed (entry 3) but with higher intensity (15 Watt), the yield percentage does

not increase with respect to the standard intensity (12 Watts) which has been utilized in general.

After screening of the solvent, the scope of this photocatalytic oxidation of benzyl alcohol was further extended to a variety of substituted benzyl alcohols with **4** as a catalyst by using dichloromethane as a solvent to study the substitution effects (Table 3.4). 4-bromo and 4-methyl benzyl alcohol showed 94% conversion with 99% selectivity which is higher than the other substituents after 3 h of stirring of the reaction mixture.

Table 3.4. *Percentage conversion of substituted benzyl alcohol by the homogeneous catalysts.*

Entry	Substrates	Conversion [%] Com-**4**/Com-**5**	Product	Selectivity [%] Com-**4**/Com-**5**
1	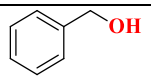	97/95	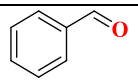	94/94
2	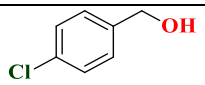	98/95	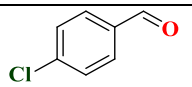	99/99
3	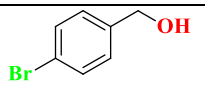	99/96	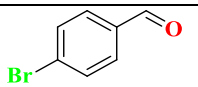	99/99
4	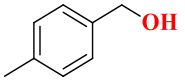	99/96	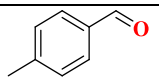	99/99
5	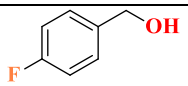	81/75	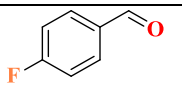	99/99
6	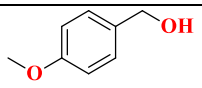	67/64	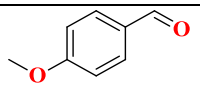	99/99
7	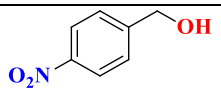	20/18	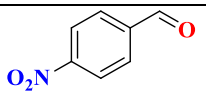	99/99

General reaction conditions: benzyl alcohol (1 mmol), catalyst (0.5 mol%), TEMPO (2 mol%), DCM (1mL), light intensity (12 Watt LED bulb, 400−800 nm wavelength range), room temperature (~25 °C), stir for 1h.

It has been observed that these photocatalytic reactions follow a regular trend according to the electronic properties of the functional group which is attached to the benzyl alcohol. The conversion of benzyl alcohol to benzaldehyde was found to be decreasing with decreased electron density at the benzene ring. The presence of a strong electron-withdrawing group such as the nitro group resulted in lower conversion in respective of other electron-donating groups such as chloro, bromo, methyl, or methoxy groups. 4-bromo and 4-methyl substituted benzyl alcohol showed a better conversion rate than other substituted benzyl alcohol such as 4-chloro, 4-methoxy, 4-fluoro, or 4-nitro and as well as benzyl alcohol.

3.3.5. Mechanism for Photocatalytic Oxidation

The plausible simplified mechanism based on ESI-MS data for the oxidation of benzyl alcohol by complex **4** is depicted in scheme 3.4. The reaction begins with the binding of benzyl alcohol to complex **A** through an unshared pair of electron; forming **B**. TEMPO is converted into TEMPOH by the abstraction of hydrogen from benzyl alcohol to form an intermediate **C**. In the presence of visible light, the phenoxide ion gets oxidized to phenoxyl radical by donating a single electron to Cu(II) which gets reduced to Cu(I) and then generates the species **D** by releasing the acetate ion, which gives the desired product benzaldehyde. After that, the intermediate **D** gets converted into **E**. ESI-MS spectrometry of the reaction mixture reveals a molecular ion peak at 571.18, 499.12 and 416.30 indicating the formation of intermediate **B, C** and **E** respectively (figure 3.8). TEMPO is regenerated from TEMPOH which leads to the formation of Cu(II) complex (A) by the oxidation of Cu(I) species in the presence of molecular oxygen under visible light irradiation.

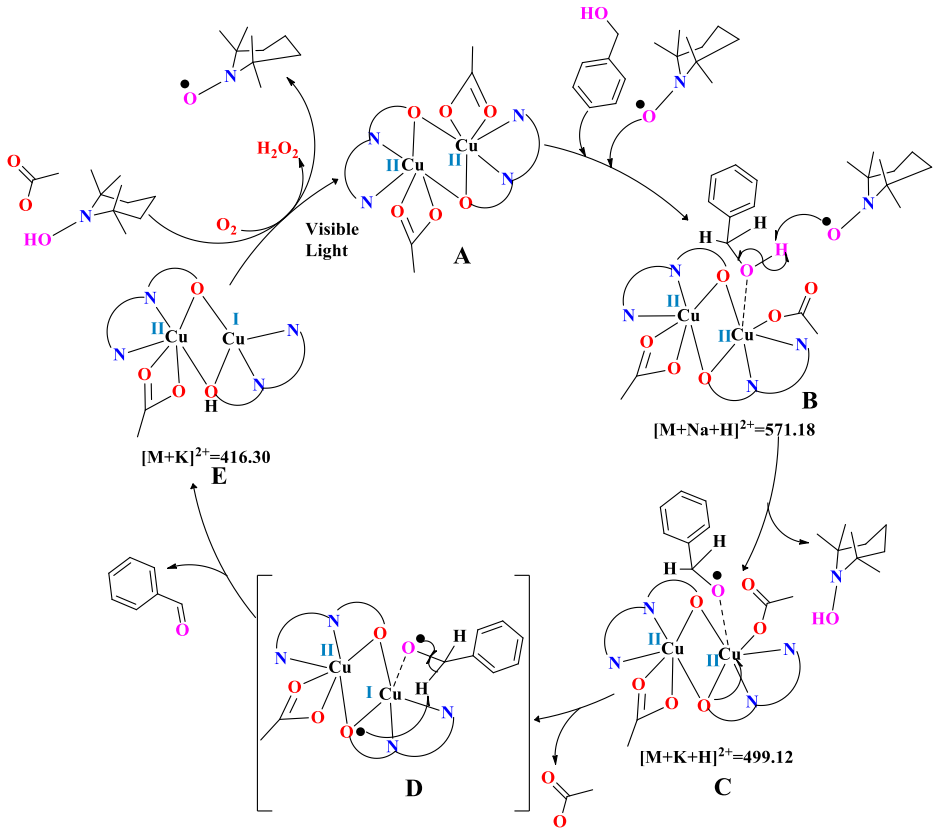

Scheme 3.4. *Proposed Mechanism for the Photocatalytic Oxidation of Benzyl Alcohol.*

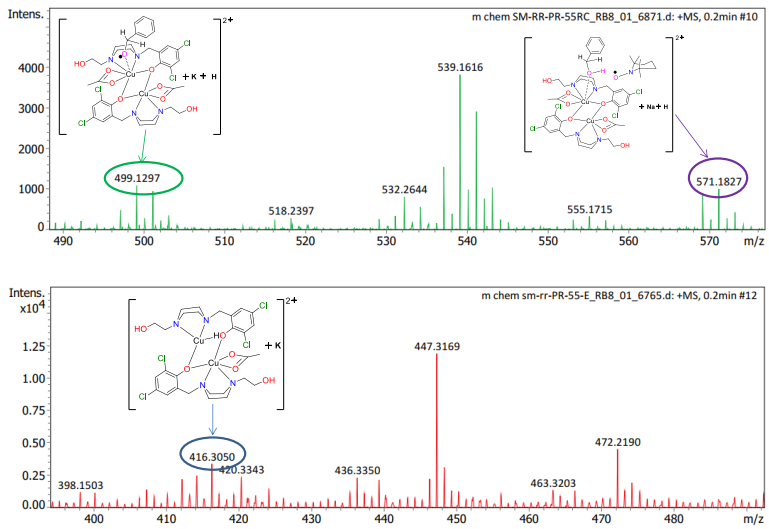

Figure 3.8. *ESI-MS Spectrum in MeOH of the photocatalytic alcohol oxidation reaction intermediates.*

3.3.6. Catalytic activity for the Borrowing hydrogen reaction

After having optimized the reaction condition for the oxidation of benzyl alcohols to benzaldehydes, the N-alkylation reaction was explored by adding aniline along with benzyl alcohol in the same reaction condition. The formation of benzyl-

phenyl-amine is recorded in good yield. The scope of the reaction was extended further with various substituted benzyl alcohols (**1a-f**) using aniline 3 for the N-alkylation reaction (Table 3.5). 4-chlorobenzyl alcohol afforded the desired product 4b with 88% and 84% yields in the presence of complex **4** and **5** respectively, which is higher than any other substituents. After that, the reaction was further extended by increasing the scope using several substituted anilines (**3a-d**) along with benzyl alcohol (**1a**) (Table 3.6). In this series, P-toluidine afforded a higher yield than the other substituted reactants. This result indicates the rate of formation of the phenoxyl radical intermediates increases with increased electron density on the benzene ring. The electron-withdrawing substituents decrease the stability of the radical intermediate by decreasing the electron density of the ring.

Table 3.5. Substrate scope for the N-alkylation of aniline with substituted benzyl alcohols

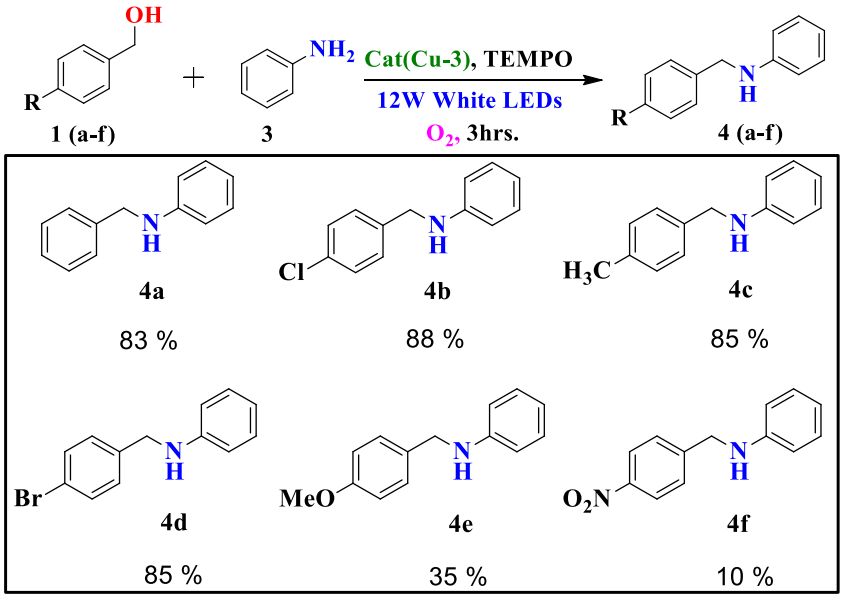

*Scope of Benzyl alcohols. Reaction conditions: Benzyl alcohol (1 mmol), Aniline (1 mmol), catalyst **4** (0.5 mol%), TEMPO (2 mol%), DCM (1mL), O_2 atmosphere (balloon pressure), light intensity (12 Watt LED bulb, 400−800 nm wavelength range), room temperature (~25 °C), stir for 3h.*

Table 3.6. Substrate scope for the N-alkylation of substituted anilines with benzyl alcohol

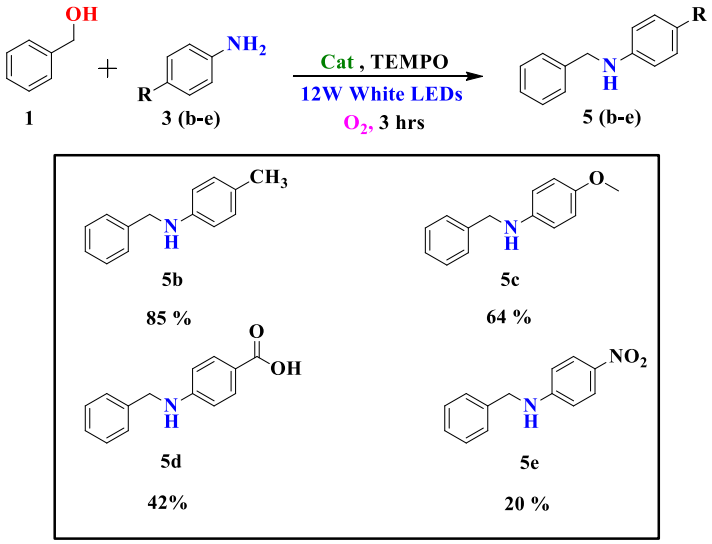

*Scope of Anilines. Reaction conditions: Benzyl alcohol (1 mmol), Aniline (1 mmol), catalyst **4** (0.5 mol%), TEMPO (2 mol%), DCM (1mL), O_2 atmosphere (balloon pressure), light intensity (12 Watt LED bulb, 400−800 nm wavelength range), room temperature (~25 °C), stir for 3h.*

3.3.7. Mechanism for Photocatalytic N-alkylation Reaction

To determine the prospective mechanistic pathway for N-alkylation of aromatic amine reaction several interesting observations were taken into account with complex **4**, which establishes the active role of the presence/absence of certain reactants in the process. First and foremost, the catalyst remains ineffective in absence of exposure to light confirming the role of visible light in the catalytic procedure. Furthermore, we found that the reaction cannot proceed without the presence of TEMPO, confirming its vital role in the whole process. In addition to that during the reaction, no generation of hydrogen peroxide was detected and it has been found that the reaction can proceed even in an inert atmosphere (without the presence of molecular oxygen). This factor indicates that aerial oxygen is not involved at least directly in the whole procedure.

Based on the above facts and the ESI-MS analysis done during the reaction process a plausible mechanism is proposed herewith. The reaction gets initiated by the binding of the benzyl alcohol to one of the copper centers in complex **I**, forming an intermediate **II**. In this process, the acetate ion attached to the same Cu(II) center might become monodentate from chelating bidentate coordination.

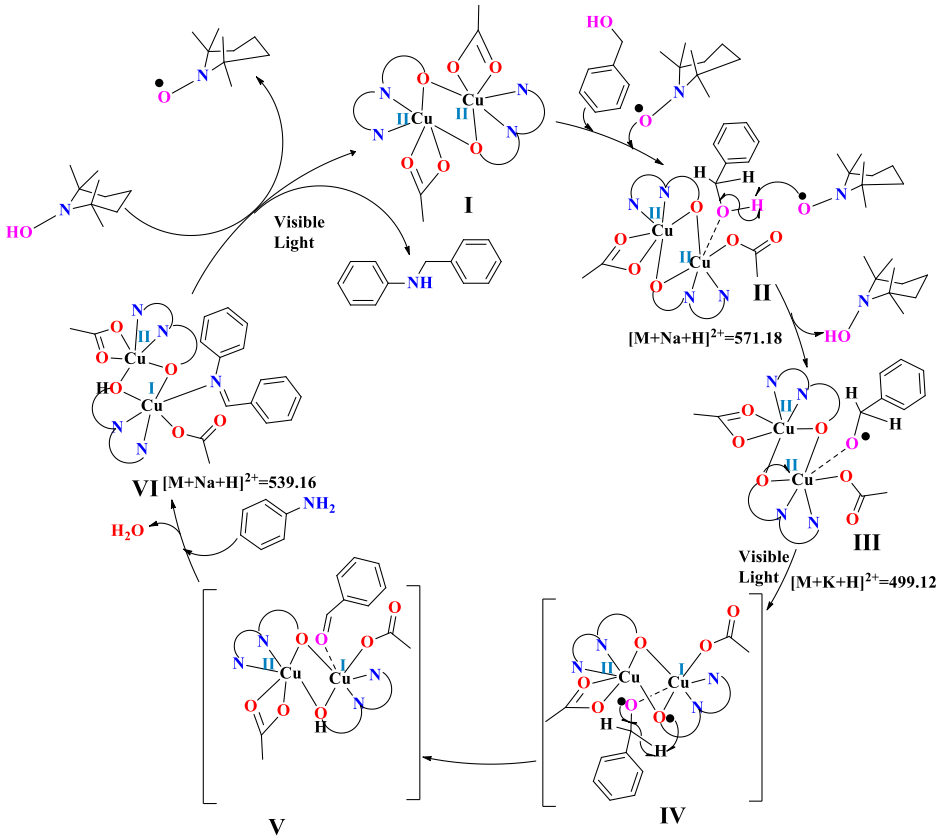

Scheme 3.5. *Proposed Mechanism for the Photocatalytic Borrowing Hydrogen Reaction.*

After that TEMPO abstracts the alcoholic hydrogen to get self-converted into TEMPOH and forms intermediate state **III** which is observable in the ESI-MS at 499.12. Interestingly the ESI-MS data show peaks around 571.18 indicating the formation of an aggregation similar to **II**. In the next step upon irradiation with visible light, the negative charge on the phenoxide ion donates a single electron to Cu(II) to convert it into a Cu(I) species and itself gets transformed into a phenoxyl radical giving a transition state **IV**. Subsequently the phenoxyl radical abstracts a benzylic proton converting it into benzaldehyde **V**. In presence of aniline the aldehyde gets converted into a corresponding Schiff base generating complex **VI** completing the C-N coupling which might get assisted in the presence of metal ion. The presence of the corresponding metal complex can be observed in ESI-MS at 539.16 (figure 3.9). In the final step the hydrogens borrowed by TEMPO and phenoxyl ligand are given back to the Schiff base moiety to generate N-alkylated aromatic amine and the original complex gets generated completing the catalytic cycle. The uniqueness of the process here is that unlike in other hydrogen borrowing scheme where metal ion borrows the hydrogen; here the phenoxide ligand and TEMPO does the same under the

influence of photon-assisted electron transition. It is also important to note that the ESI-MS peaks corresponding to the free Schiff base and N-alkyl amine are observed at 182.09 and 184.12 at the time interval of 60 minutes and 120 minutes after the initiation of the reaction (figure 3.10).

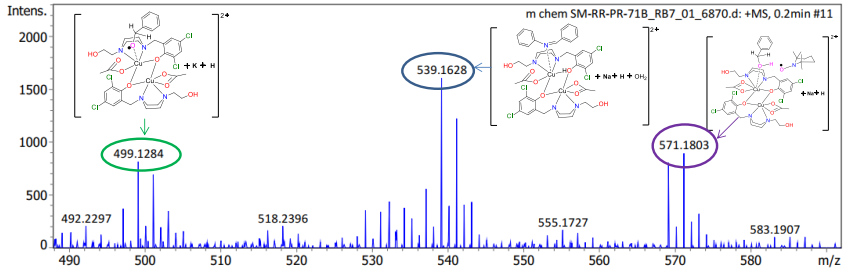

Figure 3.9. *ESI-MS Spectrum in MeOH of the borrowing hydrogen reaction intermediates.*

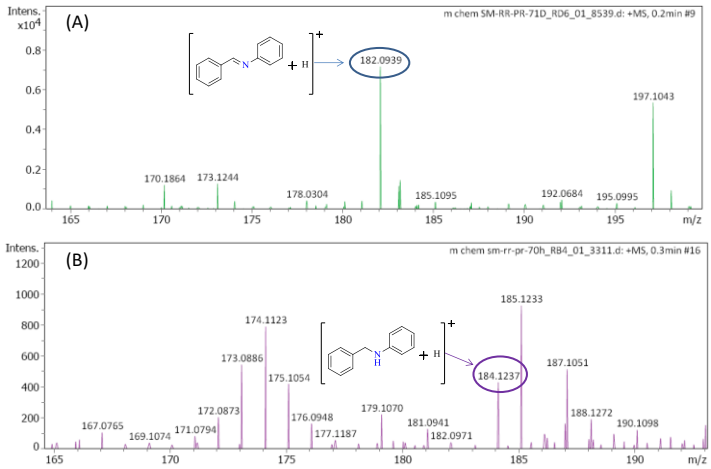

Figure 3.10. *ESI-MS Spectrum in MeOH of (A) free Schiff base intermediate and (B) N-alkyl amine product.*

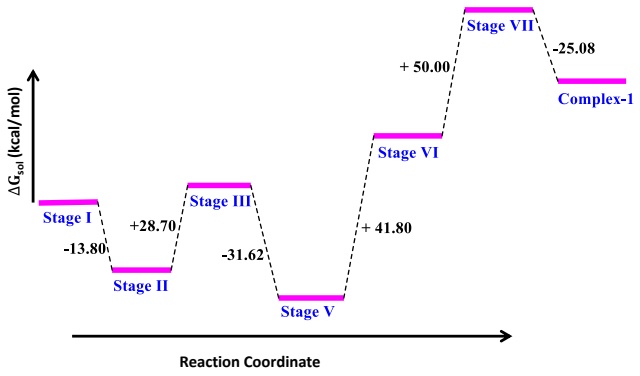

Scheme 3.6. *Reaction-free energy profile diagram of Proposed Mechanism for the Photocatalytic C-N coupling.*

Furthermore, DFT calculation is taken up to elucidate the proposed photocatalytic coupling mechanism (scheme 3). The active catalyst is complex 'I', in which both the copper are present in a +2 oxidation state. According to the reaction free energy profile diagram (scheme 3), the free energy of (cat I + BnOH + TEMPO) is higher than the free energy of (intermediate-II + TEMPO), so the first step is energetically favorable; whereas, 28.7 kcal/mol energy are required for the progress of the reaction from stage-II to stage-III, which may be provided by the visible light irradiation. The energy of intermediate 'III' is higher than the energy of intermediate 'V', so this step is also energetically favorable. 41.80 Kcal/mol and 50.00 kcal/mol of energy are required to further proceed with the reaction in the consecutive fourth and fifth steps, which might be again provided by visible light. The free energy of (VII + TEMPOH) is higher than the energy of (cat I + TEMPO + product), therefore we can expect the last step of the catalytic cycle is energetically favorable. At last, the intermediate VII can be converted easily to produce the active catalyst I for the re-initiation of the next cycle with the release of the valuable C-N coupling product.

3.3.8. Detection of hydrogen peroxide during catalysis

The predominant band in UV-vis data for oxidation of alcohol to aldehyde at 286 nm is the combination of I_3^- and benzaldehyde and the band at 349 nm for I_3^- (figure 3.11). Hence, all the above experiments hereby support the radical mechanism pathways for catalysis. Interestingly the borrowing hydrogen reaction mixture not shown any absorption band of I_3^- ruling out the possibility of the generation of H_2O_2.

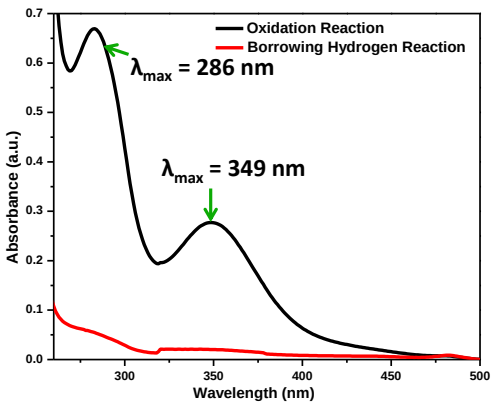

Figure 3.11. *UV-Vis spectra for Detection of hydrogen peroxide in the catalytic reaction.*

3.3.9. Recyclability and reusability of Catalyst

Photocatalysts **4** and **5** have been tested for recyclability and reusability with N-alkylation as well as benzyl alcohol oxidation reaction. The catalyst can be recovered almost quantitatively from the reaction mixture by column filtration. The molecular structure of the catalyst remains almost intact as can be seen from the PXRD pattern before and after the reaction (figure 3.12) The recovered catalyst-**4** can be utilized for four cycles without much decrement of its activity (figure 3.13) or significant change in PXRD, IR and LCMS pattern (figure 3.14 and 3.15).

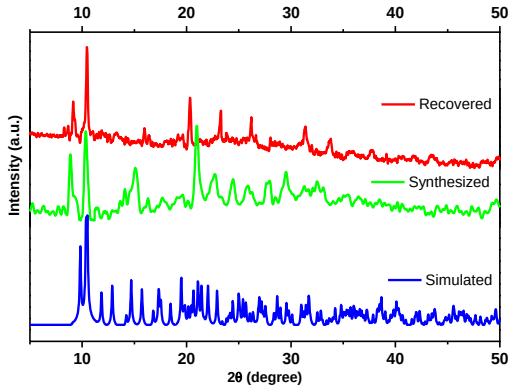

Figure 3.12. *Powder X-ray diffraction patterns for complex* ***4.***

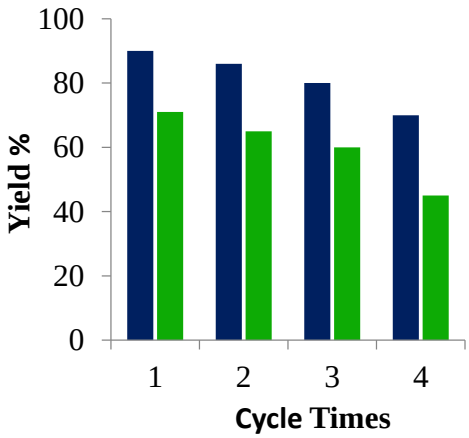

Figure 3.13. *Recyclability of the complex* ***4****. The blue and green bar indicates the yield of benzaldehyde and N-benzylamine in the presence of a catalyst for a separate run, respectively.*

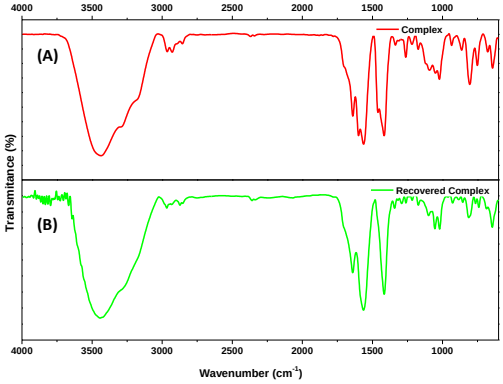

Figure 3.14. *FTIR stretching frequencies of complex* ***4****, (a) before and (b) after catalytic reaction.*

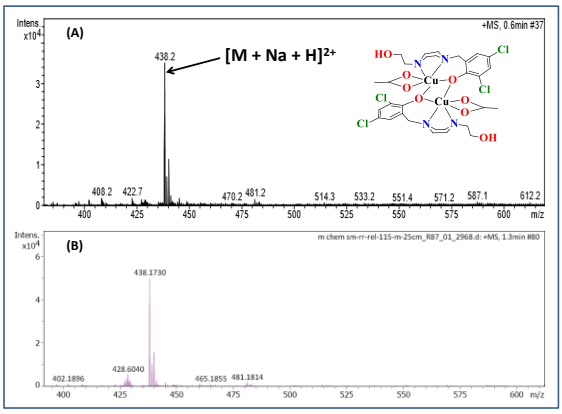

Figure 3.15. *ESI-MS Spectra in MeOH for complex* ***4*** *(A) synthesized and (B) recovered from catalytic reaction.*

3.4. Conclusions

In summary, two new binuclear Cu(II) **[CuHL^1(OAc)]$_2$** and **[CuHL^2(NO$_3$)]$_2$** photocatalyst, which was effective in N-alkylation of aromatic amines under visible light irradiation with no application of other sources of energy in presence of TEMPO have been synthesized and characterized. The phenoxyl radical of the ligand is generated by the transfer of an electron to the copper center and TEMPO plays important roles by abstracting hydrogen from the substrate and acting as the borrower of hydrogen instead of metal ions as per all the literature reports so far. Furthermore, the catalysts can also oxidize benzyl alcohol in presence of oxygen to selectively produce only benzaldehyde with a percentage conversion of 97 and 95% for complex **4** and **5** respectively in 3 h in the presence of visible light. The flexidentate acetate group attached to the central copper ion might be responsible for the better catalytic activity of complex **4**. The

synthesized catalysts survived many cycles of reuse without significant loss of catalytic activity.

3.5 Declaration:

This chapter is adapted from Dalton Trans.**,** 2022, 51**,** 13288-13300. (DOI: 10.1039/D2DT01771G)

3.6 References

[1] Yan, L., Xin-Xin Liu and Fu, Y. (2016), N-Alkylation of amines with phenols over highly active heterogeneous palladium hydride catalysts, RSC Adv. 6 109702-109705.(DOI: 10.1039/ C6RA22383D)

[2] Marina, M., Adrian, P. R., Silvia, G. R., Victoria, F. G., Regadera, J., Zazpe, A., Artaiz, I., Martín-Sanz, P., Ledo, F., Boscá, L., Front. Oncol. 8 (2018) 328.(DOI: 10.3389/fonc.2018.328)

[3] Boehm, H. J., Banner, D., Bendels, S., Kansy, M., Kuhn, B., Muller, K., Obst-Sander, U., Stahl, M. (2004), Fluorine in Medicinal Chemistry, ChemBioChem., 5, 637-643.(DOI: 10.1002/cbic.200301023)

[4] Ismail, F. M. D. (2002), Important fluorinated drugs in experimental and clinical use, J. Fluor. Chem. 118 27-33.(DOI: 10.1016/S0022-1139(02)00201-4)

[5] Hoshimoto, Y., Kinoshita, T., Hazra, S., Ohashi, M., Ogoshi, S. (2018), Main-Group-Catalyzed Reductive Alkylation of Multiply Substituted Amines with Aldehydes Using H_2, J. Am. Chem. Soc., 140, 7292-7300.(DOI: 10.1021/ jacs.8b03626)

[6] Murugesan, K., Chandrashekhar, V. G., Senthamarai, T., Jagadeesh, R. V., Beller, M. (2020), Reductive amination using cobalt-based nanoparticles for synthesis of amines, Nat. Protoc. 15, 1313-1337.(DOI: 10.1038/s41596-019-0258-z)

[7] Bissember, A. C., Lundgren, R. J., Creutz, S. E., Peters, J. C., Fu, G. C. (2013) Transition-Metal-Catalyzed Alkylations of Amines with Alkyl Halides: Photoinduced, Copper-Catalyzed Couplings of Carbazoles, Angew. Chem. Int. Ed., 52, 5129-5133.(DOI: 10.1002/ange. 201301202)

[8] Federica, S., Rinaldo, P., Nicoletta, R., Federica Z. (2012), Reductive Amination of Ketones or Amination of Alcohols over Heterogeneous Cu Catalysts: Matching the Catalyst Support with the NAlkylating Agent, ChemCatChem, 4, 1249-1254.(DOI: 10.1002/cctc.201200213)

[9] Ju, Y., Varma, R. S. (2004), Aqueous *N*-alkylation of amines using alkyl halides: direct generation of tertiary amines under microwave irradiation, Green Chem., 6, 219-221.(DOI: 10.1039/ B401620C)

[10] Corma, A., Navas, J., Sabater, M. J. (2018), Advances in One-Pot Synthesis through Borrowing Hydrogen Catalysis, Chem.Rev, 118, 1410-1459.(DOI: 10.1021/acs.chemrev. 7b00340)

[11] Kodama, T., Kawashima, Y., Deng, Z., Tobisu, M. (2021), Synthesis of 4,5-Benzotropone π Complexes of Iron, Rhodium, and Iridium and Their Potential Use in Catalytic Borrowing-Hydrogen Reactions, Inorg. Chem., 60, 4332–4336.(DOI: 10.1021/acs.inorgchem.0c03587)

[12] Bian, Y., Tam, C. M., To, C. T., Qu, X., Chan, K. S. (2019), Alkylation of Rhodium Porphyrin Complexes with Primary Alcohols under Basic Conditions, Organometallics, 38, 3662-3670.(DOI: 10.1021/acs.organomet.9b00454)

[13] Wong, C. M., Peterson, M. B., Pernik, I., McBurney, R. T., Messerle, B. A. (2017), Highly Efficient Rh(I) Homo- and Heterogeneous Catalysts for C–N Couplings via Hydrogen Borrowing, Inorg. Chem., 56, 14682-14687.(DOI: 10.1021/acs.inorgchem.7b02586)

[14] Guerin, V., Legault, C. Y. (2021), Synthesis of NHC-Iridium(III) Complexes Based on *N*-Iminoimidazolium Ylides and Their Use for the Amine Alkylation by Borrowing Hydrogen Catalysis, Organometallics, 40, 408-417.(DOI: 10.1021/acs.organomet.0c00726)

[15] Yao, W., Duan, Z. C., Zhang, Y., Sang, X., Xia, X. F., Wang, D. (2019), Iridium Supported on Phosphorus-Doped Porous Organic Polymers: Active and Recyclable Catalyst for Acceptorless Dehydrogenation and Borrowing Hydrogen Reaction, Advanced Synthesis & Catalysis 361, 5695-5703.(DOI: ATES DOI: 10.1002/adsc.201900929)

[16] Huang, M., Li, Y., Liu, J., Lan, X. B., Liu, Y., Zhao, C., Ke, Z. (2019), A bifunctional strategy for N-heterocyclic carbene-stabilized iridium complex-catalyzed *N*-alkylation of amines with alcohols in aqueous media, Green Chem., 21, 219-224.(DOI: 10.1039/C8GC02298D)

[17] Zhang, J., Wang, J. (2018), Atropoenantioselective Redox-Neutral Amination of Biaryl Compounds through Borrowing Hydrogen and Dynamic Kinetic Resolution, Angew. Chem. Int. Ed., 57, 465-469.(DOI: 10.1002/anie. 201711126)

[18] Donthireddy, S. N. R., Illam, P. M., Rit, A. (2020), Ruthenium(II) Complexes of Heteroditopic N-Heterocyclic Carbene Ligands: Efficient Catalysts for C–N Bond Formation via a Hydrogen-Borrowing Strategy under Solvent-Free Conditions, Inorg. Chem, 59, 1835-1847.(DOI: 10.1021/acs.inorgchem.9b030 49)

[19] Kaithal, A., Schmitz, M., Hoelscher, M., Leitner, W. (2020), On the Mechanism of the Ruthenium-catalyzed β- methylation of Alcohols with Methanol, ChemCatChem, 12, 781-787.(DOI: 10.1002/cctc.20190)

[20] Ogata, O., Nara, H., Fujiwhara, M., Matsumura, K., Kayaki, Y. (2018), *N*-Monomethylation of Aromatic Amines with Methanol via $PN^{H}P$-Pincer Ru Catalysts, Org. Lett. 20, 3866-3870.(DOI: 10.1021/acs.orglett.8b01449)

[21] Chelucci, G. (2017), Ruthenium and osmium complexes in C-C bond-forming reactions by borrowing hydrogen catalysis, Coordination Chemistry Reviews 331, 1-36.(DOI: 10.1016/ j.ccr.2016.10.002)

[22] Buil, M. L., Esteruelas, M. A., Herrero, J., Izquierdo, S., Pastor, I. M., Yus, M. (2013), Osmium Catalyst for the Borrowing Hydrogen Methodology: α-Alkylation of Arylacetonitriles and Methyl Ketones, ACS Catalysis, 3, 2072-2075.(DOI: 10.1021/cs4005375)

[23] Saravanakumar, E., Jacob, N., Kathrin, J., Matthias, B., Jean-Baptiste, S., Christophe, D. (2016), Efficient and selective *N*-alkylation of amines with alcohols catalysed by manganese pincer complexes, Nat. Comm., 7, 12641.(DOI: 10.1038/ncomms12641)

[24] Fertig, R., Irrgang, T., Freitag, F., Zander, J., Kempe, R. (2018), Manganese-Catalyzed and Base-Switchable Synthesis of Amines or Imines via Borrowing Hydrogen or Dehydrogenative Condensation, ACS Catal., 8, 8525-8530.(DOI: 10.1021/acscatal.8b02530)

[25] Rana, S., Biswas, J. P., Paul, S., Paik, A., Maiti, D. (2021), Organic synthesis with the most abundant transition metal–iron: from rust to multitasking catalysts, Chemical Society Reviews, 50, 243-472.(DOI: 10.1039/D0CS00688B)

[26] Zhang, G., Yin, Z., Zheng, S. (2016), Cobalt-Catalyzed N-Alkylation of Amines with Alcohols, Org. Lett., 18, 300-303.(DOI: 10.1021/acs.orglett. 5b03461)

[27] Mastalir, M., Tomsu, G., Pittenauer, E., Allmaier, G., Kirchner, K. (2016), Co(II) PCP Pincer Complexes as Catalysts for the Alkylation of Aromatic Amines with Primary Alcohols, Org. Lett., 18, 3462-3465.(DOI: 10.1021/acs. orglett.6b01647)

[28] Rosler, S., Ertl, M., Irrgang, T., Kempe, R. (2015), Cobalt-Catalyzed Alkylation of Aromatic Amines by Alcohols, Angew. Chem. Int. Ed., 54, 15046-15050.(DOI: 10.1002/anie. 201507955)

[29] Zhang, G., Hanson, S. K. (2013), Cobalt-Catalyzed Acceptorless Alcohol Dehydrogenation: Synthesis of Imines from Alcohols and Amines, Org. Lett. 15, 650-653.(DOI: 10.1021/ ol303479f)

[30] Das, J., Banerjee, D. (2018), Nickel-Catalyzed Phosphine Free Direct N-Alkylation of Amides with Alcohols, J. Org. Chem., 83, 3378-3384.(DOI: 10.1021/acs.joc.7b03215)

[31] Yang, P., Zhang, C., Ma, Y., Zhang, C., Li, A., Tang, B., Zhou, J. S. (2017), Nickel-Catalyzed N-Alkylation of Acylhydrazines and Arylamines Using Alcohols and Enantioselective Examples, Angew. Chem. Int. Ed., 56, 14702-14706.(DOI: 10.1002/anie.201708949)

[32] Vellakkaran, M., Singh, K., Banerjee, D. (2017), An Efficient and Selective Nickel-Catalyzed Direct N-Alkylation of Anilines with Alcohols, ACS Catal., 7, 8152-8158.(DOI: 10.1021/acscatal.7b02817)

[33] Xu, Z., Yu, X., Sang, X., Wang, D. (2018), BINAP-copper supported by hydrotalcite as an efficient catalyst for the borrowing hydrogen reaction and dehydrogenation cyclization under water or solvent-free conditions, Green Chem., 20, 2571-2577.(DOI: 10.1039/C8GC00557E)

[34] Zhaojun, Z., Wang, D. S., Yu, X., Yang, Y., Wang, D. (2017), Tunable Triazole-Phosphine-Copper Catalysts for the Synthesis of 2-Aryl-1H-benzo[d]imidazoles from Benzyl Alcohols and Diamines by Acceptorless Dehydrogenation and Borrowing Hydrogen Reactions, Advanced Synthesis & Catalysis, 359, 3332-3340.(DOI: 10.1002/adsc.201700179)

[35] Liu, H., Chuah, G. K., Jaenicke, S. (2015), Self-coupling of benzylamines over a highly active and selective supported copper catalyst to produce N-substituted amines by the borrowing hydrogen method, Journal of Catalysis, 329, 262-268.(DOI: 10.1016/j.jcat.2015.05.029)

[36] Santoro, F., Psaro, R., Ravasio, N., Zaccheria, F. (2014), N-Alkylation of amines through hydrogen borrowing over a heterogeneous Cu catalyst, RSC Advances, 4, 2596-2600.(DOI: 10.1039/C3RA44364G)

[37] Paul, A., Martins, L. M. D. R. S., Karmakar, A., Kuznetsov, M. L., da Silva, M. F. C. G., Pombeiro, A. J. L. (2020), Zn(II)-to-Cu(II) Transmetalation in an Amide Functionalized Complex and Catalytic Applications in Styrene Oxidation and Nitroaldol Coupling, Molecules, 25, 2644.(DOI: 10.3390/molecules 25112644)

[38] Ju, S., Yusuf, M., Jang, S., Kang, H., Kim, H. S., Park, K. H. (2019), Simple Transformation of Hierarchical Hollow Structures by Reduction of Metal–Organic Frameworks and Their Catalytic Activity in the Oxidation of Benzyl Alcohol, Chem. Eur. J., 25 7852-7859.(DOI: 10.1002/chem.201900231)

[39] Kundu, B. K., Ranjan, R., Mukherjee, A., Mobin, S. M., Mukhopadhyay, S. (2019), Mannich base Cu(II) complexes as biomimetic oxidative catalyst, J. Inorg. Biochem, 195, 164-173.(DOI: 10.1016/j.jinorgbio.2019.03.023)

[40] Seneque, O., Campion, M., Douziech, B., Giorgi, M., Le Mest, Y., Reinaud, O. (2003), Supramolecular control of an organic radical coupled to a metal ion embedded at the entrance of a hydrophobic cavity, Dalton Trans., 22**,** 4216-4218.(DOI: 10.1039/B308255E)

[41] Gennarini, F., David, R., Lopez, I., Le Mest, Y., Reglier, M., Belle, C., Thibon-Pourret, A., Le Poul, N. (2017), Influence of Asymmetry on the Redox Properties of Phenoxo- and Hydroxo-Bridged Dicopper Complexes: Spectroelectrochemical and Theoretical Studies, Inorg. Chem., 56**,** 7707-7719. (DOI: 10.1021/acs.inorgchem.7b00338)

[42] Chebout, O., Trifa, C., Bouacida, S., Boudraa, M., Imane, H., Merzougui, M., Mazouz, W., Ouari, K., Boudaren, C., Merazig, H. (2022), Two new copper (II) complexes with sulfanilamide as ligand: Synthesis, structural, thermal analysis, electrochemical studies and antibacterial activity, journal of Molecular Structure 1248, 131446. (DOI: 10.1021/acs.inorgchem.7b00338)

[43] Biswas, S., Naiya, S., Gómez-García, C. J., Ghosh, A. (2012), Synthesis of the first heterometalic star-shaped oxido-bridged MnCu3 complex and its conversion into trinuclear species modulated by pseudohalides (N3−, NCS− and NCO−): Structural analyses and magnetic properties, Dalton Transactions, 41, 462-462. (DOI: 10.1039/c1dt11333j)

[44] Sajidu, S. M. I.,Persson, I.,Masamba, W. R. L.,Henry, E. M. T. (2008), Mechanisms of heavy metal sorption on alkaline clays from Tundulu in Malawi as determined by EXAFS, Journal of Hazardous Materials, 158, 401-409.(DOI: 10.1016/j.jhazmat.2008.01.087)

[45] Köppel, H., Yarkony, D. R., Barentzen, H., (08-Dec-2009), The Jahn-Teller Effect: Fundamentals and Implications for Physics and Chemistry.Springer Science & Business Media, Springer Heidelburg Dordrecht London New York.

Chapter 4

Employing Cu(II) complexes of N,O-donor ligand for catalysis in visible light driven cleavage of lignin C-C bonds

Chapter 4

Employing Cu(II) complexes of N,O-donor ligand for catalysis in visible light driven cleavage of lignin C-C bonds

4.1 Introduction

Lignocellulosic biomass is a significant renewable feedstock for the fabrication of valuable chemicals and petrochemicals that could reduce dependence on fossil-based resources [1]. It is a heterogeneous aromatic biopolymer of three phenyl propane units, namely coniferyl (G), p-coumaryl (H) and sinapyl (S) units [2-4]. The aromatic units of lignocellulose can be converted into valuable chemicals and high-grade fuels, which can solve the present concerns regarding the limited fossil fuel resources [5,6].

The phenyl propane units of the lignin biopolymer are linked by various C-C and C-O bonds, including β-1, β-O-4, 4-O-5, β-β, 5-5′, α-1 and so on [2-4,7]. The β-O-4 linkage contributes around 40% to 64% of all the bonds present in lignin [5, 8, 9]. Therefore, the breaking of the β-O-4 bonds are producing low molecular weight aromatic chemicals. The oxidative cleavage of C–O or C–C bonds can cause the depolymerization of β-O-4 linkages. At present, researchers are focusing on the depolymerization of lignin through the C–O bonds cleavage [10-16]. The selective cleavage of stable inter-unit C–C bonds is challenging for researchers [2, 17]. Therefore, to selectively break the C–C bonds of lignin, an efficient catalytic system should be developed. CuCl with pyridine can catalyze the oxidative cleavage of C–C bond [18]. From the green chemistry point of view, the copper-catalyzed aerobic oxidative depolymerization of lignin in water solvent in the absence of any bases or acids is better than the use of harmful organic solvents [19–21]. Phenols are readily oxidized or repolymerized under oxidative conditions, resulting in undesired products [22]. Previously researchers have reported the poor yields of phenols by oxidative cleavage of lignin models [23-25]. Thus, the oxidative cleaving of lignin under mild ambient conditions could maximize the yield of desired monomers. Changzhou Chen and co-workers reported a photocatalytic degradation of the lignin model compound (2-phenoxyacetophenone) by using Ni/TiO_2/DMF affording phenol almost quantitatively [26]. So far, only a few reports have been published in which

photocatalytic degradation of lignin is pursued [27-29].

In continuation to the effort to extend the photocatalysis by copper(II) complexes in the realm of organic transformation, degradation of lignin by cleaving the β-O-4 linkage has been taken up and hereby a flexible ligand viz. Synthesis of 2-(((3-(dimethylamino)-2,2-dimethylpropyl)imino)(phenyl)methyl)phenol (HL^3) is employed to synthesize binuclear copper(II) complexes **$[Cu(L^3)Cl]_2$ (6)** and **$[Cu(L^3)(N_3)]_2$ (7)** to act as catalysts for such conversions. In the presence of visible light, it has found that the complexes **6** and **7** can selectively cleave the C–C bonds of lignin model substrates into corresponding phenols and benzoic acids under mild conditions in the water.

4.2 Experimental Section

4.2.1 Materials and methods

All the chemical reagents required were purchased from sigma and used without further purification. The specifications of all the instruments used for analysis purposes were the same as described in section 2A.2.1 of the previous chapter 2A.

4.2.2 X-ray crystallography

Single crystal X-ray structural studies of **6** and **7** were performed following a similar protocol as mentioned in section 2A.2.2 of previous chapter 2A. The crystal refinement data are summarized in Table 4.1.

Table 4. 1. *Crystallographic data and structure refinement parameters for* ***6****, and* ***7****.*

Complex	**6**	**7**
Empirical Formula	$C_{40}H_{50}Cl_2Cu_2N_4O_2$	$C_{40}H_{50}Cu_2N_{10}O_2$
Formula weight	816.82 g/mol	830.00 g/mol
Crystal system	orthorhombic	Monoclinic
Space group	P c a 21	P 21/n
a (Å)	18.723(5)	13.1604(6)
b (Å)	8.784(2)	12.1030(4)
c (Å)	23.229(5)	13.4284(7)
α (°)	90	90
β (°)	90	111.818(6)
γ (°)	90	90
V ($Å^3$)	3820.3(16)	1985.67(17)
λ (Å)	0.71073	0.71073
ρcalcd (g cm^{-3})	1.420	6.247
Z	4	4
T(K)	100(2)	273(2)
μ (mm^{-1})	1.293	1.119
F(0 0 0)	1704	868
Crystal size (mm^3)	0.08 × 0.08 × 0.10	0.40 × 0.20 × 0.08
θ ranges (°)	2.18 to 27.16	6.42 to 58.22
h/k/l	-24,24/-11,11/-29,29	-16,16/-13,13/-17,17
Reflections collected	58107	15422
Independent reflections	8429	4694
Tmax and Tmin	0.904 and 0.882	0.764 and 0.639
Data/restraints/ parameters	8429 / 0 / 460	4694 / 0 / 109
Goodness-of-fit	1.055	1.973
Final R indices [I > 2σ(I)]	R1 = 0.0247, wR2 = 0.0640	R1 = 0.1022, wR2 = 0.2861
R indices (all data)	R1 = 0.0281, wR2 = 0.0652	R1 = 0.1250, wR2 = 0.03062
Largest peak and hole (e $Å^{-3}$)	0.314 and -0.438	2.94 and -2.02

4.2.3 Synthesis of 2-(((3-(dimethylamino)-2,2-dimethylpropyl)imino)(phenyl) methyl)phenol (HL^3)

A mixture of 2-hydroxy-benzophenone (1.19 g, 6 mmol) and N,N,2,2-tetramethyl-propane diamine (0.78 g, 6 mmol) was refluxed in 20 mL of ethanol for 3 hrs and then allowed to cool up to room temperature. After that, the solvent was removed under vacuo to obtain viscous yellowish oil (1.85 g, 6 mmol, yield 94 %). This oil was utilized without any further purification. ^{1}H NMR (500 MHz, 298 K, $CDCl_3$): δ 7.51 (3H, d, ArH), 7.28 (1H, t, ArH), 7.20 (2H, d, ArH), 7.00 (1H, d, ArH), 6.80 (1H, d, ArH), 6.64 (1H, t, ArH), 3.19 (2H, s, =NCH_2-), 2.30 (6H, s, -$N(CH_3)_2$), 2.26 (2H, s, N-CH_2-C), 0.96 (6H, s, C-$C(CH_3)_2$-C) ppm; ^{13}C NMR (100.61 MHz, 298 K, $CDCl_3$): δ 174.19 (C of $(Ar)_2C$=N), 164.19 (C of ArOH), 133.98 (C of Ar-C), 132.46 (C of Ar), 131.41 (C of Ar), 128.96 (C of Ar), 128.70 (C of Ar), 127.41 (C of Ar), 119.63 (C of Ar-C), 118.21 (C of Ar), 116.91 (C of Ar), 68.25 (C of C-N-C) , 59.91 (C of C-N=C), 48.81 (C of $N(CH_3)_2$), 36.99 (C of C-$C(CH_3)_2$-C) and 24.62 (C of $C(CH_3)_2$) ppm (figure 4.2). Anal. Calcd (%) for $C_{20}H_{26}N_2O$: 77.38 for C; 8.44 for H; 9.02 for N. Found 77.34 for C; 8.50 for H; 9.03 for N. FTIR in KBr (υ in cm^{-1}): 3690–3010 {υO-H, (m)}; 2980–2725 {υC-H, (m)}; 1750-1525 {υC=N, C=C (m)}; 1350–1235 {υC-N,C-O (m)};. ESI-MS (HPLC MeOH) (m/z): 311.215 (100%) $[M+H]^+$ (figure 4.3).

4.2.4 Synthesis of complex $[Cu(L^3)Cl]_2$ (6)

A 10 mL acetonitrile solution of **HL^3** (0.186 g; 0.6 mmol) and triethylamine (85 µL; 0.6 mmol) was taken and it was followed by the dropwise addition of 10 mL acetonitrile solution of $CuCl_2.2H_2O$ (0.102 g; 0.6 mmol). The resulting green solution, after 4 hrs of stirring, was concentrated up to 4-5 mL by evaporation under vacuo. After filtration, the concentrated reaction mixture was left for slow evaporation. After four or five days, green square-shaped crystals are obtained. Filtration and diethyl ether washing were used to collect the crystals. ESI-MS $[C_{40}H_{50}Cl_2Cu_2N_4O_2 + Na]^+$ 839.175 (figure 4.4); Anal. Calcd. (%) for $C_{40}H_{50}Cl_2Cu_2N_4O_2$: 58.81 for C; 6.17 for H; 6.86 for N. Found (%): 58.76 for C; 6.14 for H; 6.80 for N; FTIR in KBr (υ in cm^{-1}): 3100–2800 {υC-H, (m)}; 1750-1480 {υC=N, C=C (m)}; 1350–1105 {υC-N,C-O (m)} (figure 4.5). Yield 75%

4.2.5 Synthesis of complex $[Cu(L^3)(N_3)]_2$ (7)

A binuclear complex **7** was prepared by refluxing the reaction mixture of 0.222 g (0.6 mmol) $Cu(ClO_4)_2.6H_2O$, 0.186 g (0.6 mmol) **HL^3** and triethylamine

(85 µL; 0.6 mmol) followed by addition of 0.040 g (0.6 mmol) of sodium azide in 25 mL of methanol. A crystalline green precipitate appears after 4 hrs then the reaction was stopped and allowed to cool up to room temperature and filtered.The suitable single crystals for X-ray diffraction were obtained by the diffusion of MeOH into the solution of DMF after 7-8 days. ESI-MS $[C_{40}H_{50}Cu_2N_{10}O_2 - N_3]^+$ 789.215 (figure 4.4). Anal. Calcd (%) for $C_{40}H_{50}Cu_2N_{10}O_2$: 57.88 for C; 6.07 for H; 16.88 for N. Found (%): 57.85 for C; 6.06 for H; 16.89 for N; FTIR in KBr (υ in cm^{-1}): 3030–2800 {υC-H, (m)}; 2080-2000 {υN=N, (s)}; 1750-1485 {υC=N, C=C (m)}; 1350–1100 {υC-N,C-O (m)} (figure 4.5). Yield 72%

4.2.6 Synthesis of β-O-4 model compounds

β-O-4 model compounds are synthesized by previously reported procedures [30]. The synthesized compounds were analyzed by LCMS (figure 4.1).

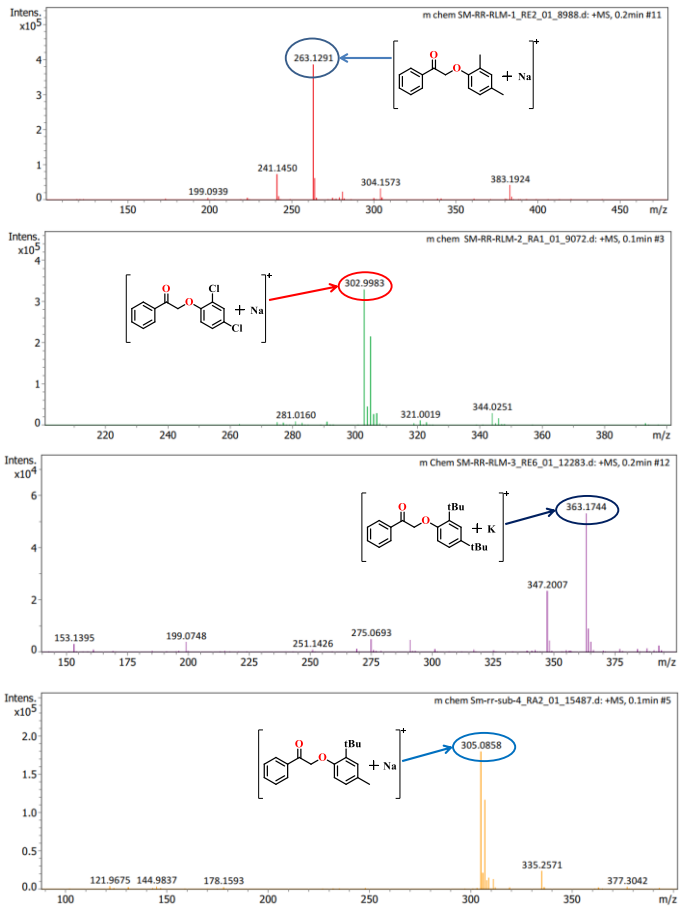

***Figure 4.1**. ESI-MS Spectra in MeOH for Substituted 2-Phenoxy-1-phenylethanone substrates.*

4.2.7 Authentic lignin extraction Procedure

Lignin was extracted from natural biomass resources by a previously reported method [31]. The purity of the compound was confirmed using two-dimensional

heteronuclear single quantum coherence nuclear magnetic resonance (HSQC) NMR. As reported earlier they have correlated the subunits of extracted lignin from the data obtained by HSQC NMR [32, 33].

4.2.8 General procedure for the photocatalytic cleavage reaction

4.2.8.1 Procedure for the model compounds cleavage reaction

All the photocatalytic activities of complexes **6** and **7** were also studied following a similar procedure as described in section 2A.2.6 of previous chapter 2A.

4.2.8.2 Degradation Procedure for authentic lignin material.

The degradation of authentic lignin was performed in a 25 mL round bottom flask by taking 0.1 g of extracted lignin sample (from pineapple stem), catalyst (40 mg, 0.05 mmol), and H_2O (15 mL) as the solvent. The reaction mixture was stirred at room temp in air for 8 hrs in the presence of 12 watts of visible light LEDs. After the reaction, the residue was analyzed through two-dimensional HSQC NMR and HPLC.

4.3 Results and discussion

4.3.1 Syntheses of the ligands and complexes

The ligand (**HL^3**) was synthesized by using a conventional Schiff base condensation method in ethanol (scheme 4.1).

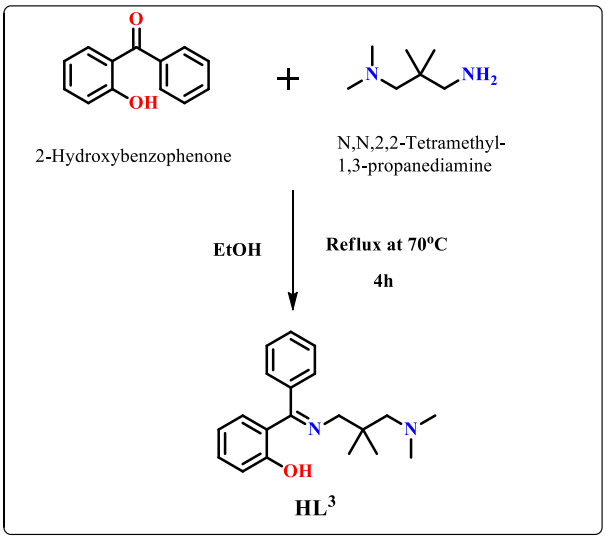

Scheme 4.1. *Synthesis of Ligand*

The compound (**HL^3**) was obtained with a good yield and further characterized by mass spectrometry and ^{1}H, ^{13}C NMR spectroscopy (figure 4.2). The molecular ion peak of the ligand was obtained at 311.21 $[M + H]^+$ (figure

4.3). The bands at 3490 cm^{-1} and 1605 cm^{-1} in the FTIR spectrum of the ligand indicate the presence of phenolic –OH and C=N, which is in analog with previously reported similar compounds [34].

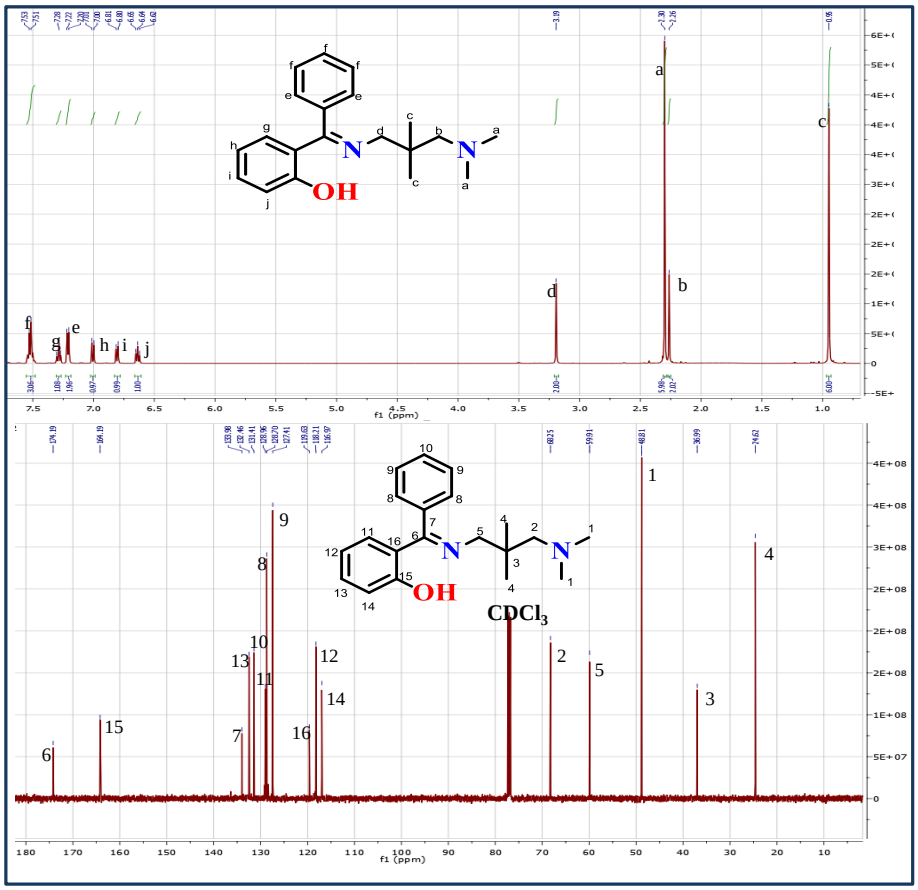

Figure 4.2. *^{1}H and ^{13}C NMR of* ***HL³***.

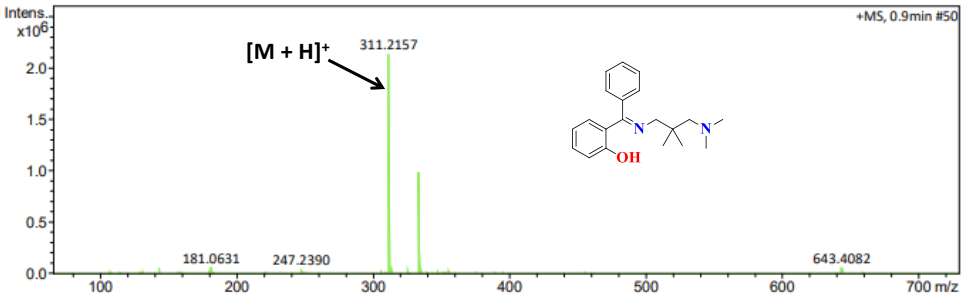

Figure 4.3. *ESI-MS spectrum of* ***HL³***.

A mixture of metal salt precursors with ligand and triethylamine, upon stirring/refluxing for 4 hours furnished the desired binuclear metal complexes **6** and **7** according to scheme 4.2.

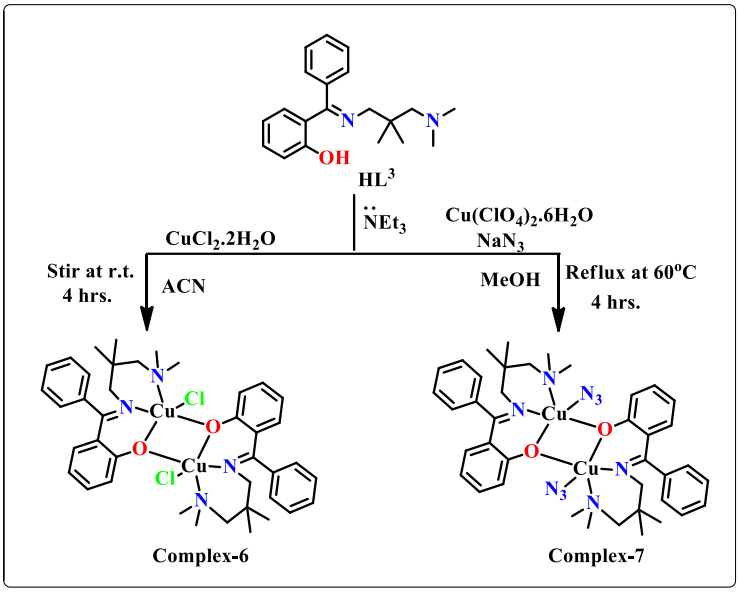

Scheme 4.2. *Synthesis of Complexes.*

The obtained green-colored compounds were characterized using elemental analysis, FTIR, mass spectrometry, SCXRD and PXRD. Molecular ion peak $[M + Na]^+$ for complex **6** and $[M – 2(N_3)]^{2+}$ for complex **7** was obtained at 839.175 and 789.218, respectively (figure 4.4). Both the metal complexes have shown the shifting of C=N from 1605 to 1650 cm^{-1}. The stretching frequency at 2048 cm^{-1} indicates the presence of N=N bonds of the azide group in the case of complex **7** (figure 4.5).

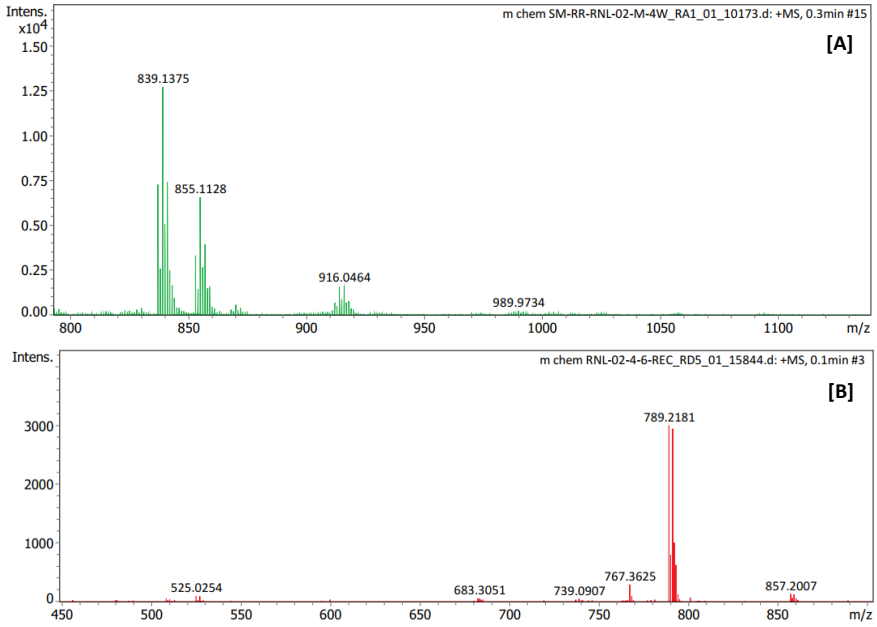

Figure 4.4. *ESI-MS Spectra in ACN for [A] complex **6** and [B] complex **7**.*

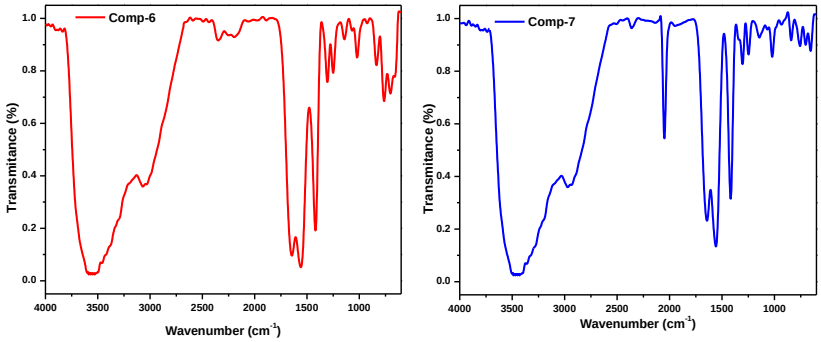

Figure 4.5. *FTIR Spectra for complex **6** and complex **7**.*

4.3.2 Description of Crystal Structures of Complexes 6 and 7.

The single crystal X-ray crystallographic technique was used to determine the solid-state structures of both metal complexes. Figure 4.6(a) and 4.6(b) represent the distorted square pyramidal structure of the copper complexes.

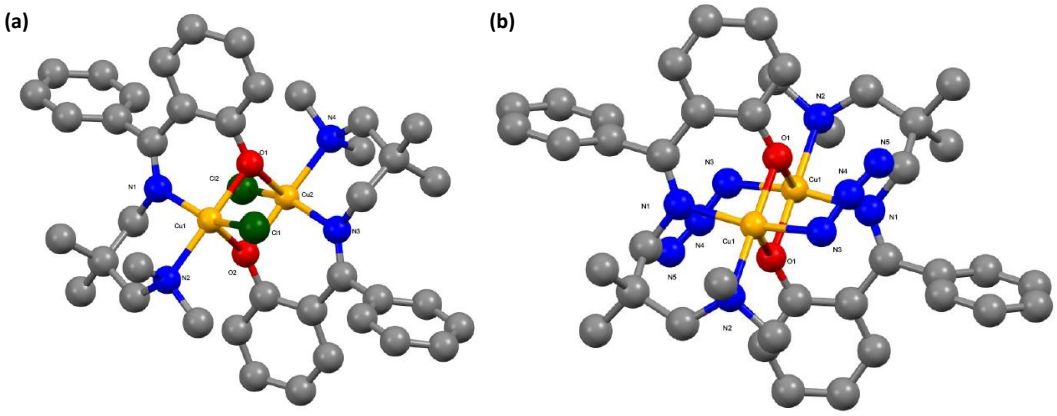

Figure. 4.6. *The solid-state crystal structure for (a) complex **6** (b) complex **7**, Hydrogen atoms are omitted for clarity.*

Table 4.2 represents the selected bond distances and angles. Complex **6** and **7** are crystallizes in orthorhombic space group Pca21 and monoclinic space group p-2 1/n, respectively. Both structures show binuclear complex formation in which the copper ions are found to be penta-coordinated. Ligand bounded tetradentedly with copper ions by two O- and two N-donor sites in both complexes **6** and **7**. The Cu(II) ions are bounded with one Cl^- and one N_3^- ion in the case of complex **6** and **7** respectively. The calculated **τ** values for compound **6** are 0.40 and 0.42 for two metal centers indicating the distorted square-pyramidal geometry. In complex **7** the **τ** value is 0.295 also indicates the distorted square-pyramidal geometry.

***Table 4. 2**. Selected bond lengths (Å) and bond angles (°) for **6** and **7**.*

Complex 6		Complex 7	
Cu1-O1	1.943(2)	Cu1-O1	1.950(2)
Cu1-O2	2.257(2)	Cu1-O1	2.350(3)
Cu1-N1	2.034(3)	Cu1-N1	2.021(4)
Cu1-N2	2.053(2)	Cu1-N2	2.080(3)
Cu1-Cl1	2.3014(11)	Cu1-N3	1.978(3)
Cu2-O2	1.944(2)	N3-N4	1.194(2)
Cu2-O1	2.254(2)	N4-N5	1.153(2)
Cu2-N3	2.034(3)		
Cu2-N4	2.054(2)		
Cu2-Cl2	2.2997(11)		
O1-Cu1-N1	86.11(10)	O1-Cu1-O1	83.04(12)
O1-Cu1-N2	178.88(10)	O1-Cu1-N1	87.97(11)
N1-Cu1-N2	93.17(10)	O1-Cu1-N2	178.07(13)
O1-Cu1-O2	83.57(8)	O1-Cu1-N3	90.29(12)
N1-Cu1-O2	90.56(10)	N1-Cu1-N2	93.17(12)
N2-Cu1-O2	95.58(9)	N1-Cu1-N3	160.32(14)
O1-Cu1-Cl1	87.56(7)	N2-Cu1-N3	88.11(11)
N1-Cu1-Cl1	153.44(8)	N3-N4-N5	177.34(12)
N2-Cu1-Cl1	93.46(8)		
O2-Cu1-Cl1	114.32(7)		
O2-Cu2-N3	86.10(10)		
O2-Cu2-N4	179.17(10)		
N3-Cu2-N4	93.19(10)		
O2-Cu2-O1	83.64(8)		
N3-Cu2-O1	90.28(10)		
N4-Cu2-O1	95.93(9)		
O2-Cu2-Cl2	87.23(7)		
N3-Cu2-Cl2	154.73(8)		
N4-Cu2-Cl2	93.60(8)		
O1-Cu2-Cl2	113.15(7)		

4.3.3. Electrochemistry

Upon oxidation of the Schiff-base ligand **(HL^3)** a prominent oxidation peak at +1.30 V and another at +1.65 V was observed, which suggests the irreversible oxidation behavior of the ligand. Among the complexes, upon

oxidation a reversible oxidation peak at +0.55 V is found in the case of complex **6**, whereas complex **7** shows an irreversible oxidation peak at +0.86 V, both indicate that the generation of phenoxyl radical from phenoxide ion.[35] Apart from that the Cu(II)/Cu(I) redox couple peaks are observed in the cases of both the complexes. Complex **6** has shown a stronger reduction peak for the reduction of Cu(II) to Cu(I) at ($E_{1/2}$ = -0.86 V) whereas in the case of complex **7** we got the reduction peak at ($E_{1/2}$ = -1.18 V) (figure 4.7).

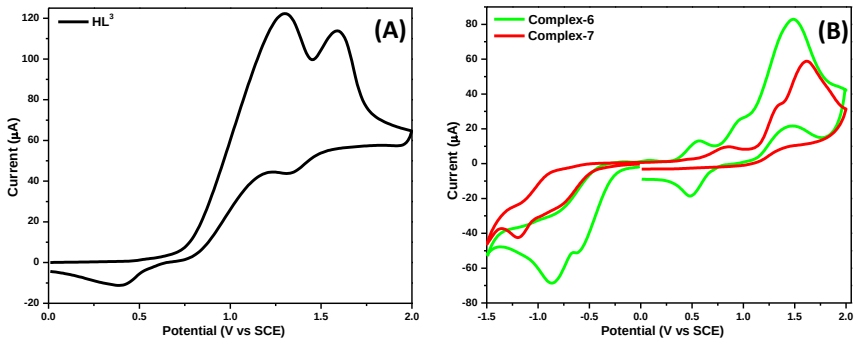

Figure 4.7. *Cyclic voltammograms of (1.0 × 10^{-4} M) solution of (a) Ligand,* ***HL³*** *and (b) complexes* ***6*** *and* ***7*** *in CH_2Cl_2 containing 0.1 M Bu_4NPF_6 as the supporting electrolyte. The data were recorded at a scan speed of 100 mV s^{-1} at 25 °C.*

4.3.4 Electronic spectra

Acetonitrile was used to record the electronic spectra of complexes **6** and **7**. A broad peak arises at 510 nm for the d-d absorption band in the cases of both complexes, which indicates the square pyramidal geometry (figure 4.8) [36]. The band around 390 nm arises due to the ligand to metal charge transfer (LMCT) transition. Bands observed below 360 nm are due to internal transitions of the ligand.

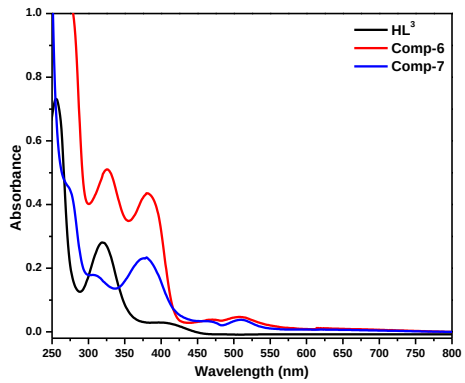

Figure 4.8*. UV-Vis spectra in dichloromethane for ligand and complexes.*

4.3.5 Photocatalytic cleavage of model compounds

Under visible light irradiation, both complexes were investigated for their ability to catalyze the oxidative cleavage of the lignin β-O-4 model compound, 2-phenoxy-1-phenylethanone (1a). The cleavage of lignin into phenols and carboxylic acids is an important reaction in organic and biochemistry because of the significant nature of such a depolymerization reaction.

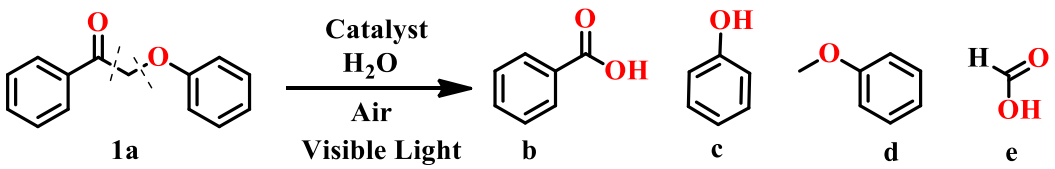

Table 4.3. Photocatalytic degradation of 2-phenoxy acetophenone by complex 6/H_2O/base[a]

Entry No	Base	Conversion [%]	Selectivity [%] b	c	d	Yield [%] b	c	TON (h^{-1})
1	none	85	50	50	None	85	85	113
2[b]	none	40	50	50	None	40	40	53
3	KOH	92	50	25	25	92	46	122
4	NaOH	90	50	30	20	90	54	120
5	Na_2CO_3	90	50	35	15	90	63	120
6	Cs_2CO_3	90	50	35	15	90	63	120
7	K_2CO_3	90	50	30	20	90	54	120

[a]General reaction conditions: Substrate (0.1 mmol), catalyst ***complex 6*** *(5 mol%), Base (0.2 mmol), solvent volume (2 mL), light intensity (12 Watt white LED bulb, 400−800 nm wavelength range), room temperature (~25 °C), Stir for 3h. [b]stirring.*

The photocatalytic ability of lignin degradation by the prepared copper complexes was verified in the presence of visible light. Both compounds have shown promising ability towards the depolymerization of β-O-4 bond. To optimize the reaction conditions, 2-phenoxy-1-phenylethanone has been chosen as the model substrate and the degradation reaction was studied in different reaction conditions by using different bases for better reactivity as per Table 4.3. The reaction was executed upon visible light irradiation (12 watts of the LEDs) for 3 h at room temperature in air. Complex **6** with H_2O as a solvent in the presence of two equivalents of KOH afforded 92% degradation of the model

substrate (entry 3). In the presence of other bases like NaOH, Na_2CO_3, Cs_2CO_3 and K_2CO_3 the reaction afforded 90% degradation product, but the selectivity towards the valuable phenol product is low (entry 4, 5, 6 and 7 respectively). In the absence of base, we got 85% degradation product with an equal selectivity towards benzoic acid as well as phenol, which is best with respect to other reaction conditions (entry 1). The degradation of model substrate was observed only up to 40% after 3 hrs, without irradiation of visible light (entry 2). The photocatalytic degradation reaction does not proceed in the absence of Cu complex.

Table 4.4. Percentage conversion of substituted 2-phenoxy acetophenone by catalysts 6 and 7.

Entry No	Substrates	Conversion [%]		Products (selectivity %)	
		Cat-6	Cat-7		
1	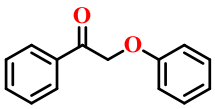	85	79	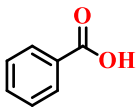 (50)	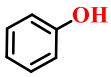 (50)
2	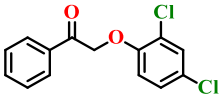	93	88	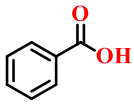 (50)	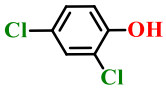 (50)
3	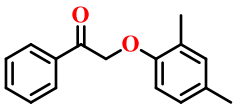	88	80	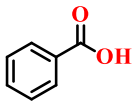 (50)	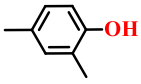 (50)
4	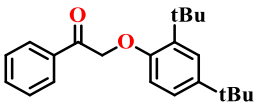	90	80	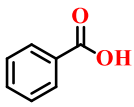 (50)	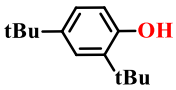 (50)
5	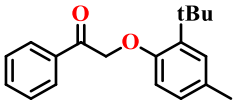	86	80	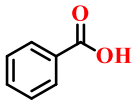 (50)	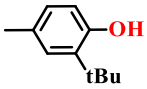 (50)

[a]*General reaction conditions: Substrate (0.1 mmol), catalyst (5 mol%), H_2O (2 mL), light intensity (12 Watt white LED bulb, 400−800 nm wavelength range), room temperature (~25 °C), Stir for 3h.*

The optimized reaction conditions was further extended with other β-O-4 linkage containing substrates by catalysts **6** and **7**, using H_2O as a solvent to investigate the substitution effects (Table 4.4).

The photocatalytic reaction results a general trend according to the electronic influence of the phenoxyl moiety. The conversion of the substrate increases with increasing electron density at the phenoxyl moiety. When the strong electron-donating group, such as chloro, is present, it affords higher conversion than the other similar groups, such as methyl or ^{t}Bu. In the presence of photocatalyst **6**, chloro- substituent afforded 93% conversion, whereas photocatalyst **7** afforded 88% conversion.

4.3.6 Kinetic study of the degradation raeaction

The degradation of a model substrate at different time intervals is shown in figure 4.9a. The Langmuir-Hinshelwood kinetic model equation was used to estimate the kinetic model of photocatalytic reaction.

$$\mathbf{ln(C_0/C_t) = kt}$$

Where C_0 and C_t are the percentage amount of the reactant at t = 0 and t minutes of the reaction, k is the slop of the linear curve and it represents the rate constant of the reaction.

According to Langmuir-Hinshelwood kinetic model, the photocatalytic cleavage reaction follows the pseudo-first-order reaction kinetics (figure 4.9b) [37].

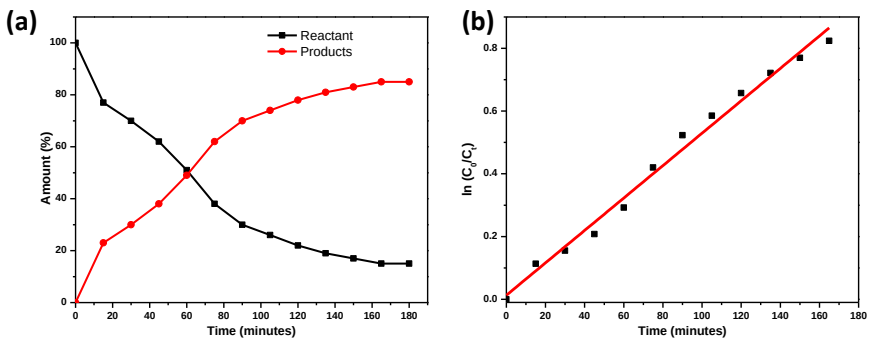

Figure 4.9. *(a) Percentage amount of reactant and products at different time intervals (b) plot of ln(C_0/C_t) versus time (minutes) showing the kinetics of photocatalytic cleavage reaction.*

4.3.7 Mechanistic study of the degradation reaction of the model substrate

To know the plausible reaction pathway I have done some control experiments. The involvement of molecular oxygen was checked by using the

nitrogen atmosphere instead of air as it is interesting to observe that in the absence of oxygen there is no conversion occurred (scheme 4.3). Only 20% of conversion was observed in the case of 2-hydroxyacetophenone instead of the model substrate, whereas no conversion was observed in the case of benzil in the standard reaction conditions (scheme 4.3). These results suggest that 2-Hydroxy-1-phenylethanone or benzil does not form as an intermediate during the cleavage reaction.

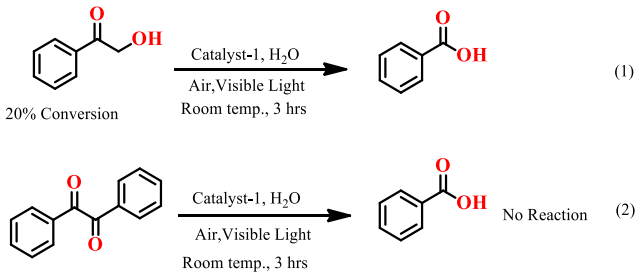

Scheme 4.3. *Control experiments for the possible intermediates*

In order to know the possibility of generation of free radical during the cleavage of the model substrate, TEMPO (2,2,6,6-tetramethyl-1-piperidinyloxy) is used as a radical scavenger. The yields of the products **b** and **c** considerably get reduced from 85% to 43% and 30%, in the presence of 0.5 and 1 equivalent of TEMPO respectively (Table 4.5). The significant inhibition of the reaction in the presence of a free radical scavenger, suggests that the C-C bond cleavage reaction occurs through a free radical pathway.

Table 4.5. *Oxidative cleavage of lignin model substrate by complex-6 in the presence of TEMPO.*

Substrate	**Quantity (equiv.)**	**Conversion (%)**	**Yield (%)**	
			b	**c**
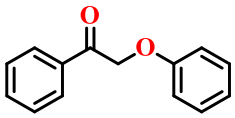	None	85	85	85
	0.5	43	43	43
	1.0	30	30	30

The NMR analysis has been used as a tool to elucidate the formation of benzoic acid and formic acid during the degradation of the model substrate. In the absence of base, we got the ^{13}C peaks for formic acid, benzoic acid and phenol at 171.48 (C of HCOOH), 164.87(carboxylic carbon of benzoic acid) and 155.81

(α–C of phenol) ppm, respectively (figure 4.10). There were no additional products detected, which indicates that intermediates like benzaldehyde or formaldehyde get oxidized in the course of the β-O-4 cleavage reaction in the presence of air and water.

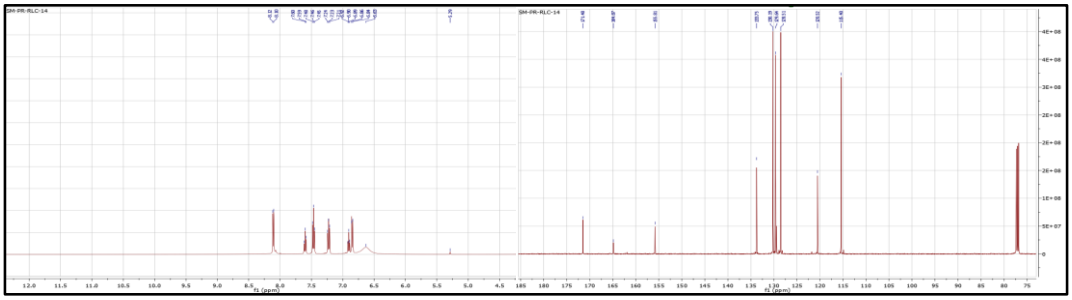

Figure 4.10. *NMR Spectra of degraded product of model substrate 2-Phenoxy-1-phenylethanone in $CDCl_3$ (400.13 MHz, 298K): ^{1}H NMR and ^{13}C NMR.*

On the basis of the above observation and UV-Vis, CV and ESI-MS study, a simplified probable mechanism for C-C cleavage reaction is proposed which is depicted in scheme 4.4. At the beginning of the reaction, model substrate approaches the complex in enol form and binds to the Cu center with an unshared electrons pair of the oxygen and forms the intermediate **'B'** by releasing **HCl**. As per UV-Vis and cyclic voltammetry data analysis, phenoxide ion getting oxidized by visible light into phenoxyl radical by providing a single electron to the Cu(II) which is reduced to Cu(I) species **'C'** [35]. The reduced Cu(I) species can produce the superoxide by providing a single electron to the molecular oxygen from Cu(I), and itself getting oxidized into Cu(II), forming intermediate **'D'** [38]. Afterward the superoxide ion attacks on the double bond of substrate forming the intermediate **'E'**, which gives the benzoate and phenyl formate intermediates, with the formation of species **'F'**, through rearrangement and donating a single electron to the Cu(II) [38, 39]. Subsequently, phenyl formate gets hydrolyzed by water and gives the products phenol and formic acid [39]. In the final step, benzoate gives the product benzoic acid by accepting the H^+ ion from **HCl,** and species F regenerates the **complex A** by the concomitant oxidation of Cu(I).

As support of the proposed mechanism, the mass spectrometric analysis was performed. The result indicates that the intermediate 'B' and 'D' are formed during the catalytic reaction. Molecular ion peaks at 1029.45 and 987.42 for $[B + K]^+$ and D.

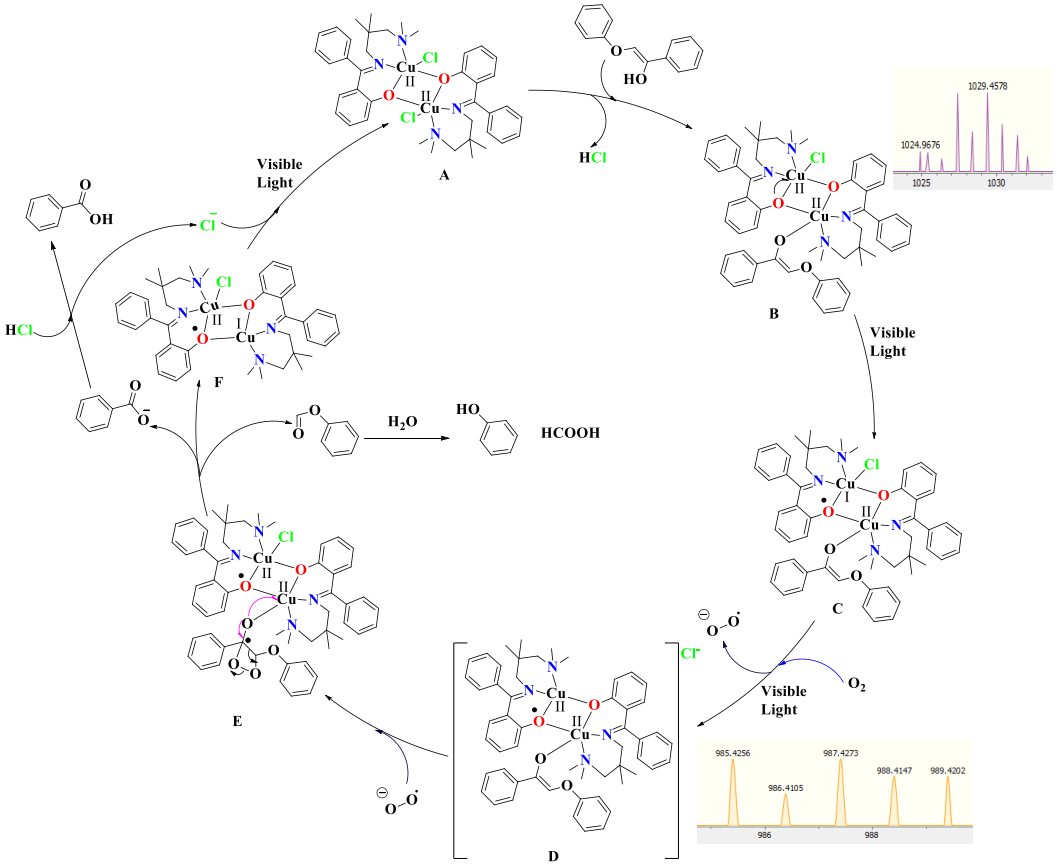

Scheme 4.4. *Proposed mechanism for the photocatalytic C-C cleavage reaction by complex-**6.***

To investigate the proposed photocatalytic cleavage mechanism the DFT calculations studies was carried out (scheme 4.5) to optimize the energy of different intermediates and transition states. In the active catalyst complex 'A', both the copper centers are present in '+2' oxidation state. The reaction free energy profile diagram (scheme 4.5) reveals that (B + HCl) has a lower free energy than (cat A + substrate), making this step favorable. While the mechanism requires 0.8 and 24 kcal/mol more energy in the second and third steps, this may be supplied by visible light. The intermediate E has lower energy than (D + superoxide), similarly (F + benzoate + phenyl formate) has lower free energy than E, so the conversion of D to E and E to F is energetically favorable. The free energy of active catalyst A is higher than the energy of (F + HCl). 34.5 kcal/mol energy is required in the last step of the mechanism for the generation of active catalyst A from the intermediate F, which can be achieved by the visible light, for re-initiation of the next cycle.

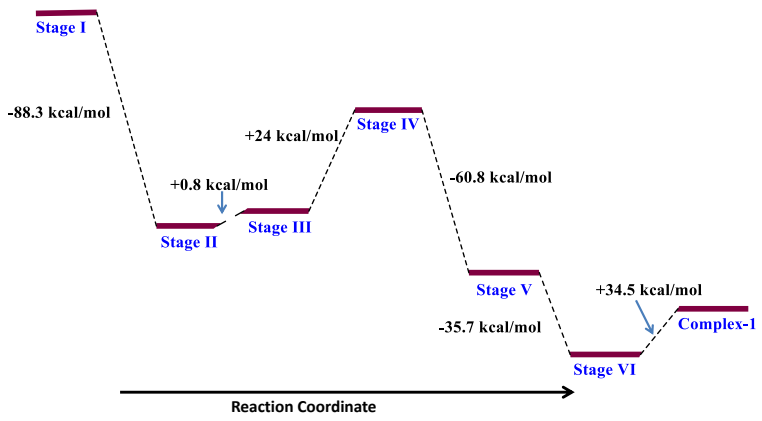

Scheme 4.5. *Reaction free energy profile diagram of proposed mechanism for the photocatalytic C-C cleavage reaction by complex* ***6****.*

4.3.8. Recyclability and reusability of catalyst

The catalyst was utilized for six consecutive cycles without much depreciation of its catalytic activity (figure 4.11).

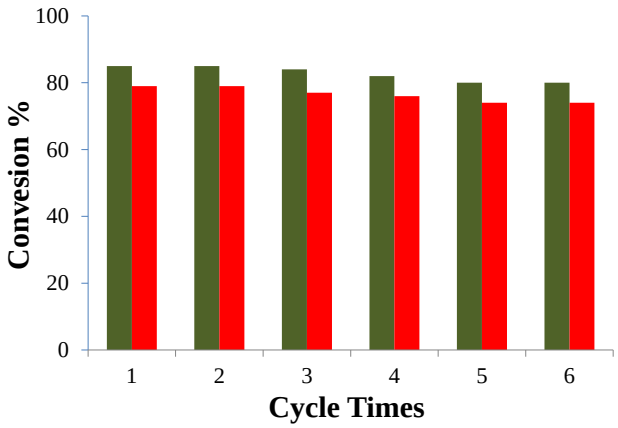

Figure 4.11. *Recyclability of the photocatalyst* ***6*** *and* ***7****. The green and red bar indicates the cleavage of model substrate in the presence of catalyst* ***6*** *&* ***7*** *at 3 h for separate run, respectively.*

After the reaction, both the catalysts can be recovered almost quantitatively from the reaction mixture by filtration, the precipitate catalyst was washed with dichloromethane followed by diethyl ether and dried in vacuum. The PXRD pattern of the recovered and synthesized catalyst indicates the molecular structure of the catalyst almost intact after the photocatalytic reaction (figure 4.12).

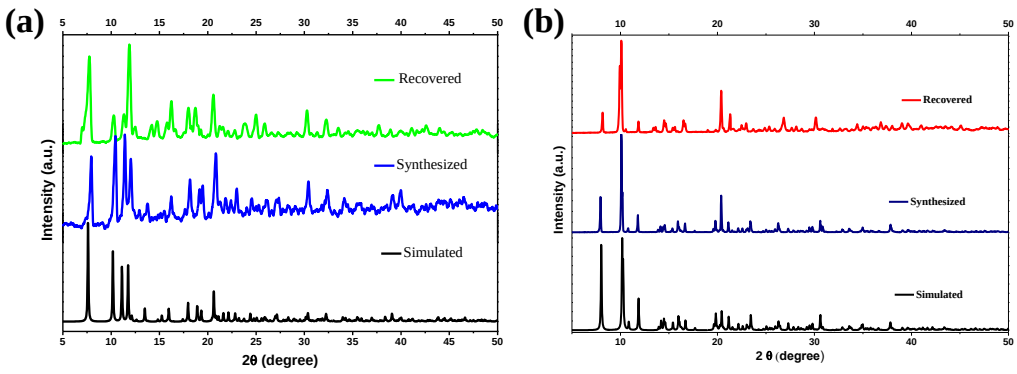

Figure 4.12. *Powder X-ray diffraction patterns for (a) photocatalyst* ***6*** *and (b) photocatalyst* ***7*** *before and after six catalytic cycles.*

4.3.9 The degradation of authentic lignin feedstocks

The photocatalytic degradation results of the lignin model substrates by synthesized catalysts encouraged further to apply it for the conversion of the natural lignin. Cu(II) complexes were used to degrade the lignocellulosic feedstocks, viz. pineapple stem, with the optimized condition. The optimized reaction condition was applied for the depolymerization of extracted lignin for 8 hrs. The aromatic aldehydes syringaldehyde and vanillin, as well as other chemicals including syringic acid and vanillic acid, were produced by the cleavage of pineapple lignin (figure 4.13).

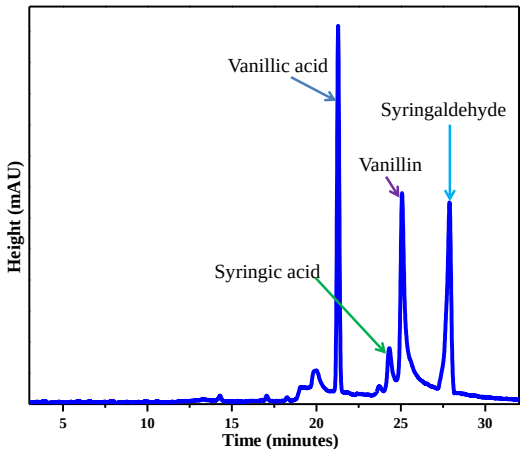

Figure 4.13. *HPLC interpretation of degraded product of authentic pineapple lignin.*

The structural changes of extracted lignin from the pine apple and the degraded products were explained using two-dimensional heteronuclear single quantum coherence nuclear magnetic resonance (2D HSQC-NMR, figure 4.14). In the aliphatic regions of the HSQC data of natural lignin (figure 4.14 (A) and (B)), shows the presence of β-O-4 linkages (structure A of figure 4.14), β–β (structure B of figure 4.14) and β-5 (structure C of figure 4.14) which upon

depolymerization were disappeared, demonstrating that these bonds have been successfully cleaved; whereas in the aromatic region (figure 4.14 (C) and (D)), the signals of G and H peaks decreases and the signal corresponding to S′ appears most prominently in the organic oil. According to the HSQC results, this catalytic system degraded the pineapple lignin into benzylic ketone analogues.

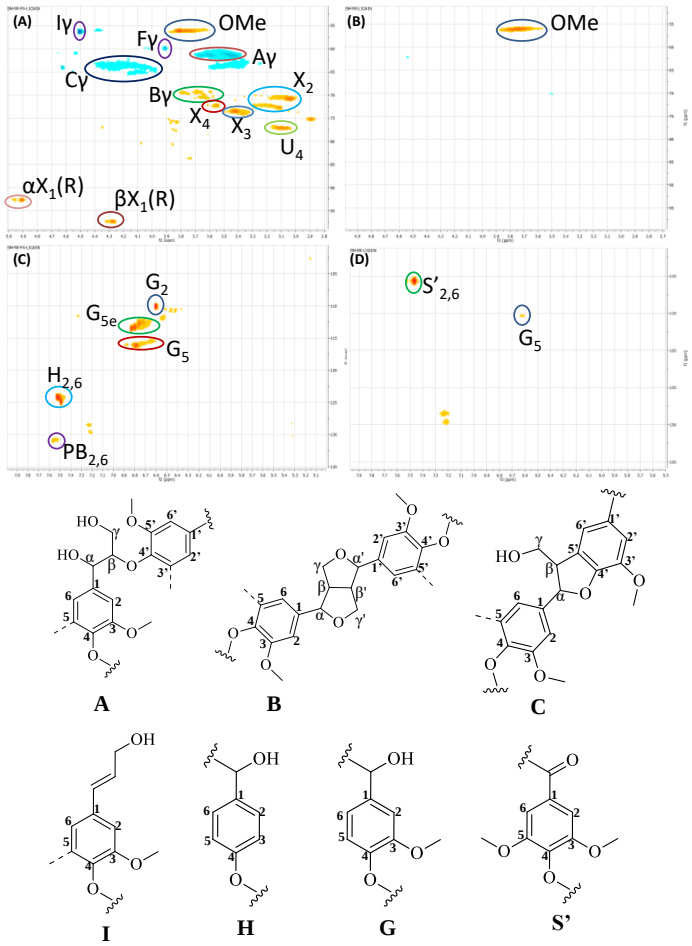

Figure 4.14. *2D HSQC-NMR spectra of pineapple stem lignin sample before (A and C) and after (B and D) reaction. Cross peaks are assigned according to the previous literature.[32,33] Reaction conditions: 0.1 g extracted lignin, 0.05 mmol complex* ***6****, H_2O (15 mL) as the solvent, r.t. (~25°C), 12 Watt LEDs, 8 hrs.*

4.4 Conclusions

In conclusion, two new binuclear Cu(II) containing complexes *viz.* **[CuL(Cl)]$_2$ (6)** and **[CuL(N$_3$)]$_2$ (7)** have been synthesized which show square pyramidal geometry around Cu. Both the complexes efficiently cleaved the lignin model compound (2-phenoxy-1-phenylethanone) as well as authentic lignin (extracted from pineapple stem) at room temperature and in presence of water as a solvent in an environmentally friendly manner. Photocatalyst **6** shows 85% conversion whereas photocatalyst **7** shows up to 79% conversion in 3 h. The

synthesized catalysts have been used for six consecutive cycles without significant decline of catalytic efficiency. A plausible mechanistic pathway for cleavage reaction has been explored through ESI-MS spectrometry, cyclic voltammetry, UV-vis and computational study. The mechanism follows radical pathway which was supported by the observed slow reaction rate in the presence of radical scavenger TEMPO. In the nitrogen atmosphere, no product was observed which indicates that the molecular oxygen plays an important role in the C-C bond cleavage reaction. Most importantly, the photocatalysts can cleave the extracted lignocellulose sample into aromatic aldehydes and acids in a water medium in the presence of visible light in 8 hrs of stirring at room temperature.

4.5 Declaration

This chapter is adapted from **Molecular Catalysis,** 2023, **537,** 112947. (DOI: 10.1016/j.mcat2023.112947)

4.6 References

[1]Tuck, C. O., Pérez, E., Horváth, I. T., Sheldon, R. A., Poliakoff, M. (2012),Valorization of Biomass: Deriving More Value from Waste, Science, 337, 695–699.(DOI: 10.1126/science. 1218930)

[2] Rinaldi, R., Jastrzebski, R., Clough, M. T., Ralph, J., Kennema, M., Bruijnincx, P. C. A., Weckhuysen, B. M. (2016), Paving the Way for Lignin Valorisation: Recent Advances in Bioengineering, Biorefining and Catalysis, Angew. Chem. In. Ed. En., 55, 8164–8215.(DOI: 10.1002/anie.201510351)

[3] Key, R. E., Bozell, J. J. (2016), Progress toward Lignin Valorization via Selective Catalytic Technologies and the Tailoring of Biosynthetic Pathways, ACS Sustainable Chem. Eng., 4, 5123–5135.(DOI: 10.1021/ acssuschemeng.6b01319)

[4] Ragauskas, A. J., Beckham, G. T., Biddy, M. J., Chandra, R., Chen, F., Davis, M. F., Davison, B. H., Dixon, R. A., Gilna, P., Keller, M., Langan, P., Naskar, A. K., Saddler, J. N., Tschaplinski, T. J., Tuskan, G. A., Wyman, C. E. (2014),Lignin valorization: improving lignin processing in the biorefinery, Science, 344, 1246843.(DOI: 10.1126*/science.1246843)*

[5] Zakzeski, J., Bruijnincx, P. C. A., Jongerius, A. L., Weckhuysen, B. M. (2010),The Catalytic Valorization of Lignin for the Production of Renewable Chemicals, Chem. Rev., 110, 3552–3599.(DOI: 10.1021/cr900354u)

[6] Wang, H., Pu, Y., Ragauskas, A., Yang, B. (2019), From lignin to valuable products-strategies, challenges, and prospects, Bioresour. Technol., 271, 449–461.(DOI: 10.1016/j.biortech.2018.09.072)

[7] Xu, C., Arancon, R. A. D., Labidi, J., Luque, R. (2014), Lignin depolymerization strategies: towards valuable chemicals and fuels, Chem. Soc. Rev., 43, 7485–7500.(DOI: 10.1039 /C4CS00235K)

[8] Li, C., Zhao, X., Wang, A., Huber, G. W., Zhang, T. (2015), Catalytic Transformation of Lignin for the Production of Chemicals and Fuels, Chem. Rev., 115, 11559–11624.(DOI: 10.1021/acs.chemrev.5b00155)

[9] Behling, R., Valange S., Chatel, G. (2016), Heterogeneous catalytic oxidation for lignin valorization into valuable chemicals: what results? What limitations? What trends? Green Chem., 18, 1839–1854.(DOI: 10.1039/C5GC03061G)

[10] Lancefield, C. S.; Ojo, O. S.; Tran, F.; Westwood, N. J. (2015), Isolation of Functionalized Phenolic Monomers through Selective Oxidation and C-O Bond Cleavage of the β-O-4 Linkages in Lignin, Angew. Chem. In. Ed. En., 54, 258–262.(DOI: 10.1002/anie.201409408)

[11] Rahimi, A., Ulbrich, A., Coon, J. J., Stahl, S. S. (2014), Formic-acid-induced depolymerization of oxidized lignin to aromatics, Nature, 515, 249–252.(DOI: 10.1038/nature13867)

[12] Rahimi, A., Azarpira, A., Kim, H., Ralph, J., Stahl, S. S. (2013), Chemoselective Metal-Free Aerobic Alcohol Oxidation in Lignin, J. Am. Chem. Soc., 135, 6415–6418.(DOI: 10.1021/ja401793n)

[13] Li, L., Kong, J., Zhang, H., Liu, S., Zeng, Q., Zhang, Y., Ma, H., He, H., Long, J., Li, X. (2020), Selective aerobic oxidative cleavage of lignin C-C bonds over novel hierarchical Ce-Cu/MFI nanosheets, Applied Catalysis B: Environmental, 279, 119343.(DOI: 10.1016/ j.apcatb.2020.119343

[14] Liu, S.; Bai, L.; van Muyden, A. P.; Huang, Z.; Cui, X.; Fei, Z.; Li, X.; Hu, X.; Dyson, P. J. (2019), Oxidative cleavage of β-O-4 bonds in lignin model compounds with a single-atom Co catalyst, Green Chem., 21, 1974–1981.(DOI: 10.1039/C9GC00293F)

[15] Nichols, J. M.; Bishop, L. M.; Bergman, R. G.; Ellman, J. A. (2010), Catalytic C-O Bond Cleavage of 2-Aryloxy-1-arylethanols and Its Application to the Depolymerization of Lignin-Related Polymers, J. Am. Chem. Soc., 132, 12554–12555.(DOI: 10.1021/ja106101f)

[16] Liu, Y., Li, C., Miao, W., Tang, W., Xue, D., Li, C., Zhang, B., Xiao, J., Wang, A., Zhang, T., Wang, C. (2019), Mild Redox-Neutral Depolymerization of Lignin with a Binuclear Rh Complex in Water, ACS Catal., 9, 4441–4447. (DOI: 10.1021/acscatal.9b00669)

[17] Liu, C., Wu, S., Zhang, H., Xiao, R. (2019), Catalytic oxidation of lignin to valuable biomass-based platform chemicals: A review, Fuel Processing Technology, 191, 181–201.(DOI: 10.1016/j.fuproc.2019.04.007)

[18] Lanfranchi, M., Prati, L., Rossi, M., Tiripicchio, A. (1993), The Oxidation of Ethane-1,Z-diol resulting from Molecular Oxygen Activation by Copper: Formation of an Oxoethanoate Complex precedes Carbon-Carbon Bond Cleavage, J. Chem. Soc., Chem. Commun., 22, 1698–1699.(DOI: 10.1039/C39930001698)

[19] Schutyser, W., Kruger, J. S., Robinson, A. M., Katahira, R., Brandner, D. G., Cleveland, N. S., Mittal, A., Peterson, D. J., Meilan, R., Román-Leshkov, Y., Beckham, G. T. (2018) Revisiting alkaline aerobic lignin oxidation, Green Chem., 20, 3828–3844.(DOI: 10.1039/ C8GC00502H)

[20] Liang Y.-F., Jiao, N. (2014), Highly Efficient C-H Hydroxylation of Carbonyl Compounds with Oxygen under Mild Conditions, Angew. Chem. In. Ed. En., 53, 548–552.(DOI: 10.1002/ anie.201308698)

[21] Wendlandt, A. E., Suess, A. M., Stahl, S. S. (2011), Copper-Catalyzed Aerobic Oxidative C-H Functionalizations: Trends and Mechanistic Insights, Angew. Chem. In. Ed. En., 50, 11062–11087.(DOI: 10.1002/anie.201103945)

[22] Cheng, C., Wang, J., Shen, D., Xue, J., Guan, S., Gu, S., Luo, K. H. (2017), Catalytic oxidation of lignin in solvent systems for production of renewable chemicals: a review, Polymers, 9, 240.(DOI: 10.3390/polym9060240)

[23] Mathieu, Y., Vidal, J. D., Arribas, M. L., Abad Fernández, N., Iborra, S., Corma, A. (2020), Molecular Oxygen Lignin Depolymerization: An Insight into the Stability of Phenolic Monomers, ChemSusChem, 13, 4743–4758.(DOI: 10.1002/cssc.202001295)

[24] Bhargava, S., Jani, H., Tardio, J., Akolekar, D., Hoang, M. (2007), Catalytic Wet Oxidation of Ferulic Acid (A Model Lignin Compound) Using Heterogeneous Copper Catalysts, Ind. Eng. Chem. Res., 46, 8652–8656.(DOI: 10.1021/ie070085d)

[25] Wang, M., Gu, X.-K., Su, H.-Y., Lu, J.-M., Ma, J.-P., Yu, M., Zhang, Z., Wang, F. (2015), Preferential cleavage of C-C bonds over C-N bonds at

interfacial CuO-Cu_2O sites, J. Catal., 330, 458–464.(DOI: 10.1016/j.jcat. 2015.08.001)

[26] Chen, C., Liu, P., Xia, H., Zhou, M., Zhao, J., Sharma, B. K., Jiang, J. (2020), Photocatalytic cleavage of β-O-4 ether bonds in lignin over Ni/TiO2, Molecules, 25, 2109.(DOI: 10.3390/molecules25092109)

[27] Sharma, S., Kumar, S., Arumugam, S. M., Elumalai, S. (2020), Promising photocatalytic degradation of lignin over carbon quantum dots decorated TiO2 nanocomposite in aqueous condition, Appl. Catal. A: Gen., 602, 117730.(DOI: 10.1016/j.apcata.2020.117730)

[28] Li, W., Zhang, M., Du, Z., Ma, Q., Jameel, H., Chang, H. (2015), Photocatalytic degradation of lignin model compounds and kraft pine lignin by CdS/TiO2 under visible light irradiation, Bioresources, 10, 1245–1259.

[29] Li, H., Lei, Z., Liu, C., Zhang, Z., Lu, B. (2015), Photocatalytic degradation of lignin on synthesized Ag-AgCl/ZnO nanorods under solar light and preliminary trials for methane fermentation, Bioresour. Technol., 175, 494–501. (DOI: 10.1016/j.biortech.2014.10.143)

[30] Luo, N. C., Wang, M., Li, H. J., Zhang, J., Hou, T. T., Chen, H. J., Zhang, X. C., Lu, J. M., Wang, F. (2017), Visible-Light-Driven Self-Hydrogen Transfer Hydrogenolysis of Lignin Models and Extracts into Phenolic Products, ACS Catal., 7, 4571–4580.(DOI: 10.1021/acscatal. 7b01043)

[31] Wtkins, D., Nuruddin, Md., Hosur, M., Narteh, A. T., jeelani, S. (2015), Extraction and characterization of lignin from different biomass resources, J. Mater. res. technol., 4, 26-32.(DOI: 10.1016/j.jmrt.2014.10.009)

[32] del Rio, J.C., Rencoret, J., Marques, G., Li, J., Gellerstedt, G., J.-Barbero, J., Martínez, Á. T., Gutiérrez, A. (2009), Structural Characterization of the Lignin from Jute (Corchorus capsularis) Fibers, J. Agric. Food Chem., 57, 10271–10281.(DOI: 10.1021/ jf900815x)

[33] Sun, X., Xu, F., Sun, R., Wang, Y., Fowler, P., Baird, M. (2004), Characteristics of degraded lignins obtained from steam exploded wheat straw, Polym. Degrad. Stab., 86, 245–256.(DOI: 10.1016/j.polymdegradstab. 2004.05.003)

[34] Kundu, B. K., Chhabra, V., Malviya, N., Ganguly, R., Mishra, G. S., Mukhopadhyay, S. (2018), Zeolite encapsulated host-guest Cu(II) Schiff base complexes: superior activity towards oxidation reactions over homogenous

catalytic systems, Microporous Mesoporous Mater., 271, 100-117.(DOI: 10.1016/ j.micromeso.2018.05.046)

[35] Ranjan, R., Kundu, B. K., Kyarikwal, R., Ganguly, R., Mukhopadhyay, S. (2022), Synthesis of Cu(II) complexes by N,O-donor ligand transformation and their catalytic role in visible-light-driven alcohol oxidatin, appl. Organomet Chem., 36, e6450.(DOI: 10.1002/aoc.6450)

[36] Christina Chai, L. L., Elix, John A., Huleatt, Paul B. (2005), The synthetic versatility of alkoxycarbonyl- and hydroxymethyl-piperazine-2,5-diones, Tetrahedron, 61, 8722–8739.(DOI: 10.1016/j.tet.2005.06.084)

[37] Preet, K., Gupta, G., Kotal, M., Kansal, S. K., Salunke, D. B., Sharma, H. K., Sahoo, S. C., Voort, P. V. D., Roy, S. (2019), Mechanochemical Synthesis of a New Triptycene-Based Imine-Linked Covalent Organic Polymer for Degradation of Organic Dye, cryst. Growth Des., 5, 2525-2530.(DOI: 10.1021/acs.crd.9b00166)

[38] Hayyan, M., Hashim, M. A., Alnashef, I. M. (2016), Superoxide Ion: Generation and Chemical Implications, Chem. Rev., 116, 3029-3085.(DOI: 10.1021/acs.chemrev.5b00407)

[39] Hu, Y., Yan, L., Zhao, X., Wang, C., Li, S., Zhang, X., Ma, L., Zhang, Q. (2021), Mild selective oxidative cleavage of lignin C–C bonds over a copper catalyst in water, Green Chem., 23, 7030-7040. (DOI: 10.1039/D1GC02102H)

Chapter 5

Zeolite encapsulated host-guest Cu(II) Schiff base complexes: superior activity towards degradation of lignin C=C bonds

Chapter 5

Zeolite encapsulated host-guest Cu(II) Schiff base complexes: superior activity towards degradation of lignin C=C bonds

5.1 Introduction

The selective oxidative cleavage of carbon-carbon double bonds is an important reaction from the synthetic point of view which can play an important role even to degrade polymeric complex compounds like lignin. Obtaining smaller monomeric fragments from lignin, which can be used as alternative sources of fuels in an environment-friendly method is one of the key topic of research in recent past [1-3]. In last few decades, researchers have shown much attention towards the oxidative cleavage of C=C bonds, and in the process they have developed many protocols. Ozonolysis is a classical method for the oxidative cleavage of olefins into aldehydes, ketones, and carboxylic acids [4, 5]. However as the reactivity, and toxicity of the ozone are high and it causes pollution of the ground-level air, therefore it is considered as a dangerous reagent and researchers have moved to find some alternative oxidants. The following reagents have been developed as useful oxidants in recent past which can selectively cleave the olefin bonds after oxidation, viz. Oxone, [6, 7] $OsO_4/NaIO_4$ [8], H_2O_2 [9], m-CPBA [10], $KMnO_4$ [11], etc. These oxidants have some disadvantages, such as toxicity and the generation of oxidant waste. On the other hand t-BuOOH is known as a photoactive oxidant and it provides free radicals in the presence of light under mild conditions [12]. The photochemical reactions are considered as environmentally friendly and greener approach. Visible light is an economic and greener source of energy and has attracted much attention of the researchers in last decades.

Vanillin is a natural product and one of the popular substances for flavoring and it is used as an additive in the cosmetic, food, and pharmaceutical industries [13]. However, approximately 98% of the total worldwide vanillin production happens through artificially synthesis [14, 15]. Vanillin can be synthesized by the oxidative cleavage of several chemical compounds such as isoeugenol [16], guaiacol [17], ferulic acid [18-21], and lignin [14]. Ferulic acid

is a highly abundant compound in the lignocellulosic biomass as pectin and lignin in the cell walls of the seeds cover, flowers, grasses, leaves and stems [22, 23]. Therefore, this type of compound can work as a remarkable feedstock for the production of valuable aromatic molecules through the environmentally friendly process. Gonzalez *et al.* [24], and Flores *et al.* [20] reported in 2017 and 2018 a Cu(II) based metal-organic polyhedron and MOF respectively which are capable to cleave the C=C bond of trans-ferulic acid in the presence of H_2O_2 oxidant. After that, in 2019 Lopez *et al.* [25] reported that Cu/TiO_2 can also cleaves the carbon-carbon double bond of ferulic acid in the presence of light and oxidant H_2O_2. However, in these cases the selectivity towards the vanillin is low and the over-oxidized product vanillic acid is found as the major product.

Zeolites have a high surface area and also show excellent ion exchange properties in the presence of light making them a good base for designing the host-guest photo catalysts [26]. The recent reports on Cu(II) photocatalysts indicate that the N_2O_2-donor ligand system with the aromatic moiety can provide an ideal environment to Cu to shuttle between the Cu(II) and Cu(I) oxidation state easily [27-29]. To provide an environment suitable photocatalysis, two phenol-based ligand systems viz. 2-(((3-(dimethylamino)-2,2-dimethylpropyl) imino)(phenyl)methyl) phenol **[HL^3]** and 2-(((2-(methylamino)ethyl)imino) (phenyl)methyl)phenol **(HL^4)** are designed to synthesize the following Cu(II) complexes viz. **[$CuL^3(OAc)]_2$ (8)** and **[$CuL^4(OAc)]_2$ (9)**. Furthermore, as heterogeneous system can have some added advantages over the homogeneous system like thermal stability and reusability [30, 31]. The synthesized compounds are encapsulated into the zeolite pore and to fabricate the heterogeneous systems like **[CuL^3(OAc)@Y](10)** and **[CuL^4(OAc)@Y] (11)** to explore their photocatalytic activity for lignin degradation.

5.2 Experimental Section

5.2.1 Materials and Instrumentation

Zeolite-Y having the chemical formula $Na_{48}Al_{48}Si_{144}O_{384}$ (Al/Si = 1/3) was purchased from Sigma Aldrich, and used without purification. The specifications of all the instruments used for analysis purposes were the same as described in section 2A.2.1 of the previous chapter 2A.

5.2.2 X-ray crystallography

Table 5. 1. *Crystallographic data and structure refinement parameters for* ***8****, and* ***9****.*

Complex	**8**	**9**
Empirical Formula	$C_{44}H_{56}Cu_2N_4O_6$	$C_{36}H_{40}Cu_2N_4O_6$
Formula weight	864.03 g/mol	751.81 g/mol
Crystal system	Monoclinic	Monoclinic
Space group	P 21/n	P 21/n
a (Å)	13.451(3)	11.942(7)
b (Å)	11.382(2)	9.240(10)
c (Å)	14.121(3)	17.719(16)
α (°)	90	90
β (°)	101.82(2)	103.22(7)°
γ (°)	90	90
V ($Å^3$)	2116.03(8)	1903.6(3)
λ (Å)	0.71073	0.71073
ρcalcd (g cm^{-3})	2.509	2.616
Z	4	4
T (K)	300(2)	300(3)
μ (mm^{-1})	7.435	2.326
F(0 0 0)	1541.1	1555.5
Crystal size (mm^3)	0.080 x 0.060 x 0.080	0.40 × 0.30 × 0.08
θ ranges (°)	6.18 to 58.16	5.78 to 58.24
h/k/l	-18,17/-15,14/-18,17	-15,15/-12,12/-22,22
Reflections collected	25735	13778
Independent reflections	5212	4572
T_{max} and T_{min}	0.9040 and 0.8820	0.764 and 0.639
Data/restraints/parameters	5212 / 0 / 113	4572 / 0 / 105
Goodness-of-fit	2.164	2.243
Final R indices [I > 2σ(I)]	R1 = 0.1038, wR2 = 0.3129	R1 = 0.1744, wR2 = 0.4108
R indices (all data)	R1 = 0.1312, wR2 = 0.3237	R1 = 0.2197, wR2 = 0.4480
Largest peak and hole (e $Å^{-3}$)	4.01 and -2.20	5.16 and -4.63

Single crystal X-ray structural studies of **8** and **9** were performed following a similar protocol as mentioned in section 2A.2.2 of previous chapter 2A.

5.2.3 Synthesis of 2-(((2-(methylamino)ethyl)imino)(phenyl)methyl)phenol (HL^4)

The ligand HL^4 was synthesized by following the similar procedure as the synthesis of HL^3, by using N-Methylethylenediamine instead of N,N,2,2-tetramethylpropanediamine, which is described in section 4.2.3 of the previous chapter 4. The ligand HL^4 was furnished as a viscous orange oil (1.85 g, 6 mmol, yield 93%).^{1}H NMR (400.13 MHz, 298 K, $CDCl_3$): δ 7.56 (3H, d, ArH), 7.31 (3H, d, ArH), 6.88 (1H, d, ArH), 6.66 (2H, d, ArH), 3.35 (2H, t, =NCH_2-), 3.18 (3H, s, N-CH_3), 2.76 (2H, t, CH_2-N-C), ppm (figure 5.1); ^{13}C NMR (100.61 MHz, 298 K, $CDCl_3$): δ 174.57.41 (C of Ar-C-Ar), 163.48 (C of Ar-OH), 133.73 (C of Ar), 132.83 (C of Ar), 131.47 (C of Ar), 129.59 (C of Ar), 129.24 (2C of Ar), 127.76 (2C of Ar), 119.80 (C of Ar-C), 118.17 (C of Ar), 117.60 (C of Ar), 52.10 (C of C-N-C), 51.17 (C of C-N=C) and 36.24 (C of NH-CH_3) (figure 5.1). Anal. Calcd (%) for $C_{16}H_{18}N_2O$: C, 75.56; H, 7.13; N, 11.01. Found (%): C, 75.54; H, 7.12; N, 11.03. FTIR (υ in cm^{-1}): 3500–3100 {υO-H, (s)}; 3000–2725 {υC-H, (m)}; 1750-1525 {υC=N, C=C (m)}; 1350–1235 {υC-N,C-O (m)}; (figure 5.2). ESI-MS in HPLC MeOH (m/z): 255.15 (100%) $[M+H]^+$ (figure 5.3).

5.2.4 Preparation of homogeneous catalysts

5.2.4.1 Synthesis of complex $[CuL^3(OAc)]_2$ (8)

A 8 mL methanolic solution of $Cu(OAc)_2.H_2O$ (0.1 g; 0.5 mmol) was added drop-wise to a 12 mL MeOH solution of HL^3 (0.155 g; 0.5 mmol) and tri-ethylamine (70 μL; 0.5 mmol). The resulting green solution, after 4 hrs of stirring, was reduced to 4 mL by evaporating the solvent in vacuo. The dark green square-shaped crystals appeared after four days of slow evaporation of the filtered concentrated reaction mixture. Crystals are collected by filtration followed by washing with diethyl ether. ESI-MS $[C_{44}H_{56}Cu_2N_4O_6 - 2(OAc)]^{2+}$ 372.129 (figure 5.4); Anal. Calcd (%) for $C_{44}H_{56}Cu_2N_4O_6$: C, 61.16; H, 6.53; N, 6.48. Found (%): C, 61.23; H, 6.49; N, 6.50; FTIR (in KBr υ in cm^{-1}): 3030–2830 {υC-H, (m)}; 1680-1510 {υC=O, C=N (s)}; 1470-1360 {υC=C (s)}; 1350-980 {υC-N,C-O (m)}; (figure 5.5). Yield 75%

5.2.4.2 Synthesis of complex $[CuL^4(OAc)]_2$ (9)

The binuclear complex-**9** was obtained following the same procedure as above by using the ligand HL^4 in place of HL^3. ESI-MS $[C_{36}H_{40}Cu_2N_4O_6 + K]^+$ 791.225 (figure 5.4); Anal. Calcd (%) for $C_{36}H_{40}Cu_2N_4O_6$: C, 57.51; H, 5.36; N, 7.45.

Found (%): C, 57.48; H, 5.40; N, 7.39; FTIR (in KBr υ in cm^{-1}): 3070-2830 {υC-H, (m)}; 1720-1500 {υC=O, C=N (s)}; 1490-1370 {υC=C (s)}; 1360-990 {υC-N,C-O (m)}; (figure 5.5). Yield 72%

5.2.5 Preparation of heterogeneous catalysts:

This is a two steps process as described below

A. **Synthesis of Cu(II)-exchanged zeolite, [Cu(II)@Y(OAc)].** The mixture of $Cu(OAc)_2.H_2O$ (200 mg, 1 mmol) and zeolite Y (1 gm) was refluxed at 100° C in 80 mL of water for 24 h with constant stirring. The pH of the reaction mixture is maintained at 3.0-3.5, by using buffer tablets. This slurry was filtered and washed with deionized water followed by the Soxhlet extraction for 5 hrs with methanol and acetonitrile. After that, the solid was kept at 200° C for 14 hrs in an oven for drying to get Cu-exchanged zeolite [Cu(II)@Y(OAc)] as a faint blue powder.
B. **Synthesis of zeolite-Y encapsulated Cu(II) complexes, [CuL^3(OAc)@Y] (10) and [CuL^4(OAc)@Y] (11):** The metal ion exchanged zeolites (Cu(II)@Y(OAc); 0.3 g) and ligand **HL^3/ HL^4** (0.2 g) were refluxed separately in CH_3CN for 24 hrs. Afther that, blue-violet precipitate was obtained and filtered. The obtained precipitate was dired after washing by Soxhlet extraction (MeOH, ACN and diethyl ether) to eliminate the undesired species. The finally blue-violet powder of the compounds [CuL^3(OAc)@Y] **(10)** or [CuL^4(OAc)@Y] **(11)** was obtained after 24 hrs of oven dryness.

5.2.6 Procedure for the extraction of authentic lignin

Lignin was extracted and characterized by following the same procedure which is described in section 4.2.7 in the previous chapter 4.

5.2.7 General procedure for the photocatalytic cleavage reaction

5.2.7.1 Procedure for the cleavage reaction of the model compounds.

All the photocatalytic activities of the complexes **8**, **9**, **10** and **11** were also studied following a similar procedure as described in section 2A.2.6 of previous chapter 2A.

5.2.7.2 Procedure for the degradation of the authentic lignin material.

Oxidation experiments were performed in a 50 mL round bottom flask charged with 0.1 g of authentic lignin sample (extracted by coconut husk), catalyst (20 mg, of homogeneous or 50 mg heterogeneous catalysts), ^{t}BuOOH (1 mmol, 130 mg) and acetonitrile (15 mL) as the solvent. The reaction mixture was stirred at room temp in the open air for 8 hrs in the presence of 12 watts of visible light LEDs. After the reaction, the residue was analyzed through two-dimensional HSQC-NMR and HPLC.

5.3 Results and discussion

5.3.1 Synthesis and characterization of ligand

The ligands **HL^3** and **HL^4** were synthesized by using a conventional Schiff base condensation method using previously reported methodology describe in an earlier chapter with sufficient purity and yield. The compound **(HL^4)** was obtained in good yield and was characterized by mass spectrometry and ^{1}H and ^{13}C NMR spectroscopy (scheme 5.1).

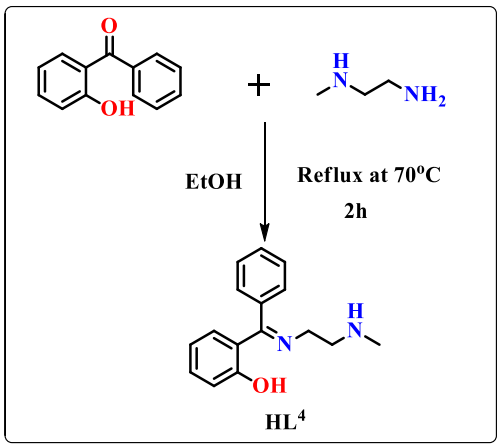

Scheme 5.1. *Synthesis of Ligand* ***HL^4.***

The proposed ligand structure has been confirmed by ^{1}H and ^{13}C spectra (Figure 5.1). The bands around 1576 and 3440 cm^{-1} in FTIR arises due to C=N and phenolic –OH stretching frequency (figure 5.2). The ESI-MS spectrometry shows a molecular ion peak for **HL^4** at 255.15 [M + H]$^+$ (figure 5.3).

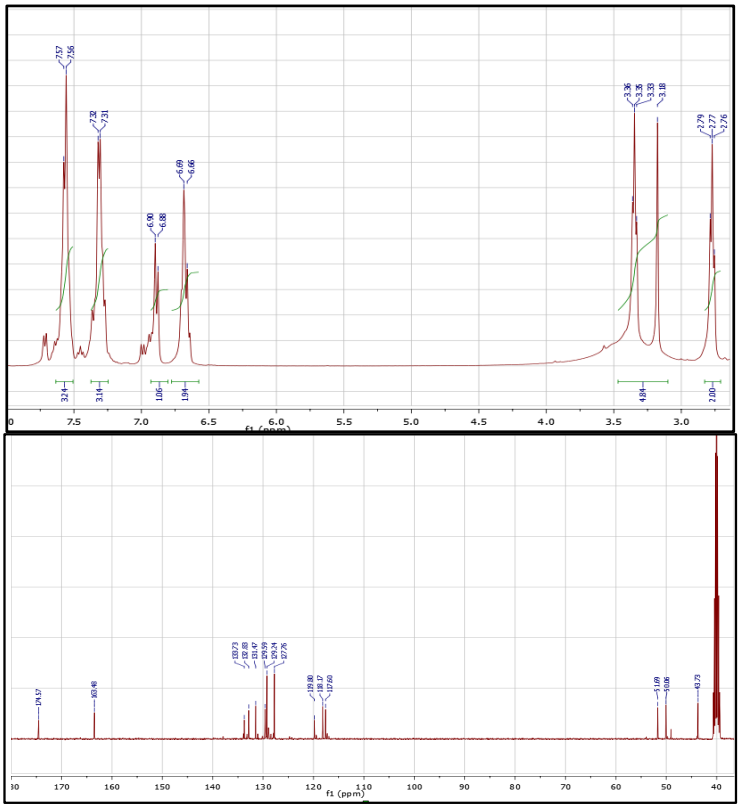

Figure 5.1. *^{1}H and ^{13}C NMR of* ***HL^{4}***.

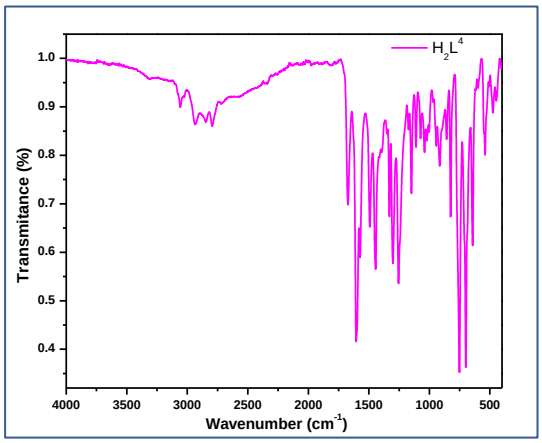

Figure 5.2. *FTIR spectrum of* ***HL^{4}***.

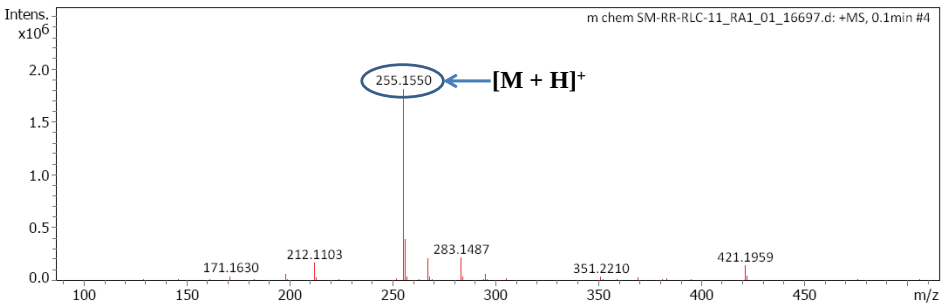

Figure 5.3. *ESI- Mass spectrum of* ***HL^{4}***.

5.3.2 Synthesis and characterization of homogeneous catalysts

In the presence of triethylamine, a methanolic solution of $Cu(OAc)_2.H_2O$ upon stirring with ligands (**HL**^{3}) / (**HL**^{4}) for 4 hours furnished the desired binuclear metal complexes **8** and **9** respectively (scheme 5.2). The compounds obtained were characterized by mass spectrometry, FTIR, elemental analysis, and SCXRD. Molecular ion peak $[M - 2(OAc)]^{2+}$ for complex **8** and $[M + K]^+$ for complex **9** was obtained at 372.129 and 791.225, respectively (figure 5.4). Both the metal complexes have shown the shifting of C=N from 1576 to 1580 cm^{-1}. The bands at 1580 and 1320 cm^{-1} are appeared in both the cases for asymmetric and symmetric stretching of carboxylate ion (figure 5.5).

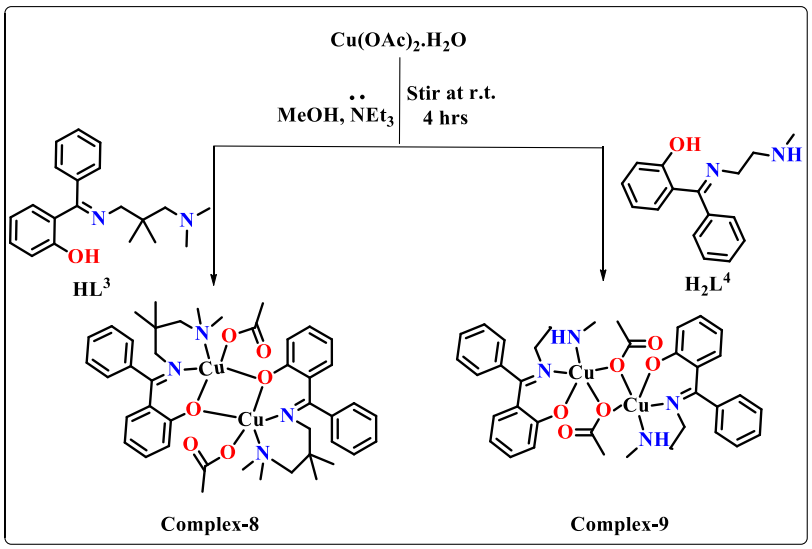

Scheme 5.2. *Synthesis of homogeneous catalysts.*

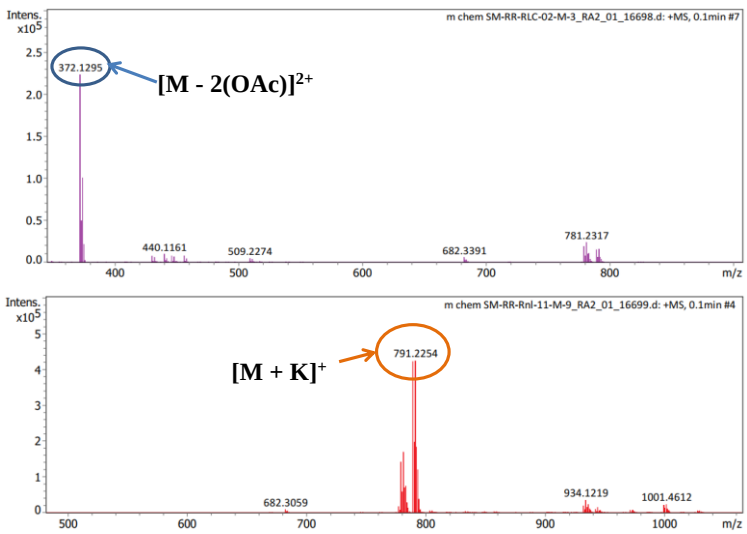

Figure 5.4*. ESI- MS spectrum of* ***8*** *and* ***9****. (top to bottom)*

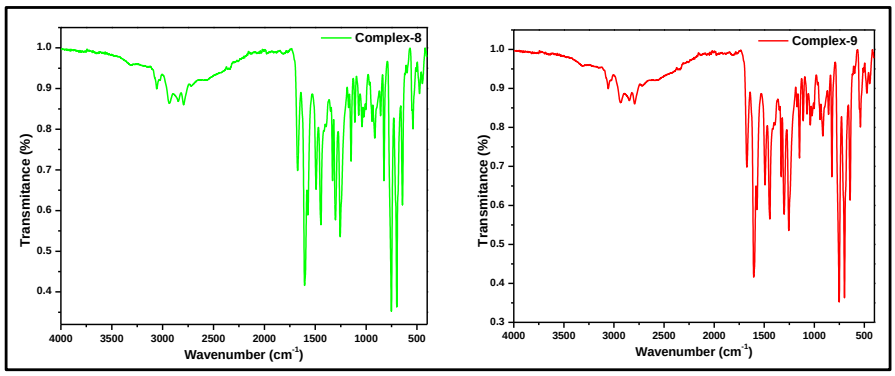

***Figure 5.5**. FTIR spectrum of **8** and **9**.*

5.3.2.1 Electronic spectra

The UV-vis spectra of **8** and **9** were recorded in methanol. A broad band for d-d transition was appeared at 620 nm in both the complexes **8** and **9** (figure 5.6). The peak appearing at 378 and 372 nm for complexes **8** and **9** is due to the ligand-to-metal charge transfer (LMCT) transition. Furthermore, the peak shifting from 260 to 273 nm of the ligand is also responsible for the ligand-to-metal charge transfer (LMCT) transition.

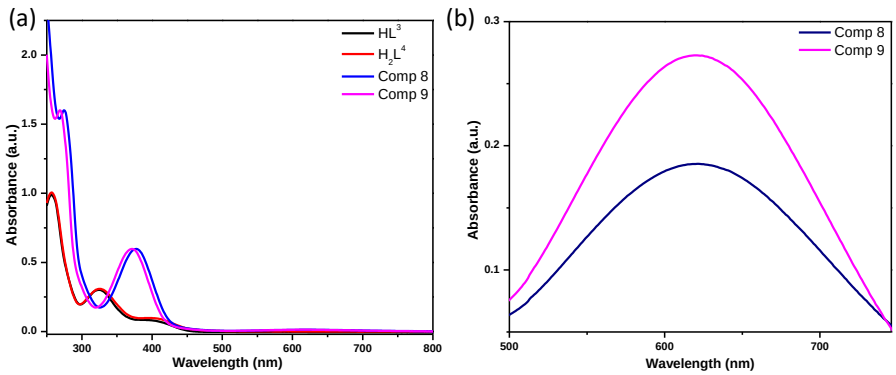

***Figure 5.6**. UV-Vis spectra in methanol for ligands and complexes.*

5.3.2.2 Description of crystal structure

The structures of both the complexes were determined by single crystal X-ray crystallography. Both the complexes are crystallized as binuclear Cu(II) complexes. Complex **8** shows distorted square pyramidal geometry around the Cu(II) ions whereas complex **9** shows the distorted octahedral geometry around the Cu(II) ions (figure 5.7). The selected bond distances and angles are given in Table 5.2. Both complexes **8** and **9** crystallize in monoclinic space group $P2_1/n$.

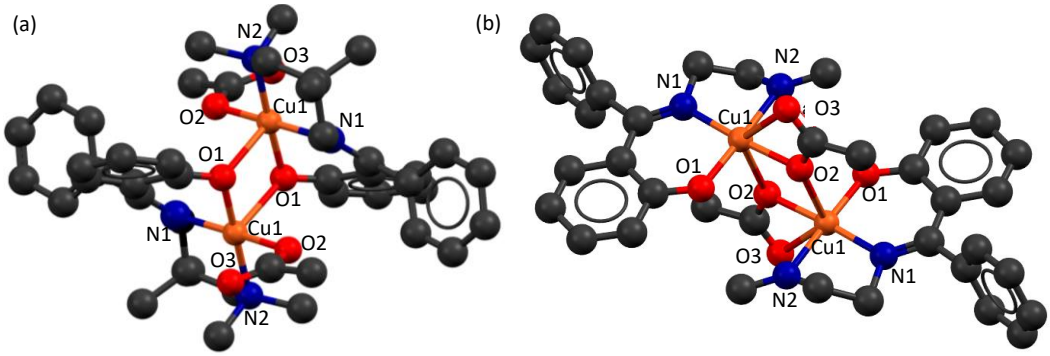

Fig. 5.7. *The solid-state crystal structure for (a) complex* ***8*** *and (b) complex* ***9****, hydrogen atoms are omitted for clarity.*

Table 5. 2*. Selected bond lengths (Å) and bond angles (°) for* ***8*** *and* ***9****.*

Complex 8		Complex 9	
Cu1-O1	2.394(2)	Cu1-O1	1.912(2)
Cu1-O2	1.958(2)	Cu1-O2	1.971(3)
Cu1-N1	2.056(3)	Cu1-N1	1.971(4)
Cu1-N2	2.078(2)	Cu1-N2	2.048(3)
Cu1-O1	1.984(2)	Cu1-O3	2.722(3)
		Cu1-O2	2.511(3)
O1-Cu1-N1	87.14(10)	O1-Cu1-O2	94.24(12)
O1-Cu1-N2	175.50 (10)	O1-Cu1-N1	92.60(11)
N1-Cu1-N2	94.28(10)	O1-Cu1-N2	177.29(13)
O1-Cu1-O2	87.28(8)	O1-Cu1-O3	132.00(12)
N1-Cu1-O2	172.56(10)	N1-Cu1-N2	85.17(12)
N2-Cu1-O2	90.69(9)	O2-Cu1-O3	53.32(12)
O1-Cu1-O1	85.79(12)	O2-Cu1-N1	101.88(11)
		O2-Cu1-N2	84.73(12)

5.3.3 Synthesis and characterization of heterogeneous catalysts

After the synthesis of binuclear copper complexes, the zeolite-Y super-cage was used for the encapsulation of complexes **8** and **9.** The complexes were successfully encapsulated into cages in two-step processes; copper exchange

followed by ligand exchange and the desired compounds in zeolite environment are formed and identified as compounds **10** and **11**.

The bands in the regions of 900-1180 cm^{-1} and 670-820 cm^{-1} in the FTIR spectrum of **10** and **11** are appeared due to the $\upsilon_{asymmetric}$ (OTO) and $\upsilon_{symmetric}$ (OTO) stretching of zeolite Al–O–Si framework. A band shift for C=C and C=N was observed in the case of encapsulated compound upto ~30 cm^{-1} and the recovered catalysts also possess similar frequencies as that of heterogeneous counter parts shown in figure 5.8. Additionally, the vibrations for Cu-N and Cu-O stretching were obtained at 511 and 579 cm^{-1}, which were, verified by Raman spectroscopy. It shows characteristic peaks at 500 (Cu-O) in the encapsulated complexes. A sharp peak at 948 cm^{-1} is responsible for $\upsilon_{symmetric}$ (SiO_4 framework) in Cu@Y(OAc) (Figure 5.9). The peaks at 1324 cm^{-1} and 1588 cm^{-1} are accountable due to the $\upsilon_{symmetric}$ and $\upsilon_{asymmetric}$ (COO) stretches revealing the presence of acetate.

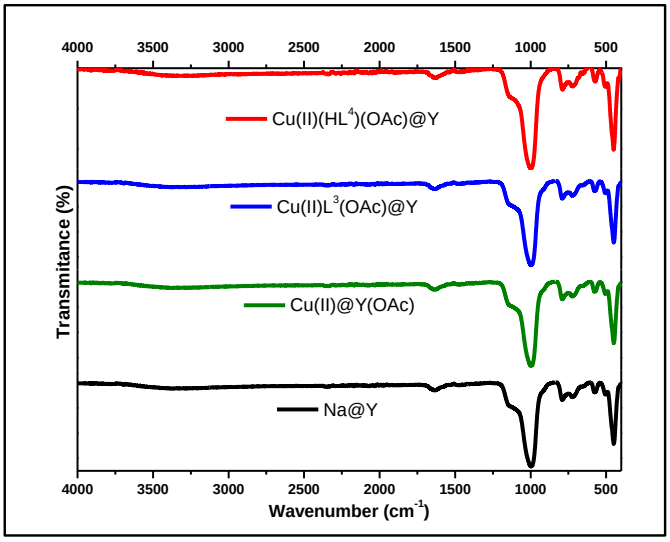

Figure 5.8. *FTIR spectra of (where υ are the stretching frequencies, and represented in cm^{-1}): (a) NaY, (b) Cu@Y(OAc), (c) CuL^3(OAc)@Y, (d) Cu(HL^4)(OAc)@Y (bottom to top).*

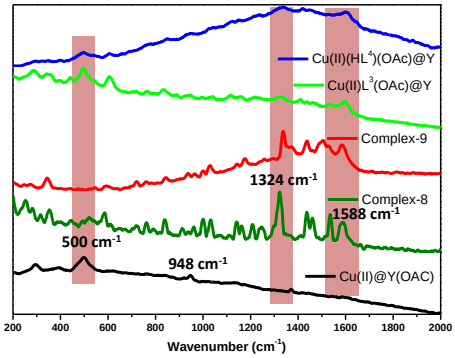

Figure 5.9. *Raman spectra (in cm^{-1}) homogeneous complexes and zeolite immobilized complexes.*

The thermal stability profiles of parent and exchanged zeolites show the presence of physical or chemisorbed water molecule which evaporates up to 360 °C. Furthermore, in the temperature range 361-470 and 361-460 °C in the case of encapsulated **[CuL^3(OAc)@Y]** and **[CuL^4(OAc)@Y]** shows ~4% loss in mass due to the dissociation of Schiff base ligand (figure 5.10). N_2 adsorption decreases after encapsulation of complexes, the Langmuir surface area 419.603 and 409.077 m^2/g for **[CuL^3(OAc)@Y]** and **[CuL^4(OAc)@Y]** respectively which are smaller with respect to the pure or copper ion-exchanged zeolite 626.547 and 568.075 m^2/g (figure 5.11 and Table 5.3). Hence, TG and BET studies show the formation of a host-guest complex inside the super cage of zeolites.

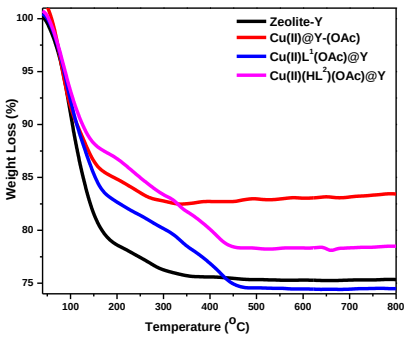

Figure 5.10 *TGA-DTA profile of pure NaY and zeolite encapsulate complexes.*

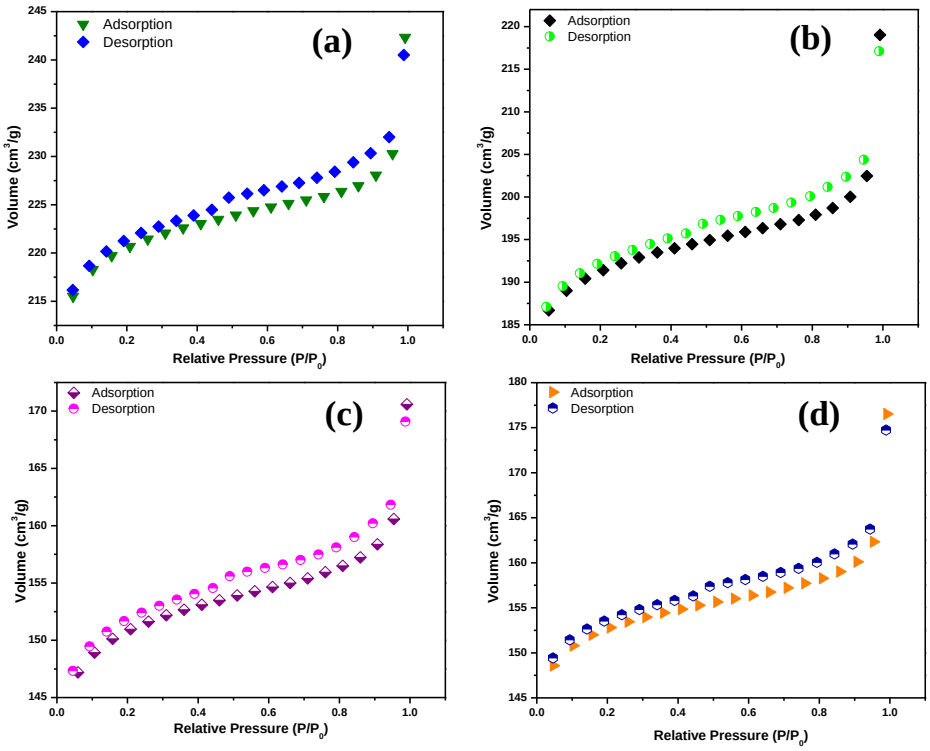

Figure 5.11. *N_2 adsorption isotherms of pure zeolite and encapsulated catalysts. (a)* ***NaY****,(b)* ***Cu@Y(OAc)****, (c)* ***CuL^3(OAc)@Y****, and (d)* ***Cu(HL^4)(OAc)@Y****.*

Table 5.3. *BET adsorption results of zeolite exchanged and encapsulated catalysts*

Catalyst	Multi Point BET (m^2/g)	Langmuir Surface Area (m^2/g)	Pore Volume (cc/g)	Average Pore Size
Zeolite-Y	626.547	1018.700	3.749×10^{-1}	2.52178 nm
Cu@Y(OAc)	568.075	902.811	3.388×10^{-1}	2.39319 nm
CuL^3(OAc)@Y	419.603	711.890	2.645×10^{-1}	2.52178 nm
Cu(HL^4)(OAc)@Y	409.077	724.094	2.730×10^{-1}	2.66990 nm

After the encapsulation of homogeneous complexes inside the cavity of zeolite, the morphology remains unchanged (figure 5.12). The PXRD pattern suggests that, after the incorporation of copper complex inside the matrix of zeolite, the Bragg faces of pure zeolite do not change. NaY has 2θ value at 10° and 12° corresponding to 220 and 311 planes respectively. After the formation of the host-guest complex, the relative peak intensities of zeolite-Y ($I_{220} > I_{311}$) are reversed ($I_{220} < I_{311}$) (figure 5.13). This is a characteristic of the bulky complex formation inside the cavity of the zeolite.

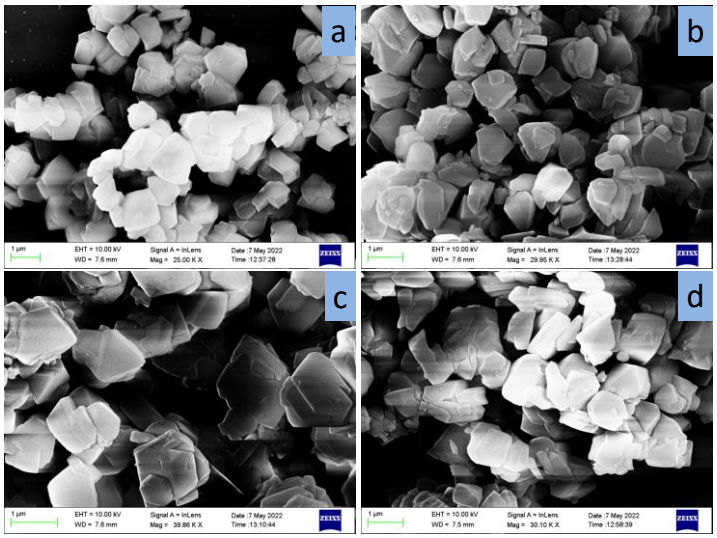

Figure 5.12. *FESEM images (EHT, 10 kV; Signal A, SE2; Scale bar, 1 μm) of (a)* ***NaY****, (b)* ***Cu@Y(OAc)****, (c)* ***CuL^3(OAc)@Y****, and (d)* ***Cu(HL^4)(OAc)@Y****.*

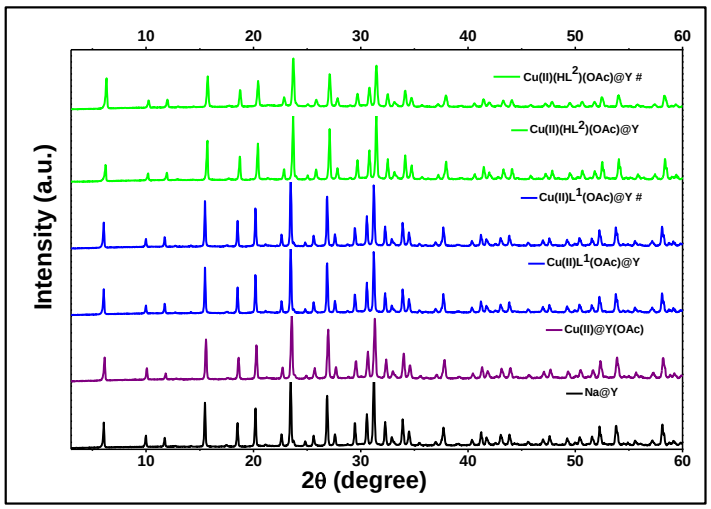

Figure 5.13. *PXRD patterns of pure zeolite, copper ion-exchanged zeolites, and zeolite encapsulated complexes. # signifies the reused catalyst.*

Although, the information regarding the encapsulation inside the zeolite super-cages is confirmed by the TGA and BET studies. But to confirm the presence of Cu(II) and ligands inside the zeolite, the binding energy studies have been performed using X-ray photoelectron spectroscopy.

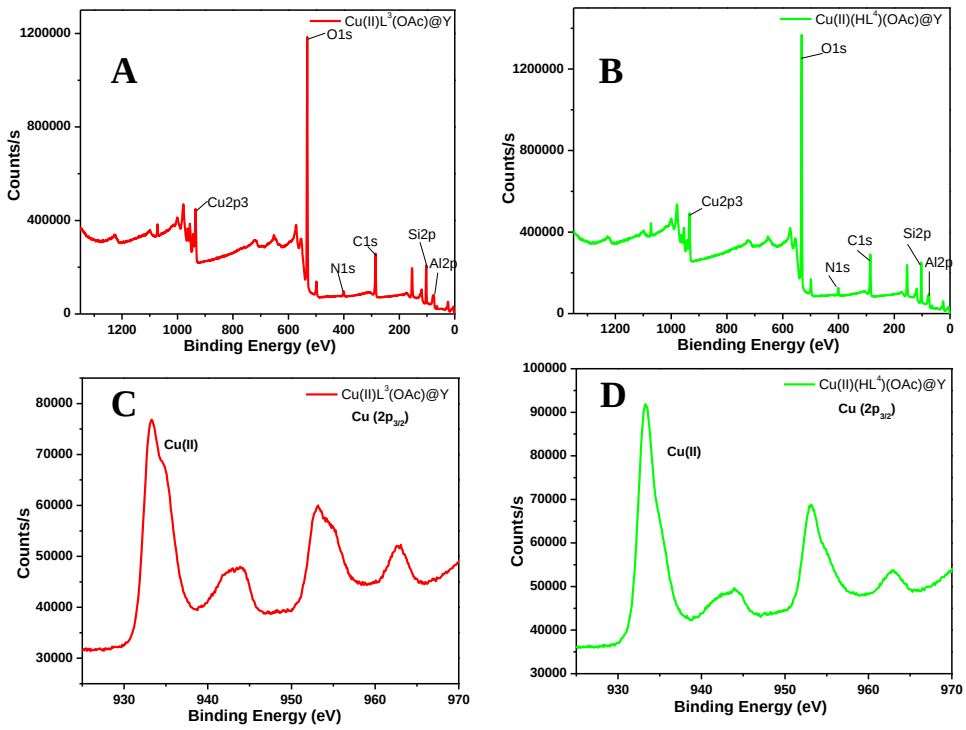

Figure 5.14. *(a) and (b) represent XPS survey spectrum of* ***CuL^3(OAc)@Y****, and* ***Cu(HL^4)(OAc)@Y*** *respectively. (c) and (d) display the XPS patterns of copper(II) in 2p$_{3/2}$ state.*

Binding energies of CuL^3(OAc)@Y at 77.66, 101.05, 400.32, 284.57 and 531.91 eV are corresponding to Al(2p), Si(2p), N(1s), C(1s) and O(1s) shell, respectively (figure 5.14). Similarly, CuL^4(OAc)@Y having an energy value of 77.63, 101.16, 401.22, 284.27 and 531.96 eV defines Al(2p), Si(2p), N(1s), C(1s) and O(1s) shell, respectively. Peaks at 933.35 and 953.15 eV are corresponding to the Cu(2p$_{3/2}$), and Cu(2p$_{1/2}$) shells in case of both the catalysts. Furthermore, the peak at 531 eV in both compounds **10** and **11**, proves the presence of the acetate group. Apart from that, a peak associated with N(1s) in both cases is shown at 400.32 eV, revealing the presence of ligands in encapsulated compounds. The presence of satellite peak in both the heterogeneous catalysts (**10** and **11**) indicates the presence of paramagnetic Cu (+2, d^9) [32, 33]. Further, the percentage of the elements is calculated by using the area covered by the curve, and the composition data have been summarized in the Table 5.4.

Table 5.4. *XPS elemental composition for the encapsulated catalysts*

	Element detection (in %)					
Samples	O(1s)	Cu($2p_3$)	C(1s)	Al(2p)	Si(2p)	N(1s)
Catalyst-**10**	48.48	5.28	25.13	1.60	16.73	2.79
Catalyst-**11**	49.05	4.16	24.49	1.49	17.63	3.19

5.3.4. Photocatalytic cleavage of model compounds

All the homogeneous and heterogeneous complexes have been tested towards the oxidative cleavage of the C=C bond of ferulic acid (1a), under the visible light irradiation. The C=C bond cleavage into the corresponding aldehydes and carboxylic acids is an important reaction from an organic as well as biochemistry viewpoint [4-11]. The catalytic ability of the synthesized Cu(II) containing compounds were verified for the oxidative cleavage of the C=C bond of the lignin upon visible light irradiation. All the compounds have shown encouraging results toward the cleavage of the C=C bond. Ferulic acid has been taken as model substrates for optimization of reaction conditions of the oxidative cleavage of the C=C bond as per Table 5.5. The reaction was carried out under visible light (irradiated by 12 watts of the LED bulb) at room temperature in an open atmosphere. Complex **8** with acetonitrile (1 mL) as a solvent in the presence of five equivalents of H_2O_2 afforded only 12% and 21% cleavage of a model substrate with 100% selectivity towards the vanillin after 1 hr and 2 hrs of light irradiation respectively (entry 1 and 2), whereas upon visible light irradiation for 3 hrs, 6 hrs and 8 hrs afforded 40%, 62% and 70% cleavage of substrate respectively (entry 3, 4 and 5). The over oxidation product vanillic acid has obtained from this cleavage reaction, this reaction afforded 25%, 50% and 50% selectivity towards the vanillic acid after 3 hrs, 6 hrs and 8 hrs of the irradiation of visible light respectively (entry 3, 4 and 5). When tert-Butyl hydroperoxide (TBHP) was used in place of H_2O_2 as oxidant, 95% and 98% of conversion were obtained along with the 87% and 92% selectivity towards the vanillin in 1 hr and 2 hrs of light irradiation (entries 6 and 7).

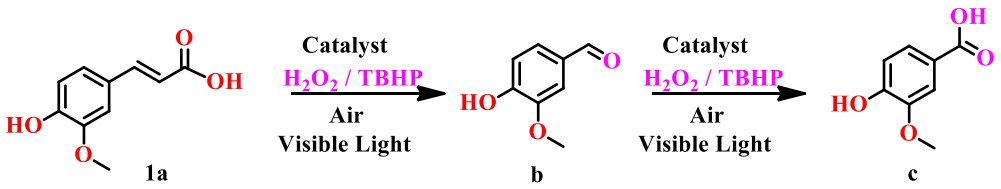

Table 5.5. *Photocatalytic C=C cleavage of ferulic acid by complex* ***8***

Entry No	Oxidant	Time (h)	Conversion [%]	Selectivity [%] b	Selectivity [%] c	Yield [%] b	Yield [%] c
1	H_2O_2	1	12	100	00	12	00
2	H_2O_2	2	21	100	00	21	00
3	H_2O_2	3	40	75	25	30	10
4	H_2O_2	6	62	50	50	31	31
5	H_2O_2	8	70	50	50	35	35
6	TBHP	1	95	87	13	83	12
7	TBHP	2	98	92	8	90	8

[a]*General reaction conditions: Substrate (0.1 mmol), catalyst* ***complex 8*** *(5 mol % / 5 µmol, 4.3 mg), Oxidant (5 equivalent / 0.5 mmol), ACN 1 mL, light intensity (12 Watt white LED bulb, 400−800 nm wavelength range), Stir at room temperature (~25 °C).*

Afterward, some common solvents were screened for their suitability by using the above reaction condition for the C=C bond cleavage reaction in the presence of **complex 8** (Table 5.6). Among these solvents, 97 % of conversion in the presence of acetonitrile as a solvent was obtained with 87 % selectivity towards the vanillin (entry 1 of Table 5.6).

Furthermore, the above-optimized reaction was further optimized with varying quantitiy of TBHP to know the suitable amount for this reaction. In the presence of 5 equivalent of TBHP with respect to the substrate better results were obtained than the other conditions as represented in entry number 4 (Table 5.7)

Table 5.6. *The effect of the solvent on the oxidative cleavage of ferulic acid 1a with TBHP*

Entry No	Solvent (1 mL)	Conversion [%]	Selectivity [%]		Yield [%]	
			b	c	b	c
1	ACN	97	87	13	84	13
2	H_2O	21	00	100	00	21
3	DCM	40	75	25	30	10
4	MeOH	10	40	60	4	6
5	EtOH	10	40	60	4	6
6	THF	5	80	20	4	1
7	DMF	40	85	15	34	6
8	DMSO	36	80	20	29	7
9	EtOAc	30	80	20	24	6

[a]*General reaction conditions: Substrate (0.1 mmol), catalyst* ***complex 8*** *(5 mol % / 5 µmol, 4.3 mg), Oxidant TBHP (5 equivalent / 0.5 mmol), solvent 1 mL, light intensity (12 Watt white LED bulb, 400−800 nm wavelength range), Stir at room temperature (~25 °C) for 1h.*

Table 5.7*. The effect of TBHP on the oxidative cleavage of the C=C bond of ferulic acid 1a.*

Entry No	Equiv. of TBHP	Conversion [%]	Selectivity [%]		Yield [%]	
			b	c	b	c
1	1	10	100	00	10	00
2	2	12	100	00	12	00
3	4	80	86	14	69	11
4	5	97	87	13	84	13
5	6	97	80	20	77	20
6	8	98	70	30	74	24
7	10	99	48	52	48	51

[a]*General reaction conditions: Substrate (0.1 mmol), catalyst* ***complex 8*** *(5 mol % / 5 µmol, 4.3 mg), ACN 1 mL, light intensity (12 Watt white LED bulb, 400−800 nm wavelength range), Stir at room temperature (~25 °C) for 1h.*

After optimization of the reaction conditions, the photocatalytic reaction by using all homogeneous (complexes **8** and **9**) and heterogeneous (complexes **10** and **11**) catalysts was carried out with different substrates. In all the cases, the heterogeneous system afforded higher conversion than the homogeneous catalyst. In the case of *p*-coumeric acid, I got 100% selectivity towards the aldehyde whereas in all other cases the over oxidation product (acid) was found (Table 5.8).

Table 5.8. *Percentage conversion of ferulic acid and other similar compounds by homogeneous and heterogeneous catalysts (**8, 9, 10** and **11**).*

Entry SL. No	Substrates	Conversion [%]		Products (selectivity % in all cases)	
		Cat-8/9	**10/11**		
1	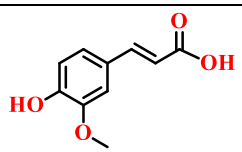	97/95	99/97	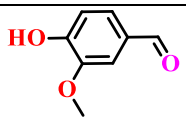 (87)	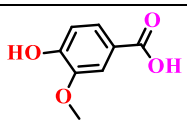 (13)
2	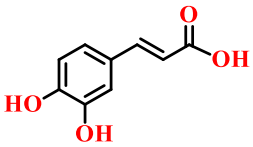	93/90	95/92	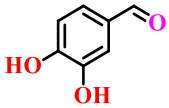 (70)	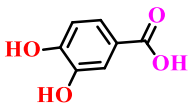 (30)
3	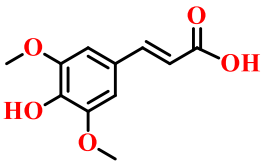	92/89	95/93	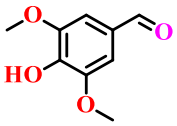 (84)	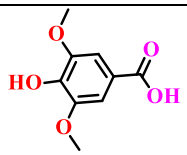 (16)
4	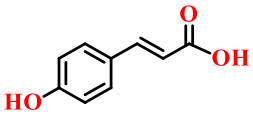	93/89	95/91	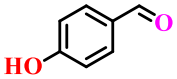 (100)	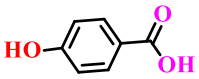 (00)

[a]*General reaction conditions: Substrate (0.1 mmol), catalyst (5 mol % / 5 µmol), Oxidant TBHP (5 equivalent / 0.5 mmol), ACN 1 mL, light intensity (12 Watt white LED bulb, 400−800 nm wavelength range), Stir at room temperature (~25 °C) for 1h.*

5.3.5 The degradation of authentic lignin feedstocks

The results of the photocatalytic cleavage of C=C bond of ferulic acid by synthesized catalysts encouraged further to apply the optimized reaction conditions to degrade the natural lignin into monomers. The optimized reaction condition was applied for the depolymerization of extracted lignin for four hrs. The aromatic aldehydes syringaldehyde and vanillin, as well as other chemicals including syringic acid and vanillic acid, were produced by the cleavage of coconut lignin (figure 5.15).

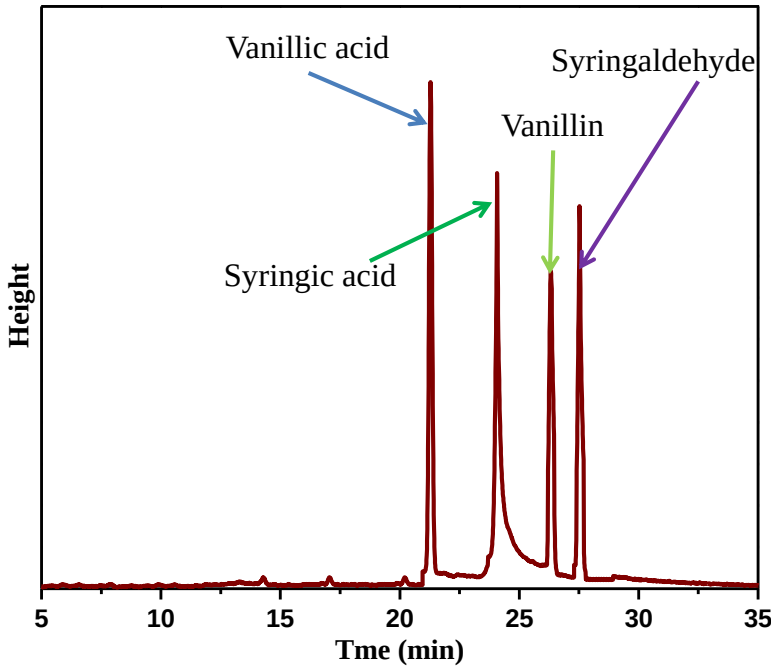

Figure 5.15. *HPLC interpretation of degraded product of authentic coconut husk lignin.*

The structural changes of the extracted lignin from the coconut husk and the degraded residue were analyzed through two-dimensional heteronuclear single-quantum coherence nuclear magnetic resonance (2D HSQC-NMR, figure 5.16). HSQC and HPLC results suggest that the catalytic system degraded the coconut husk lignin into the monomers.

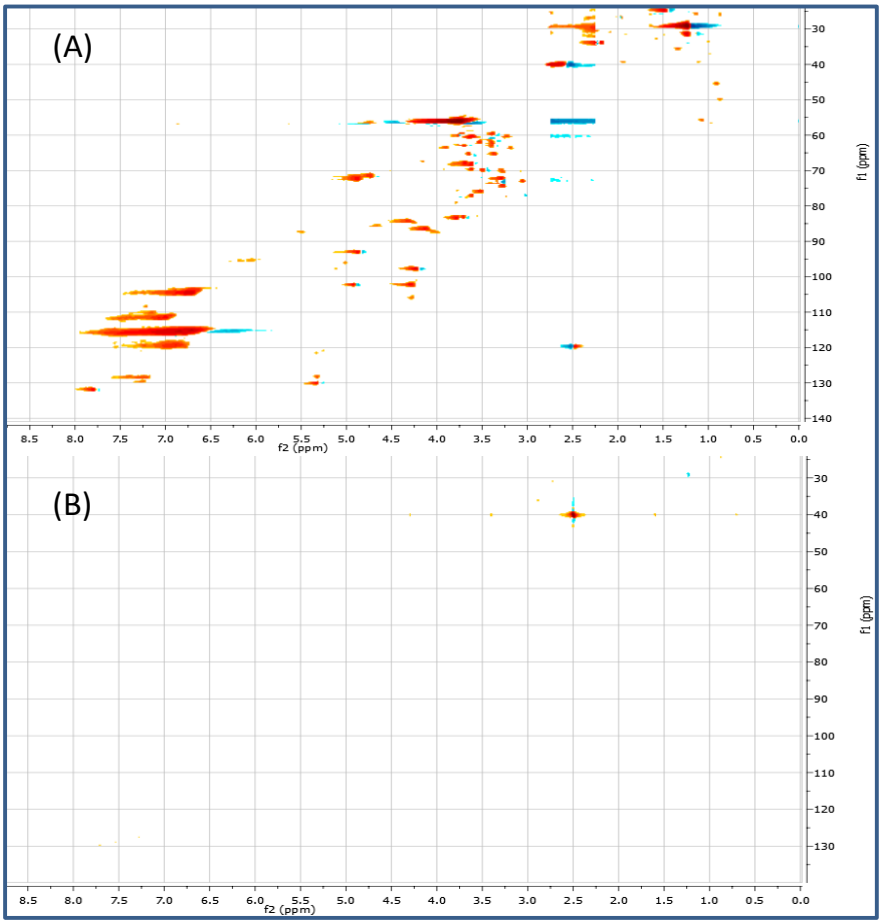

Figure 5.16. *2D HSQC-NMR spectra of coconut husk lignin sample (A) before and (B) after degradation reaction.*

5.4 Conclusions

Two new binuclear Cu(II) complexes *viz.* $[CuL^3(OAc)]_2$ **(8)** and $[CuL^4(OAc)]_2$ **(9)** have been synthesized by reacting with $\mathbf{HL^3}$ and $\mathbf{HL^4}$ respectively in MeOH. Complexes **8** and **9** were characterized by single crystal X-ray crystallography, LCMS, FTIR and power X-ray diffraction techniques. The heterogeneous catalysts **10** and **11** were synthesized by encapsulation of the copper(II) ion and the corresponding ligands within the zeolite core. The incorporation of the Cu(II) complexes inside the zeolite core were indicated by Raman spectroscopy and BET analysis, further confirmed by X-ray photoelectron spectroscopy. The Cu(II) complexes 8 and 9 along with its heterogeneous counter parts 10 and 11 have shown their ability towards the photocatalytic cleavage of the C=C bond of the lignin at room temperature in the presence of TBHP (tert-Butyl hydroperoxide). The photocatalytic degradation of lignin into the valuable monomers was confirmed by HPLC and 2D HSQC NMR. The heterogeneous catalysts show better catalytic activity than its homogeneous counterparts.

5.5 References

[1] Allpress, C. J., Berreau, L. M. (2013), Oxidative aliphatic carbon–carbon bond cleavage reactions, Coord. Chem. Rev., 257, 3005–3029.(DOI: 10.1016/j.ccr.2013. 06.001)

[2] Chen, F., Wang, T., Jiao, N. (2014), Recent Advances in Transition-Metal-Catalyzed Functionalization of Unstrained Carbon–Carbon Bonds, Chem. Rev., 114, 8613– 8661.(DOI: 10.1021/cr400628s)

[3] Chan, A. P. Y., Sergeev, A. G. (2020), Metal-mediated cleavage of unsaturated C-C bonds, Coord. Chem. Rev., 413, 213213. (DOI: 10.1016/j.ccr.2020.213213)

[4] Koike, K., Inoue, G., Fukuda, T. (1999), Explosion Hazard of Gaseous Ozone, J. Chem. Eng. Jpn., 32, 295–299. (DOI: 10.1252/jcej.32.295)

[5] Hassan, Z., Stahlberger, M., Rosenbaum, N., Bräse, S. (2021), Criegee Intermediates Beyond Ozonolysis: Synthetic and Mechanistic Insights, Angew. Chem., Int. Ed., 60, 15138–15152. (DOI: 10.1002/anie.202014974**)**

[6] Travis**,** B. R., Narayan**,** R. S., Borhan**,** B. (2002), Osmium Tetroxide-Promoted Catalytic Oxidative Cleavage of Olefins: An Organometallic Ozonolysis, J. Am. Chem. Soc., 124, 3824–3825.(DOI: 10.1021/ja017295g)

[7] Moorthy, J. N., Parida, K. N. (2014), Oxidative Cleavage of Olefins by In Situ-Generated Catalytic 3,4,5,6-Tetramethyl-2-iodoxybenzoic Acid/Oxone, J. Org. Chem., 79, 11431–11439.(DOI: 10.1021/jo502002w)

[8] Yu, W., Mei, Y., Kang, Y., Hua, Z., Jin, Z. (2004), Improved Procedure for the Oxidative Cleavage of Olefins by OsO_4–$NaIO_4$, Org. Lett., 6, 3217–3219.(DOI: 10.1021/ol0400342)

[9] Mang, H., Gross, J., Lara, M., Goessler, C., Schoemaker, H. E., Guebitz, G. M., Kroutil, W. (2007), Optimization of a biocatalytic single-step alkene cleavage of aryl alkenes, Tetrahedron, 63, 3350-3354.(DOI: 10.1016/j.tet.2007.02.034)

[10] Singh, F. V., Milagre, H. M. S., Eberlin, M. N., Stefani, H. A. (2009), Synthesis of benzophenones from geminal biaryl ethenes using *m*-chloroperbenzoic acid, Tetrahedron Lett., 50, 2312–2316.(DOI: 10.1016/j.tetlet.2009.02.164)

[11] Lai, S., Lee, D. G. (2001), Heterogeneous Permanganate Oxidation of Styrene and Cinnamic Acid Derivatives: A Simple and Effective Method for the Preparation of Benzaldehydes, Synthesis, 11, 1645–1648.(DOI: 10.1055/s-2001-16760)

[12] Sarma, D., Majumdar, B., Deori, B., Jain, S., Sarma, T. K. (2021), Photoinduced Enhanced Decomposition of TBHP: A Convenient and Greener Pathway for Aqueous Domino Synthesis of Quinazolinones and Quinoxalines, ACS Omega, 6, 11902−11910.(DOI: 10.1021/acsomega. 1c00211)

[13] Wang, W., Rodrigue, H. Ahn, S. H. (2016), Deployable Soft Composite Structures. Sci. Rep., 6, 20869.(DOI: 10.1038/srep20869)

[14] Fache, M., Boutevin, B., Caillol, S. (2016), Vanillin Production from Lignin and Its Use as a Renewable Chemical, ACS Sustain. Chem. Eng., 4, 35–46.(DOI: 10.1021/acssuschemeng. 5b01344)

[15] Gallage, N. J., Hansen, E. H., Kannangara, R., Olsen, C. E., Motawia, M. S., Jørgensen, K., Holme, I., Hebelstrup, K., Grisoni, M., Møller, B.L. (2014), Vanillin formation from ferulic acid in *Vanilla planifolia* is catalysed by a single enzyme, Nat. Commun., 5, 4037.(DOI: 10.1038/ncomms5037)

[16] Furuya, T., Kuroiwa, M., Kino, K. (2017), Biotechnological production of vanillin using immobilized enzymes, J. Biotechnol., 243, 25–28.(DOI: 10.1016/ j.jbiotec.2016.12.021)

[17] Hu, J., Hu,Y., Mao, J., Yao, J., Chen, Z., Li, H. (2012), A cobalt Schiff base with ionic substituents on the ligand as an efficient catalyst for the oxidation of 4-methyl guaiacol to vanillin, Green Chem., 14, 2894–2898. (DOI: 10.1039/C2GC36049G)

[18] Yan, L., Chen, P., Zhang, S. (2016), Biotransformation of ferulic acid to vanillin in the packed bed-stirred fermenters, Sci. Rep., 6, 34644. (DOI: 10.1038/srep34644)

[19] Yepez, R., García, S., Schachat, P., Sánchez, M. S., González-Estefan, J. H., Zamora, E. G., Ibarra, I. A. (2015), Catalytic activity of HKUST-1 in the oxidation of trans-ferulic acid to vanillin, New J. Chem., 39, 5112–5115.(DOI: 10.1039/ C5NJ00247H)

[20] Flores, J. G., González, E. S., Alejandre, A. G., Pliego, J. A., Martínez, A., Vázquez, T. J., Lima, E., Zamora, E. G., García, M. D., Sánchez, M. S., Ibarra, I. A. (2018), Greener synthesis of Cu-MOF-74 and its catalytic use for the generation of vanillin, Dalton Trans., 47, 4639–4645. (DOI: 10.1039/C7DT04701K)

[21] Horvat, M., Iskra, J. (2022), Oxidative cleavage of C–C double bond in cinnamic acids with hydrogen peroxide catalysed by vanadium (V) oxide, Green Chem.**,** 24**,** 2073-2081. (doi: 10.1039/D1GC04416H)

[22] Ni, J., Tao, F., Du, H. (2015), Mimicking a natural pathway for de novo biosynthesis: natural vanillin production from accessible carbon source, Sci. Rep. 5, 13670. (DOI: 10.1038/ srep13670)

[23] Banerjee, G., Chattopadhyay, P. (2019), Vanillin biotechnology: the perspectives and future, J. Sci. Food Agric., 99, 499–506. (DOI: 10.1002/jsfa.9303)

[24] Sánchez-González, E., López-Olvera, A., Monroy, O., Aguilar-Pliego, J., Flores, J.G., Islas-Jácome, A., Rincón-Guevara, M. A., González-Zamora, E., Rodríguez-Molina, B., Ibarra, I. A. (2017), Synthesis of vanillin via a catalytically active Cu(II)-metal organic polyhedron, CrystEngComm, 19, 4142–4146.(DOI: 10.1039/C6CE02621D)

[25] Gómez-López, P., Lázaro, N., Alvarado-Beltrán, C. G., Pineda, A., Balu, A. M., Luque, R. (2019),One-Pot Cu/TiO_2 Nanoparticles Synthesis for Trans-Ferulic Acid Conversion into Vanillin, *Molecules*, *24*, 3985.(DOI: 10.3390/ molecules24213985)

[26] Dubey, N., Rayalu, S. S., Labhsetwar, N. K., Naidu, R. R., Chatti, R. V., Devotta, S. (2006), Photocatalytic properties of zeolite-based materials for the photoreduction of methyl orange. Applied Catal. A: General, 303, 152-157. (DOI: 10.1016/j.apcata.2006.01.043)

[27] Hossain, A., Vidyasagar, A., Eichinger, C., Lankes, C., Phan, J., Rehbein, J., Reiser, O. (2018), Visible-Light-Accelerated Copper (II)-Catalyzed Regio-and Chemoselective Oxo-Azidation of Vinyl Arenes. Angew. Chem. Int. Ed., 57, 8288-8292.(DOI: 10.1002/anie.201801678)

[28] Zheng, Y. W., Narobe, R., Donabauer, K., Yakubov, S., König, B. (2020), Copper (II)-photocatalyzed N–H alkylation with alkanes, ACS Catal., 10, 8582-8589.(DOI: 10.1021/acscatal.0c01924)

[29] Reichle, A., Sterzel, H., Kreitmeier, P., Fayad, R., Castellano, F. N., Rehbein, J., & Reiser, O. (2022), Copper (ii)-photocatalyzed decarboxylative oxygenation of carboxylic acids, Chem. Commun., *58*(28), 4456-4459.(DOI: 10.1039/D2CC00570K)

[30] Kundu, B. K., Chhabra, V., Malviya, N., Ganguly, R., Mishra, G. S., & Mukhopadhyay, S. (2018), Zeolite encapsulated host-guest Cu (II) Schiff base complexes: Superior activity towards oxidation reactions over homogenous catalytic systems, Microporous and Mesoporous Mater., *271*, 100-117.(DOI: 10.1016/j.micromeso.2018.05.046)

[31] Kundu, B. K., Das, M., Ganguly, R., Bhobe, P. A., & Mukhopadhyay, S. (2020), Role of zeolite encapsulated Cu (II) complexes in electron transfer as well as peroxy radical intermediates formation during oxidation of thioanisole, J. catal., 389, 305-316.(DOI: 10.1016/j.jcat.2020.06.005)

[32] Fujiwara, M., Matsushita, T., Ikeda, S. (1993). X-ray photoelectron spectroscopy of copper (II) complexes with donor sets of O_4, N_2O_4, N_2O_2, N_4, N_2S_2, and S_4, Analytical sciences, 9, 289-291.(DOI: 10.2116/analsci.9.289)

[33] Reddy, G. R., Balasubramanian, S., Chennakesavulu, K. (2014), Zeolite encapsulated Ni (ii) and Cu(ii) complexes with tetradentate N2O2 Schiff base ligand: catalytic activity towards oxidation of benzhydrol and degradation of rhodamine-B, Journal of Materials Chemistry A, 2(37), 15598-15610.(DOI: 10.1039/ C4TA01869A)

Chapter 6

General conclusions and future scopes

Chapter 6

General conclusions and future scopes

6.1 General conclusions

Over the past few decades, there has been widespread interest in the identification of transition metal-based compounds for various applications. Among the various kinds of ligand systems N, O-donor-based ligands are found to be very attractive because of their intermediate strength which can be tuned further with denticity, flexibility, and formal charge on them. There is an impetus among inorganic chemists to explore the versatility of Mannich bases and Schiff bases ligands, with N, O-donor based ligand backbone. Details of the studies on the synthesis, characterization, and applications, particularly of biological and ecological relevances for some new N, O-donor based ligands and their copper complexes are presented in this thesis. In this aspect, the thesis is divided into six chapters. The essences of these chapters are delineated hereunder.

Chapter 1 under the heading of 'Introduction' explains the novelty of N, O-donor based ligands and their transition metal complexes mainly composed of Cu(II). The biological importance, photocatalytic ability, and sensing behavior of these compounds have been presented. A brief review of recent reports is incorporated in this chapter.

Chapter 2 describes the materials and methods used for the synthesis of ligands and metal complexes. Various characterization techniques used to study the structures of the synthesized compounds have also been summarized. Metallo-enzyme mimicking properties *via* Mannich base Cu(II) complexes (**1** and **2**) have been explored. Apart from that, one hexanuclear Cu(II) Mannich base complex (**3**) has been synthesized and investigated for their sensing ability towards the picric acid.

Chapter 3 deals with the template synthesis of binuclear Cu(II) complexes (**4** and **5**) from Mannich base ligands and their photocatalytic ability towards the benzyl alcohol oxidation as well as N-alkylation of aniline reactions.

Chapter 4 defines the synthesis and characterization of binuclear Schiff base Cu(II) complexes (**6** and **7**) and their catalytic efficiency towards the

photocatalytic cleavage of C-C bonds of lignin model substrate as well as authentic (pineapple) lignin.

Chapter 5 pronounces the importance of zeolite-encapsulated Schiff base copper complexes in oxidative C=C bond cleavage reactions and degradation of extracted (coconut husk) lignin. Moreover, the stability of these copper complexes inside the super cages of zeolites has been explored in this chapter.

6.2 Comparison of photocatalytic ability of synthesized mono- and bi-nuclear Cu(II) complexes

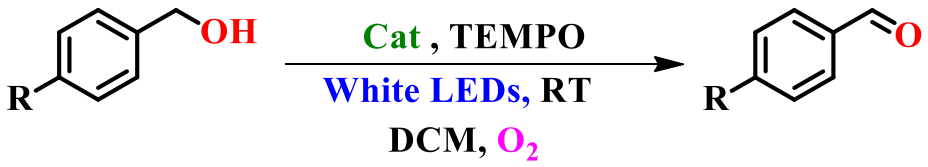

Table 6.1. *Photocatalytic oxidation of benzyl alcohol by synthesized complexes.*

Entry No	Catalyst	Conversion [%]	Selectivity [%]	Yield [%]	TON
1	Comp-1	90	99	90	89
2	Comp-2	89	99	89	88
3	Comp-4	92	99	92	92
4	Comp-5	87	99	87	86
5	Comp-6	85	99	85	84
6	Comp-7	72	99	72	71
7	Comp-8	92	99	92	92
8	Comp-9	89	99	89	88
9	Comp-10	95	99	95	95
10	Comp-11	92	99	92	90

[a]*General reaction conditions: benzyl alcohol (1 mmol), catalyst (1 mol%), TEMPO (2 mol%), DCM (1 mL), Air, light intensity (12 Watt LED bulb), room temperature, stir 1 h.*

The synthesized mono- and bi-nuclear (homogeneous and heterogeneous) copper complexes have been tested for the photocatalytic oxidation of benzyl alcohol into an aldehyde. Complex **4** and **8** afforded 92 % conversion with 99 %

selectivity towards the benzaldehyde in 1 h, which is better among the homogeneous complexes (Table 6.1). In the presence of heterogeneous compound **10**, 95 % conversion with 99 % selectivity of benzaldehyde (Table 6.1) was observed. The acetate group abstracts the hydrogen more easily than the other weak base co-ligand present in the complexes, making complexes **4** and **8** better catalysts. The heterogeneous compound showed better catalytic ability among all synthesized Cu(II) containing compounds.

6.3 Future scopes

N, O-donor-based ligands are dynamic in geometry, electron affinity, and reactivity, making them excellent choices to feed the ongoing field of catalysis and sensing. This area of research is still of much relevance and continously expanding. Results obtained from the present work would be very useful for the synthesis of organic compounds and drugs in environmentally friendly processes. Furthermore, the selective design of Cu(II) complexes can be useful for the degradation of bio-polymers into valuable chemicals and fuels. The present work concludes that heterogeneous complexes might be a better catalyst for various catalysis. The study of the intrinsic properties and stability of heterogeneous catalysts after several times of use would be supportive for efficient design. Apart from that, these Cu(II) complexes can be investigated as electrocatalysts in H_2O-splitting as well as in the CO_2 reduction reactions [1, 2].

6.4. References

[1] Chen, Q. F., Cheng, Z. Y., Liao, R. Z., Zhang, M. T. (2021) Bioinspired Trinuclear Copper Catalyst for Water Oxidation with a Turnover Frequency up to 20000 s-1, J. Am. Chem. Soc., 143, 19761−19768.(DOI: 10.1021/jacs.1c08078)

[2] Kim, K., Wagner, P., Wagner, K., Mozer, A. J. (2022) Electrochemical CO_2 Reduction Catalyzed by Copper Molecular Complexes: The Influence of Ligand Structure, Energy & Fuels, 4653-4676.(DOI: 10.1021/acs.energyfuels.2c00400)